MOLECULAR AND ENVIRONMENTAL ASPECTS OF LATEX FILM FORMATION

by

Jianrong Feng

A thesis submitted in conformity with the requirements for the Degree of Doctor of Philosophy, Graduate Department of Department of Chemistry, in the University of Toronto

MOLECULAR AND ENVIRONMENTAL ASPECTS OF LATEX FILM FORMATION

Ph.D. 1997

Jianrong Feng

Department of Chemistry
University of Toronto

ABSTRACT

This thesis examines mainly the formation mechanism and structure of latex films. We investigated the drying behavior of latex dispersions by monitoring simultaneously the loss of water mass and the contraction of the wet dispersion area. A soft latex dries slower than a hard latex, and their blends dry even more slowly. The presence of hydrophilic material facilitates drying. We propose a drying model to explain the results. We examined our strategy for zero VOC (volatile organic compound) coatings, by blending latex particles of a low Tg polymer [e.g. poly(butyl methacrylate-co-butyl acrylate)] and of a high Tg polymer [e.g. poly(methyl methacrylate)]. Transparent films can be obtained from blend dispersions when the volume fraction of soft polymer exceeds a critical value (Φ_C) ca. 0.5, and when the hard spheres are uniformly distributed in a soft polymer matrix. The hard particles in blends improve significantly the mechanical properties. Interface structure in blend films was characterized by direct non-

radiative energy transfer (DET) technique. A finite efficiency of DET, which is proportional to the interfacial area, characterizes a sharp interface between the polymer components, and its slight increase upon annealing the films represents the evolution of interface thickness (up to 7 nm at 140 °C). The DET technique is also employed to analyze polymer diffusion in latex films and to examine the effect of various components on diffusion rate. We find that water has little effect on the diffusion of a hydrophobic polymer [poly(butyl methacrylate), PBMA]. For a hydrophilic polymer [a copolymer of BMA with 5 wt% methacrylic acid], the presence of water increases the diffusion coefficient by a factor of 5 in the protonated sample, and by 2 orders of magnitude for the sample neutralized by a base (e.g. NaOH). The BMA oligomers enhance significantly the diffusion rate of high molar-mass PBMA. Finally, we examine strategies for ambient crosslinking of latex films. Films with acetoacetoxy functionality can be crosslinked rapidly with diamine as a crosslinker. Films with unsaturated bonds can be cured with the addition of an organic salt (e.g. cobalt octoate) in several days during which a high degree of polymer interdiffusion can be achieved.

SUMMARY

In this thesis, some important aspects in latex film formation were studied. These aspects include the kinetics and mechanism of drying, morphologies and properties for latex blend films, interface structures as characterized by fluorescent energy transfer, polymer diffusion and factors affecting the diffusion rate, as well as strategies for film crosslinking for structural stability and improved performance.

The latex samples used for various projects were synthesized by emulsion polymerization. These include fluorescent-labeled latex, low Tg film-forming latex, nano-sized latex, and reactive latex. The strategies for the synthesis of these latexes and some experimental details are described in Chapter II.

Chapter III describes our experiments on drying of latex dispersions and their interpretation. We carried our experiments in which we monitored the loss of water mass and the contraction of the area of the wet dispersion (or the propagation of the drying front) simultaneously. This kind of measurements enables us to have a more complete image for the drying process than that of the classic three-stage drying model proposed by Vanderhoff: drying is accompanied by not only the concentration of particles in the bulk but also the contraction of the wet dispersion area in the substrate plane. We find that the decrease in area of the wet dispersion precedes the decrease in water evaporation rate, establishing that the dry boundary region plays an important role in water evaporation. We find that a soft latex (minimum film-forming temperature, MFT, below 22 °C) dries slower than a hard latex (MFT well above 22 °C), and blends of them dry even more slowly with a distinct composition for slowest drying. The presence of hydrophilic material (ionic surfactant) facilitates the drying. These results lead to a conclusion that drying is influenced by the particle packing structure at close-contact in the drying boundary region. Combined with recent literature, we develop a new model for the drying mechanism of latex dispersions that takes into account the propagating drying front.

One project involves our strategy for zero VOC (volatile organic compound) coatings. Our approach involves mixtures of particles of a low Tg polymer [e.g. a copolymer of butyl methacrylate and butyl acrylate, P(BMA-co-BA)] and a high Tg polymer [e.g. poly(methyl methacrylate), PMMA]. A dispersion of a latex with a low MFT will form a transparent film upon evaporation, even when blended with a substantial amount of high Tg latex. There is a critical volume fraction of low Tg polymer ($\Phi_C \approx 0.5$) above which one can obtain transparent films. Transparency requires that the hard latex be sufficiently small and well dispersed in the final film and that the two components have similar refractive indices. When the size ratio between the hard and soft particles is far from unity, macroscopic phase separation occurs, giving rise to films with a clear region and a turbid region associated with hard-particle clustering. Film morphologies were examined by atomic force microscopy (AFM), scanning electron microscopy (SEM), and freeze-fracture transmission electron microscopy (FFTEM). In all films, the hard particles retain their original size and spherical shape. In the transparent films, they are uniformly distributed in a polymer matrix generated from deformed soft particles, whereas clustering of PMMA microspheres is observed in turbid films. Dynamic mechanical analysis (DMA) indicates that the hard particles in blends improve significantly the mechanical properties of the films. These results are presented in Chapter IV.

Interface structure in polymer blend films is an important factor affecting the film properties. While the structure at interfaces can be observed by electron microscopy, one can only obtain poor depth resolution. We employed the direct non-radiative energy transfer (DET) technique to characterize the interface. Fluorescence decay measurements on films consisting of a polymer component labeled with donor and the other component labeled with acceptor give the quantum efficiency of DET (Φ_{ET}) occurring in the interfacial region. A certain value of Φ_{ET} is observed across a sharp interface which is proportional to the interfacial area (and for spheres, inversely proportional to the diameter of donor-labeled particles). Upon annealing the films, the Φ_{ET} value increases, characterizing the increase in interface thickness. For PMMA/P(BMA-co-BA) blends, the interface thickness increases upon heating (e.g. to 4 nm at 140 °C for 1 h), but

only up to a finite extent (e.g. 7 nm) with extended annealing time owing to limited miscibility. We are able to obtain information about the interface structure with a fine depth resolution by the DET technique. This part is presented in Chapter V.

In the newly formed latex films, the particles deform into polyhedra and the polymer molecules are essentially separated in individual cells. It is believed that the film mechanical properties will be developed only after the polymer molecules have diffused across the interfaces. We employed the DET technique to monitor the polymer diffusion process for films formed from mixtures of donor- and acceptor- labeled particles composed of otherwise identical polymers. With time or upon annealing, the efficiency of DET increases which can be used to characterize the increasing extent of interdiffusion of the labeled polymers and to calculate the diffusion coefficient. The major focus for this part of this thesis is to examine the effects of various components, including water and oligomers, on the polymer diffusion rate. We found that water has little effect on the diffusion rate of a hydrophobic polymer [poly(butyl methacrylate), PBMA], but increases the diffusion coefficient by more than 5 times for a hydrophilic polymer [i.e. a copolymer of BMA with 5 wt% methacrylic acid, P(MAA-co-BMA)]. For P(MAA-co-BMA) polymer neutralized by base (e.g. NaOH), the diffusion coefficient values found in the presence of water are 2 orders of magnitude larger than those measured for the same polymer in dry state. The BMA oligomers can enhance significantly the diffusion rate of high molar-mass PBMA. These results establish that not only those added traditional plasticizers can plasticize the polymer but also those components inherently present in the system can change the diffusion rate and hence alter the process of development of film properties. These results are presented in Chapter VI. The energy transfer technique allows us to obtain information about the film formation process at a molecular level.

It is well-known that curing of the polymer films is essential for coatings applications for obtaining chemical resistance and improved performance. One of the target for novel coatings is to cure the coatings under ambient conditions. We examined strategies for ambient crosslinking of latex films. We chose two types of reactive functionalities, acetoacetoxy and unsaturated groups. The results about film crosslinking and its characterization are presented in Chapter VII.

The rate of crosslinking is also compared with the rate of polymer interdiffusion in our model systems. Latex films formed from acetoacetoxy functionalized latex can be crosslinked with a diamine (e.g. hexane diamine) as a crosslinker. The crosslinking reaction between amino and acetoacetoxy groups occurs at a rapid rate, giving rise to a high degree of crosslinking even before the completion of drying of the dispersions. The crosslinking process precedes the polymer interdiffusion in such a reactive system, even when the molecular weight or the Tg of the polymers is low. Films with unsaturated bonds can be cured with the addition of certain organic salts (e.g. cobalt octoate). Curing can be achieved on the time scale of days during which the latex films can undergo a high degree of coalescence.

ACKNOWLEDGMENTS

I must express first my deep appreciation to my supervisor, Professor Mitchell A. Winnik. Owing to him I started my research related to emulsion polymers and began a somewhat different type of life in Toronto 5 years ago. Since then he has been continuously offering me opportunities of pursuing several research projects and participating in various group activities. By the time of my graduation from his lab, my overall strength of scientific research has grown by a significant level that I become more confident than before in my work. I thank Mitch for his constant supervision and support, his pleasant style of communication, and his special help in my English Writing throughout this period.

Special thanks are given to Dr. Yuansheng Liu, Ms. Ewa Odrobina, Mr. Abhi Patel, Mr. Hung Pham, Dr. Ahmad Yekta, Dr. Stan Sosnowski, Dr. Lin Li, Dr. Yongcai Wang, Prof. Julia Vancso, and Prof. Peter Macdonald in the Chemistry Department of University of Toronto for various collaborations. Thanks are extended to Prof. Anton L. German, Prof. Steven van Es, and their students at the Department of Chemical Engineering of University of Technology in Eindhoven, Holland for their help in the collaborative work during my visit in their lab. These above-mentioned have been or will be co-authors with me in various publications or projects and contribute in some ways to the work presented here, and hence their credits will be mentioned in the thesis. I also thank Prof. Xigao Jin and Prof. Liusheng Chen at the Institute of Chemistry of Chinese Academy of Sciences for the co-authored paper on dye-labeling of poly(ethylene) resin and its thermal stability, although this part is not discussed in this thesis.

I would also like to thank all other members in the Polymer and Colloid Chemistry Group at the University of Toronto for many valuable discussions with them and for the friendly atmosphere they have created in the lab, although their individual names are not listed here due to a large number. I wish this friendship and memory will be extended in the future of my life.

It is my pleasure to appreciate the Federation of Societies for Coatings Technology for awarding Prof. Winnik and myself the First Prize of 1995 Roon Awards, and the Polymer Divisions of the American Chemical Society for selecting me as the finalist and awarding me a certificate of merit in the 1995 Sherwin-Williams Graduate Award Competition. These will encourage me to pursue my future career as a researcher. Various scholarships offered by University of Toronto during my graduate study are also greatly appreciated.

Finally, I must stress that this thesis research is made possible by the full support and love from my family, my daughters, Nina and Betty, my wife, Jian Ni, and my parents. This Ph.D. thesis is thus also written for them.

CONTENTS

ABSTRACT ii

SUMMARY iv

ACKNOWLEDGMENTS viii

CHAPTER I GENERAL INTRODUCTION 1

I-1 EMULSION POLYMERIZATION AND LATEX 1

I-1-1 General Description of Emulsion Polymerization System 1

I-1-2 The Process of Emulsion Polymerization 2

I-1-2-1 Qualitative features of the process 2

I-1-2-2 The kinetics of emulsion polymerization 4

I-1-2-3 The degree of polymerization and molecular weight distribution 5

I-1-2-4 The particle number concentration and size distribution 6

I-1-3 Batch and Semi-continuous Processes 7

I-1-4 The Product of Emulsion Polymerization - Latex 7

I-2 LATEX FILM FORMATION 8

I-2-1 Brief Description of the Process 8

I-2-2 The Drying Process of Latex Dispersions 9

I-2-3 Deformation Mechanism and Packing Structure 10

I-2-4 Polymer Diffusion 12

I-2-5 Current Research Directions 13

I-2-5-1 Strategies for low and zero VOC coatings 13

I-2-5-2 Strategies for improved performance 14

I-3 SCOPE OF THIS RESEARCH WORK 14

CHAPTER II SYNTHESIS AND CHARACTERIZATION OF LATEX PARTICLES 16

II-1 BRIEF DESCRIPTION 16

II-2 EXPERIMENTAL 17

II-2-1 Materials 17

II-2-2 Typical Reaction Recipe and Set-up 18

II-2-3 Latex Purification 21

II-2-3-1 Purification by ion-exchange 21

II-2-3-2 Purification by serum replacement 21

II-2-3-3 Purification by centrifugation 21

II-2-4 Techniques and Instrumentation in Latex Characterization 22

II-2-4-1 Particle sizer 22

II-2-4-2 Scanning electron microscopy (SEM) 22

II-2-4-3 Gel permeation chromatography (GPC) 22

II-2-4-3 UV-visible spectrophotometer 22

II-2-4-4 Nuclear magnetic resonance (NMR) spectroscopy 23

II-2-4-5 Infrared (IR) spectroscopy 23

II-2-4-6 Differential scanning calorimetry (DSC) 23

II-2-4-7 Gravimetric measurements 23

II-2-4-8 Acid-base titration 23

II-3 IMPORTANT FEATURES OF TWO-STAGE EMULSION POLYMERIZATION 24

II-3-1 Conversion of Polymerization 24

II-3-2 Particle Size and Size Growth 25

II-3-3 Variation of Molecular Weight 28

II-4 SYNTHESIS AND CHARACTERIZATION OF FLUORESCENT LABELED LATEXES 30

II-4-1 Synthesis of Fluorescent Comonomers 30

II-4-1-1	Vinyl phenanthrene comonomer	
II-4-1-2	Phenanthryl methyl methacrylate comonomer	31
II-4-1-3	Anthryl methacrylate comonomer	31
II-4-2	Preparation of Labeled Latex Polymers	31
II-4-3	Dye Distribution Analysis	33
II-4-3-1	Illustration of the GPC graphs and their analysis	33
II-4-3-2	Batch and semi-continuous polymerizations	35
II-4-3-3	Analysis of Phe and An labeled polymer	38
II-5	SYNTHESIS OF LOW-Tg FILM-FORMING LATEXES	40
II-6	SYNTHESIS OF 30 NM LATEX PARTICLES	43
II-7	SYNTHESIS OF REACTIVE LATEX	45
II-7-1	Acetoacetoxy-functional Latexes	45
II-7-2	Carboxylated Latexes	47
II-7-3	Unsaturated Latex	51

CHAPTER III	THE PROCESS OF LATEX DRYING	54
III-1	INTRODUCTION	54
III-2	EXPERIMENTAL	55
III-2-1	Latex Samples	55
III-2-2	Film Formation	56
III-2-3	Measuring Water Loss During Drying	56
III-3	RESULTS AND DISCUSSIONS	57
III-3-1	The Drying Front	57
III-3-2	The Kinetics of Drying	59
III-3-2-1	The water evaporation rate at low solids	59
III-3-2-2	The drying of hard and soft latex dispersions	60
III-3-3	The Drying of Latex Blends	65
III-3-4	Surfactant Effects on the Drying Rate	68

III-3-5 Models for The Drying Process 71
III-3-5-1 Classic models of drying 71
III-3-5-2 Recent views of the drying process 71
III-3-5-3 Our view of the drying process 72
III-4 SUMMARY 75

CHAPTER IV LATEX BLEND FILMS FOR ZERO VOC COATINGS 76

IV-1 INTRODUCTION 76
IV-1-1 Latex Blends 76
IV-2 EXPERIMENTAL 78
IV-2-1 Latex Samples 78
IV-2-2 Film Formation 79
IV-2-3 Film Characterization 79
IV-3 RESULTS AND DISCUSSIONS 80
IV-3-1 Film Transparency 80
IV-3-2 Film Morphology 83
IV-3-2-1 A random distribution of hard particles in transparent films 83
IV-3-2-2 Clustering of hard particles in turbid films 85
IV-3-2-3 Surface morphology in relation to transparency phase diagram 87
IV-3-2-4 Morphology Evolution upon Annealing 89
IV-3-3 Mechanical Properties 90
IV-4 SUMMARY 93

CHAPTER V INTERFACE CHARACTERIZATION IN BLEND LATEX FILMS BY DIRECT NON-RADIATIVE ENERGY TRANSFER 94

V-1 INTRODUCTION 94
V-1-1 Direct Non-radiative Energy Transfer 94
V-1-2 Interface Characterization by DET 96
V-1-3 Latex Films 97
V-2 EXPERIMENTAL 98
V-3 RESULTS AND DISCUSSIONS 99
V-3-1 Energy Transfer Across An Interface 99
V-3-1-1 Varying blend composition and hard particle size 101
V-3-1-2 The dependence of energy transfer on surface area 105
V-3-1-3 Variation of the means of labeling 108
V-3-1-4 Influence of the presence of surfactant 108
V-3-2 Interface Structure in Nascent Blend Films 109
V-3-3 Interface Evolution in Annealed Films 110
V-4 SUMMARY 114

CHAPTER VI POLYMER DIFFUSION ANALYSIS BY FLUORESCENCE ENERGY TRANSFER IN LATEX FILMS AND FACTORS AFFECTING THE DIFFUSION RATE 115

VI-1 INTRODUCTION 115
VI-1-1 Polymer Diffusion 115
VI-1-2 Analysis of Polymer Diffusion by DET 116

VI-1-3 Examining Factors Affecting Polymer Diffusion Rate 118
VI-2 EXPERIMENTAL 119
VI-2-1 Latex Sample 119
VI-2-2 Film Formation and Characterization 120
VI-3 RESULTS AND DISCUSSIONS 121
VI-3-1 Energy Transfer and Diffusion Analysis 121
VI-3-2 Role of Water in Polymer Diffusion 124
VI-3-2-1 Film Transparency and Water Content 124
VI-3-2-2 Effect of Water on Polymer Diffusion 127
VI-3-2-3 Effect of Water on Neutralized P(MAA-co-BMA) 130
VI-3-3 Effect of Oligomers on Polymer Diffusion 133
VI-4 SUMMARY 135

CHAPTER VII FORMATION AND CHARACTERIZATION OF LATEX FILMS CROSSLINKABLE UNDER AMBIENT CONDITIONS 136

VII-1 INTRODUCTION 136
VII-1-1 Brief Review of Thermal-cure Systems 136
VII-1-2 Brief Review of Ambient-cure Systems 137
VII-1-3 Our Approaches to Ambient-cure 138
VII-2 EXPERIMENTAL 138
VII-2-1 Latex Sample 138
VII-2-2 Film Formation, Crosslinking, and Measurements 140
VII-3 RESULTS AND DISCUSSIONS 141
VII-3-1 Acetoacetoxy (AA) System 141
VII-3-1-1 The drying behavior and pseduoplastic rheological effect 141
VII-3-1-2 Characterization of crosslinking reaction 143

VII-3-1-3 Polymer diffusion rate Vs. crosslinking rate 147
VII-3-1-4 Loss of functionality during storage and upon heating 152
VII-3-2 Unsaturated (U) SYSTEM 154
VII-4 SUMMARY 155

APPENDICES 156

Appendix II-1 Recipes for Preparation and Characteristics of P(BMA-co-BA) Latexes 156
Appendix II-2 Recipes for Preparation and Characteristics of P(BMA-co-BA-co-MAA) latexes 157
Appendix III-1 Calculation of the percent solids and thickness of the wet dispersion domain during latex drying 159
Appendix VI-1 Comparison of polymer diffusion analysis by DET for film samples of different number ratio of donor to acceptor-labeled particles or with different sample geometries and by using different analytical techniques 160
AVI-1-1 Objectives 160
AVI-1-2 Experimental 160
AVI-1-3 Comparison between 1 : 1 and 1 : 12 D/A mixture 161
AVI-1-3-1 Geometric consideration 161
AVI-1-3-2 Analysis of energy transfer efficiency 164
AVI-1-3-3 The net increase of energy transfer efficiency 166
AVI-1-3-4 Calculation of diffusion coefficient 168
AVI-1-3-5 The $t^{1/2}$ dependence of energy transfer at short times 170
AVI-1-3-6 Evidences of non-uniform chromophore concentration distribution (the correlation holes) 171
AVI-1-3-7 Calculation of the characteristics distance for energy transfer (R_o) 173

AVI-1-4 Strategies for Comparison Between Latex-Structured and Lamellar-layered Films 174
AVI-1-5 Comparison of analysis between the "three-region" approach and the "concentration-gradient" approach 176
AVI-1-5-1 Simulated data 176
AVI-1-5-2 Experimental data 177
AVI-1-6 Concluding Remarks 178

REFERENCES 179

LIST OF PUBLICATIONS 189

CHAPTER I GENERAL INTRODUCTION

I-1 EMULSION POLYMERIZATION AND LATEX

I-1-1 General Description of Emulsion Polymerization

Emulsion polymerization refers to a process in which the monomers are dispersed in a continuous medium with the aid of emulsifier and polymerized with free-radical initiators.[1-3] Typical components in the system are the monomer, emulsifier (surfactant), water-soluble initiator, and water as the dispersant. The concentration of surfactant is usually above its critical micelle concentration (CMC) in the system before polymerization. The number of micelles formed and their size depend on both the total amount of surfactant used and the relative amount of monomer to surfactant present. A typical size for spherical surfactant micelles is 2 to 5 nm in diameter in its original state, increasing to >10 nm when swollen by monomer. For most monomers, only a very small fraction is dissolved in water. A larger but still small portion of monomer enters the interior hydrophobic part of the micelles. The largest portion of monomer is dispersed as monomer droplets whose size is usually above a micrometer and is dependent on the intensity of agitation. The droplets are probably stabilized by surfactant molecules adsorbed on their surfaces. The typical concentration of micelles is 10^{17}-10^{18} per milliliter, and that for monomer droplets is 10^{10}-10^{11} per milliliter.

The locus of polymerization is very important. The initiator is present in the water phase where the initiating radicals are produced, and the rate of radical production R_i is typically of the order of 10^{13} radicals per milliliter per second. Polymerization in aqueous solution undoubtedly takes place but does not contribute significantly when the monomer solubility (concentration) is low and propagating radicals would precipitate out of the aqueous solution at very small oligomer size. It has been found that for many hydrophobic monomers polymerization is initiated mainly in the monomer swollen micelles where particle nucleation occurs. The micelles act as a meeting place for the organic monomer and the water-soluble free radicals. The site of particle nucleation is not the monomer droplets. The reason for this is that the micelles have much higher total surface area available for entry of radicals than the monomer droplets, and that the initiator concentration in a micelle is much higher than that in a larger-sized monomer droplet if they both contain one radical. The micelles are also favored as the nucleation site because of their higher monomer concentration than the monomer in solution.

A simplified schematic representation of the initial stage of an emulsion polymerization is shown in Figure I-1. Surfactant molecules are shown as O- to indicate that one end (O) is polar or ionic and the other end (-) nonpolar. The system consists of three types of particles: monomer droplets, inactive micelles in which polymerization is not occurring, and active

micelles in which polymerization is occurring. Once "active micelles" become sufficiently large, they are referred to as polymer particles.

The mechanism for particle nucleation is best described as proceeding by two simultaneous processes. One is the entry of radicals from the aqueous phase into the micelles (micellar nucleation). The other, homogeneous nucleation,[4,5] involves solution-polymerized oligomeric radicals becoming insoluble and precipitating on themselves (or on dead oligomer). The precipitated species become stabilized by adsorbing surfactant (from solution, inactive micelles, and the monomer droplets) and upon subsequent absorption of monomer. The species formed in this way are the equivalent of polymer particles formed by micellar nucleation. The relative extents of micellar and homogeneous nucleation would be expected to vary with the water solubility of the monomer and the surfactant concentration. Higher water solubility and low surfactant concentration favor homogeneous nucleation;[6,7] micellar nucleation is favored by low water solubility and high surfactant concentration.[8]

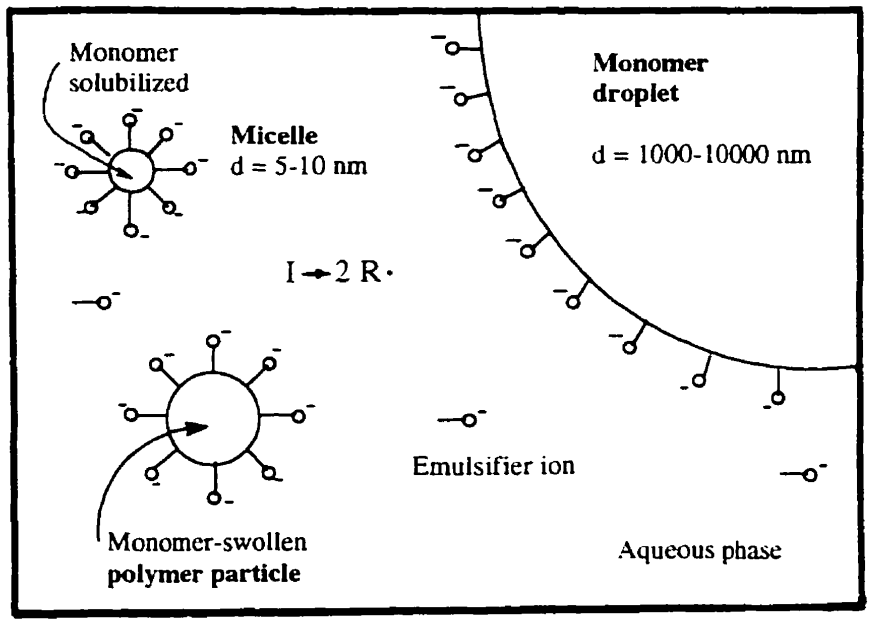

Figure I-1. Simplified representation of the initial stage of an emulsion polymerization system.

I-1-2 The Process of Emulsion Polymerization

I-1-2-1 Qualitative features of the process

The qualitative interpretation of the main features of emulsion polymerization was put forward by Harkins in 1946.[9] Although there have been additions and modifications of the concepts, the overall view of emulsion polymerization remains accepted. It was considered that

the polymerization took place mainly in the micelles in which a small fraction of monomer dissolved and polymer particles were formed by continuously polymerizing the monomer initiated by entry of free-radicals from the aqueous solution. Three Intervals (I, II, III) can be discerned in all emulsion polymerizations based on the particle number concentration N (number of particles per milliliter) and the existence of a separate monomer phase (i.e. monomer droplets). Interval I is a particle nucleation period in which polymerization starts in micelles to form particles, and the particle number increases. The polymerization rate increases with time as the particle number builds up. A large fraction of monomer is present in the monomer droplets. Monomer is transferred from the monomer droplets into the particles to replenish the monomer that has reacted. The reaction system undergoes a very significant change during Interval I. The particle number stabilizes at some value (in the range of 10^{13}-10^{15} particles per milliliter) which is only a small fraction, typically about 0.1%, of the concentration of micelles initially present. As the polymer particles grow in size, they absorb more surfactant from solution to maintain stability. The point is quickly reached at which the surfactant concentration in solution falls below its CMC.

By the end of Interval I, almost all of the surfactant originally present as micelles has been absorbed by the polymer particles. Interval I is generally the shortest of the three Intervals, its duration varying in the range of 2-15% conversion. The transition from Interval I to II occurs when the surfactant in the inactive micelles moves to the active particle surface and hence no new particles will form. Thus ideally the particle number remains constant during the subsequent Intervals (II and III). Polymerization proceeds in the polymer particles as the monomer concentration in the particles is maintained at the equilibrium (saturation) level by diffusion of monomer from solution, which in turn is maintained at the saturation level by dissolution of monomer from the monomer droplets. During this period, the polymerization rate is nearly constant, since the monomer concentration within each particle remains constant. The monomer concentration (volume fraction Φ_m) in the polymer particles for styrene is 0.60, and that for methyl methacrylate is 0.71.[10] The polymer particles increase in size as the monomer droplets decrease. Interval II ends when all the monomer in the monomer droplets is consumed and the droplets disappear. The particle number remains the same in Interval III as in Interval II, but the monomer concentration decreases with time, since there is no longer a supply of monomer from the initial monomer droplets. Polymerization continues but at a steadily decreasing rate as the monomer concentration in the particles decreases. Figure I-2 is a typical plot of polymerization rate vs. time, showing schematically the difference in rates for three Intervals of polymerization. Final conversions of essentially 100% are usually achieved. The final polymer particles have sizes intermediate between that of the initial micelles and that of the monomer droplets, of the order of 50 - 200 nm.

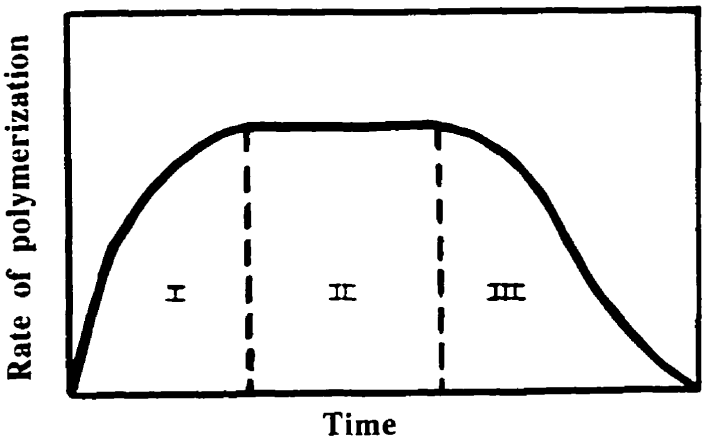

Figure I-2. Schematic illustration of the change of the polymerization rate with time in emulsion polymerization.

I-1-2-2 The kinetics of emulsion polymerization

The first quantitative treatment of emulsion polymerization kinetics was by Smith and Ewart.[11] One of the important assumptions of the Smith-Ewart theory is that the polymerization rate is determined by the ingress of radicals into the growing particles and not by the competing rates of propagation and polymer radical termination reactions as in the case of bulk polymerization. In this theory polymerization is considered to be initiated in the micelle and to continue within the monomer-polymer particle. Following initiation within the surfactant micelles, three limiting cases are considered relating to the average number of free-radicals (n) in a particle: (1) n is much smaller than unity; (2) n is approximately 0.5; (3) n > 0.5.

The rate of polymerization R_p is related to the monomer concentration in the swollen particles ([M], in moles/liter), the average number of free radicals per particle (n), and the concentration of particles (N, in number of particles / ml) by

$$R_p = (1000/N_A)\, k_p\, [M]\, n\, N \qquad (I\text{-}1)$$

where k_p is the rate constant, and N_A is the Avogadro constant.

At the start of Interval I, the number of particles is small and polymerization rate is low. During Interval II, the particle concentration has reached its steady-state value N. n may also reach an constant value. [M] is also relatively constant since there is equilibrium swelling of the particles by monomer during this stage, with a value as high as 5M (50-80% monomer volume fraction). During Interval III, monomer concentration decreases sharply and the rate decreases. One can see that these results are consistent with the plot of rate vs. time shown in Figure I-2.

The value of n is of critical importance in determining R_p. Three cases can be distinguished based on the work of Smith and Ewart and others.

Case 2 (n = 0.5) is usually described in texts as applicable to most emulsion polymerizations. It occurs when desorption of radicals is negligible compared to the rate of radicals entering particles (absorption) and the particle size is too small, relative to the bimolecular termination rate constant, to accommodate more than one radical. Under these conditions, a particle normally contains one radical which is trapped within that particle and undergoes propagation until another radical enters, at which point there is essentially instantaneous termination. Any polymer particle will be active half of the time and dormant the other half of the time. In other words, at any given moment half of the polymer particles contain one radical and are growing while the other half are dormant. The number of radicals per particle n averaged over all the particles is 0.5.[12]

In case 1, the average number of radicals per particle (n) can drop below 0.5 if radical desorption from particles and termination in the aqueous phase are not negligible. The decrease in n is larger for small particle sizes and low initiator rates. As for the monomers, it is found that certain monomers (e.g., vinyl acetate and vinyl chloride) follow case 1 behavior.[10]

Case 3 is characterized by $n > 0.5$. Some fraction of the polymer particles must contain two or more radicals per particle in order for n to be > 0.5, since there will always be a very significant fraction of zero radical per particle. This occurs if the particle size is sufficiently large (100-1000 nm) and the initiation rate is sufficiently high relative to the termination rate constant, while termination in the aqueous phase and desorption are not important. This effect is more pronounced as the percent conversion increases. Under these conditions, two or more radicals coexist in a polymer particle without instantaneous termination.[13,14]

I-1-2-3 The degree of polymerization and molecular weight distribution

The number average degree of polymerization X_n in an emulsion polymerization of Case 2 behavior can be expressed as

$$X_n = r_p / r_i = Nk_p[M] / R_i \qquad \text{(I-2)}$$

where r_p is the propagation rate of a polymer chain and r_i is the rate of primary radicals entering a polymer particle. Note that r_i is equal to the radical production rate R_i divided by the polymer particle number N. For a Case 2 behavior, r_i is just equal to the rate of termination r_t of a polymer chain, since termination occurs immediately upon the entry of a radical into a polymer particle in which a polymer chain is propagating. If chain transfer occurs, the degree of polymerization will be given by

$$X_n = r_p / r_i + r_{tr} \qquad \text{(I-3)}$$

where r_{tr} is the rate of transfer reaction.

In emulsion polymerization one can attain both high molecular weight and a high polymerization rate simultaneously. As one can see from Eqs. (I-1) and (I-2), both R_p and X_n vary directly with the number of particles N. Therefore the rate and degree of polymerization

can be simultaneously increased by increasing the number of polymer particles N at a constant initiation rate R_i. These conclusions have been verified by a number of studies.[10]

The molecular weight distribution (MWD) for polymers produced from emulsion polymerization has differences from those produced from homogeneous system. In emulsion polymerization the molecular weight remains reasonably constant during a large part (i.e. Interval II) of the overall reaction, since [M], N, k_p and R_i are relatively constant. Compared to homogeneous polymerization where substantial changes occur in the molecular weight and MWD with time throughout the whole range of conversions, one would expect to obtain narrower MWD from emulsion polymerization.[1] The above point, however, does not remain true in all cases. When chain termination involves bimolecular reaction between radicals, short chains can couple or disproportionate with longer chains in homogeneous system. In emulsion polymerization, any two growing chains that undergo bimolecular termination (e.g. disproportionation) are not random, giving rise to broadening of MWD.[1] Thus in some cases one produces broader MWD by emulsion than by homogeneous polymerization. The detailed analysis or modeling for MWD in emulsion polymerization has been addressed by Gilbert.[12a]

I-1-2-4 The particle number concentration and size distribution

The number of polymer particles (N) which can be stabilized is dependent on the total surface area of surfactant present in the system a_sC_s, where a_s is the interfacial surface area occupied by a surfactant molecule, and C_s is the total concentration of surfactant in the system. N is also dependent on the rate of radical production R_i. A relationship of N to a_sC_s and R_i has been derived as [1,10]

$$N = k\,(R_i / \mu)^{2/5}\,(a_sC_s)^{3/5} \qquad \text{(I-4)}$$

where μ is the rate of volume increase of a polymer particle, which can be determined from r_p and geometrical considerations. Typical values of k vary between 0.37 and 0.53. The $^3/_5$-power dependence of N on the surfactant concentration has been a useful guide for one to adjust the particle number and hence the final particle size by varying the amount of surfactant.

The size distribution of particles prepared by emulsion polymerization is primarily due to the distribution of times at which different polymer particles are nucleated and their alternation of activity and inactivity. The maximum polydispersity occurs during Interval I. The particle size distribution (PSD) narrows considerably during the subsequent period. In general, a fast nucleation (short Interval I) favors the production of narrow PSD. There has been a significant effort to produce narrow PSD by controlling the initiation and nucleation processes, choice and amount of surfactant, the use of seeded emulsion polymerization, temperature, ionic strength, and other reaction variables.[1] Mathematical evaluation of PSD is discussed in ref. 12a.

I-1-3 Batch and Semi-continuous Processes

Emulsion polymerization can be carried out either in batch or in semi-continuous (also referred to as semi-batch) modes.

In a batch process all the reactants are present at the start of the reaction. In a semi-continuous process, either all the reactants or just part of the reactants are added into the reactor while the reaction proceeds. No products are withdrawn during the reaction. It is well-known that the semi-continuous process offers better control of reaction rate, molecular weight, chemical composition distribution in copolymers, particle size and size distribution.[15]

In semi-continuous emulsion polymerization processes two different reaction conditions can be distinguished depending on the monomer addition rate relative to the maximum rate of polymerization. When the rate of monomer addition is below the maximum polymerization rate, the monomer concentration is below the equilibrium saturation value, and the rate of polymerization is found to depend linearly on the addition rate.[16] The instantaneous conversion is generally high and no substantial accumulation of monomer in the reaction system will occur. This reaction condition is referred to as *monomer-starved* condition. This is very useful in the control of molecular weight and in the preparation of copolymers of random chemical composition distribution.[17,18] We will demonstrate this in the synthesis of latex polymers and in the labeling of the polymers with dye comonomers. At higher rates of monomer addition, a point is reached where the particles are no longer able to accommodate the added monomer and a separate monomer phase appears. This condition is generally referred to as *flooding*. In this case the rate of polymerization is no longer dependent on the rate of monomer addition and the reaction conditions are much closer to those in the batch process.

Sometimes polymerizations are carried out in a "seeded" mode for both batch and semi-continuous processes, in which the monomer and initiator are added to a previously prepared emulsion of polymer particles. The reaction conditions are arranged in such a way that particle second nucleation is avoided, and the particle number N can be held constant during polymerization. Because of this feature of seeded systems, this approach is useful for preparations where one wishes to produce particles with well-controlled size, internal composition, and morphology.

I-1-4 The Product of Emulsion Polymerization - Latex

The final product of an emulsion polymerization is called a latex dispersion. Latex dispersions are colloidal systems in which submicron polymer particles are dispersed in a liquid medium, usually water.

The first synthetic latex products were poly(vinyl acetate), produced in Germany in the mid-1930s, and styrene-butadiene rubber manufactured on a large commercial scale in the US

during the 1940s.[1,3] The styrene-butadiene products were important as a substitute for natural rubber. Emulsion polymerization is presently the predominant process for the commercial polymerization of vinyl acetate, chloroprene, various acrylates, and copolymerization of butadiene with styrene and acrylonitrile (ABS resin). It is also used for methyl methacrylate (MMA), styrene, vinyl chloride, vinylidene chloride, although it is not the predominant process. In modern polymer industry, emulsion polymerization is one of the main process for carrying out radical polymerization reactions.[1,3]

Emulsion polymerization as a reaction process has several distinct advantages. The physical state of the emulsion (colloidal) system makes it easy to control the process. Heat transfer and viscosity problems are much less significant than in bulk or in solution polymerizations. As has been mentioned earlier, emulsion polymerization affords a means of producing polymers of high molecular weight without decreasing the polymerization rate.

In many practical applications such as in coatings, adhesives, and paints, the emulsion polymerization products (latexes) can in many instances be employed directly without further separation or with only appropriate blending operations. Also, since water is commonly used as the medium, latexes are characterized by low content of volatile organic compounds (VOCs). This has been one of the major factors driving the increasing usage of latex products today.

I-2 LATEX FILM FORMATION

One of the major applications of emulsion polymers is in various water-borne coatings.[19,20] In these applications, the latex, originally present as a colloidal dispersion of microspheres in water, is transformed into a void-free and mechanically coherent polymer film.

I-2-1 Brief Description of the Process

The term "latex film formation" refers to the entire process from the aqueous latex dispersion to the fully developed coating. The process is classically divided into three consecutive major steps.[21,22] In the first step, water evaporates at a constant rate until a state is reached where particles are brought into close contact. In the second step, as more water evaporates, the particles undergo deformation and compaction to form a void-free solid structure, if the temperature exceeds a minimum film-forming temperature (MFT) of the latex. Finally, fusion occurs among adjacent particles as polymer molecules diffuse across the initial boundaries to give a mechanically coherent film. A drawing depicting this process is shown in Figure I-3.

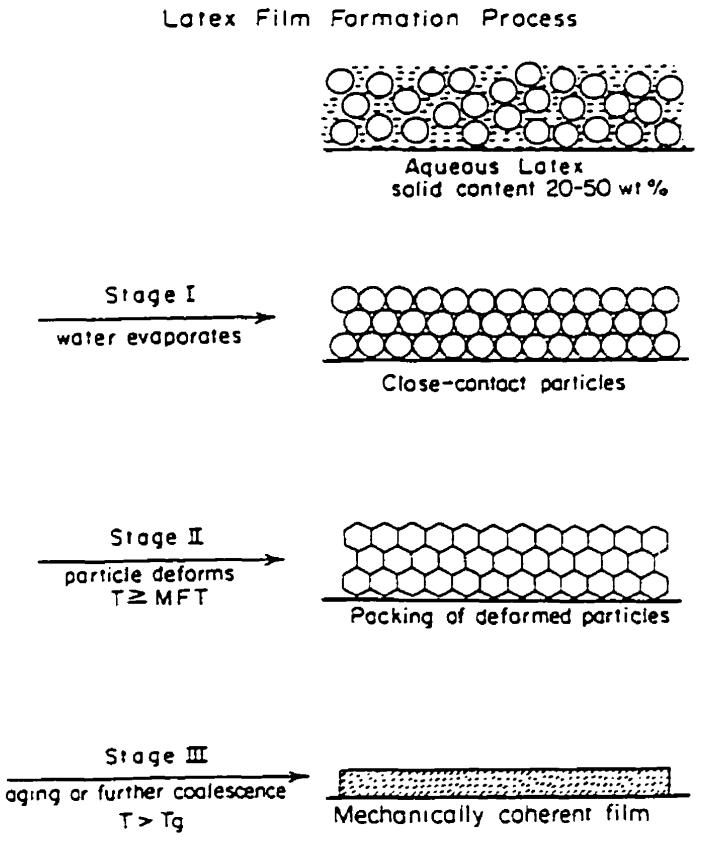

Figure I-3. A simple representation of the latex film formation process.

A comprehensive review on the topic of latex film formation has been given by Winnik.[23] I should point out here that some of the views and references present in this introduction are either cited from Professor Winnik's review or written with impact from him owing to various communications with him over the past years.

In the following I will give a brief review on the formation and structure of latex films as well as some research directions in latex coatings. The major aspects mentioned in this introduction part are related to the research presented in this thesis, and their connection is made in the next section, "Scope of This Research Work", in this chapter.

I-2-2 The Drying Process of Latex Dispersions

From a physicist's point of view, drying is one of the simplest physical processes, one in which a substance is transferred from the liquid phase to a vapor. When the external pressure, temperature and the surface area of the liquid are fixed, simple kinetics of drying are observed so that the mass of evaporation is linear in time. When the surface area of the liquid

varies, the mass of evaporation in a given time interval is different, but the rate of drying is proportional to the surface area.

Models for the drying process for latex dispersions are primarily based upon measurements of the rate of water loss.[22,24,25] The most well-known model was proposed by Vanderhoff.[22] He made a connection between the water loss rate and each of the three stages for the film formation process. In stage 1, water evaporates at its normal rate from the dispersion in which the particles remain separated. In stage 2, the particles come into close contact and deform to decrease the size of pores at the surface, and the evaporation rate slows. Eventually, coalescence leads to sealing of the surface. In stage 3, the loss of the last traces of water is very slow because water now must diffuse through the matrix of the polymer.

While the current models do capture some important features of the drying process and the Vanderhoff model is particularly often cited for its appealing simplicity, they are not complete. For example, they all neglect the propagating drying front during the drying process. This contradicts the drying behavior for most of latex dispersions[26-29] and even those observations reported by the same authors.[22,24,25] More over, there is little evidence about whether drying is dependent on the latex polymer composition or the type of particle packing structure formed at close-contact. As a consequence, reexamination of the drying process for latex dispersions is needed.

I-2-3 Particle Deformation Mechanism and Packing Structure

The particle deformation and compaction process in the second stage of film formation has both theoretical and practical importance and has received great attention. A major focus is devoted to understanding the nature of forces driving the coalescence of particles. The four main theories are the following. Bradford and coworkers[30] proposed that the major contribution to coalescence arises from the polymer surface tension which drives the polymer compaction to a fully dense film, referred to as dry-sintering theory. For Brown,[31] the acting forces were the capillary forces which develop at the surface of the drying latex when particles become partially exposed to air. According to Brown, the capillary pressure is proportional to the water-air interfacial tension and inversely proportional to the radii of the particles. Vanderhoff[32] considered that, instead of the polymer surface tension or polymer-air interfacial tension, the polymer-water interfacial tension could provide strong forces that were sufficient to drive deformation and densification of the particles immersed in water. This is referred to as the wet-sintering mechanism. Vanderhoff believed that capillary forces were also important in certain stages of the deformation process. The idea that both the interfacial tension forces and the capillary forces play complementary roles in the coalescence process has received support from others.[33] Sheetz[24] suggested another theory in which the surface of the latex is closed by a thin

layer (skin-layer) of coalesced particles. The remaining water evaporates by diffusion through this polymer layer and this evaporation gives rise to a stress which compresses the packing of particles, acting like a piston. Since the time of Bradford, Brown, and Vanderhoff, various attempts have tried to verify, extend or refine these models.[33-37] The most updated review on this topic was given recently by Holl et al.[36b] The forces arising from interfacial tensions persist in the models, and it is accepted by many scientists that the capillary forces might contribute significantly to the deformation process, and complement the interfacial tension forces.

For the particles to deform, an important requirement is that the application temperature must exceed the minimum film-forming temperature [MFT] of the system.[38] The MFT commonly corresponds to the glass transition temperature of the latex at which the modulus of the polymer greatly decrease. Under this condition, the forces tending to drive the particle deformation can overcome those resisting the deformation of particles mainly related to the viscoelastic deformation and flow properties of the polymer.[31,33,37]

The particles are transformed into space-filling polyhedra after the compaction process. Bradford and coworkers[39] pointed out that after drying the particles are packed in such a way that a most efficient packing configuration is achieved. In many latex films, patterns of hexagons are observed by electron microscopy, representing a closest packing.[39,40] Studies by Joanicot et al [26] by both transmission electron microscopy (TEM) and small angle neutron scattering (SANS) reveal that their particles form face-centered cubic packing in dispersion which give rise to a rhombic dodecahedra structure in the film. This type of structure has been clearly seen in freeze-fracture TEM (FFTEM) images by Hearn et al [41] and Winnik et al.[42] Atomic force microscopic (AFM) measurements by Winnik et al.[43] in similar latex films also support this type of ordered structure. The ordered structure is easy to see when films are prepared from dispersions without surfactant or at low ionic strength.

Films with disordered structure are also obtained. The structures generated from randomly packed particles are predicted to be Wigner-Seitz cells: polyhedra with typically 14 to 17 faces and each individual face having high possibility of being 4 to 6 sided.[42,44] It was found that monodisperse latex with added surfactant to the dispersion gave film structures much more random.[42] Polydisperse latex dispersions are not able to order.

Bradford et al[39] was one of the first who examined film morphology in binary mixtures of particles consisting of latex spheres and pigment particles. They found that latex spheres form a continuous structure which is much less ordered, but the system is still organized in a way to achieve a dense packing: large pigment particles are surrounded by small latex spheres. Here the pigment particles are much larger in size and different in other properties than the latex. Some aggregation of pigment particles always occurs. There have been few corresponding experiments reported on the morphology of films produced from latex blends in which two types

of polymer particles are used. Recently, we examined latex blend films by FFTEM, scanning electron microscopy (SEM) and AFM.[29,45] These experiments are discussed in Chapter IV. They establish that in a system consisting of hard and soft latex particles, when the hard spheres are uniformly dispersed in a matrix generated from the soft particles under certain conditions, good optical clarity and mechanical properties can be obtained.

I-2-4 Polymer Diffusion

Voyutskii[21] was probably the first to emphasize that the forces acting on particle deformation are not sufficient to produce mechanically strong films, and that there must be polymer diffusion, in his term as "autohesion", which can lead to healing of the weak boundaries and development of mechanical properties. Studies by electron microscopy revealed that upon aging, the film microstructure of the original particles gradually fades, eventually leading to a smooth continuous polymer phase.[22,46,47] Vanderhoff termed this process as "further gradual coalescence", and found that during this stage, species such as surfactant were exuded to the surface.[22,46] It was also found that during this process the gas permeability of the films decreased.[48] All these results suggest that molecular rearrangement or polymer diffusion occurs which leads to the disappearance of the initial boundaries and the increase in integrity and coherence of the polymer films.

Recently direct measurements of the diffusion of polymers have become possible by using spectroscopic techniques. The two major techniques developed for characterizing polymer diffusion in latex films are small angle neutron scattering (SANS) and direct non-radiative energy transfer (DET).

Representative contributors to the diffusion measurements by SANS for latex films are Hahn et al[49] and Sperling et al.[50-52] Hahn et al[49] examined diffusion of deuterated poly(butyl methacrylate) [PBMA] latex polymer in an excess of unlabeled PBMA. Diffusion was analyzed in terms of the growth in radius of gyration (Rg) of the deuterated microspheres. By fitting the growth of R_g in time to the Fickian diffusion model, the diffusion coefficients (in cm^2/s) of the polymer at a given temperature can be obtained. Sperling and Klein[51-53] at Lehigh have carried out many such experiments on diffusion at high temperatures of deuterated polystyrene [PS-D] in PS-H latex films prepared by compression molding of the particles at a temperature just above the Tg of the polymer. One of their major contributions was to compare the extent of polymer interdiffusion with the growth of tensile strength in their samples: the mechanical strength of the films increases with diffusion and reaches a maximum value as the polymer molecules diffuse a distance scale of one radius of gyration across the interface.

The DET method for diffusion measurements in latex polymers was developed by the Winnik group in Toronto. One needs at first to synthesize pairs of latex (e.g. PBMA), one

sample labeled with phenanthrene [Phe, the donor D], and the other labeled with anthracene [An, the acceptor A].[53] Films were prepared from mixtures (e.g. 1 : 1) of the D- and A-labeled particles in dispersion and annealed at elevated temperatures. Samples were periodically removed from the oven to arrest diffusion, and fluorescence decay profiles [$I_D(t)$] of the D emission were measured. Energy transfer causes the D emission to be quenched, leading to faster fluorescence decays, lower quantum efficiencies of donor fluorescence Φ_F, and increased efficiencies of energy transfer Φ_{ET}. The essential feature of the experiment is that the increase in Φ_{ET} in the system monitors the mixing of donor-labeled and acceptor-labeled polymer. Diffusion coefficients can also be calculated from the efficiency of energy transfer obtained at a given diffusion time. Since this technique will be used in this thesis work, I will describe the measurements and data analysis in some more detail in a later chapter.

One of the most important issues is how the various substances present in the latex systems affect the diffusion rate of the polymers. It has been found that coalescing aids,[54] or nonionic surfactant,[55] present in coatings formulations, can greatly increase the polymer diffusion rate in the films. The readers will find in Chapter VI of this thesis that the presence of water in a hydrophilic latex can increase the polymer diffusion coefficient by almost an order of magnitude, and that oligomers can enhance significantly the diffusion rate of higher molar-mass polymer.

I-2-5 Current Research Directions

Efforts are currently given to many aspects of latex film formation and of latex applications in coatings. Some of the main research directions and trends of development are discussed briefly in the following.

I-2-5-1 Strategies for low and zero VOC coatings

One of the most striking activities in the field of coatings research and development today is the effort to reduce the level of organic components as much as possible owing to the concern for a safe and healthy environment. Although latex coatings are characterized by lower levels of volatile organic compounds (VOCs) compared to traditional solvent-based coatings, a significant amount of VOCs, up to 15 wt%, is still present to promote the coalescence of latex particles as the coatings dries. The goal, then, is to lower the content of VOCs, and eventually to eliminate them entirely, while maintaining or improving the performance of the coatings.[56]

There are several obvious strategies that one can imagine for producing latex films in the absence of volatile organics (zero VOC). One could use a reactive plasticizer that could polymerize or react to form crosslinks after film formation and at the same time raise the Tg of the system. Alternatively, one could develop a latex with the surface region containing lower

molar-mass polymers which can readily deform and flow and a core with higher molar-mass polymer. One of the most attractive strategies involves blends of a soft latex and a hard latex. The soft latex can deform without VOC to form a continuous structure, and the hard latex is incorporated into the films and is expected to contribute its mechanical properties to the coatings.

I-2-5-2 Strategies for improved performance

Latex coatings have displayed excellent performance in many applications. However, latex films generally have poorer mechanical properties (e.g. strength) than solvent-cast films. With the need for zero VOC coatings, this problem is becoming even more serious, since lowering the content of organic solvents is usually accompanied by reduced performance. To solve this problem, one needs to look for appropriate systems with certain compositions and structures that can provide optimized film properties.

An efficient way to improve coatings properties is to introducing crosslinks into the systems. The properties such as tensile strength, chemical resistance, and overall durability can be improved greatly by introducing crosslinks into the system.[57] Various strategies for the preparation of reactive polymers and for the reaction routes of crosslinking used for solvent-based systems are currently being tested in latex systems.[58] There is a major difference between latex systems and solvent-based systems in that one needs to control the location of crosslinking sites in the film.[57] For example, intraparticle crosslinking will have a deleterious effect on film properties. There is also a trend towards the replacement of hazardous crosslinkers (e.g. isocyanates) with less harmful ones for water-borne coatings.

Another way to improve film properties is to vary the composition and structure of the system. Preparing structured (composite) latex particles of desired morphology is one way to combine different properties from respective polymer components to achieve an optimized performance.[59] Similarly, hybrid systems including blending particles of different polymer Tg's but of the same class of polymers [e.g. poly(acrylates)], as described in this thesis, or mixing different types of polymer components (e.g. acrylic and urethane polymers),[60] seem like attractive strategies that are currently being examined.

Steady efforts have also been devoted to studies on fundamental aspects of latex film formation. The issues concern how latex dispersions dry, the features of microstructures in the films, the polymer diffusion process, and the properties of the films.

I-3 SCOPE OF THIS RESEARCH WORK

The main focus of this thesis research is on latex film formation. The goal is to investigate the mechanism of various aspects of film formation, including the drying process, film formation from latex blends, polymer interdiffusion, and curing of latex films.

To achieve our research goal, we need appropriate samples or materials. Chapter II describes our strategies for the synthesis of various types of latexes.

Chapter III describes our experiments on the drying kinetics of latex dispersions. We carried out these experiments by monitoring both the loss of water mass and the contraction of the area of the wet dispersion simultaneously. We also compared the drying behavior for dispersions of a soft film-forming latex, a hard latex, and their blends.

Chapter IV examines the structures and properties of films formed from latex blends. We employed the scanning electron microscopy (SEM) and atomic force microscopy (AFM) for surface characterization, and freeze-fracture transmission electron microscopy (FFTEM) for bulk structural determination for our blend films. One of the most important properties for latex films is their optical clarity. The film transparency was measured and related to film morphology. I also evaluated the film mechanical properties by dynamic mechanical analysis (DMA) and demonstrate important synergistic effects in blends.

Direct non-radiative energy transfer (DET) can reveal information about interpenetration distances between phases on the order of 2 nm. We labeled the two types of polymer particles in blends with a donor (phenanthrene) and an acceptor (anthracene), and employed the DET technique to characterize the interfaces between the two components in films. This part is presented in Chapter V.

Mechanically tough latex films require polymer molecules to diffuse across the particle interfaces. We employed the DET technique to monitor the diffusion process, using poly(butyl methacrylate)-based polymers as model samples. With time or upon annealing, the efficiency of DET increases, which can be used to characterize the extent of polymer diffusion and to calculate the diffusion coefficients. The major focus for this part of this thesis is to examine the effects of various components in the system on the polymer diffusion rate. The description of the principles and our results are presented in Chapter VI. The examination of different sample geometries and other technical aspects are presented in Appendix-VI.

In Chapter VII we examine strategies for ambient crosslinking of latex films. We choose two types of reactive functionalities, acetoacetoxy and unsaturated groups. The strategies for the preparation of reactive latexes are briefly described in Chapter II and the results about film crosslinking and its characterization are presented in Chapter VII.

As one can infer from the title of this thesis, one direction of the research is pointing to certain practical issues in applications of latex coatings driven by or related to *environmental* concern. The other direction is towards some fundamental issues to obtain better understanding about how one can design the structure and properties of the polymer material by varying the *molecular* structure and type, and how one can monitor the change in these polymer systems at a *molecular* level.

CHAPTER II SYNTHESIS AND CHARACTERIZATION OF LATEX PARTICLES

II-1 BRIEF DESCRIPTION

All the latex polymers used in my thesis research are either homopolymers or copolymers of methacrylates or acrylates. They were prepared by emulsion polymerization or copolymerization. The monomers include methyl methacrylate (MMA), n-butyl methacrylate (BMA), 2-ethylhexyl methacrylate (EHMA), methacrylic acid (MAA), n-butyl acrylate (BA), and others. Some important characteristics of their homopolymers are listed in Table II-1.

Table II-1. Characteristics of some poly(methacrylates) and poly(acrylates)

Polymer	Tg (°C)	n_D^{20} [f]	ρ [g] (g/cm³)	δ [h] (J/cm³)$^{1/2}$	$[M]_w^{sat}$ [i] (mol/dm³)	$[M]_p^{sat}$ [j] (mol/dm³)	$[H_2O]_p^{sat}$ [k] (wt%)
PMMA [a]	105	1.490	1.19	18.6	0.15	6.6	1.6
PBMA [b]	20	1.483	1.06	17.8	0.0025	3.8	1.2
PEHMA [c]	-10	-	-	-	-	-	1.3
PBA [d]	-55	1.474	1.08	18.0	0.0064	5.0	1.5
PMAA [e]	≈130	-	-	22.9	high	-	≈100
Ref.	1a	1a	1a	1a	1b	1b	1c

a. Poly(methyl methacrylate); b. Poly(n-butyl methacrylate); c. Poly(2-ethylhexyl methacrylate); d. Poly(n-butyl acrylate); e. Poly(methacrylic acid); f. Polymer refractive index at 20 °C; g. Polymer density at 25 °C; h. Polymer solubility parameter; i. Monomer concentration (saturated) in water at 50 °C; j. Monomer solubility in its polymer at 50 °C; k. Saturated water content in polymer at 22 °C (see ref. 1c).

Many of our latex polymers are labeled with fluorescent dyes. For this purpose I need at first to prepare dye comonomers via conventional organic reactions. These comonomers have a reactive site (i.e. a double bond) which can be reacted to form a copolymer with base monomers

during polymerization. By this we can incorporate a fluorescent dye into the polymer molecules. As mentioned earlier, the semi-continuous emulsion polymerization method under monomer-starved condition favors the production of copolymers of intermolecularly homogeneous composition, thus the labeled latex polymers were prepared by such a process. This point will be examined below.

Some latexes are prepared for forming films at ambient temperature, and thus these polymers must have a glass transition temperatures (Tg) below room temperature (e.g. 22 °C). Certain polymethacrylates (e.g. PEHMA) or polyacrylates (e.g. PBA) intrinsically have low Tg values and can be used directly for forming films. In normal practice, one would prefer to prepare copolymers consisting of a low Tg polymer component and a relatively higher Tg component. In this way one can control the Tg of the polymers simply by varying the composition of the components, as I will demonstrate in the following.

Some of our particles were prepared to have diameters of about 30 nm. One can anticipate many applications for these samples due to their very small size and high surface-to-volume ratio. We will display the usefulness of these latexes in our studies in the later chapters. In the following we propose a polymerization system which allows us to obtain such types of particles.

Latexes bearing functional groups in the particles or at the particle surfaces find their importance in many applications. We are concerned in preparing functional latexes in which the functionalities can be used to form crosslinks in the dry films through their chemical reactions under certain conditions. Among various reactive groups currently being actively investigated, we choose here two types of groups, unsaturated and acetoacetoxy groups, as the functionalities for our latex samples for crosslinking. The strategy for the preparation of these functional latexes is presented below. The detail of our film formation and film curing experiments will be presented in a later chapter.

II-2 EXPERIMENTAL

II-2-1 Materials

(1) Monomers: the monomers such as methyl methacrylate (MMA, Fluka, 99%), butyl methacrylate (BMA, Aldrich, 99%), butyl acrylate (BA, Aldrich, 99%), and methacrylic acid (MAA, Aldrich, 99%) were distilled, with addition of trace amount of hydroquinone, under reduced pressure under a N_2 (or Ar) atmosphere, and then stored in refrigerator before use. Similar procedure was used for the distillation of a reactive monomer, methacryloyl chloride (Aldrich, 90%), which was then immediately used for reaction. Other monomers such as 2-ethylhexyl methacrylate (EHMA, Aldrich, 98%), glycidyl methacrylate (GMA, Janssen, 96%) and 2-acetoacetoxy ethyl methacrylate (AAEMA, Lonza, 95%) were treated with an inhibitor-

remover resin (Aldrich) to remove the hydroquinone.

(2) Fluorescent monomers: the fluorescent monomers were synthesized in laboratory. The initial fluorescent compounds, (9-Phenanthryl) carboxaldehyde (PheCHO, Aldrich, 97%) and 9-Anthrylanol (AnOH, Aldrich, 98%), were used directly in our reactions for the synthesis of the dye comonomers.

(3) Water: deionized from Milli-Q Water System (Millipore) and then double distilled, referred to as D.D. water.

(4) Initiators: potassium persulfate ($K_2S_2O_8$, KPS, Aldrich, 99%), sodium persulfate ($Na_2S_2O_8$, NaPS, Fluka, 99%), sodium bisulfite ($NaHSO_3$, NaBS, Janssen, 98%) were used as supplied. Copper sulfate ($CuSO_4.5H_2O$, BDH, 99.9%) was used as an aqueous solution (1.0-1.5 x 10^{-3} M) with an equal molar concentration of ethylene diamine tetraacetic acid (EDTA, BDH, >99%) added to complex the copper ions.

(5) Surfactant: sodium dodecyl sulfate ($C_{12}H_{25}OSO_3^-Na^+$, SDS, Aldrich, 98%), nonyl phenol poly(ethylene oxide) ethanol (NP30, GAF), and aerosol-OT or bis(2-ethyl hexyl) sodium sulfosuccinate [AOT, Cyanamid], were used as supplied.

(6) Buffer: sodium bicarbonate ($NaHCO_3$, Caledon, 99%) was used as supplied. Aqueous ammonia solutions were prepared by dilution of the commercial reagent.

(7) Chain transfer agent: dodecyl mercaptan ($C_{12}H_{25}SH$, DM, Aldrich, 98%), used as supplied.

(8) Inhibitor: hydroquinone (E. MERCK), used as supplied.

(9) Other reagents: Triethyl amine (Et_3N, BDH, >99%) was dried over molecular sieves (4 Å) for 3 days, refluxed over CaH_2 for 3 hours, and then distilled. Tetrabutyl ammonium bromide (TBAB, Janssen, 99%), sodium borohydride ($NaBH_4$, BDH, >95%), and methyltriphenyl phosphonium iodide (Aldrich, 97%) were used as supplied.

II-2-2 Typical Reaction Recipe and Set-up

The reaction set-up for our emulsion polymerization is shown in Figure II-1. A three-neck round glass flask, equipped with a mechanical stirrer, a condenser and a nitrogen inlet, is used for the reaction. In a batch process, all the ingredients are mixed together before polymerization. In case of semi-continuous process, two metering pumps (Fluid Metering, Inc) are used to feed the monomer solution and the aqueous solution of initiator plus surfactant at a controlled rate into the reactor, in which a preformed seed has been charged. An oil bath, placed on a hot plate stirrer equipped with a temperature-control regulator, is used for heating the reactor.

Set-up for emulsion polymerization

Batch Reaction

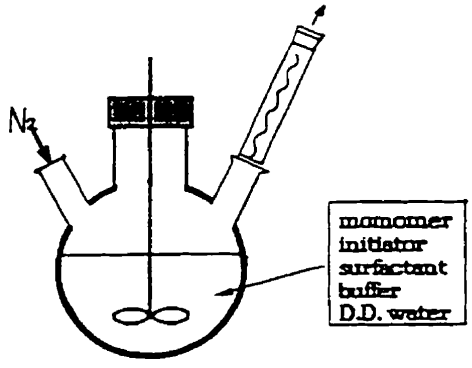

Semi-continuous Reaction

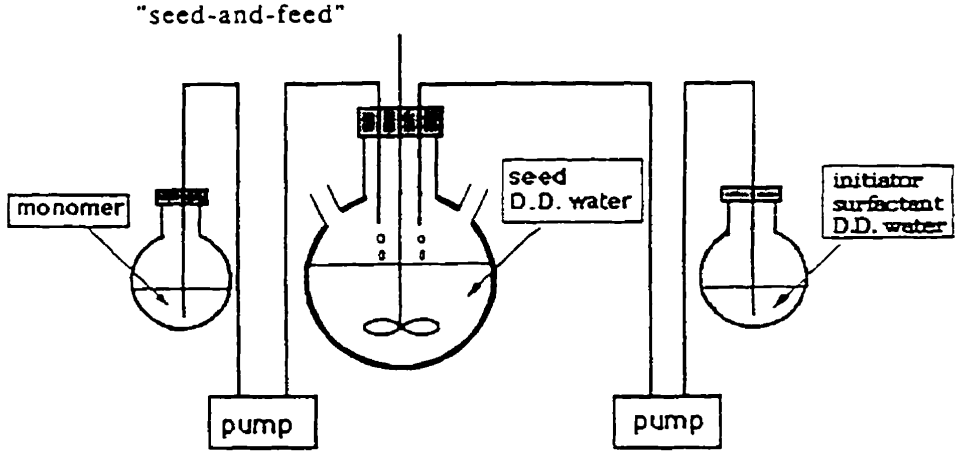

Figure II-1 Illustration for the reaction set-up of emulsion polymerization.

Various types of recipes were used in our polymerization. I shall give here two examples to illustrate our experiments of latex synthesis: one for the preparation of 110 nm PMMA latex by two-stage surfactant-containing emulsion polymerization, and the other for the preparation of large particles (400 nm) by surfactant-free batch polymerization. Other recipes for the preparation of latexes of specific characteristics will be presented in the respective sections below.

Most of the emulsion polymerizations described here are carried out at 70-80 °C by semi-continuous process, involving two stages of polymerization. The procedure described by Zhao and Wang[2] in this laboratory for similar polymerizations was used as a good guidance in my early experiments. The recipe for preparing 110 nm diameter PMMA particles is shown in Table II-2. A small amount (ca. 10% of the total) of monomer (e.g. MMA) is used in the first stage

polymerization via batch process to produce a latex seed (typically d ≈ 50 nm). In this stage, all the ingredients are mixed before heating except that the initiator is added when the reaction mixture has reached the desired temperature. The polymerization process in this stage usually takes 1 h. In the second stage, the rest of the monomer and an aqueous solution of the rest of initiator and surfactant were both fed into the reactor continuously at a slow rate (typically 0.05 - 0.1 ml/min), resulting in monomer-starvation (see Section II-3). This rate needs to be increased when the recipe is scaled up to produce larger quantity of latex, so that the total feeding time and the monomer addition rate per unit volume of the dispersion are identical.

Table II-2. Recipe for Preparing 110 nm PMMA Latex via Surfactant-containing Semi-continuous Process

First stage		**Second stage**	
MMA (ml)	3.5	MMA (ml) [a]	28
Water (ml)	45	Water (ml)	25
KPS (g)	0.04-0.05	KPS (g)	0.04
SDS (g)	0.10	SDS (g)	0.6
$NaHCO_3$ (g)	0.04		
Temp (°C)	80	Temp (°C)	80
Time (h)	1	Time (h)	20

a. When a fluorescent labeled latex is needed, a small amount (typically 1 mol%) of a dye comonomer is added in the monomer feed but other conditions are similar.

When similar particle sizes are needed for different types of polymers (e.g. PBMA), the recipe and reaction conditions can be essentially similar. For preparing samples of other sizes, in many cases one needs only to vary the concentrations of surfactant and monomer in the reaction recipe, especially for the seed stage. The procedure and other conditions are similar.

When larger particle sizes (e.g. > 300 nm) are needed, a surfactant-free polymerization is often carried out. An example of a recipe for the preparation of 400 nm PMMA via a surfactant-free batch process with persulfate initiator (KPS) is described in Table II-3.

Table II-3. Recipe for Preparing 400 nm PMMA Latex via Surfactant-free Batch Process

MMA (ml)	Water (ml)	KPS (g)	$NaHCO_3$ (g)	Temp (°C)	Time (h)
20	200	0.10	0.05	80	17

It is often found that the PMMA latex prepared in surfactant-free system is not as stable as in surfactant-containing system. Sometimes coagulation occurs during polymerization. For preparing PBMA latex via surfactant-free polymerization, however, higher stability is observed and monodisperse particles are easily obtained. The reason would be that MMA is more water-soluble with a higher tendency to undergo second nucleation (homogeneous and coagulative), and the resultant larger surface area thus has higher demand for stabilization of the system.

II-2-3 Latex Purification

II-2-3-1 Purification by ion-exchange

In some cases, latex dispersions were cleaned by the ion-exchange method to remove surfactant and other ionic substances. Before use, the mixed-bed ion exchange resin (Bio-Rad, AG-501-X8) was washed with hot deionized water (80 °C), deionized water, methanol and then deionized water. The washed resin was then added to a latex dispersion (solid content < 15 wt%), using 3-5 g resin for every 100 ml dispersion. The mixture was magnetically stirred at room temperature for 40-60 min. The resin was separated from the dispersion by filtering with glass wool or white paper. This process was repeated at least three times with each sample. Most of our dispersions remained stable upon cleaning.

II-2-3-2 Purification by serum replacement

Some latex samples were purified by serum replacement with a membrane filtration system (Millipore). The diluted dispersions were continuously pumped across a set of membranes which have certain sized pores (e.g. 10 nm) that allow the small molecule species (e.g. surfactant, initiator) to diffuse through but resist the transport of large polymer particles. By continuously transferring the impurities from the sample to the serum and repeatedly replacing the impure serum with pure water, the dispersions of particles are gradually purified.

II-2-3-3 Purification by centrifugation

Some latex dispersions were centrifuged to separate the polymer particles from the water

phase in which most of the impurities are dissolved. The polymer particles were then redispersed in pure water by stirring or ultrasonication and the formed dispersions were centrifuged again to remove more impurities from the polymer. This process needs to be repeated 3 times or more.

II-2-4 Techniques and Instrumentation in Latex Characterization

II-2-4-1 Particle sizer

Measurement of the particle size and particle size distribution of the latex samples were performed on a particle sizer (Brookhaven-BI-90). The technique employed by this instrument is photon correlation spectroscopy of quasi-elastically scattered light (QELS), also referred to as dynamic light scattering (DLS).

II-2-4-2 Scanning electron microscopy (SEM)

Some of our particles were examined by a scanning electron microscope (Hatachi S-570). The dried layer of particles on a metal sample holder was coated with a layer of gold and then examined by the microscope. This measurement provides images of the particles and reliable information about size distribution, allowing us to make good comparison of the results with those evaluated by DLS.

II-2-4-3 Gel permeation chromatography (GPC)

A small portion of a latex polymer was air-dried from dispersion and subsequently dissolved in THF to give a solution of ~0.5 wt% polymer concentration. Our GPC measurements employed a series of two Ultrastyragel columns (500 Å + 10^4 Å, or 10^4 Å + 10^5 Å for very high molecular weights), with THF as the eluent, and a flow rate of 0.8 ml/min. The detection system included a refractive index (RI) detector, WATERS Series R-400 Differential Refractometer, yielding the major signal for each chromatogram. For dye-labeled polymers, their fluorescence signal was also detected by a KRATOS FS 970 Spectrofluoro Monitor. The excitation wavelength (λ_{ex}) and emission wavelength cut-off ($\lambda_{em\text{-}cut}$) were selected based on the type of dyes: λ_{ex} = 296 nm, $\lambda_{em\text{-}cut} \approx$ 420 nm for Phenanthrene (Phe); and λ_{ex} = 350 nm, $\lambda_{em\text{-}cut} \approx$ 450 nm for Anthracene (An).

II-2-4-3 UV-visible spectrophotometer

UV absorption measurements were carried out with a Hewlett Packard 8452A Diode Array UV-visible spectrophotometer. This was used for determining the dye content of our labeled polymers. Prior to this, calibration experiments for the dye absorption were carried out using pure compounds, from which I obtained the extinction coefficients for the dyes at their maximum-absorption wavelengths: 1.150 x 10^5 $mol^{-1}cm^{-1}L$ for Phe at 298 nm and 8.10 x 10^4 $mol^{-1}cm^{-1}L$ for An at 364 nm in THF. The dye concentration in a given amount of polymer

samples can thus be determined.

II-2-4-4 Nuclear magnetic resonance (NMR) spectroscopy

NMR characterizations for latex polymers or dye compounds were performed on a 200-MHz NMR spectrometer (Varian). Most measurements were carried out for ^1H nuclei in the samples dissolved in $CDCl_3$.

II-2-4-5 Infrared (IR) spectroscopy

IR measurements were carried out either on a Fourier Transform infrared (FTIR) analyzer (Nicolet 8210E) or an infrared spectrophotometer (Perkin-Elmer 882). In most cases, the organic or polymeric powdery samples were mixed with potassium bromide (KBr) to prepare transparent disks under high pressure and examined. In some cases, a thin film was cast either from a dilute latex dispersion or from a polymer solution on a substrate suitable for IR measurements. The substrate can be NaCl crystal plate for solvent-cast film, or CaF_2 (or TiO_2) for film cast from an aqueous latex.

II-2-4-6 Differential scanning calorimetry (DSC)

The thermal transition (i.e. Tg) of a polymer sample was measured by differential scanning calorimetry (DSC, Perkin-Elmer DSC-7). Measurements were made for samples of ≈ 20 mg under N_2 atmosphere and with a heating rate of 10 °C/min.

II-2-4-7 Gravimetrical measurements

The solid content (S% by weight) of a latex was determined gravimetrically: by measuring the weight of a small portion of latex dispersion (W_L) and the weight of solid after drying (W_S) as

$$S\% = W_S / W_L \qquad (II\text{-}1)$$

The weight fraction of monomer polymerized, F_P, a measure of conversion, can be calculated from the S% after polymerization, the weight of monomer (W_M^o) added before polymerization in the dispersion of total weight W_T. One needs to subtract the weight of added non-volatile substances (e.g. surfactant, initiator, etc) (W_{NV}^o) from the total amount of solids (W_T x S%) to obtain the net weight of polymer generated (W_P), although W_{NV}^o is often small. Thus

$$F_P\% = W_P / W_M^o = (W_T \times S\% - W_{NV}^o) / W_M^o \times 100\% \qquad (II\text{-}2)$$

II-2-4-8 Acid-base titration

Acid-base titration was used to determine the surface charge (acid) concentration of particles and the fraction of acid in the serum. A pH meter was used to monitor the change in pH during titration. Sometimes a conductometer was used in conjunction with the pH meter to measure the change in conductivity during the process. The latex dispersion, cleaned by the ion-exchange technique, was titrated directly with dilute NaOH solution (e.g. 0.01 N) under a N_2 atmosphere to obtain the surface acid concentration. To determine the amount of acid in the water phase, a clear liquid was separated from the particles by centrifuging, and was directly titrated.

One can also determine the surface acid concentration by performing a back-titration, by neutralizing the latex dispersion with excess base (NaOH) first and then titrating backward with an acid (e.g. HCl) solution. By this the amount of acids at the surface plus that in the subsurface layers of the particles are obtained.[3]

II-3 IMPORTANT FEATURES OF TWO-STAGE EMULSION POLYMERIZATION

An example of typical recipes, as well as the polymerization conditions, for the preparation of poly(methyl methacrylate) (PMMA) latex via two-stage semi-continuous process is shown in Table II-1 in the previous section. A latex seed was first prepared using a small amount of MMA. The time for seed-stage polymerization was 60 min (1 h). Then the rest of MMA as well as the rest of surfactant and initiator in water were both continuously fed into the reactor. After the monomer and initiator were completely added, the polymerization was kept at 80 °C overnight. This total time (ca. 20 hrs) for polymerization was chosen mainly based on the convenience of experiment rather than a requirement for the reaction.

In the following I describe some important features observed in my own experiments for seeded semi-continuous polymerizations under monomer-starved conditions. MMA monomer is used as an example but the features presented below are similar for other monomer systems.

II-3-1 Conversion of Polymerization

The conversion of MMA to polymer during polymerization was determined gravimetrically. About 0.3 ml of the reaction mixture was pipetted out after various times. The reaction was quenched by addition of a small amount of hydroquinone and bubbling with air (oxygen is one of the most effective inhibitors for methacrylate free radical polymerization).[1,4] The yield of polymer solids was then obtained by drying each aliquot of dispersion.

The increase of conversion, or polymer fraction F_p (see Eq. II-2), with polymerization time is shown in Figure II-2. A very fast polymerization can be seen for this system. In the seed stage, at very early time (t = 5 min), the conversion has already reached ~70%. Here the starting point (t = 0) of polymerization is chosen where the liquid mixture becomes visibly cloudy, usually ≈ 5 min after the addition of initiator to the pre-heated mixture. At the end of the seed stage (1 h), a high conversion is usually achieved (93-95% or sometimes higher). The solid line in Figure II-2 separates the seed stage from the second stage polymerization. In the second stage, when the monomer feeding rate is 0.06 ml/min (0.56 mmol/min), the measured polymer fraction (F_p) rapidly reaches up to 100% and this value is kept throughout the following processes (Figure

II-2). This is a typical feature of semi-continuous reaction under monomer-starved conditions.

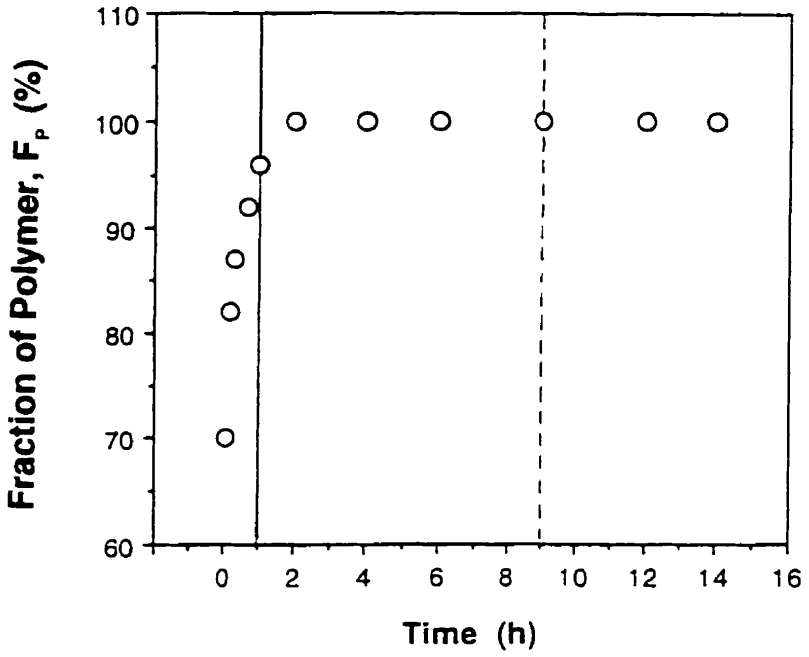

Figure II-2. Conversion or F_p during MMA polymerization in a two-stage semi-continuous process with a recipe from Table II-2. In the first stage (0 - 1 h) a small amount of seed is formed, and in the second stage monomer was fed into the reaction system (total feeding time 8 h) and polymerized. The solid line separates the first and second stage reaction, and the dashed line indicates the completion of monomer addition.

II-3-2 Particle Size and Size Growth

The particle size and size distribution of the latex samples were determined by dynamic light scattering (DLS) technique. An example of the analysis of DLS for PMMA particles prepared by recipe in Table II-2 is shown in Figure II-3. We see that a mean diameter of 109 nm was obtained, with a narrow size distribution indicated by a single line on the graph. Particles prepared by recipe in Table II-3 give similar type of results except that the mean diameter becomes larger (440 nm). SEM images were also taken for these samples as shown in Figure II-4a and Figure II-4b. Mean diameters of 110 nm and 400 nm, respectively, are obtained for the particles shown in these images. Narrow size distributions are apparent for both latex samples. It seems that in our experiments large particles (e.g. > 300 nm) more likely give higher quality of the image and apparently better monodispersity of the size.

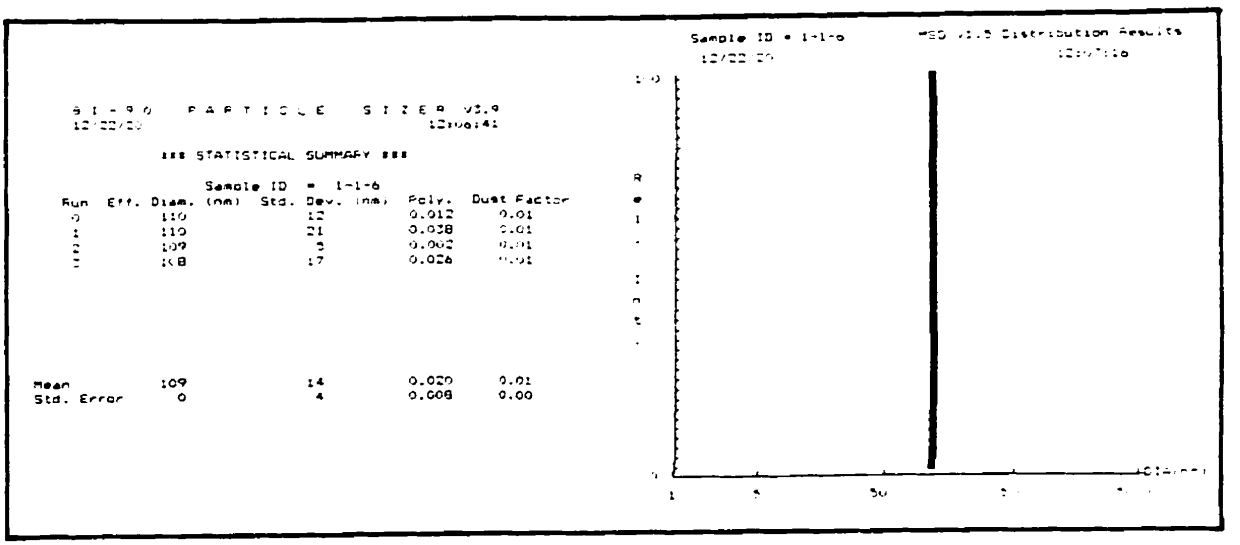

Figure II-3. An example of DLS analysis for a PMMA latex prepared with recipe in Table II-2, yielding a mean particle diameter of 109 nm.

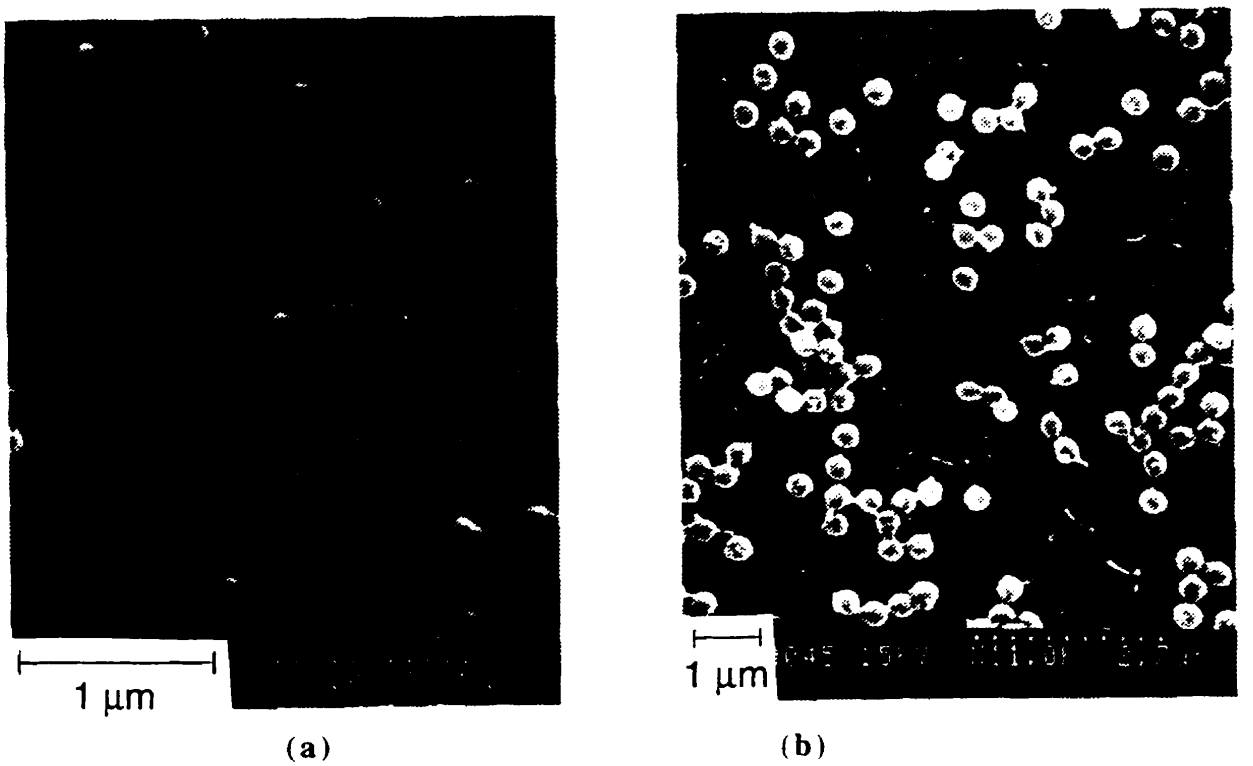

Figure II-4. SEM images of PMMA latex particles prepared by (a) recipe in Table II-2, and (b) recipe in Table II-3. Calculation of the particle sizes in these images yields a mean diameters of 110, and 400 nm, respectively.

We are also interested in how the particles grow in size in the two-stage polymerization in which a seed is formed followed by continuous, slow addition of monomer into the reaction system. The growth of particle size during polymerization using recipe in Table II-2 is shown in Figure II-5. In the first stage, seed particles form with almost a constant particle diameter (55 nm) from the beginning ($t < 10$ min) to the end ($t = 60$ min) of this stage. When additional monomer is fed into the system in the second-stage, the particles gradually grow monotonically from $d \approx 55$ nm to 110 nm. After the completion of monomer addition, the particle size (110 nm) no longer changes with time.

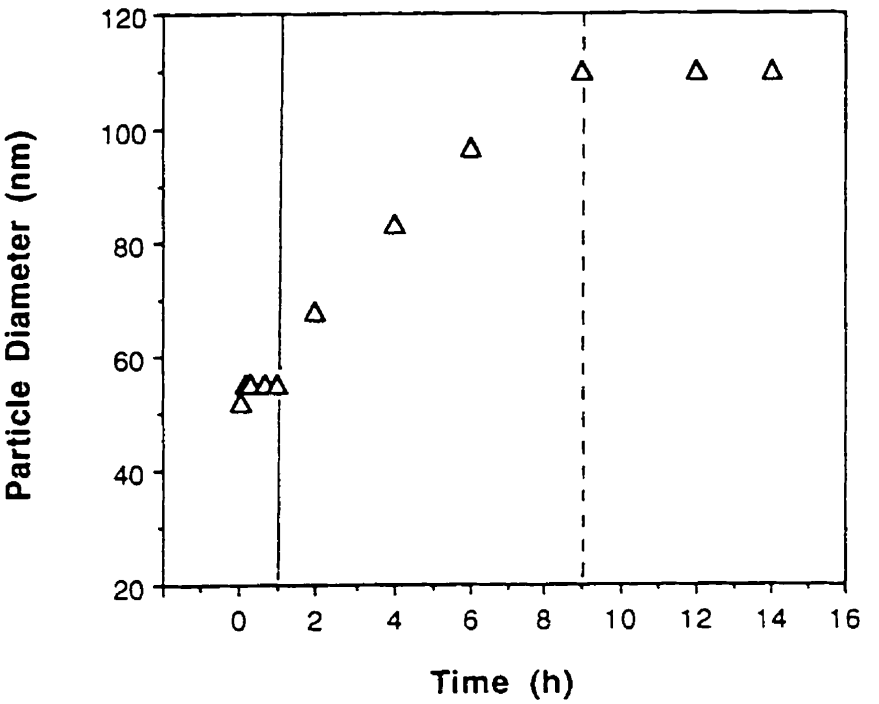

Figure II-5. Growth of particle sizes during two-stage MMA polymerization using recipe in Table II-2. The solid line separates the first and second stage reaction, and the dashed line indicates the completion of monomer addition.

The critical micellar concentration (CMC) values (in g/l) for the surfactant, SDS, at different temperatures are: 1.82 (20 °C), 2.3 (60 °C) and 2.7 (75 °C).[4] The surfactant concentration we usually use for seed stage is ca. 2.3 g/l. This may allow the formation of

micelles at low temperatures. When the temperature is elevated to 70-80 °C, polymerization occurs and polymer particles form from these micelles as nucleation sites. The concentration of emulsifier becomes much lower than the CMC at high temperature, especially at the end of seed stage where the formed particles require more emulsifier to cover them. During the second stage, the rest of emulsifier in water is fed very slowly so that the emulsifier concentration is always kept far below CMC, and a second nucleation of particles is avoided. Therefore the number of particles is constant, and the particle size should solely depend on the amount of monomer added. Figure II-6 shows a plot of the relative volume of particles, expressed by $(D/D_o)^3$, Vs. the total mass of monomer added. One sees that the particle volume is proportional to the amount of monomer added. This further confirms an important feature of monomer-starved semi-continuous process, that no second-nucleation of particles occurs.

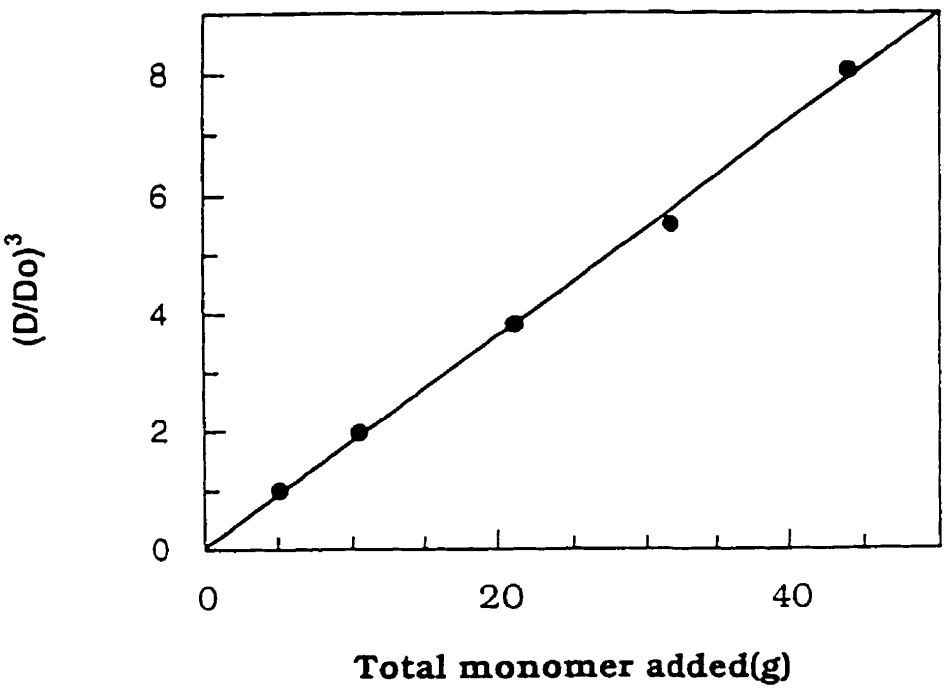

Figure II-6. Plot of $(D/D_o)^3$ Vs. the total mass of monomer (in g) added during the semi-continuous emulsion polymerization. Here D is the mean diameter of second-stage particles, and D_o is that for the seed particles.

II-3-3 Variation of Molecular Weight

Molecular weights were determined by GPC in THF on latex polymer samples dissolved in THF, using monodisperse PMMA standards to calibrate the columns.

One of the interesting results in semi-continuous monomer-starved reaction is that the average molecular weight of polymer produced in the second-stage is lower than that of the seed polymer. The reason is that the addition rate of monomer is slower than the polymerization rate, causing the termination of propagating chains at short lengths. This also implies that the average molecular weight of the two-stage latex polymer may be influenced by the monomer feeding rate. This is true in our experiments when different pump speeds are used to feed the monomer. Table II-4 shows the change of the molecular weights for latex polymers prepared under similar recipes but with different monomer feeding rates.

Table II-4 Results of molecular weights for PMMA latex samples prepared by two-stage emulsion polymerization with different monomer feeding rates in the second stage

Monomer feed rate (mmol/min)	0.53	0.64	0.79	6.72	∞ (seed)
Mw ($x10^3$)	110	140	210	830	990
Mn ($x10^3$)	50	58	67	280	430
Mw/Mn	2.3	2.4	3.2	3.0	2.3

This influence of feeding rate on molecular weights provides an additional way to adjust the molecular weight of latex polymers. Usually the molecular weights are adjusted by the variation of initiator concentration or introducing a chain transfer agent. Both of these approaches have their limitations. From Table II-4, we see that as the monomer feeding rate increases in a small range from 0.53 to 0.79 mmol/min, the average molecular weights considerably increase. When the feeding rate is 10 times faster than the normal rates (e.g. 0.6 mmol/min) we used, the molecular weight is much higher and becoming close to that of the seed polymer produced by the batch process.

In summary, it is found that in our two-stage emulsion polymerizations, a slow monomer feeding rate in the second stage results in the monomer-starved condition: a high polymer fraction F_P is maintained and no new particles form during polymerization. During the monomer feeding stage, the particle volume grows proportionally to the amount of monomer added. The molecular weights of latex polymers can also be adjusted by the variation of the monomer feeding rate.

II-4 SYNTHESIS AND CHARACTERIZATION OF FLUORESCENT-LABELED LATEXES

To prepare polymers covalently labeled with fluorescent chromophores, we need at first to synthesize reactive chromophores which can be incorporated into polymers. One of the most effective ways is to attach a double bond into a dye molecule and the dye monomer is then introduced into polymer chains by copolymerization with the base monomers. The synthesis of dye comonomers is described first below.

II-4-1 Synthesis of Fluorescent Comonomers

The dye comonomers examined in this research are (9-phenanthryl) methyl methacrylate (PheMMA), 9-vinyl phenanthrene (V-Phe), and (9-anthryl) methacrylate (AnMA). Their chemical structures are represented in Figure II-7.

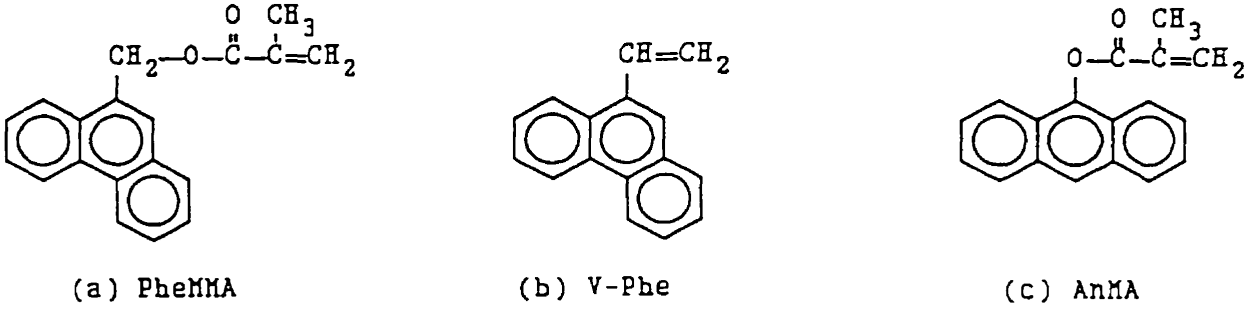

Figure II-7. A representation of chemical structures of the dye comonomers.

II-4-1-1 Vinyl phenanthrene comonomer

9-vinyl phenanthrene (V-Phe) was synthesized by a Wittig reaction in the following procedure: 6 g (0.029 mol) of (9-Phenanthryl) carboxaldehyde (PheCHO) was dissolved in 90 ml benzene, followed by the addition of 22.6 g (0.056 mol) of solid methyltriphenyl phosphonium iodide into the solution. A white suspension was formed. Then 300 ml aqueous solution of NaOH (5N) was added to the reactor. The mixture was kept stirring at room

temperature for 72 hours. TLC (silica gel, CH_2Cl_2) showed the appearance of one major spot at $R_f = 0.89$ and another spot at $R_f = 0$, and the disappearance of $R_f = 0.76$ for PheCHO.

Prior to the above experiment, a reaction on a small scale using CH_2Cl_2 instead of benzene as the medium was carried out, and it was found that the reaction in CH_2Cl_2 was not completed after 3 days. References for Wittig reactions are also available.[5,6]

After the reaction, the organic substances in the mixture were extracted with toluene (2 x 100 ml), neutralized to pH 7 with dilute HCl solution, washed with water, and then dried over anhydrous Na_2SO_4 to give a clear yellow solution. After evaporation of toluene, a viscous oil remained. When benzene/hexane (1:1) was added, a white powder was formed and separated, which was identified as a by-product, triphenylphosphine oxide ($R_f = 0$ on TLC), produced from the Wittig reaction. The remaining crude products did not give solids when adding solvents such as hexane, pentane or alcohols. Column chromatography (silica gel, CH_2Cl_2 as eluent) was used to separate the substances and the fraction at $R_f = 0.89$ was collected. After solvent evaporation on a rotation-evaporator followed by vacuum drying the final product was obtained, which turned wax-like solid when stored in refrigerator. Yield: 5.1 g, 85%; M.P.: 38.5 - 39.5 °C; TLC (silica gel, CH_2Cl_2): $R_f = 0.89$. ^{1}H-NMR: 5.55 ppm (1H doublet -CH=C$\underline{H}_a$), 5.90 ppm (1H doublet -CH=C$\underline{H}_b$), 7.45 ppm (1H quadrate for -C$\underline{H}$=CH$_2$), and 7.60-8.80 ppm (9H multiplet for aromatic protons).

II-4-1-2 Phenanthryl methyl methacrylate comonomer

(9-phenanthryl) methyl methacrylate (PheMMA) was synthesized by reacting (9-phenanthryl) methanol with methacryloyl chloride in dry THF and in the presence of dry triethylamine (Et_3N). The phenanthryl methanol was first prepared from reduction of (9-phenanthryl) carboxaldehyde with $NaBH_4$ in iso-propanol. The procedure is similar to that reported previously.[7]

II-4-1-3 Anthryl methacrylate comonomer

(9-anthryl) methacrylate (AnMA) was synthesized by a reaction between 9-Anthrylanol and methacryloyl chloride in dry THF in the presence of dry Et_3N. The reaction procedure and product purification were very similar to those reported previously.[2,7]

II-4-2 Preparation of Labeled Latex Polymers

Latex polymers labeled with fluorescent dyes were prepared simply by copolymerizing a base monomer with a small amount of a dye comonomer via a two-stage emulsion polymerization. The latex seed was formed first by using a small amount of base monomer. Subsequently, the rest of initiator in water and the fluorescent monomer (FLM) dissolved in the base monomer (molar ratio 1 : 100) were both fed continuously at a slow speed into the reactor.

Both the base monomer and FLM reach high conversion (> 97%), with the result that the labeling content is almost the same as the ratio of monomers added, typically 1 mol%. The conversion of base monomer was determined gravimetrically, and that of FLM was determined by measuring the dye content by UV absorption. Before UV measurement the labeled latex polymer was dried and purified by extraction for 2 days with water and then 2 days with methanol with a Soxhlet extractor. As we will mention later, the fraction of FLM attached to polymers can also be obtained from GPC analysis equipped with both fluorescent and refractive index detectors. This can be obtained by comparing the integrated peak area of fluorescence signal for the high polymer portion to that for unreacted dye molecules in longer retention times.

In the case of labeled PMMA particles of 110 nm, the recipes are very similar to that shown in Table II-2 except that in the second stage 1 mol% dye comonomer is included in the monomer feed. Since the second-stage polymer represents ca. 90% of the total polymer, the final particles are nearly fully labeled.

Many of my experiments involve poly(butyl methacrylate) (PBMA) latex, labeled with either phenanthrene (Phe) or anthracene (An). In Table II-5 a typical recipe for the preparation of labeled PBMA latexes is presented. The procedure is described as follows: A small amount of PBMA latex seed (diameter ≈ 55 nm) was prepared in the first stage. Potassium persulfate (KPS), sodium dodecyl sulfate (SDS), and sodium bicarbonate ($NaHCO_3$) were used as the initiator, surfactant, and PH buffer, respectively. In some cases, a certain amount (e.g. 2 wt% based upon the monomer weight) of a chain transfer agent (i.e. dodecyl mercaptan, DM) was used to adjust the molecular weights for the latex polymers. In the second stage of polymerization, a monomer solution composed of 1 mol% of a fluorescent comonomer (PheMMA, or V-Phe, or AnMA), certain amount of DM, and the rest of BMA were continuously fed into the seed latex dispersion. The monomer feeding rate was slow (< 0.1 ml/min). KPS and SDS dissolved in water were added into the reactor concurrently. To prepare a more hydrophilic latex, 5 wt% (based upon BMA) methacrylic acid (MAA) was premixed in the monomer solution and the monomers were then polymerized in the second stage under identical conditions to those shown in Table II-5, to give a copolymer of 5 wt% MAA / 95 wt% BMA [P(MAA-co-BMA)]. A high conversion of the monomers (> 98.5%) was obtained for all reactions, as evaluated gravimetrically. The particle size is ca. 125 nm (with a narrow size distribution) when prepared by this recipe.

Table II-5. Recipe for the preparation of labeled PBMA latex

First stage		Second stage	
BMA (ml)	3.5	BMA (ml) [a]	32
DM (ml)	0 - 0.074	DM (ml)	0 - 0.68
Water (ml)	60	V-Phe[b] (g)	0.48
KPS (g)	0.062	Water (ml)	26
SDS (g)	0.11	KPS (g)	0.060
$NaHCO_3$ (g)	0.060	SDS (g)	0.60
Temp (°C)	80	Temp (°C)	80
Time (h)	1	Time (h)	20-24

a: For preparing the P(MAA-co-BMA) copolymer, a mixture of 32 ml (28.6 g) BMA + 1.5 g MAA was used to replace pure BMA; b: When using PheMMA dye comonomer, this quantity becomes 0.65 g; For preparing the An-labeled latex, 0.62 g AnMA was used to replace 0.48 g V-Phe.

II-4-3 Dye Distribution Analysis for Labeled Polymers

In the labeling experiments, it is often desired that the chromophores are randomly distributed. This consideration allows one to presume that the physical behavior of the labeled polymer reflects the overall reality of the polymer. In this case, two assumptions are usually made: (1) the dyes are randomly distributed along each chain; and (2) the dye population is proportional to the chain length. It is important to characterize not only the overall labeling content but also the distribution of labels in the polymer.

In this section, a simple, qualitative method is used to examine the dye distribution, based on the GPC analysis for the samples produced under different polymerization conditions and with different dyes. The method involves analyzing the uniformity of dye distribution by examining the ratio of intensity between a signal (e.g. fluorescence or UV) related to the dye concentration and that reflecting the overall monomer units (e.g. refractive index) in the chromatogram. This analysis was suggested by Dr. Sosnowskii in this lab, as seen in our publication.[8] A similar idea has also been used by others previously for analyzing other polymers.[9]

II-4-3-1 Illustration of the GPC graphs and their analysis

Figure II-8a shows a sample chromatogram. The solid curve represents the refractive index (RI) signal; and the dotted curve, the fluorescence (FL) signal. Our procedure of analysis is as

follows: First, both the FL and RI curves are normalized to their maximum signals, by subtracting their baselines and dividing by their peak intensity values. The normalized chromatogram is shown in Figure II-8b. Under circumstances which result in a uniform labeling of polymer molecules, one would expect that the two normalized curves should overlap completely. Note that in the sample given here the overlap is not perfect. In our system, the FL detector was placed in front of the RI detector. This results in a small time shift (3 sec) between two curves, and this difference could be neglected in our calculation. We are particularly interested in how the intensity ratio between FL and RI signals varies for polymer molecules having different chain lengths. Since in gel permeation chromatography of linear polymers, each retention time corresponds to a certain molecular weight, we used a computer software (Sigma Plot Version 4.1, Jandel Scientific, USA) to calculate the ratio of FL to RI intensity (FL/RI) or its inverse (RI/FL) for the normalized chromatograms at each time along the elution profile. We found it convenient to plot both the FL/RI and RI/FL ratios versus retention time, as shown in Figure II-8c.

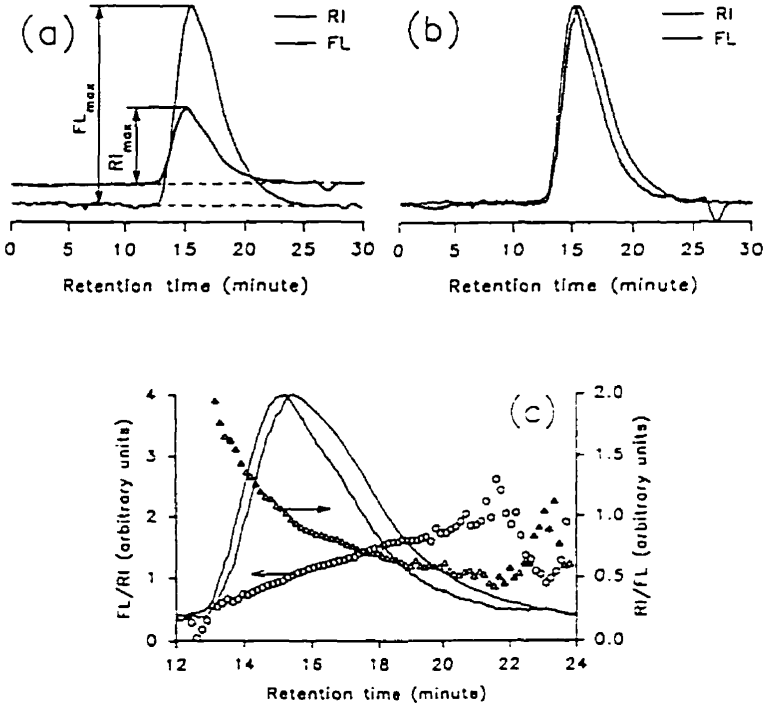

Figure II-8. A sample of GPC chromatogram and analysis: (a) a plot of GPC curves using RI and FL detectors; (b) the RI and FL signals after normalizing by their maximum intensities; (c) a typical plot showing the two normalized signals (RI and FL), the FL/RI ratio (circle), and the RI/FL ratio (triangle) versus retention time.

At low concentrations in the GPC effluent, the fluorescence intensity is proportional to the chromophore concentration. This presumes that the quantum yield for the chromophores is independent of the molar mass of the polymers to which they are attached. The intensity of RI signal is proportional to the concentration of monomer units passing through the detector. Therefore, at each time point of the chromatogram, the signals that are monitored can be expressed as:

$$FL \propto [Dye] = N_{Dye} \cdot [Polymer] \qquad (II\text{-}3)$$

$$RI \propto DP \cdot [Polymer] \qquad (II\text{-}4)$$

where [Dye] is the dye concentration in solution in mole·L^{-1}, [Polymer] is the polymer concentration in solution in mole·L^{-1}, and N_{Dye} is the number of dye units per polymer chain. Since the dye content of the polymer is very low, the degree of polymerization (DP) can be replaced by the number of MMA units (N_{MMA}) per polymer chain, giving:

$$FL/RI \propto N_{Dye} / N_{MMA} \qquad (II\text{-}5)$$

Thus, the FL/RI ratio in the GPC analysis measures the dye label content for polymers of each molar-mass. When the polymer labeling is homogeneous, N_{Dye}/N_{MMA} should be constant, and the FL/RI ratio should be independent of molecular weight (or N_{MMA}).

II-4-3-2 Batch and semi-continuous polymerizations

We employed the seeded semi-continuous polymerization to prepare our labeled polymers. One interesting advantage for us is that the unlabeled seed often has a higher molecular weight than the polymer formed in the second stage. An example of such a system is shown in Figure II-9. This polymer (PMMA) was prepared by the recipe similar to that shown in Table II-2 but with vinyl phenanthrene as the fluorescent comonomer in the second stage. A very slow monomer feed rate (0.37 mmol/min) was used in the process. Since the seed polymer doesn't fluoresce, it exhibits only an RI signal (curve 1). In the second stage, both the FLM and MMA were incorporated with a high conversion after the complete addition of the monomers. The RI and FL signals for this polymer are plotted in the Figure. The FL curve (curve 3) shows a polymer peak and a negligible signal for low molar mass species (unreacted fluorescent monomer) with a retention time between 22 to 23 minutes, indicating that almost all the FLM has been incorporated into the host polymer chains. The RI trace (curve 2) shows a major peak at ca. 14.5 min and a smaller peak at ca. 11.5 min. The latter signal has the same retention time as the unlabeled seed polymer. It corresponds to a small amount of PMMA produced in the first stage of the polymerization. The fraction of this seed polymer is kept small in all our experiments and sometimes this bimodal molar mass distribution is not apparent.

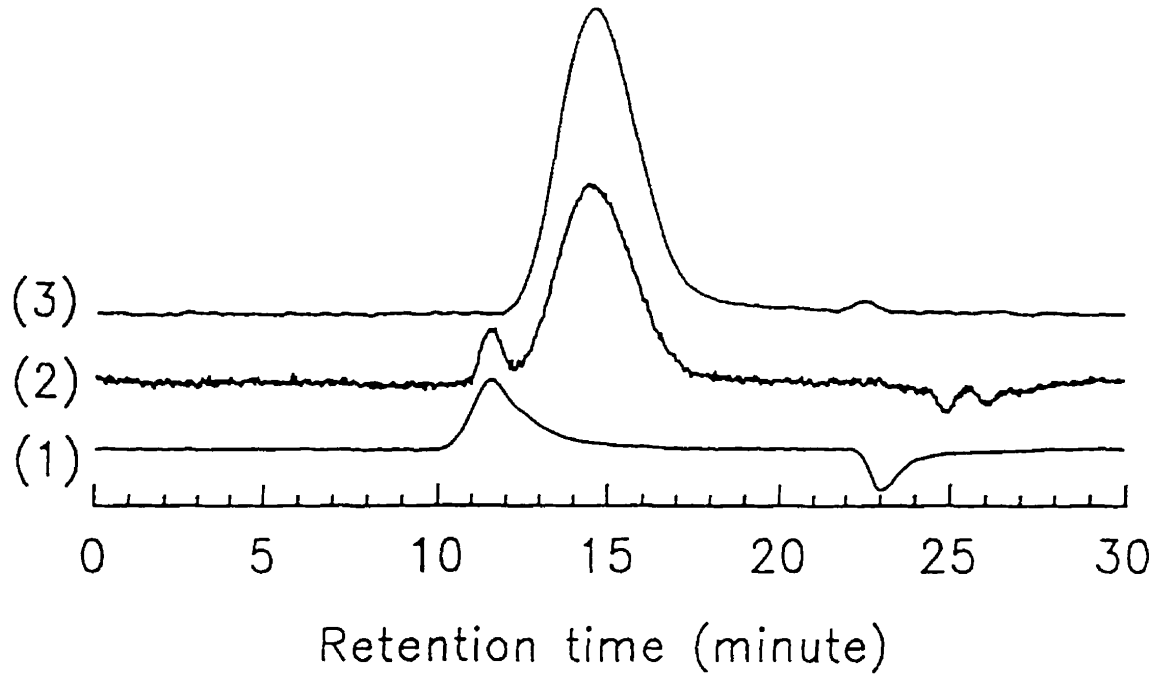

Figure II-9. An example of GPC curves for the seed and two stage PMMA. The polymer was prepared by the recipe as in Table II-2 with V-Phe as the fluorescent comonomer and a slow monomer feeding rate (0.37 mmol/min) in the second stage. Curve (1): the RI signal for seed polymer; curve (2) and (3): the RI and FL signal for the two-stage polymer.

In Figure II-10 we compare the results of a batch polymerization in which all the ingredients were combined at the start of the reaction, with that of a two-stage semi-continuous polymerization with a slow monomer feed rate in second stage, for the preparation of PMMA using recipe in Table II-2. We see from Figures II-10a, b that the GPC signals for polymers resulting from the two polymerizations are different not only in position but also in shape. The FL curve in Figure II-10a exhibits a peak at the high molecular weight side and a long tail into the low molecular weight region. In contrast, the FL curve in Figure II-10b shows a more symmetrical peak. More information about the dye distribution in these two samples can be inferred from the FL/RI ratio. At short retention time in Figure II-10b, this ratio shows a gradual increase, as the fraction of second-stage polymer gradually increases, and then remains flat over the peak range of retention times. In Figure II-10a, the FL/RI ratio increases significantly with

retention time. These results indicate that the semi-continuous polymerization method provides a more uniform labeling, whereas the batch polymerization results in a lower level of labeling for the higher molar-mass molecules and a much higher labeling content for smaller molar-mass polymers. While there is no unambiguous explanation available for this, we suspect that in the last stage of batch polymerization where there is no longer sufficient supply of MMA to the particles, the dye monomer or its radicals may be readily trapped (e.g. by solidification) in the PMMA glassy matrix and terminated at short chain lengths. This part of the chains with short lengths should have high dye content.

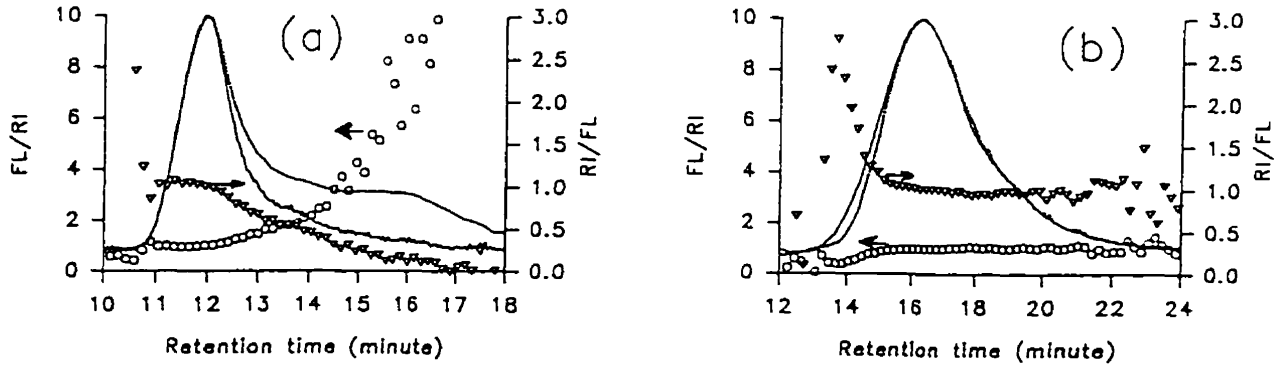

Figure II-10. GPC analysis of PheMMA labeled PMMA prepared by (a) batch process and (b) semi-continuous process at slow monomer addition rate (0.5 mmol/min).

An important feature of semi-continuous emulsion polymerization worth mentioning here is that one can apply various monomer addition strategies. The monomer-starved conditions are often applied for the preparation of homogenous copolymers.[10] One can imagine from the results mentioned above that one will possibly obtain a non-uniform dye labeling if a fast monomer addition rate is applied so that the polymerization conditions are close to that of batch polymerization. Most of our experiments for latex polymer labeling were carried out under monomer-starvation conditions.

II-4-3-3 Analysis of Phe and An labeled polymer

In the following paragraphs, we will present our results of dye distribution analysis for labeled polymers prepared with different dye comonomers.

The factors that control the copolymer structure, or dye distribution in this study, is very complex. The reactivity ratios of monomers and the monomer concentration distribution between various phases play important roles.[10,11] Also, other factors, such as initiator concentration and monomer addition rate which can affect the copolymerization kinetics, may also affect the copolymer structure formed.

(a) Labeling with phenanthrene

Both PheMMA and V-Phe, can be used to introduce the Phe chromophores into PMMA. Although there are no polymerization-kinetics data available for these two monomers, their chemical structures suggest that their polymerization reactivity as well as their solubility in water may differ from each other and from the growing polymer chains. Since in emulsion copolymerization, the chemical microstructure of the copolymers formed depends upon the reactivity ratios of the monomers and the monomer partitioning behavior between the various phases in the emulsion system, it is important to know if there are differences in dye distribution in polymers for these dye monomers.

When the monomer addition rate is sufficiently low (e.g. 0.5 mmol/ml), both dyes can be randomly incorporated into the host polymers and show similar distribution behavior in our GPC analysis. This can be seen in Figures II-9 and II-10b for PMMA samples labeled with V-Phe and PheMMA dyes, respectively.

We observed an interesting result for labeling of PBMA with these dye compounds. The polymers were prepared and labeled with PheMMA and V-Phe, respectively, using the same recipe in Table II-5 and with an identical monomer addition rate of 1.0 mmol/ml (0.16 ml/min). The GPC analysis is shown in Figure II-11. Both samples with PheMMA and V-Phe dyes gives quite flat FL/RI lines across the polymer peak, indicating uniform dye labeling in the polymers. A clear difference is that the sample with V-Phe gives a significant fraction of low molar mass species in the FL signal with much high FL/RI values in this region, while that with PheMMA only exhibits FL signal in the polymer region.

One reason for the above results would be that the V-Phe has much lower reactivity than the PheMMA and part of the growing chains with V-Phe would be terminated before they grow further into high polymer. Another major difference between PheMMA and V-Phe observed in our experiments is that the V-Phe has much lower solubility than PheMMA in both water and MMA monomer. One consequence of this is that during polymerization not all V-Phe is carried forward by BMA into the particles to polymerize. For example, we notice that part of the dye

species is lost as a precipitate on the wall surface of the flask or on the stirring bar, and the labeling content of the final polymer is noticeably (e.g. ca. 20 wt%) lower than the amount in the monomer mixture. These may be responsible for the high FL signal for low-molar-mass in Fig. II-11b. Nevertheless, a high extent, random labeling of latex polymers with Phe can be obtained when one properly chooses the polymerization conditions, especially under monomer-starvation.

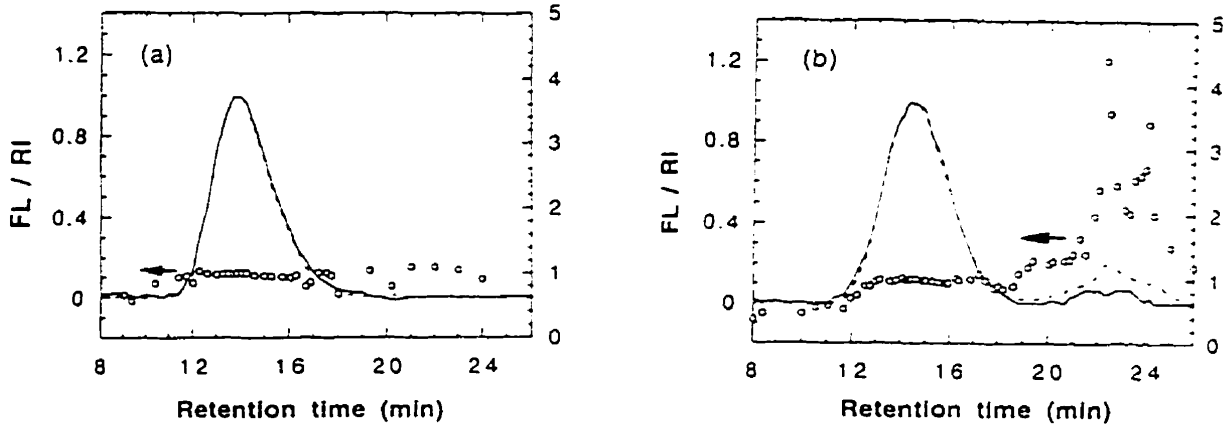

Figure II-11. GPC analysis of Phe-labeled PBMA. Samples were prepared by the recipe in Table II-5 with a monomer feeding rate of 1.0 mmol/min using a dye comonomer of (a) PheMMA, and (b) V-Phe, respectively.

(b) Labeling with anthracene

Figure II-12 presents similar data for an AnMA labeled PMMA sample prepared under almost identical conditions as the sample shown in Figure II-10b. Here, too, we see that the FL and RI peaks are very similar to those in Figure II-10b. Labeling of the second stage polymer is uniform.

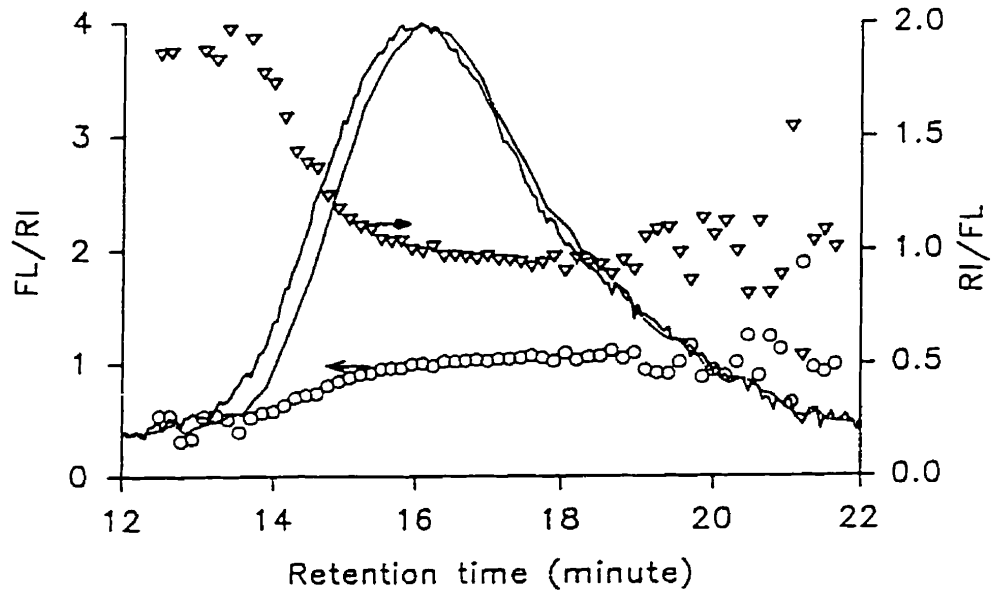

Figure II-12. GPC curves of AnMA-labeled PMMA sample prepared with the recipe as in Table II-2 at the monomer feeding rate of 0.58 mmol/min.

In summary, the dye distribution between polymer molecules can be analyzed from GPC signals detected by FL and RI. It is shown that the semi-continuous method, particularly with slow monomer feed, gives a more homogenous dye distribution in the host polymer molecules than the batch method in emulsion polymer system. However, non-uniform labeling is also observed in some cases. GPC analysis is useful for monitoring both the molecular weight distribution and the dye comonomer distribution in the same chromatogram.

II-5 SYNTHESIS OF LOW-Tg FILM-FORMING LATEXES

Many (meth)acrylic ester polymers have Tg values that are below or close to room temperatures. Those examined in this study included PEHMA, PBA, and copolymers of BMA and BA [P(BMA-co-BA)] and of MMA and BA [P(MMA-co-BA)] (For homopolymer Tg values see Table II-1).

The preparation of single component latexes (e.g. PEHMA) is straightforward. Here I

will describe the preparation of copolymers, using P(BMA-co-BA) as an example, to illustrate the control of polymer properties (e.g. Tg) by varying the polymer composition.

P(BMA-co-BA) is an important type of film-forming latexes used in our studies. These copolymer latexes were prepared by both batch and semi-batch emulsion polymerizations. The recipes for the preparation of various samples are presented in Table AII-1-1 and their properties are listed in Table AII-1-2 in Appendix II-1.

The glass transition temperatures (Tg) of polymers were evaluated by DSC. The Tg value for pure dry PBMA latex is 22.9 °C, and that of PBA is -57.5 °C. When their latex copolymers are prepared, a single Tg value is observed for all the compositions. An example of DSC traces is shown in Figure II-13. This is for the sample prepared with the weight ratio of BA to BMA of 0.25 : 1, yielding a Tg value of -1.9 °C. This value is well below 22 °C and its latex product is expected to readily deform at room temperature.

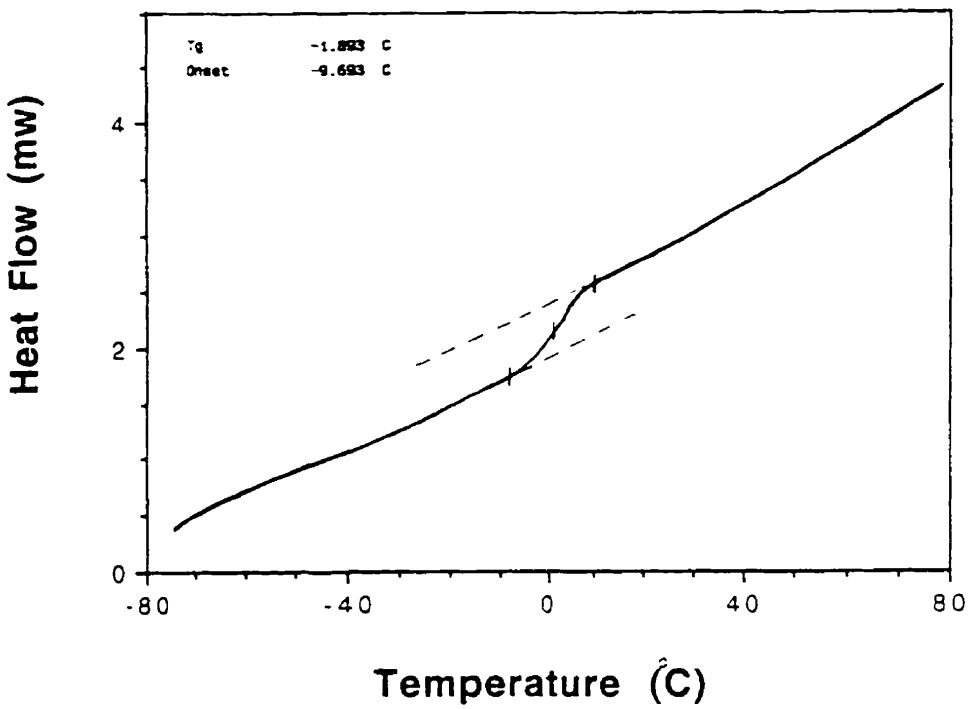

Figure II-13. DSC trace for a P(BMA-co-BA) copolymer sample with the weight fraction of BA component of 0.2. Heating rate: 10 °C/min, N_2 atmosphere.

When the weight fraction of BA component (W_{BA}) increases, the Tg decreases. Table II-6 shows the variation of Tg with the copolymer composition.

Table II-6. Variation of Tg with the copolymer composition

BA : BMA	0 : 1	0.25 : 1	1 : 1	1 : 0
W_{BA}	0	0.2	0.5	1
Tg (°C)	22.9	-1.9	-33.8	-57.5
$1/T_g$ (10^{-3}/K)	3.38	3.69	4.18	4.64

The Tg value for a copolymer can also be estimated from a knowledge of the weight fraction of each monomer type and the Tg of each homopolymer, according to the Fox equation.[12] In our P(BMA-co-BA) polymer, the expression is as in Eq.(II-6):

$$\frac{1}{Tg} = \frac{W_{BA}}{Tg_{BA}} + \frac{W_{BMA}}{Tg_{BMA}} = W_{BA}\left(\frac{1}{Tg_{BA}} - \frac{1}{Tg_{BMA}}\right) + \frac{1}{Tg_{BMA}} \quad \text{..... (II-6)}$$

From the data in Table II-6, a plot of 1/Tg versus W_{BA} can be made (Figure II-14) and an approximately linear correlation as predicted by Eq.(II-6) is obtained.

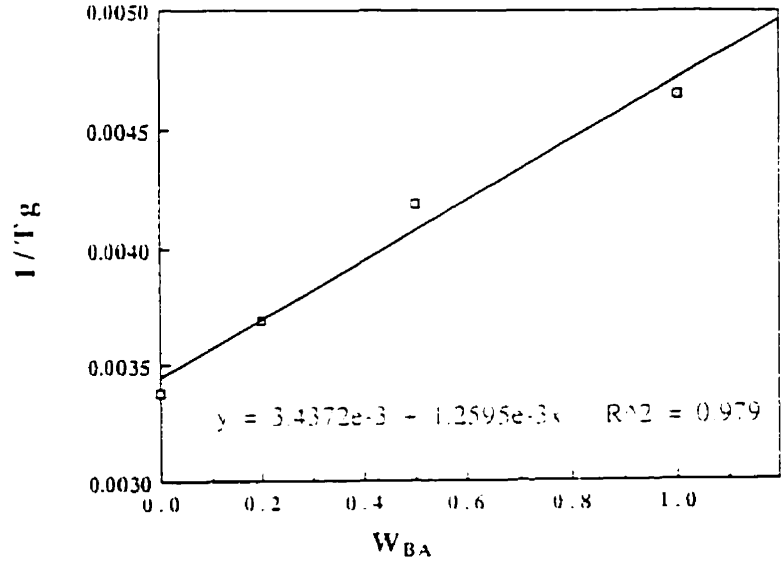

Figure II-14. Plot of 1/Tg (in 1/K) Vs. W_{BA} in P(BMA-co-BA) copolymers.

For the copolymerization of two monomers, the composition of the copolymer chain depends on the composition of the monomer mixtures and the monomer reactivity ratios. The

monomer reactivity ratios r_1 and r_2 are the ratios of the rate constants of different propagation reactions as defined by Eqs (II-7) to (II-11)

$$\sim M_1^{\cdot} + M_1 \rightarrow \sim M_1M_1^{\cdot} \text{ (Rate constant } k_{11}) \qquad \text{(II-7)}$$

$$\sim M_1^{\cdot} + M_2 \rightarrow \sim M_1M_2^{\cdot} \ (k_{12}) \qquad \text{(II-8)}$$

$$\sim M_2^{\cdot} + M_2 \rightarrow \sim M_2M_2^{\cdot} \ (k_{22}) \qquad \text{(II-9)}$$

$$\sim M_2^{\cdot} + M_1 \rightarrow \sim M_2M_1^{\cdot} \ (k_{21}) \qquad \text{(II-10)}$$

$$r_1 = k_{11}/k_{12}\,, \qquad r_2 = k_{22}/k_{21} \qquad \text{(II-11)}$$

where $\sim M^{\cdot}$ represents a polymer chain ending in a radical derived from M.

When BMA (M_1) and BA (M_2) are used, the reactivity ratio will be $r_1 = 2.2$, $r_2 = 0.27$ and $r_1 \times r_2 = 0.60$.[4,13] From the above data it seems that the probability for BA to copolymerize with BMA is much larger than to polymerize with BA itself ($r_2 = 0.27$), and the total copolymerization probability is comparable with the homo-polymerization probability ($r_1 \times r_2 = 0.60 < 1$), even though the propagation rate of BA is much larger than BMA in almost all of the cases.[4] A random copolymer is expected. Each copolymer sample we prepared has only one glass transition temperature both in batch polymerization, where the monomers were added and mixed before polymerization; and in two-stage polymerization, where the monomer mixture were slowly fed and a starved polymerization could lead to a more random copolymer.

In summary, a random copolymer with a single Tg can be obtained for P(BMA-co-BA). The Tg of the polymer can be controlled by varying the composition of the polymer components.

II-6 SYNTHESIS OF 30 NM LATEX PARTICLES

Latex particles of diameters below ca. 50 nm are conventionally prepared by microemulsion polymerization.[14] For particles ≤ 30 nm, a high weight ratio of surfactant-to-monomer, typically 1 - 3, and a large amount of organic alcohols as a cosurfactant, are used to stabilize the emulsion and to produce small particles.[15,16] These additives are difficult to get rid of by conventional latex-purification methods or, if they are removed in some way, destabilization of the system usually occurs. Thus the final latex product obtained from a typical microemulsion system is essentially a mixture of small amount of polymer particles with a larger amount of emulsifier and organic cosurfactant. What one desires to obtain are polymer particles with little impurity.

We intended to employ a normal emulsion polymerization system with smaller amount of ionic surfactant (stabilizer) to prepare small particles. We started with the recipe and condition for preparing 50 nm particles. The recipe is used very often in our laboratory to make latex seeds in a typical emulsion polymerization involving two-stages, as one can see in Tables II-2 for PMMA and II-5 for PBMA. For 50 nm P(BMA-co-BA) latex, the recipe is shown in Table II-7 below and identified as Sample ID III-1-0. To prepare smaller particles, an increased amount of emulsifier is usually needed. When double amount of surfactant was added into the system, the particle size did not change considerably (III-1-1). The particle size decreases more efficiently when the monomer concentration is decreased. As seen in Table II-7 for the preparation of small size P(BMA-co-BA) latex, as the concentration of monomer in water varies, the particle size changes obviously and can be adjusted from 25 nm to 38 nm (III-1-4,5,7,9). It is also possible to employ the two-stage polymerization method, making a seed (e.g. 20-25 nm) and then feeding the monomer slowly, to produce particles of 40-50 nm. This is important when one intends to label tiny particles with fluorescent dyes.

Table II-7. Examples of recipes for the preparation of P(BMA-co-BA) small particles and their properties

Sample ID	III-1-0	III-1-1	III-1-4,5	III-1-7	III-1-9
Recipe					
Water (ml)	100	100	100	100	100
Monomer (g)	6.25-6.75	6.26	1.8	2.2	2.5
KPS (g)	0.085	0.085	0.085	0.085	0.085
SDS (g)	0.22	0.44	0.44	0.44	0.44
$NaHCO_3$ (g)	0.18	0.18	0.18	0.18	0.18
Temp (°C)	70	70	70	70	70
Time (h)	1-2	1	2	2	6
Property					
Diameter (nm)	50-55	43	25-26	32	38
Polydispersity	~0.05	0.008	0.042	0.026	0.027
%Solid (wt%)	6.3	6.2	2.3	2.6	2.8

We are able to prepare particles as small as 25 or 30 nm in diameter, by increasing the surfactant concentration and simultaneously decreasing the monomer concentration in the polymerization systems. Only one ionic surfactant is used, and its amount varies from 0.04 to 0.25 (with respect to the polymer), much smaller than that used in a common system of microemulsion. The procedure can be easily extended to the preparation of nanoparticles of PBMA, PMMA, and polystyrene (PS). It is worth mentioning here that most of our dispersions of small latex particles (e.g. PBMA, PS) remain colloidally stable following repeated treatment by an ion-exchange resin.

II-7 SYNTHESIS OF REACTIVE LATEX

We are concerned with preparing functional latexes in which the functionality can be used to form crosslinks in the dry films through their chemical reactions. I choose here two types of groups, acetoacetoxy (AA) groups and unsaturated (U) bonds, as the reactive functionalities for our latex samples.

II-7-1 Acetoacetoxy-functionalized Latex

A poly(butyl methacrylate) latex bearing acetoacetoxy functional groups (AA-PBMA) was prepared by emulsion copolymerization of butyl methacrylate and 2-acetoacetoxyethyl methacrylate (AAEMA) (weight ratio BMA : AAEMA = 10 : 1). The copolymerization here was carried out by a batch process at 20 °C with a redox initiator system ($Na_2S_2O_8$/$NaHSO_3$/ $CuSO_4$.EDTA). The choice of low polymerization temperature was based on the consideration that the functional groups (i.e. acetoactoxy) may be hydrolyzed at high temperatures. A similar method was used for the preparation of a poly(ethylhexyl methacrylate-co-acetoacetoxy ethyl methacrylate) (AA-PEHMA) latex. The recipes for preparing the latex samples and their characteristics using low T polymerization with redox initiation system are summarized in Table II-8. This recipe was suggested by the group of Prof. German at the University of Technology in Eindhoven, Holland.

Table II-8. Recipes for the preparation of AA-PBMA and AA-PEHMA latex samples and their characteristics

	AA-PBMA	AA-PEHMA
Recipe		
BMA (g)	85.50	-
EHMA (g)	-	85.33
AAEMA (g)	8.60	8.53
Water (g)	847.5	850.4
NaPS (g)	2.316	2.364
$NaHSO_3$ (g)	1.040	1.06
$CuSO_4$.EDTA (μ mol)	1.50	1.50
SDS (g)	2.883	2.887
$NaHCO_3$ (g)	0.804	0.804
Temp (^oC)	20-22	20-22
Time (h)	24	20
Characteristics		
Solids content (wt%)	10.6	10.5
Monomer conversion (%)	100	99
Mean diameter (nm) [a]	54.2	50.8
Size polydispersity [a]	0.082	0.078
Tg [b]	20	-7

---

a. Measured by dynamic light scattering particle sizer. **b.** Measured by differential scanning calorimetry.

The latex samples were characterized by conventional techniques for emulsion polymers. Some characteristics are listed in Table II-8. The content of acetoacetoxy functional groups were determined by NMR spectroscopy. Figure II-15 shows an example of ^{1}H-NMR spectrum for an AA-PBMA sample freshly prepared.

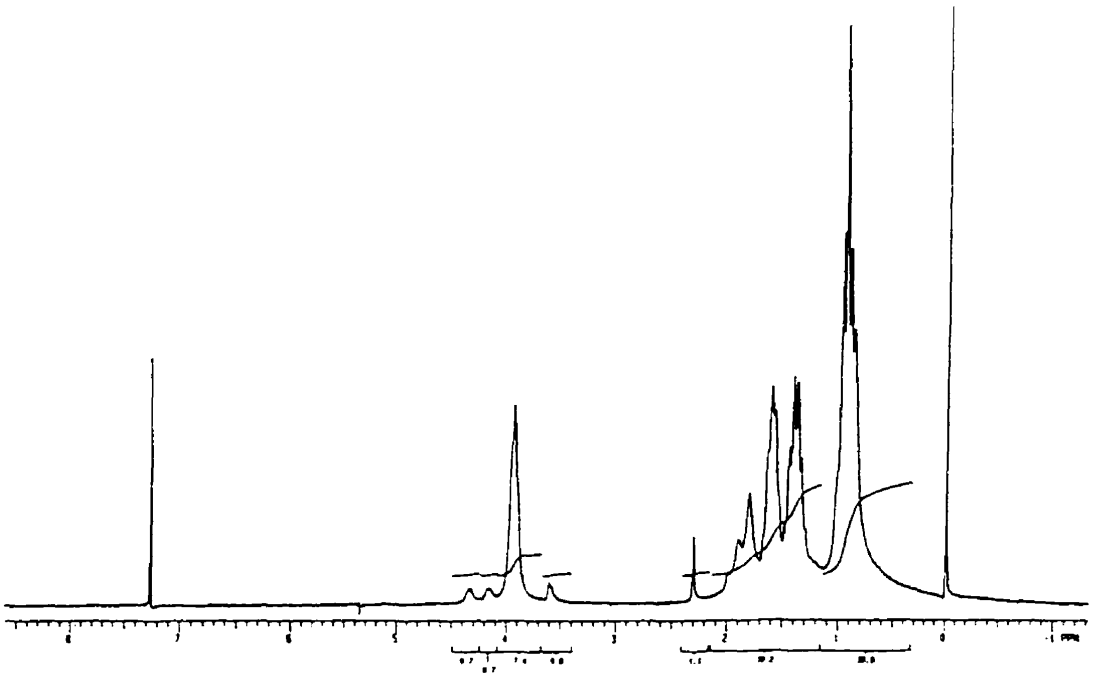

Figure II-15. ^{1}H-NMR spectrum for an AA-PBMA sample dissolved in $CDCl_3$

The integrated areas of the peaks characteristics for the acetoacetoxy units (2.30 ppm for the methyl and 3.60 ppm for the methylene group in -OCO$\underline{CH_2}$CO$\underline{CH_3}$) and those for the BMA units (e.g. 3.95 ppm for the -COO$\underline{CH_2}$-) match the ratio of monomers added before polymerization. By comparing the integrated areas and comparing the spectrum with pure PBMA, it is also likely that the two small peaks at 4.15 and 4.35 ppm arise from the two ester methylene groups of AAEMA units [-CH_2-C(CH_3)-CO-O-$\underline{CH_2}$-$\underline{CH_2}$-O-CO-CH_2-CO-CH_3]. These characteristic peaks are useful for us to quantify the acetoacetoxy (AA) content.

II-7-2 Carboxylated Latexes

An example of preparation of carboxylated PBMA latex has been described in Table II-5 in the previous section, by copolymerizing the MAA monomer with BMA.

I also prepared carboxylated P(BMA-co-BA) latexes. These samples were prepared by emulsion terpolymerization of BMA, BA and MAA, with a monomer weight ratio of BMA : BA : MAA = 70.5 : 23.5 : 6.0. This composition was chosen based on the consideration that the resulting Tg of the polymer should be below 22 °C and the amount of BA should be small enough to avoid premature branching or crosslinking. The recipes are given in Table AII-2-1 in

Appendix II-2, and are similar to that shown in Table II-8, except that the monomers here are a mixture of BMA, BA with a carboxylic monomer (MAA). With redox initiation, one such a sample was prepared at 20 °C, referred to as C-1 latex below, and the other was prepared at 60 °C with the addition of chain transfer agent (DM), referred to as C-2 latex.

Ion-exchange cleaning was carried out to remove the initiator, surfactant and other ionic materials from the latex samples before characterization. Following this procedure, the dispersion had a conductivity nearly 1/100 of that of the dispersion before cleaning, as monitored by a conductometer. The carboxylated latex remained highly stable during cleaning, with almost constant particle size and size distribution.

The acid concentrations in the latex dispersion were determined by potentiometric and conductometric titrations. The cleaned latex dispersion was titrated directly with NaOH solution (0.00984 M) under a nitrogen atmosphere. In this way, the total amount of acid groups at the particle surface plus those possibly present in the water-phase were measured. To determine the amount of acid in the water phase, the aqueous part was separated from the particles by centrifuging at a speed of 50,000 rpm for 3 h, and the clear liquid was directly titrated.

Figure II-16a shows the titration curves for the dispersion of C-1 latex, and for comparison we present in Figure II-16b the curves for the aqueous phase of the latex dispersion, after separation from the particles. The titration of the dispersion includes the neutralization of surface -OSO_3H and -COOH groups as well as that of -COOH groups attached to the PMAA oligomers present in the water phase. These are difficult to distinguish in one titration. We evaluated these values separately. We estimated the level of surface -OSO_3H concentration by using a latex prepared without MAA but under otherwise similar conditions. Since the amount of aqueous -COOH was known by titration of the water phase, we therefore obtained the surface COOH concentration by titrating the latex dispersion and by subtracting the surface -OSO_3H from the model latex as well as the -COOH measured in the aqueous serum. Table II-9 lists the acid concentrations in the particle surface and in the water phase. The total amount of MAA added in the polymerization recipe is also given.

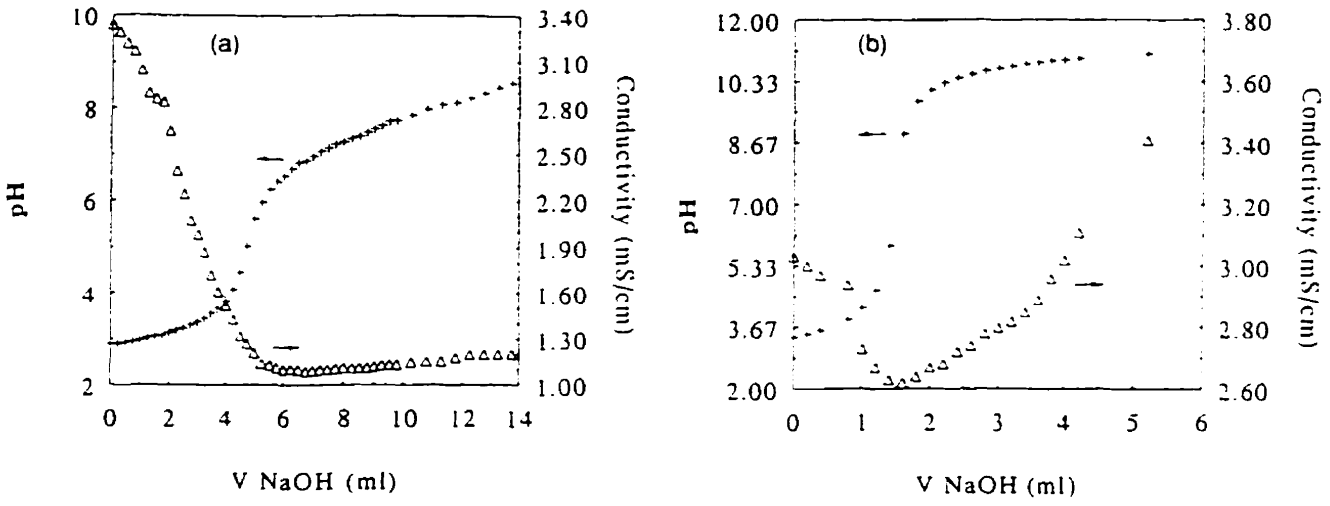

Figure II-16. Potentiometric and conductometric titration curves for the ion-exchanged carboxylated P(BMA-co-BA) (C-1) latex: (a) the dispersion sample (5 g, polymer content 10.75 wt%), and (b) the aqueous phase (5 g) separated from the particles. The concentration of NaOH is 0.00984 M.

Table II-9. Surface and water-phase acid concentrations (in μ mol/g polymer)

Latex	Total -COOH	Aqueous -COOH	Surface -COOH	Surface -OSO_3H
C-1	700	25	75	≈ 9.5
C-2	700	-	160 [a]	≈ 9.5

a. including the small fraction in the water phase

The level of surface -OSO_3H is low (9.5 μ mol/g polymer), as compared to the -COOH groups. This is similar to what observed in most carboxylated latex systems.[17] We find that there are also acid groups present in the water phase in our latex dispersions. This part of acids in aqueous phase is always found in varying concentrations in carboxylated latex prepared with a carboxylic comonomer (e.g. MAA), especially those prepared by a batch reaction.[18] In our systems the detected water-phase -COOH is 25 μ mol/g polymer for C-1 latex, corresponding to a very small fraction (3.6 %) of the total -COOH (700 μ mol/g polymer).

The surface -COOH density we found from titration was about 75 μ mol/g polymer (ca. 10% of total -COOH) for the C-1 latex, and about 140-160 μ mol/g polymer ($\approx$ 20% of total COOH) for the C-2 latex. Polymerization at 60 °C for C-2 latex may permit the rearrangement of the polymer chains, allowing the acid groups to move toward the surface, so that it has higher surface acid content than the C-1 latex. The smaller particle size of C-2 latex (40 nm) than that of C-1 latex (58 nm) should also be reflected in a larger number of titratable surface acid groups. In both cases, there is only a small fraction of -COOH at the surface. The major fraction is buried inside the particles. This distribution behavior is consistent with results reported by many others for similar latex systems, including those by Emelie etal[18] in their MMA-BA-MAA and Zosel et al[19] in their BA-MAA latex polymer systems.

There are two kinds of views regarding this type of titrations. One is to use the forward titration technique, in which the acid groups in the dispersion is directly titrated with a base (e.g. NaOH), to determine the surface acid concentration. The other suggests a back-titration method,[3,20] involving the neutralization of the acids by an excess of base and then the dispersion is titrated backward by an acid (e.g. HCl). The surface acid density found by back-titration of the neutralized dispersion is often higher than that obtained by forward-titration performed in a similar time scale, indicating that the former technique gives the acid concentrations not only on the immediate surface but also of the inside layers of the particles. According to El-Aasser and Vanderhoff et al[21], the amount of titratable acids is strongly dependent on the time of titration. With the titration time extending from instantaneous interval (e.g. sec) to as long as 10 mins, the acids from both the surface and sub-surface layers of particles can be titrated, and in 24 hrs a major fraction of acids within the particles can be detected even with a forward titration.[21] Thus, a key factor for the titration is the time of the process. By forward titration at a fast speed, one may obtain the acid density at or immediately near the surface. By equilibrium neutralization and back-titration in a long time scale, one obtains a much larger fraction of acids from deep inside of

the particles.

We used the forward titration in a short time scale (e.g. in mins) in our surface characterization here. This determines those groups immediately accessible on the surface of the particles. As expected, many -COOH groups are located just beneath the surface and are accessible when the dispersion is allowed to stand in the presence of base for a long time (hours). In support of this idea, we note a slow fall-off in pH (or change in conductivity) with time at each point in the course of titration. The pH and conductivity values we report were those recorded immediately (ca. 3 s) after the addition of each volume of NaOH solution. This phenomenon is also evident in the titration curves shown in Figure II-16. In the aqueous serum titration (Figure II-16b), where there is no such a "dynamic" process involved, one sees that at the equivalence-point, the pH increases sharply and reaches above 10 as the V_{NaOH} increases. The conductivity exhibits a minimum at this point and increases rapidly after the equivalence-point. In the case of the latex titration (Figure II-16a), the equivalence-point is less distinct. The pH rises but with a broader transition, and the increase in pH levels off at a much lower pH (below 7), indicating that some exchange between the protons inside the particles and the added NaOH takes place during the process. In the conductivity curve, it is seen that after the minimum, the conductivity increases very little with further addition of NaOH up to a V_{OH} (in ml) three times of that at the equivalence-point $[(V_{OH})_{eq}]$, further implying that additional neutralization occurs during the titration process.

We intend to use these -COOH groups as the reactive sites for attaching other functional groups to the latex polymer. Although the fraction of surface acid is often low in carboxylated latex prepared with MAA, we expect that under certain circumstances, both -COOHs at the surface and in the particles are available for reaction with other species. For example, reaction at elevated temperature will allow the polymer to readily diffuse within the low Tg particles and the acid groups can be easily redistributed during the reaction.

II-7-3 Unsaturated Latex

A carboxylated P(BMA-co-BA) latex is used and the unsaturated (U) groups were introduced into the latex by reacting the -COOH groups with a compound containing an epoxy group and a double bond (i.e. GMA). The reaction between -COOHs attached to the latex polymer and epoxys in GMA is described as follows.

To 250 g cleaned latex dispersion (C-2, polymer content 10.75%) in a 400 ml reactor was added 0.27 g NP30 surfactant and the dispersion was heated to 80 ^{o}C with magnetic stirring. Triethyl amine (Et_3N) was added slowly until the dispersion pH reached about 7. At least 0.4 g

Et_3N was needed to neutralize the -COOH groups in the particle surface layers plus a small amount in the water phase. When the temperature and pH were stable, 0.05 g hydroquinone was directly added into the dispersion, followed by the dropwise addition of a liquid mixture consisting of 2.27 g GMA, 0.085 g Tetrabutyl ammonium bromide (TBAB), and 0.27 g aerosol-OT (AOT) surfactant into the dispersion. The amount of GMA corresponded to 85% of total moles of the carboxylic acid in the latex. The reaction mixture was then kept stirring at 80 ^oC for 5 h. The latex was stable during reaction with no observable coagulum and no significant change in size. The unsaturated latexes prepared from C-1 and C-2 samples are referred to as U-1 and U-2, respectively.

To characterize the reacted polymer, steps were taken for the separation of the polymer from the mixture of the dispersion or of the dry solids. At first, centrifuging was used to separate the particles from the aqueous phase; however, on one attempt at this separation, the small soft particles coalesced together and could not be redispersed for further purification. A small portion of the reacted latex dispersion was then freeze-dried, and the sample was cleaned as follows: the mixture was dissolved in CH_2Cl_2, and an excess of heptane was added and the precipitate was separated. Methanol was found not a good precipitating agent for our carboxylated copolymer. The purification process was repeated for 4 times. The polymer was finally vacuum dried.

To characterize the reaction, i.e. the incorporation of unsaturated groups into the latex polymer, NMR measurements were carried out for the purified samples dissolved in $CDCl_3$. Figure II-17 shows the ^1H-NMR spectrum for the reacted latex polymer (U-2 latex). The peaks between 0.9 and 2 ppm arise from the poly(meth)acrylates, and that at ca. 4 ppm is attributed to the ester methylene protons (-CH_2-O-CO-) in all the (meth)acrylic ester monomer units (BMA, BA, and GMA). At 5.62 ppm and 6.15 ppm, one clearly sees two characteristic peaks for the vinyl protons (-C=CH_2). The peaks are broadened to some extent, as compared to the solvent peaks (e.g. 7.26 ppm for $CHCl_3$), due to the attachment of vinyl protons to polymer chains. We calculate from the spectrum the molar ratio of the C=CH_2 groups to the -CH_2-O-CO- groups using the peaks at 5.62 ppm (or 6.15 ppm) and 4.0 ppm. We found a value of 7.2%. The molar ratio of GMA to all acrylic ester monomers added in the reaction was 7.6%. This means that about 94% of the GMA has reacted with the -COOH groups in the polymers. For -COOH groups initially bound into the latex, ca. 80 % have been converted to unsaturated groups after the reaction. It is interesting to note that a similar extent of reaction was obtained by Taylor et al[22] in a reaction between carboxyl groups and carbodiimide derivative. We think that the small size, the soft nature of the particles, as well as the elevated temperature of reaction would favor the high extent of chemical reactions occurring within the entire particles.

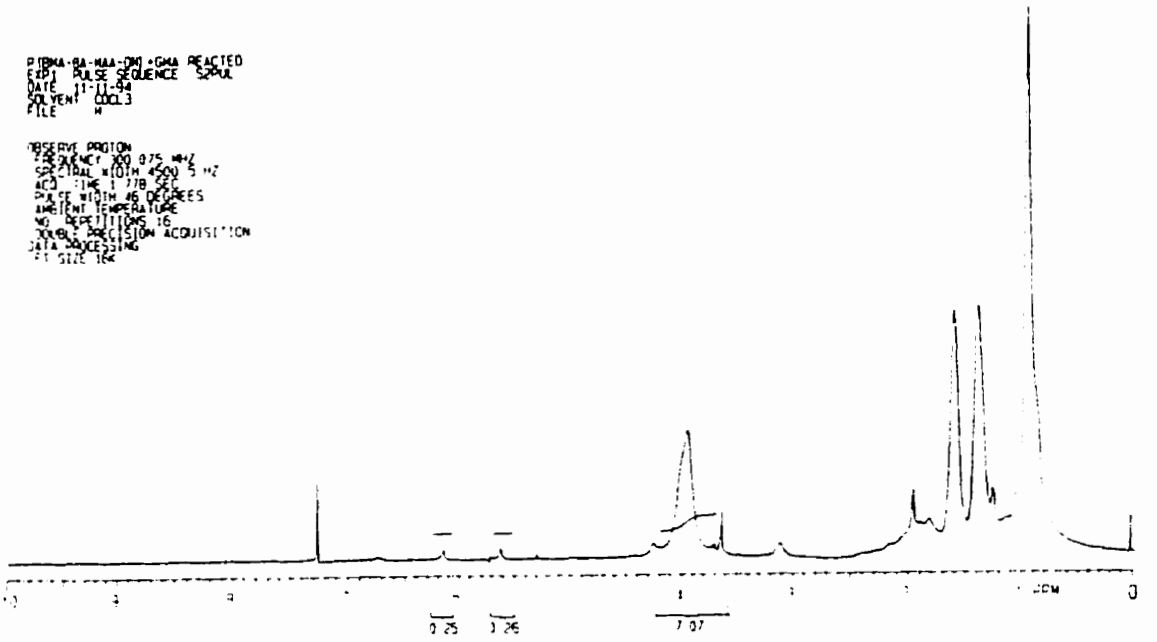

Figure II-17. ^{1}H-NMR spectrum for a unsaturated latex polymer (U-2) in $CDCl_3$.

CHAPTER III THE PROCESS OF LATEX DRYING

III-1 INTRODUCTION

Latex film formation is accompanied by evaporation of water. Early understanding of the mechanism of latex film formation largely came from investigations of the drying process by water loss measurements.[1-4]

Typically, two types of plots from water loss measurements can be used to characterize the drying process: the cumulative mass of water loss and the polymer solid content of the dispersion as a function of drying time, as shown in Figure III-1. Vanderhoff [3] pointed out that there are three regions which can be discerned from the drying curves, corresponding to three states of the film during the film formation process, as depicted in the bottom of the Figure. In stage I, all the particles are separated and dispersed in the mobile dispersion state with a solid content < ~70%, and water evaporates at a relatively fast rate which is linear in time. In the second stage, particle deformation starts, and the surface area for water evaporation decreases which leads to a decrease in the water loss rate. In the third stage, a continuous polymer phase is formed with a solid content > 90%, and the water loss rate is determined by its relatively slow diffusion through the polymer phase.

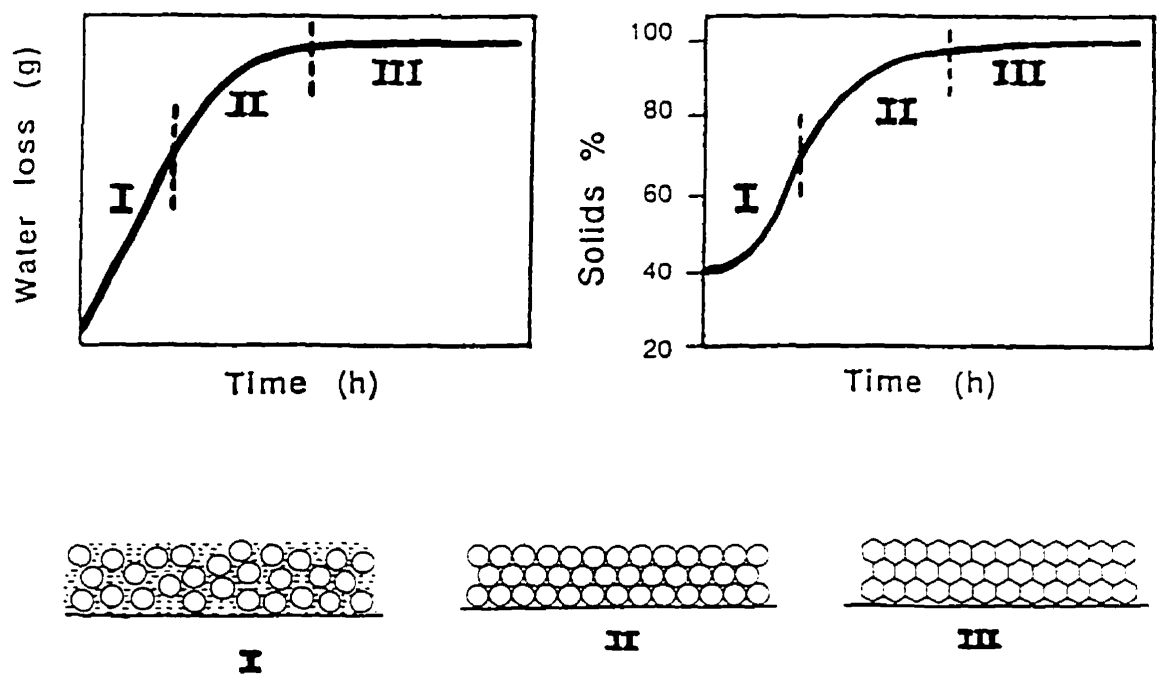

Figure III-1. Typical drying plots: (a) cumulative water loss (in g) and (b) percent solids (either in vol% or in wt%) Vs. time. The conceptualized three states during the drying process is also shown.

Classic models [3,5-7] of latex drying presume that drying occurs uniformly over the entire surface. Moreover, in these models it is assumed that there is a rather well-defined three-stage process which correlates to the water evaporation rate in a simple fashion, as shown in Figure III-1. What one actually observes is that on a flat surface drying occurs faster at the edges. A dry film forms first at the edge, and the boundary between the film and the central wet dispersion propagates inward as water evaporates. This means that at each time during the drying process, there is not a single state corresponding to the stages shown in Figure III-1. Rather, one has in the film a combination of all these states, with the fraction of each varying during the process.

In addition, the models have assumed that the drying rate of latex dispersions is not dependent on the composition and characteristics of the particles. It is hard to believe that water evaporation from a low Tg latex sealed at the surface is the same as that from porous non-deformable particle layers, and that there is no difference between drying from deformed particle layers with full polymer contact and from those with hydrophilic materials separating the polymer particles. All these indicate that classic models of drying are incomplete or problematic, and reexamination of the process is required.

In this chapter, we will examine in detail the drying behavior of single component and blend dispersions. We emphasize the feature that latex dispersions dry with a drying front, which separates a dry film part from the wet dispersion region, and that this front propagates during the drying process. We report and explore the finding that blends of hard and soft latex dry more slowly than either individual dispersion. This kind of rate difference can only occur if the drying rate is controlled by the boundary between the wet and dry regions of the film. From these observations, we develop a new model of the drying process.

III-2 EXPERIMENTAL

III-2-1 Latex Samples

The latex samples include poly(methyl methacrylate) [PMMA] and various butyl methacrylate-butyl acrylate copolymer [P(BMA-co-BA)]. Their synthesis has been described in Chapter II. The important characteristics for the samples employed here are collected in Tables III-1. Some dispersions contained an anionic surfactant [sodium dodecyl sulfate (SDS), 2-6 wt% based on total solids], whereas other dispersions were cleaned carefully by the ion-exchange technique to remove all the salts and surfactant.

Table III-1. PMMA and P(BMA-co-BA) Latex Characteristics

Sample	PMMA			P(BMA-co-BA)	
Diameter (nm)	44	110	167	43	49
Polydispersity	0.01	0.01	0.01	0.01	0.08
Tg (°C)	-	105	-	-33.0	9.9
Mw ($x10^{-5}$)	4.6	2.1	-	8.4	1.1
Mw/Mn	2.0	2.3	-	1.7	6.9

III-2-2 Film Formation

To prepare films, latex dispersions were placed on a flat glass substrate or quartz plate and air dried. Latex blends were prepared by simply mixing the two types of latex, e.g. hard and soft, in dispersion and drying the dispersions to give films. Most samples here were dried directly in the open air. The films had a thickness of 30-50 μm.

III-2-3 Measuring Water Loss During Drying

All dispersions were adjusted to an initial solids content of 5 wt%. For each set of samples to be compared, the initial quantities of dispersion (e.g. 0.300 g) were weighed as identically as possible (± 0.3%). The dispersions were spread on individual glass plates to produce wet films with similar surface areas (e.g. 5.0 ± 0.2 cm^2). With practice I could achieve this reproducibility. Films were dried at ambient temperature (22 ± 1 °C) and humidity in an area of the laboratory free from drafts. The relative humidity (RH) changed from 45 to 65 % day-to-day, but it was fairly constant (with a small deviation < ± 2 %RH) during the measurement time

of each set of samples. The samples were weighed at regular time intervals using an analytical balance: each half hour at early stages, and each 10-15 minutes at later stages, of drying. The changes in solids content with time were calculated from the water loss data. In our experiments, the latex drying occurs as a moving front, showing a decrease in surface area of the wet part of the film. A ruler was placed over the film surface after each time interval to measure the dimensions of the wet region.

III-3 RESULTS AND DISCUSSIONS

III-3-1 The Drying Front

Published models of latex drying assume that water evaporation occurs uniformly over the entire film surface. In all of our experiments, the films dried as a propagating front. When the dispersions were placed in a small circular dish with a vertical wall, a concave meniscus was formed with a thicker edge near the wall and a thin central region. Here drying took place first at the center where the liquid was the thinnest and moves outward towards the thick edge. Concurrently, drying from the top of the liquid at the wall surface also occurred, progressing downward to the bottom of the dish. The film formed at the bottom of the dish had a much thicker edge (e.g. 200 μm) and a very thin center (e.g. 10 μm).

When the dispersions are spread onto a flat glass surface, a flat liquid drop with a slightly convex surface forms spontaneously. Here the liquid center is relatively thick with a thinner edge. Drying occurs initially at the outermost region, and the dry region grows inward toward the center. We illustrate in Figure III-2 the drying process of our latex dispersions spread on a flat glass surface. A dry region forms at the edge of the film. There is a thin transition region which represents the drying front that separates the dry region from the inner wet dispersion. With time, the drying front moves inward, accompanied by a decrease in surface area of the wet center. This drying behavior characterized by a drying front is also observed when latex coatings are directly applied onto a large wall surface.

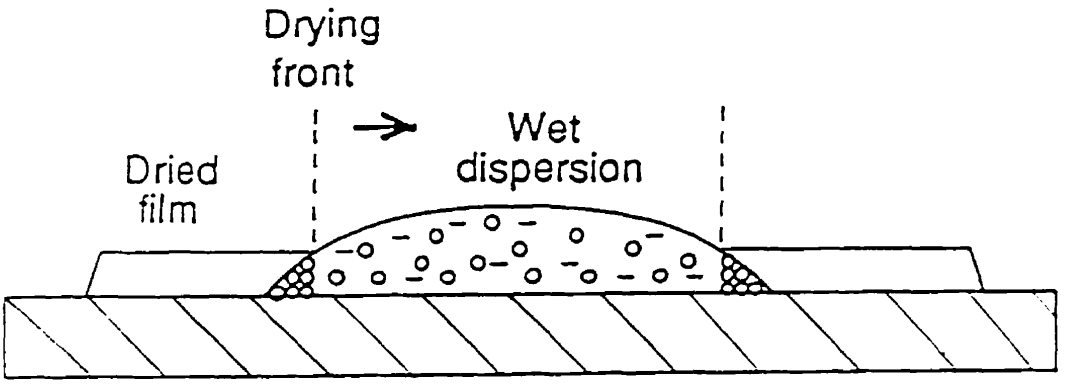

Figure III-2. A drawing illustrating the latex film formation process on a flat substrate. A transparent film at the edge is separated from an inner wet dispersion by a boundary referred to as the drying front. The drying process is characterized by the movement of the drying front towards the center until the wet dispersion fades, and the film is entirely dry.

We observe this behavior for both surfactant-containing and surfactant-free dispersions. Films formed on a flat glass surface for surfactant-containing latex dispersions often have a relatively thick edge surrounding a large flat portion in the center. An example of such a kind of film dimensions is shown in Figure III-3. Here the small portion at film edge has a thickness of 60 μm and the flat part of film center is 45 μm thick. This difference in thickness is even larger (e.g. 80 Vs. 40 μm) in some films.

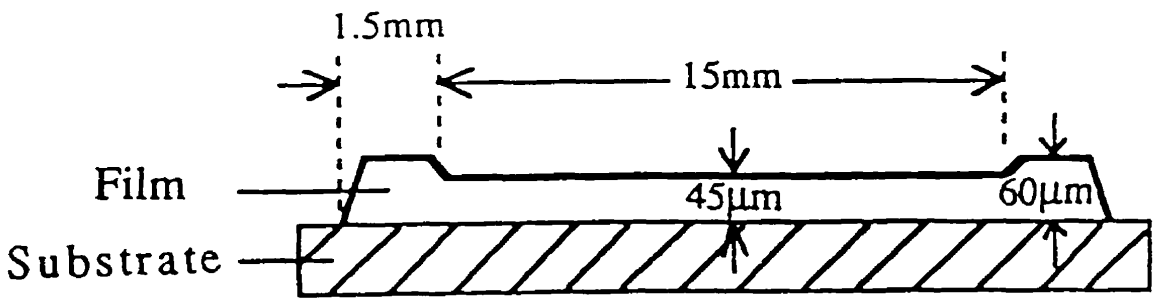

Figure IV-3. A cross-section view with the dimensions of a film produced from a surfactant-containing dispersion, showing a thick rim surrounding a flat center.

When the surfactant and salts are removed from the dispersions, the drying front is also seen but its propagation is slower than for the surfactant-containing dispersions. Films prepared from these surfactant-free dispersions have a much more uniform thickness, and in many cases, the rim at the edge is barely discernible. On some occasions, however, a thicker edge is also observed.

Joanicot et al[8,9] have reported that their surfactant-free dispersions dry differently from corresponding dispersions containing surfactant. Their surfactant-free dispersions dry uniformly over the surface, with no propagating drying front. In our cases, dispersions in which surfactant is removed by ion-exchange also dry with a propagating drying front. Interestingly, films formed with a moving front from our surfactant-free dispersions have thicknesses that are more uniform, as measured by a micrometer. The reason for the uniform drying observed by Joanicot et al would be that their surfactant-free dispersions contained particles with a very narrow size distribution, which ordered into a colloidal crystalline phase throughout the drying process.[8,9] Under these circumstances, particle motion would be suppressed. Our small soft latex particles show a larger size distribution which increases upon washing with ion-exchange resin. We have never observed formation of a colloidal crystalline structure in these dispersions. Clearly, the binary dispersions do not order at all.

III-3-2 The Kinetics of Drying

Most coatings formulations contain latex dispersions at relatively high solids, i.e. > 40 wt%. As a consequence, most previous studies of the drying process began with dispersions at high concentrations. Since we wished to look carefully at the early stages of drying, we chose to dilute all dispersions including blends to 5.0 wt% solids.

In the following paragraphs we compare the rates of water loss from samples of soft latex, hard latex, and their blends. When examining a given variable, we compare samples prepared to have equal initial area, mass, and wet film thickness and whose water-loss rates were measured simultaneously. The reproducibility between identical samples examined in this way was excellent, and the data quality can be judged by reference to the Figures presented below.

III-3-2-1 The water evaporation rate at low solids

An example of a water evaporation experiment is shown in Figure III-4, where we compare mass loss as a function of time from three liquid films: pure water, a soft latex dispersion [P(BMA-co-BA), d = 43 nm, Tg = -33 °C], and a hard latex dispersion (PMMA, d = 110 nm). The two dispersions were cleaned to remove surfactant. The first feature that one notices is that water loss over 2/3 of the drying is linear in time. In addition, the water loss curves of pure water

and the dispersions overlap in this linear region, indicating an identical drying rate, with a water flux of $3.5 \pm 0.1 \times 10^{-4}$ g min^{-1} cm^{-2}. This value is not very different from those reported in the literature. Vanderhoff[3] reported in his early paper that latex dispersions dried at a similar rate to thin films of water. Croll[6,7] found that latex dispersions and various pigment dispersions dried initially at a constant rate which was about 85% of that of pure water. Numerical simulations by Vanderhoff and coworkers using heat and mass transfer equations also gave a similar factor of about 85%.[5] We find a negligible difference in initial drying rates between water and latex dispersions. Note that our latex drying experiments begin at a much lower solids content (5 wt%) than those of Vanderhoff and Croll (ca. 50 wt%).

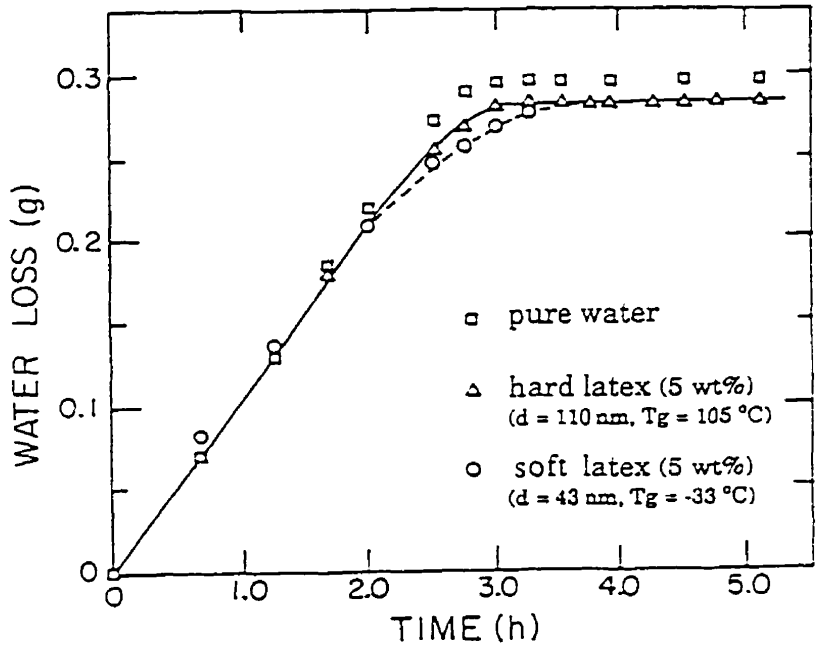

Figure III-4. Water loss as a function of time for water (squares), a dispersion of soft latex (circles), and of hard latex (triangles). In the soft latex: d = 43 nm, Tg = -33 °C and in the hard latex: d = 110 nm. The latex samples are surfactant-free, and initially at a concentration of 5 wt%.

III-3-2-2 The drying of hard and soft latex dispersions

In our experiments, we monitored both water loss and the area of the wet domain during drying. We are thus able to relate the loss of water and the growth in percent solids to the propagation of the drying front during the entire process from a dilute dispersion to a solid film.

a. The drying curves. An example of one of our experiments is given in Figure III-5, where we show drying curves for two latex samples, one hard and one soft. We plot in Figure III-5A the solids content (in weight percent) and the fraction of water remaining ($W_{H_2O}/W^{o}_{H_2O}$, in %) in the latex samples as a function of time. In Figure III-5B, for the same samples, we compare the area of the wet region relative to its initial value (A_{wet}/A^{o}_{wet}, in %) as a function of time. The plots of solids content versus time are sigmoidal, with a slow upward curvature, and a sharp break as the lines approach 100% solids. Initially, the solids content changes slightly with time. This is a consequence of starting the experiment at a low solids concentration: when half the water has evaporated, the solids content has only increased from 5 wt% to 10 wt%. In the very beginning, the wet area does not change very much, but after about 40 min, a dry edge appears, and the drying front starts to move inward.

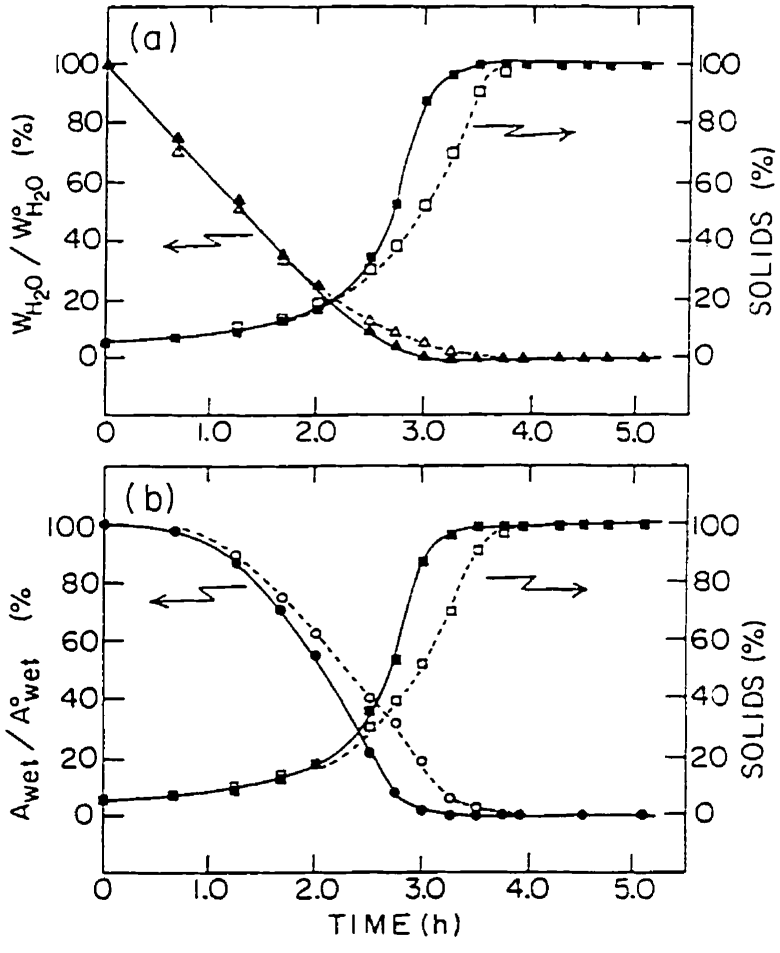

Figure III-5. The drying process for a dispersion of soft latex (d = 43 nm, Tg = -33°C, open symbols) and of hard latex (PMMA, d = 110 nm, filled symbols). In (A) the percent solids (squares) and the fraction of water remaining (triangles) are plotted, while in (B) we plot the relative area of the wet dispersion (circles), as a function of time. Both dispersions are surfactant-free.

Over the first 2.5 hr, the weight fraction of water remaining in the dispersion decreases linearly with time. The linearity of water loss persists even when the measured wet area has decreased by a significant extent (e.g. by 60% of its initial value). This implies that water evaporation occurs not only in the wet dispersion part, where water loss rate is proportional to the surface area, but also in other regions of the film, which must be near the wet-dry boundary. We will discuss this important issue below. After 2.5 hr, when the solids content has reached 30 wt%, the wet area has already decreased to 30% of its initial value. At this point, the rate of water loss for both dispersions begins to decrease, characterized by non-linearity in the water loss curves. Further water loss corresponds to a large, rapid increase in solids content. Above 60% to 80% solids, there is a marked slowing of the water evaporation rate. The wet drop is very much reduced in size and disappears during this stage of the drying process. The solids content eventually reaches its equilibrium value (typically 97-99%).

Once these latex films become transparent or apparently dry to the eye, no further weight decrease is detected during further aging in air. The residual water content, measured by the weight lost during heating the films under vacuum, is small (< 3 wt%). This result differs from that reported by Vanderhoff,[3] who observed significant water loss (ca. 10 wt%) over a prolonged aging period.

An interesting observation is that the drying front moves at different rates during the experiment. At very early times, there is only a wet dispersion. After a certain period (here, 40 min), the dry edge appears. The propagation of the drying front is initially slow, but becomes rapid at the transition region where most of the water has evaporated, and the polymer changes from the minor to the major component. Near the end of the drying process, the propagation rate diminishes. Finally the liquid dispersion fades, and the wet area approaches zero. One can see that the rapid rate of decrease in the area of the wet drop (t = 1.5 to 3 hr in Fig III-5B) precedes the rapid rate of increase of latex solids (t = 2.5 to 3.5 hr) in the system.

b. <u>The concentration of particles in the wet domain during drying.</u> As has mentioned above, during the drying process a solid film is formed at the edge surrounding a wet circular domain which remains as a mobile colloidal dispersion. It is interesting to know the concentration of particles in this wet region and how this concentration varies during the drying process.

From the drying curves (Figure III-5), we obtain both the fractional area of the wet domain (A_{wet}/A^{o}_{wet}, or F_{wet}) and the total solids content (Solids %, or S_{total}) of the film at each stage (or time) of the drying process. These data allow us to estimate the solids contents in the wet domain (S_{wet} %) and the thickness of the wet dispersion (δ_{wet}, in μm) at each point of the

process. Table III-2 shows the results for drying of the hard and soft latex dispersions. The procedure of calculation of S_{wet} % and δ_{wet} is presented in App. III-1.

Table III-2 The percent solids (S_{wet} %) and the thickness (δ_{wet}) of the wet dispersion region during the drying process of a hard and a soft latex

Time (h)	**Hard latex** (PMMA, 110 nm)				**Soft latex** [P(BMA-co-BA), 43 nm]			
	F_{wet}	S_{total} %	S_{wet} %	δ_{wet} (μm)	F_{wet}	S_{total} %	S_{wet} %	δ_{wet} (μm)
1.5	0.77	12	9.5	320	0.80	12	9.8	300
2	0.55	17	10	300	0.62	17	11	270
2.5	0.27	33	12	260	0.41	26	13	240
2.75	0.08	58	10	300	0.31	37	15	200
3	0.02	90	15	210	0.17	50	14	210
3.25	-	-	-	-	0.065	70	13	230
3.5	-	-	-	-	0.02	90	15	200

We note that the percent solids in the wet dispersion all vary within 10-15 %, both for a hard and a soft latex, when the total solids content changes from ca. 10 % to 90 %, and when the fractional area of the wet dispersion changes from ca. 0.8 to 0.02. This level of concentration of particles is quite low. This indicates that the wet domain remains as a dilute dispersion from the early stages to the very end of the process.

We also note that the thickness of the dispersion region changes slowly from ca. 300 μm at intermediate drying times to ca. 200 μm near the end of the process. This thickness is much larger than the dried film part (e.g. 30 μm).

It can be inferred from the above results that those events occurring in the plane of the substrate are as important as those occurring in the bulk. In the above systems, the dispersions have an initial solids content of ca. 5% and thickness of 600 μm. In the first 1 hr, drying occurs across the entire film surface, with no dry film apparent. The solids content increases to about

10% and the thickness of the dispersion decreases to about 300 μm. As drying proceeds, the drying front appears and the area of wet dispersion contracts. The dominant feature of the remaining part of the process is the propagation of the drying front in the substrate plane. There are no significant changes in the wet dispersion: the particle concentration in the wet domain does not increase significantly, and the thickness of this region shows a large decrease (from ca. 200 to 30 μm) only when the wet domain nearly vanishes.

c. Comparison of hard and soft latex dispersions. The most interesting result in Figure III-5 is that the dispersion of PMMA particles dries significantly faster than that of the P(BMA-co-BA) latex with a Tg below room temperature: it takes shorter for the hard latex to reach 97% solids than for the soft latex (i.e. 3.25 Vs. 3.75 h here). Also, the hard latex dispersion contracts its area faster than the soft one.

As we will discuss below, this rate difference is related to a fundamental difference in drying behavior between dispersions of hard and soft latex particles. In the cases we have examined, dispersions of latex with Tg well above room temperature (non-film forming) dry more rapidly than dispersions of low Tg latex.

III-3-3 The Drying of Latex Blends

Latex blends were prepared by mixing dispersions of a hard latex with those of a soft latex. Figure III-6 shows drying curves for a set of surfactant-free dispersions, in which percent solids is plotted vs. time in Fig. III-6A, and the relative wet area is plotted vs. time in Fig. III-6B.

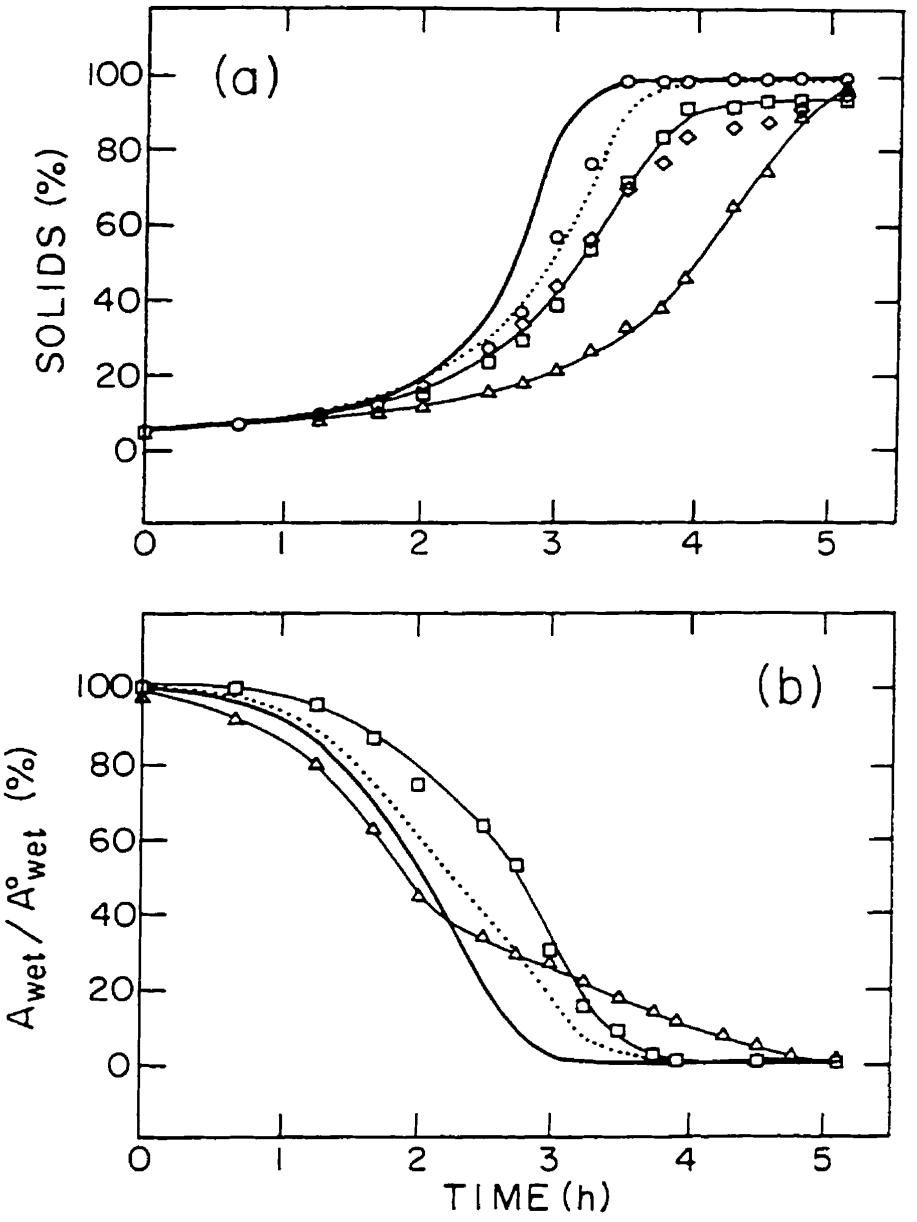

Figure III-6. Drying curves for surfactant-free blends of various hard-component weight fractions: (A) growth in percent solids as a function of time for dispersions of a hard latex (solid line), a soft latex (dashed line) and blends of Φ_{hard} = 0.33 (squares), 0.47 (diamonds), 0.56 (triangles), and 0.78 (circles); (B) decrease in wet area for dispersions of pure hard latex (solid line), pure soft latex (dashed line) and latex blends of Φ_{hard} = 0.33 (squares) and 0.56 (triangles). The soft and hard latexes used for preparing the blends are those of Fig. III-5, and $\Phi_{hard} = 1-\Phi_{soft}$.

The first feature one notices in the drying curves is that latex blends dry differently from the dispersions of soft and the hard latex alone. As seen in Figure III-5, the hard latex dispersion dries faster than the dispersion of soft latex. One might imagine that blending these samples would lead to intermediate drying rates. What one observes is that for most of the compositions studied, the blends dry much slower than the dispersions of either pure component. As the weight fraction of hard component increases from 0 to 0.56, the time taken for the dispersions to reach high solids increases systematically, implying a decrease in drying rates. One also observes that the drying front propagates more slowly for blend samples with Φ_{hard} below ~0.5 than that for either the soft or hard latex dispersion (cf. Φ_{hard} = 0.33 in Figure III-6B). It is only when the blends become non-film-forming (e.g. Φ_{hard} = 0.78), that they exhibit rapid drying.

We also observed a decrease in the drying rate in blends in which the hard latex was replaced by samples of d_{hard} = 167 or 44 nm, and when the soft latex was replaced with a sample of d_{soft} = 49 nm and Tg = 9.9°C.

There are two ways to appreciate the effect of composition on the drying rate. First, the drying process can be characterized by the instantaneous water evaporation rate, i.e. the slope at each point in the water loss curve. For a series of different blends, these water-loss rates can be compared among samples of identical solids content. In Figure III-7A, we plot the water-loss rate vs. Φ_{hard}, comparing samples at 50 wt%, 75 wt%, and 90 wt% solids. A second measure of the drying rate is the time needed to reach a given solids content. This comparison is shown in Figure III-7B.

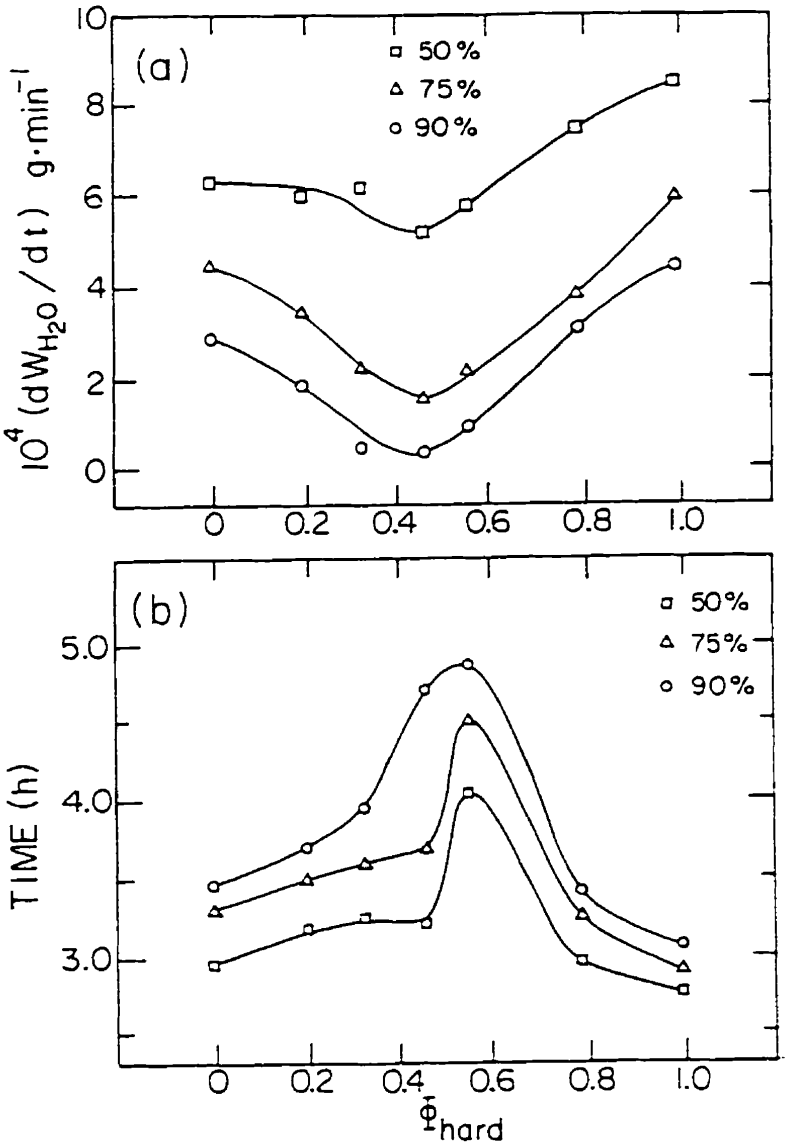

Figure III-7. Comparison of drying rates for latex blend dispersions as a function of composition: (A) instantaneous water evaporation rates (g.min^{-1}) at 50, 75, and 90wt% solids; (B) the time taken (in hr) for each dispersion to reach 50, 75, and 90wt% solids. The data are derived from Fig. III-6.

We note that there is a distinct (critical) composition at which the drying occurs at the slowest rate. At 50 wt% solids, samples of Φ_{hard} = 0.47 and 0.56 have a decreased water evaporation rate. Only the two non-film-forming samples (Φ_{hard} = 0.78 and 1) exhibit a significantly faster evaporation rate than that measured for samples of Φ_{hard} less than or equal to ~0.55. More pronounced effects are seen at the later stages of drying. At both 75 and 90% solids, the water evaporation rates exhibit a clear minimum at Φ_{hard} close to 0.5.

The same trend is seen in Figure III-7B. There is a peak in each plot of the global drying time vs. Φ_{hard} at various solids contents, representing the slowest rate of drying. There is also a

small shift in the peak position, from $\Phi_{hard} \equiv 0.5$ in Fig. III-7A to $\cong 0.55$ in Fig. III-7B. What is particularly curious about this system is that the blend with $\Phi_{hard} = 0.56$ dries very differently from those of lower values of Φ_{hard}. For example, in Fig. III-6A one finds that water evaporation of this sample occurs very slowly at early times ($t < 2.5$ hr) and after 2.5 hr, it dries more rapidly. The overall drying time for this sample is the longest, but the instantaneous drying rate at 50, 75, and 90 wt%, respectively, is not the slowest. In contrast, the dry edge is fast to develop at early times and the wet center shrinks more slowly in the later stages than for the samples of $\Phi_{hard} = 0.33$ (or 0.47), as seen in Figure III-6B. This behavior is reproducible and further effort is needed to gain more insights into the drying behavior near the critical composition.

III-3-4 Surfactant Effects on the Drying Rate

Figure III-8 shows corresponding data for surfactant-containing dispersions. These are the same samples shown in Figures III-6 and 7 but with 6 wt% SDS present (based upon solids), and dried at slightly higher humidity (55 vs. 47 %RH). The drying behavior observed is similar to that seen in Figure III-7: with increasing Φ_{hard} the drying rate passes through a minimum. These dispersions show a narrower range of drying rates than those without surfactant. This points to a surfactant effect on the drying rate itself, which is described in more detail below.

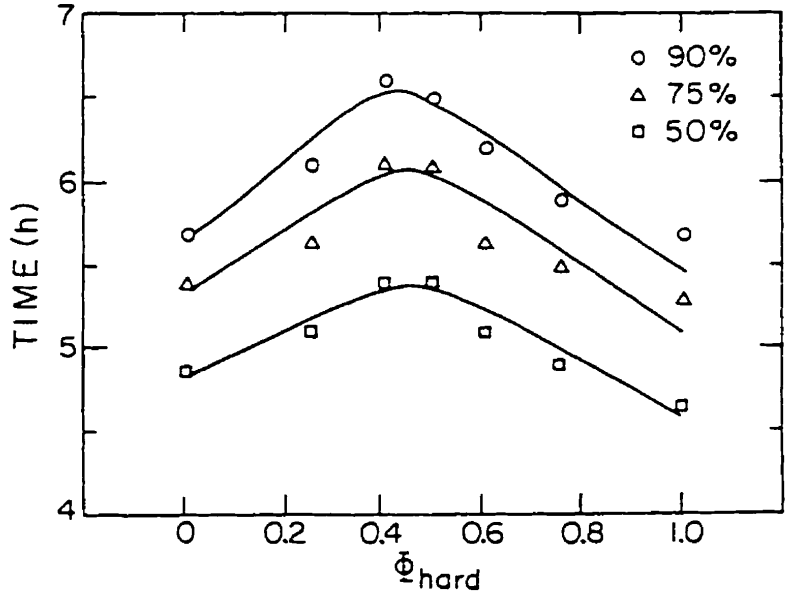

Figure III-8. Comparison of drying rates for SDS-containing latex blends as a function of composition: the time taken (in hr) during drying for each dispersion to reach 50, 75, and 90wt% solids. The samples are identical to those in Figures III-6 and 7 except that 6 wt% SDS, based upon latex solids, has been added to the ion-exchanged dispersions.

Figure III-9 presents comparisons between latex dispersions with and without surfactant (SDS). Both series were dried at the same time and under identical conditions. In the case of hard latex (d = 110 nm), there is no significant difference between the SDS-free sample and those with post-added 2 and 4 wt% SDS, respectively. For soft latex (d = 43 nm, Tg = -33 °C), addition of 4 wt% SDS to the surfactant-free dispersion leads to an increase in the drying rate. Further increases in SDS content up to 8 wt% has no additional effect on the drying rate.

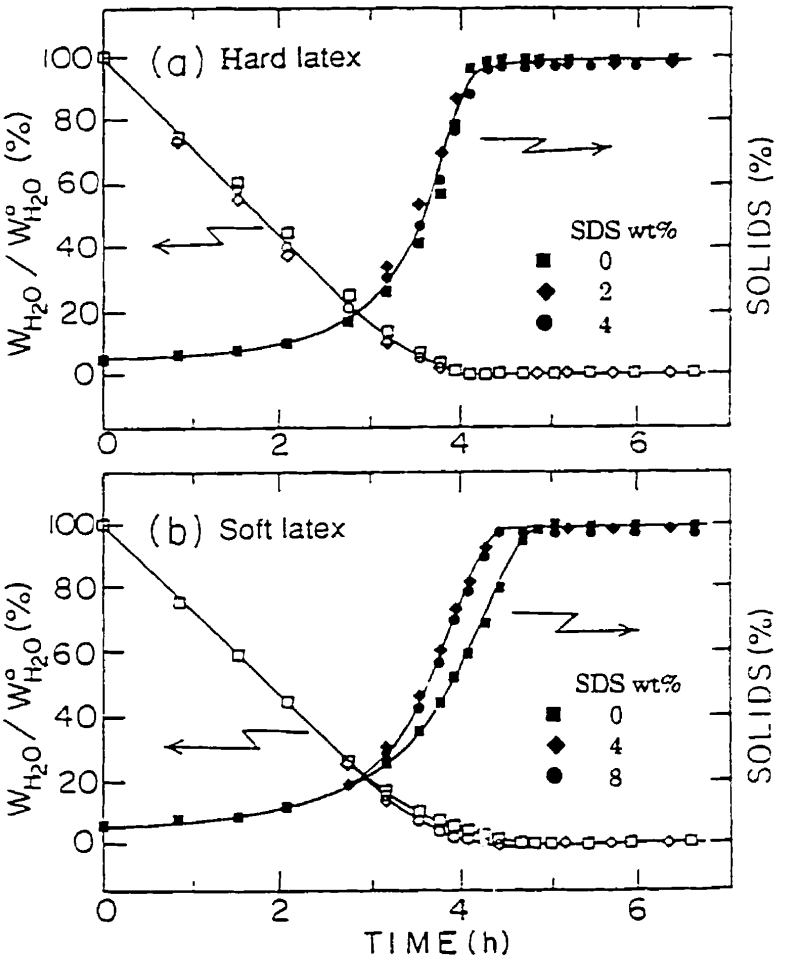

Figure III-9. Comparison of the drying process, with and without SDS, for soft and hard latex dispersions: (A) drying curves for a surfactant-free PMMA latex (d=110 nm, squares) and samples with post-added SDS: 2 wt% (diamonds), 4 wt% (circles). (B) drying curves for soft latex (d = 43 nm, Tg = -33 °C) dispersions containing 0 wt% (squares), 4wt% (diamonds), and 8 wt% (circles) SDS. The amount of surfactant is calculated based upon latex solids.

The above results indicate that the drying rate of soft latex dispersions is sensitive to the presence of SDS, but, above a certain amount, is insensitive to the amount present. Another interesting point is that for surfactant-free samples, the hard latex dispersion dries significantly faster than that of the soft latex (4 hr for the hard latex, and 4.75 hr for the soft latex dispersion to reach 97 wt% solids), whereas in the presence of SDS their drying rates become very similar.

We emphasize this point in Figure III-10, where we show the drying curves for blends of $\Phi_{hard} = 0.5$ with different amounts of SDS. The surfactant-free sample dries much slower than the surfactant-containing samples. When 2, 4, and 6 wt % SDS, were added into the latex, the drying becomes much faster, but is again independent of the SDS amount. Isaacs[10] also reported that surfactant accelerates water evaporation during the late stages of film formation. What is curious here is that the amount of surfactant needed to promote the drying rate is less than that needed for monolayer coverage of the latex. Coverage can be estimated by assuming that the area per SDS molecule at saturation is 0.8 nm^2 on a PMMA surface and 0.6 nm^2 on PBMA or PBA.[11] For monolayer coverage, one needs 2.7 wt% SDS for 110 nm PMMA latex particles, and 11 wt% for 43 nm P(BMA-co-BA) latex particles. In Figures III-9 and 10, we see that 2 wt% SDS is enough to increase the drying rate for the dispersion of the tiny P(BMA-co-BA) latex particles.

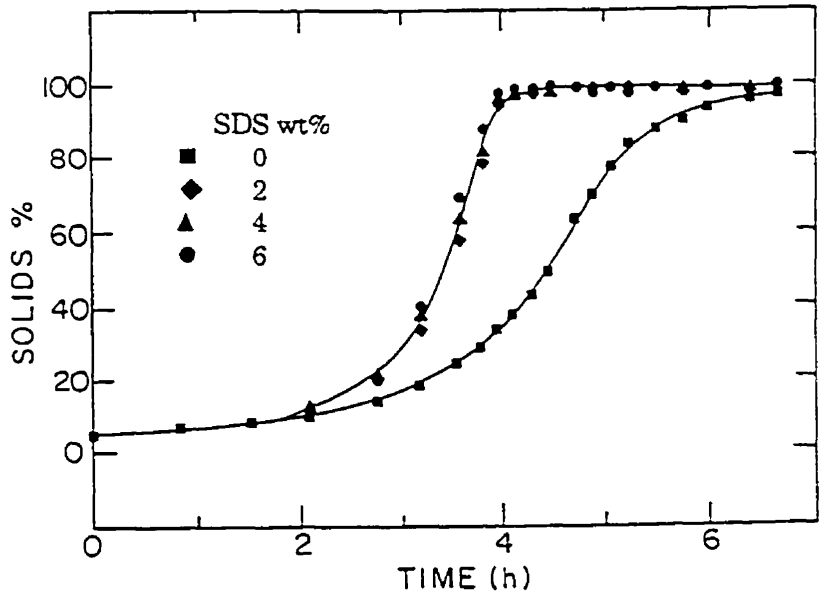

Figure III-10. Comparison of the drying process, with and without SDS, for latex blend dispersions containing 0 (squares), 2 (diamonds), 4 (triangles) and 6 wt% (circles) SDS. The blends contain a 1:1 weight ratio of soft latex (d = 43 nm and Tg = -33°C) and PMMA latex (d = 110 nm).

III-3-5 Models for The Drying Process

The above results indicate that there is a distinct composition in latex blends at which the dispersion dries at a slowest rate. For the dispersions examined, this composition corresponds to a Φ_{hard} value close to 0.5. We have some evidence that for very small PMMA particles (44 nm), the minimum is shifted to a lower value of Φ_{hard} and the range of drying rates for different compositions becomes narrower. This retardation in drying rate represents a fundamental feature of film formation which must be accommodated into realistic models of the drying process.

III-3-5-1 Classic models of drying

The classic model for the drying process for latex dispersions was proposed by Vanderhoff,[3] and was described above (see Figure III-1). Other models have been put forward for the drying process, for example by Croll,[6,7] and recently by Eckersley et al.[12] Croll also treats the drying process as occurring uniformly across the surface, with a flocculated phase separating the wet dispersion from a dry, porous top layer. Eckersley modified the Croll model to include formation of a continuous polymer layer across the dispersion surface during drying.

These models overlook important aspects of the drying process. For example, as mentioned above, they all presume that drying is uniform. This view is problematic because the area of the wet portion of the film contracts during drying.

III-3-5-2 Recent views of the drying process

It is important to mention here some related experiments described in the recent literature. First, a group at Rhône-Poulenc examined the film formation process from a latex system in which a hydrophobic core is surrounded by polar materials at the surface.[8,9] These polar materials form an interconnected membrane in newly formed films If the film is examined shortly after drying, the membrane can be rehydrated. Neutron scattering experiments on films rehydrated with D_2O give diffraction peaks corresponding to the size of the original latex particles, implying that a continuous network of membranes persists throughout the film. Note the implication that the polymer particles deform before they come into contact, a result which receives strong support from recent experiments reported by Crowley et al.[13] We believe that the structure of this kind of interconnected membrane must be important for determining the drying rates during film formation.

Another set of experiments come from an investigation of the forces which cause spherical particles in dispersion to form ordered monolayers upon drying. Denkov et al [14] monitored the drying of micron-sized polystyrene latex dispersions by optical microscopy. They observed a convective flux of the particles tending to form a close-packed particle phase, and the direction of

particle motion depended on whether the liquid droplet was concave or convex in shape. On a flat glass surface where the liquid film was convex, particle accumulation occurred first at the edge. The particle arrays built up at the periphery as a result of a particle flux from the droplet toward the boundary. When a concave liquid was formed inside a Teflon ring, the formation of close-particle-packing started from the central part of the dispersion. They argued that once the particles came in contact with the substrate so that they protruded from the water surface, the high surface area would lead to enhanced evaporation from this region, with capillary forces supplying water from the droplet. This in turn sets up a flux of water from the droplet to the drying edge, transporting latex from the bulk to the edge. When the drying rate is sufficiently slow, the forces involved are enough to lift particles above the dried particle layer at the edge, making the final particle layers thicker at the edge than in the center.

This description of the drying mechanism explains the origin of the drying front and the direction of its propagation. Moreover, it explains the observation that films formed on flat glass substrates are often thicker at the edges than in the center. Thus the model described by Denkov et al accommodates some key features of the process which other models cannot explain.

III-3-5-3 Our view of the drying process

Based on the above discussions, we believe that the faster drying rate for dispersions of hard latex than for dispersions of similar-sized soft latex is related to the magnitude of the capillary transport of water at the wet-dry interface. High Tg latex do not deform during drying. The pore structure that remains can conduct water from the wet domain into this high surface area region of the film. Deformation of the soft latex will lead to smaller capillaries and reduced flow of water. When surfactant is present, it would form a hydrophilic membrane, and this would create channels for water to transport. This has a larger effect on the capillarity of the soft latex than on the larger pores formed when the hard latex dispersions dry.

In latex blends, the soft latex can deform to fill the spaces between the hard particles. At low values of Φ_{hard}, the hard particles act as obstacles to the diffusion of water through the capillaries of the soft latex matrix. Obstacles decrease the diffusion or capillary flow rate by increasing the tortuosity of the path.[15] At high values of Φ_{hard}, the soft latex polymer plugs the pores between the hard latex. This also produces obstacles to water flow, and the drying rate is slower than for the hard particle dispersion itself.

A somewhat similar observation was reported by Sullivan[16] on evaporation of organic solvents from the newly dry pigmented latex films. He found that organic solvents (e.g. ethylene glycol) evaporated slowest from the nearly dried films when the pigment volume concentration (PVC) was ~ 50%. In these pigmented latex systems, the major components are the hard, large pigment particles and the soft binder latex. There is a critical volume concentration of the pigment

particles (CPVC) at which the polymer phase changes from continuous to discontinuous, which is close to 50%.[17,18] Sullivan explained that large pigment particles gave rise to circuitous pathways and more resistance for organic solvent transport when PVC < CPVC, while the fast evaporation observed when PVC > CPVC was also attributed to the presence of large voids.

To summarize, as water evaporates from a latex dispersion, a dry edge forms at the thinnest portion of the wet film. Drying occurs as a propagating front because water evaporates more rapidly from the high surface area region at the wet-dry boundary than from the wet surface of the droplet itself. Water is constantly wicked through the pore structure to this dry region, and this in turn creates a flux of water and particles from the droplet to the dry edge. In Figure III-11A we present a pictorial view of the flux of water and particles toward the drying boundary where fast evaporation occurs. This view may be modified for the case in which salts and surfactant have been removed from the system. Here there can be strong long-range forces between the latex particles in the liquid droplet. These can slow down the flux of particles toward the edge, and if a colloidal crystalline phase is formed, particle transport may be suppressed. In Figure III-11B we show that as a film forms from soft latex, water is transported through the hydrophilic membrane between the particles, and in blends, hard particles act as barrier to the water transport and hence reduce the evaporation rate at low Φ_{hard}.

From the systems examined in Figures III-6 - 8, we see that dispersions with a composition near $\Phi_{hard} = 0.5$ dry at the minimum rate. This composition lies in the same range as the critical composition (close to 0.5) at which the films formed from dispersions change from continuous, transparent to turbid (see Figure IV-3 in Chapter IV and ref. 19,20). We suspect that there is a connection between more rapid water loss for larger values of Φ_{hard} and the onset of turbidity in the films. Turbidity indicates the presence of voids which the soft latex is unable to fill completely. These voids can act as conduits for water transport during the later stages of drying and water evaporation occurs fast as Φ_{hard} increases from ~ 0.5 to higher values.

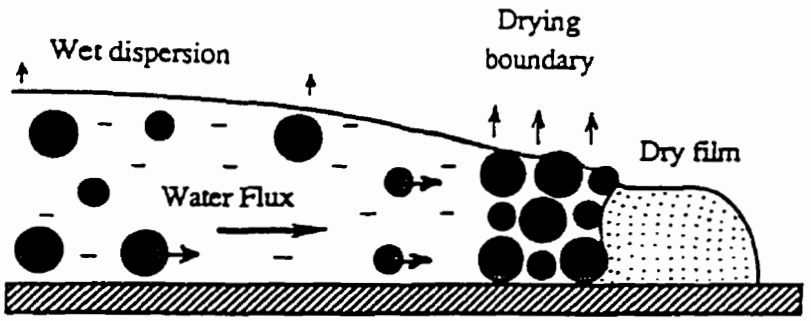

(A) Water flux at the drying boundary

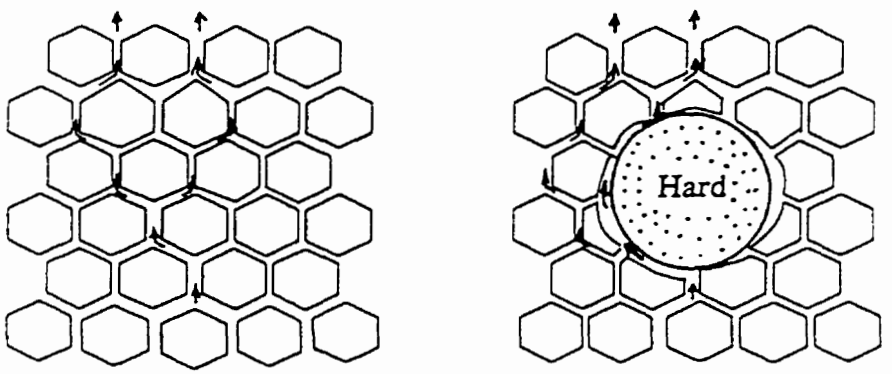

(B) Obstacle effect of hard particles in blends

Figure III-11. A pictorial view of the drying mechanism. In (A) we show that there is convective flow of water towards the drying boundary and fast evaporation of water in this region due to its high surface area. In (B) we show that as a film forms from soft latex, water is transported through the hydrophilic membrane between the particles. In the blends, hard particles form obstacles and act as a barrier to capillary transport.

III-4 SUMMARY

When latex films are spread on a flat glass surface, the drying process exhibits a drying front which separates a dry film formed first at the edge from the central wet dispersion. The drying front propagates from the edge towards the center and the liquid dispersion area contracts as drying proceeds. For dispersions of disordered particles, this process is accompanied by both a lateral liquid flux and a particle flux towards the edge from which a solid film grows continuously in size. For dispersions in an ordered state, the water dispersion area may also contract due to the curvature of the surface and the lateral water flux towards the edge may still exist, but the lateral particle flux may be suppressed due to ordering. In the later case, more uniform film thickness is observed.

Dispersions of soft latex dry more slowly than those of a corresponding latex with a Tg above room temperature. Blends of these dispersions take longer to dry, and there exists a distinct composition which dries at the slowest rate. The presence of surfactant facilitates the water evaporation rate. We propose a model to explain the drying mechanism.

CHAPTER IV LATEX BLEND FILMS FOR ZERO VOC COATINGS

IV-1 INTRODUCTION

Concern for a safe and friendly environment is leading to changes in coating technology. There is an urgent need to eliminate the volatile organic compounds (VOCs) present in most current coatings formulations. The emissions of these VOCs give undesired effects on human and are harmful to the environment. The coatings industry has responded to this challenge by trying to replace solvent-based coatings with water-borne or other alternative systems.[1-3]

Even within water-based systems, VOCs are added to promote film formation. In coatings intended for ambient temperature applications, the latex particles must deform into void-filling shapes upon water evaporation. This requires a rather low modulus for the latex polymer, on the order of 10^6 Pa.s. Such polymers form tacky films. To get good mechanical properties from a coating, the resin on the surface must have a much higher modulus, > 10^8 Pa.s. The role of the solvents added to the coatings formulation is to lower the modulus of the latex polymer to promote particle deformation during drying, and they act as plasticizers to promote polymer diffusion in the newly formed film.[1,2,4] In this way they enhance the development of good film properties. If they remained within the resin, the film would be soft and have poor mechanical properties and poor block resistance. In this technology, good film properties are achieved when the solvent evaporates from the film into the atmosphere.

Good block resistance refers to the ability of the coatings to resist the adhesion between two coatings surfaces when brought into contact. Blocking is a common problem for polymer films at temperatures near or above their Tg.

IV-1-1 Latex Blends

One attractive strategy for zero VOC coatings involves blends of low Tg and high Tg latex polymers.[5-9] One either mixes a soft latex with a hard latex in dispersion or prepares a latex with a soft shell and a hard core. The essence of this idea is to combine the different properties of the two polymer components: the soft latex component can readily deform to fill the void spaces in the blend material, and the hard latex polymer should provide enhanced mechanical properties for the coatings.

When two types of particles of different sizes are blended, to achieve a high density of packing it is desired that the small particles fill the interstitial spaces between the close-packed large particles. When the two sized particles are both hard, as is the case in ceramics, there must

be a requirement of the relative size of the particles, as depicted in Fig. IV-1A. The latex blends we choose to examine are mixtures of a hard latex and a soft latex. On one hand, if the soft particles were small in size, they would fill the volume more efficiently. On the other hand, since the soft particles can deform and flow, their size may be not a key factor. In Fig. IV-1B we depict a latex mixture in which the soft latex has exactly the volume needed to fill the interstitial spaces of a randomly close-packed array of hard spheres, assuming that the soft particle can flow readily.

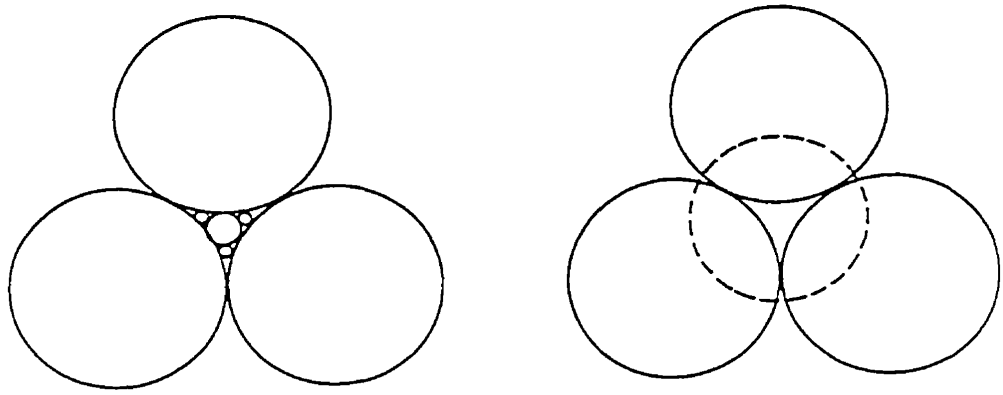

Figure IV-1. Particle arrangements in a blend to achieve high density packing. When all particles are hard, the filler particles should have well-defined smaller sizes with respect to the voids that they are intended to fill, as shown in (A); When the filler particles are soft and deformable, their size need not be so rigorously defined. In (B), the smaller central particle (dashed circle) has exactly the volume needed to occupy the void among the close-packed larger particles.

We began this project with the idea that the relative size of the soft latex compared to the hard latex would be important in producing transparent and void-free films.[3-8] As suggested in Figure IV-1, the original idea was to match the size of the low Tg latex to the void volume (Φ_V = 0.34) of randomly close-packed spheres. Thus our soft particles prepared were smaller than the hard ones. We now note that in a recent patent application[5] films with larger soft latex and small hard latex can also be prepared. Since the two materials would have somewhat different indices of refraction, achieving transparency should require that the hard latex be small with respect to the wavelength of visible light. Thus our initial target was to prepare hard microspheres with a diameter of ~100 nm, and to prepare low Tg latex much smaller in size (20-50 nm).

This chapter is divided into three parts which follow an Experimental Section. The first presents the idea of a transparency phase diagram. As the fraction of low Tg latex in the dispersion is increased, there is a sharp transition from turbid to transparent films. The second examines the surface and bulk morphologies of blend films. Finally we look at how the high Tg latex affects the mechanical properties of the blend films.

IV-2 EXPERIMENTAL

IV-2-1 Latex Samples

In most of our experiments, we chose poly(methyl methacrylate) [PMMA] as the hard latex (Tg = 105 °C) and copolymers of butyl methacrylate (BMA) and butyl acrylate (BA) [P(BMA-co-BA)] as the soft latex. In most of the films the PMMA particles used had a diameter of 110 nm. In some other films smaller (e.g. 45 nm) or larger (e.g. 400 nm) sizes were used. The soft latexes have Tg values ranging from -33 °C to 10 °C, and mean diameters between 20 and 55 nm. The synthetic procedure for both types of latex polymers was described in Chapter II, and the characteristics for some of the samples employed here are listed in Tables IV-1.

Table IV-1. Characteristics of PMMA hard Latex and P(BMA-co-BA) soft Latex

Sample	PMMA				P(BMA-co-BA)					
Diameter (nm)	44	110	230	400	43	32	21	38	49	55
Polydispersity	0.01	0.01	0.01	0.01	0.01	0.03	0.1	0.02	0.08	0.08
Tg (°C)	-	105	-	-	-33.0	-6.9	-1.9	4.1	9.9	5.1
Mw ($x10^{-5}$)	4.6	3.7	-	-	8.4	6.7	1.3	3.5	1.1	5.1
Mw/Mn	2.0	2.3	-	-	1.7	1.9	3.0	24	6.9	5.5

In some experiments we used two samples of poly(methyl methacrylate-co-butyl acrylate) [P(MMA-co-BA)] with slightly different compositions, one with Tg = 48 °C, the other with Tg = 17 °C. These samples were supplied by courtesy of The Glidden Company in Cleveland [9] and their characteristics are collected in Tables IV-2.

Table IV-2. P(MMA-co-BA) latex characteristics

Sample	High Tg latex	Low Tg latex
D_n (nm)	111	103
D_w / D_n	1.11	1.10
Tg (^oC)	48	17
Mw ($x10^{-5}$)	2.3	2.5
Mw/Mn	2.9	3.1

IV-2-2 Film Formation

A weighed quantity of a soft latex [e.g. P(BMA-co-BA)] was mixed with certain amount of a hard [e.g. PMMA] latex in dispersion and agitated for several minutes. The mixed dispersion, having a solid content of 10-15 wt%, was then coated onto a glass or quartz substrate and allowed to dry at room temperature. For some samples, the substrate with the dispersion was covered with an inverted petri dish to slow down the water evaporation rate throughout the drying process. Other samples were dried directly in the open air. The dried films have a thickness of 30-50 μm.

In some PMMA/P(BMA-co-BA) blends, the dried films were annealed at temperatures just below the Tg of PMMA, and some films were annealed at 140 °C, well above the Tg of PMMA, 105 °C.

IV-2-3 Film Characterization

Film transparency for each sample was measured with a UV-VIS spectrometer (Hewlett-Packard 8452A Diode Array). The film was mounted in front of the sample window, and its transmittance (T%) was scanned in the visible range (400 to 700 nm). When comparing the transparency for a set of samples, the T% values were recorded at 550 nm. We note that one could distinguish by eye a transparent film from a turbid film.

Film morphologies were examined by scanning electron microscopy (SEM), freeze-fracture transmission electron microscopy (FFTEM), and atomic force microscopy (AFM). FFTEM measurements were taken in the laboratory of Professor R. S. Shivers at the University of Western Ontario. Details are given elsewhere.[7,10] Scanning electron micrographs (SEM) were taken in Toronto using a Hitachi S-570 system under low voltage to prevent the melting of the soft component. Atomic force microscopy (AFM) measurements were carried out in Toronto in the laboratory of Professor J. Vancso using the Nanoscope III in the TappingMode™.[9]

Dynamic mechanical analysis (DMA) measurements were performed with a Perkin-Elmer DMA-7 system. Thick films (0.25 - 0.50 mm) were prepared by air drying the dispersions in a Teflon mold and then cutting the films into rectangular pieces (10 mm x 4 mm). Measurements were made in the extension mode to obtain E', E", and tan δ.

Some primary tests for pencil hardness and block resistance were also carried out in lab. In pencil hardness tests, a set of pencils of different hardnesses is used and the scratch hardness for each film is evaluated according to ASTM D3363-92a.[11] In the block resistance test, the two film surfaces coated on a water-proof paper were brought together, placed under a rubber stopper (size #8, smaller diameter, 3.2 cm) on which a 1000 g weight is loaded to give a pressure of 127 g/cm^2 on the film specimen. This set-up was then placed in an oven at 50 °C. After 30 min the specimen was removed, cooled, and the two film surfaces were peeled apart, during which a sound gives the degree of tack and the fraction of area of the specimen that is still sealed gives the degree of seal. Thus the block resistance (degree of tack and seal) is evaluated. These conditions were similar to those described in ASTM D4946-89.[12] We note that it is difficult to obtain rigorous scientific data from these tests with a small number of samples, but it is easy to distinguish a film of high hardness and block resistance from a film of poor hardness and block resistance.

IV-3 RESULTS AND DISCUSSIONS

IV-3-1 Film Transparency

Transparency is an important property for many latex coatings applications, especially for clear coats for automobiles and hardwood. Even in conventional pigmented coatings of complex composition which give opaque films, the formation of a clear film from the pure latex binder is important, since this ensures the full compaction of the particles and the generation of a continuous binder phase when mixed with pigments.

There are several requirements for transparency in a latex blend film. First, the number of voids in the film that can scatter light must be negligible.[1,2] In our binary latex system, the hard particles are not able to deform; therefore it is essential that the soft particles deform to fill space. In addition, the refractive indices of the two polymers must be similar,[13] or, if they differ, the dispersed domain sizes must be small.[14] In the blends described here, the latex particles are rather small. Their refractive indices are unlikely to be very different, based upon the values of the corresponding homopolymers, 1.490 for PMMA, 1.483 for PBMA and 1.474 for PBA, as listed in Table II-1 in Chapter II.

We obtain films which are transparent to the eye in blends rich in the soft component. UV-VIS measurements indicate that the percent transmittance (%T) of these samples is on the order of 85-95% over the visible wavelength range. Turbid samples, with %T only 5-20%, are obtained from blends rich in hard latex. Examples of the transmittance scan plots are shown in Figure IV-2. In films from mixtures of hard and soft latexes of different blending compositions, we found that there is a value of the volume fraction of soft polymer at which we could obtain a clear film, and below which we only could get a turbid film with cracks or, in the extreme, a white powder. We define this as the critical volume fraction of soft polymer, Φ_c.

$$\Phi_{Soft} = \frac{V_{Soft}}{V_{Total}}$$

$$\Phi_c = \left(\frac{V_{Soft}}{V_{Total}} \right)_c$$

where the volume of each polymer was calculated from its known weight and density. The density of PMMA is 1.19 g/cm^3. Since the densities of pure PBMA and PBA are very close, 1.06, and 1.08 g/cm^3, respectively, we take the value of 1.06 g/cm^3 as the density of our soft copolymer consisting of PBMA as a major component.

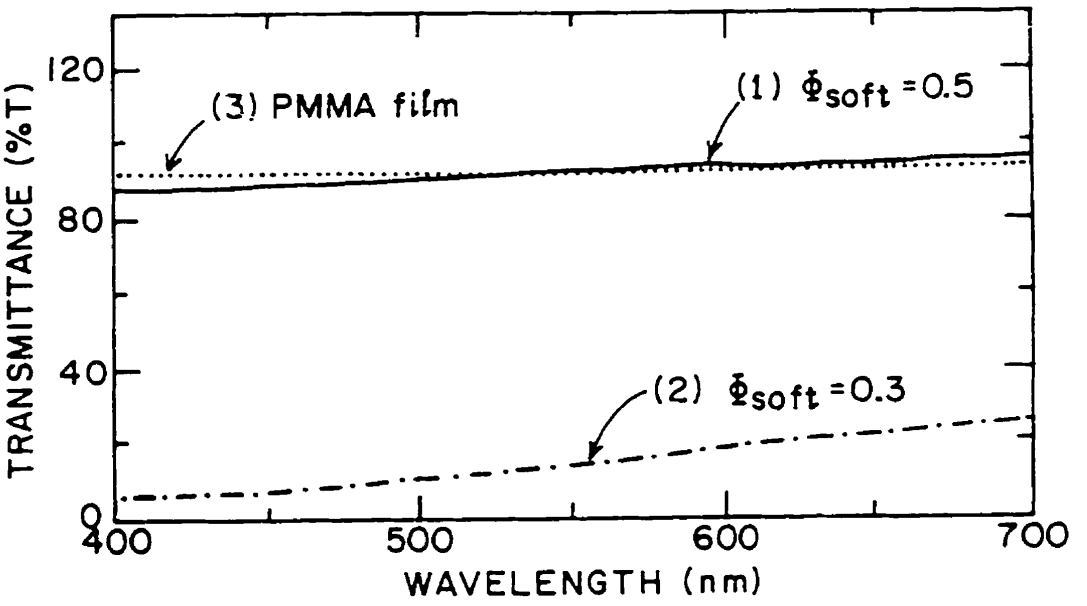

Figure IV-2. Visible transmittance spectrum of (1) a clear latex blend film, (2) a turbid latex blend film, and (3) a solvent-cast PMMA film. The two latex blend films contain PMMA hard particles of d = 110 nm and soft particles of d = 55 nm and Tg = 5.1 ^{o}C. The volume fractions of soft polymer in the films are (1) 0.5, and (2) 0.3, respectively.

Figure IV-3 shows two examples of transparency phase diagrams, i.e. plots of light transmission vs. blend composition. The plot in Figure IV-3A describes blends of 110 nm PMMA latex with 38 nm P(BMA-co-BA) latex of Tg = 4.1 °C. The transition between turbid and transparent films is extremely sharp. The two components of this blend differ in refractive index by about 0.01, which is sufficient to scatter light if the hard particles are not well separated in the blend. Figure IV-3B is for blends of P(MMA-co-BA) latex of Tg = 48 °C with that of Tg = 17 °C, both having a diameter of 110 nm. Here we observe cracks at a soft fraction between 0.3 and 0.5. Since the two components differ in refractive index by only about 0.001, the turbidity seen at lower fractions of soft component likely arises from void scattering.

Φ_c is an important parameter characterizing the formation of continuous films from binary latex systems. As one can see in ref. 7, Φ_c shows a slight increase with increasing soft particle size (e.g. from 21 to 55 nm when blended with 110 nm PMMA), but over a very small range (0.40 - 0.50), indicating relatively little dependence of Φ_c on the size ratio within certain range. It also seems that Φ_c is not sensitive to the Tg of the soft particles varying between -33 °C and 10 °C, implying that the randomness of particle distribution in the final film is not significantly influenced by the polymer composition in the particles. These results are supported by the microstructures of the films, as shown in ref. 7.

One might expect that the volume fraction of soft polymer necessary to give transparent films would correspond to that necessary to fill the void volume of close-packed hard spheres. This volume fraction Φ_{soft} would be equal to 0.26 or 0.34 depending upon whether the close packing was face-centered cubic or random. Φ_c values found in our experiments are always above these values and close to 0.5. This implies that the soft polymer forms a continuous phase in transparent films, with the hard particles dispersed in it.

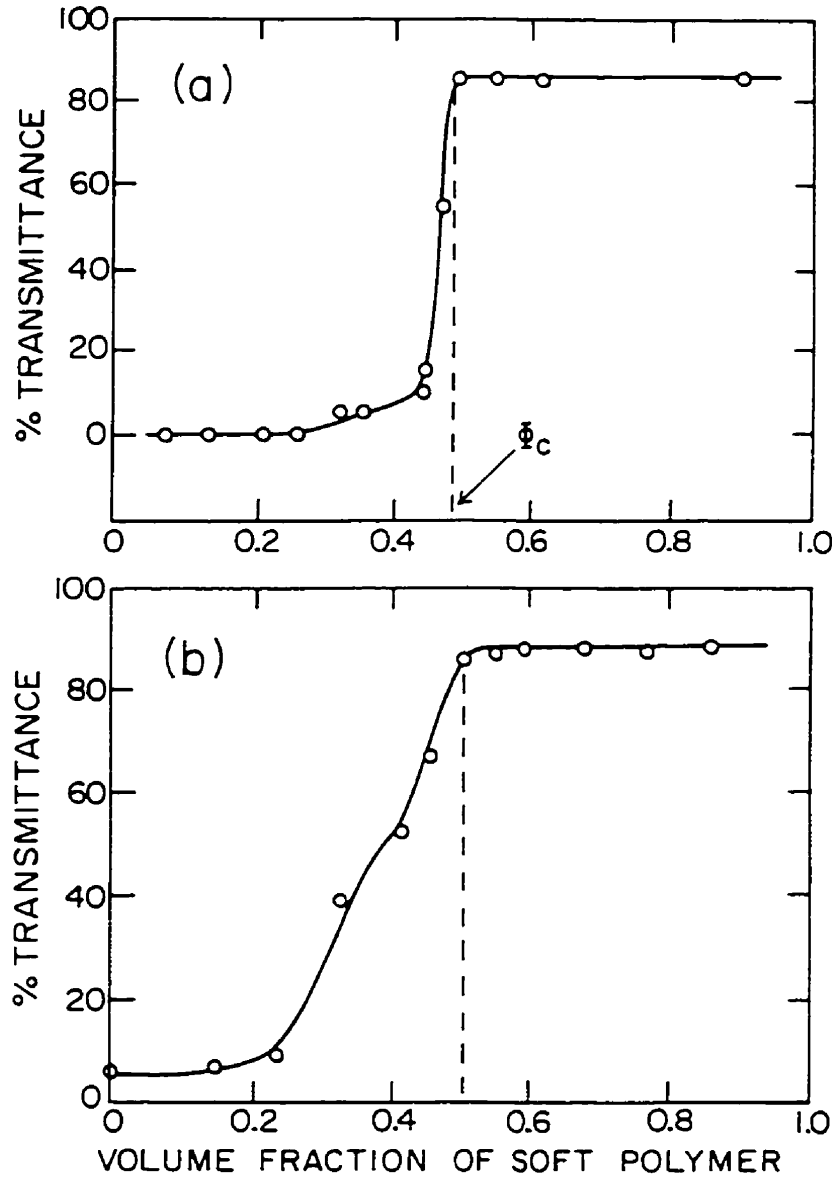

Figure IV-3. Plots of %transmittance at 550 nm Vs. blend composition: (A) blends of 110 nm PMMA latex with 38 nm P(BMA-co-BA) latex of Tg = 4.1°C; (B) blends of P(MMA-co-BA) latex of Tg = 48 °C with that of Tg = 17 °C, both samples of d ≈ 110 nm. The dashed line represents our definition of the critical volume fraction of the soft component for film transparency.

IV-3-2 Film Morphology

IV-3-2-1 A random distribution of hard particles in transparent films

Film surface morphologies were examined by scanning electron microscopy (SEM). In blends of PMMA and P(BMA-co-BA) particles, SEM images show that transparent films are characterized by a random distribution of hard particles in the low Tg matrix. A typical packing

pattern for transparent films composed of about 1 : 1 volume ratio of hard to soft components are presented in Figure IV-4. In this sample, the hard spheres are randomly distributed and embedded in the continuous phase generated by the soft latex.

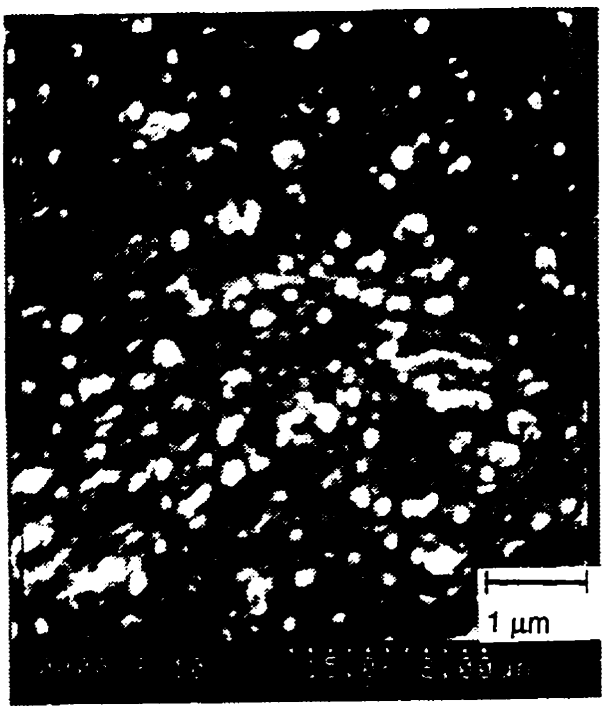

Figure IV-4. A SEM image of the pattern of random distribution of hard particles seen in transparent latex blend films. In this sample, the hard particles have a diameter of 110 nm and the soft particles have a d = 55 nm and Tg = 5.1 °C with a Φ_{soft} = 0.5.

A number of these film samples were examined by FFTEM. This technique provides a rich view of the fracture surface of the film interior with high resolution and with minimal distortion. In Figure IV-5, we present a FFTEM image of a transparent film comprised of a 1:1 mixture of 110 nm PMMA particles and small soft P(BMA-co-BA) latex. One can see that the hard (PMMA) particles preserve their size and spherical shape. The soft particles have deformed and result in a void-free internal structure. The hard particles are uniformly distributed in the soft polymer matrix. These results support the idea that film transparency is dependent on the distribution of hard particles in the soft polymer matrix.

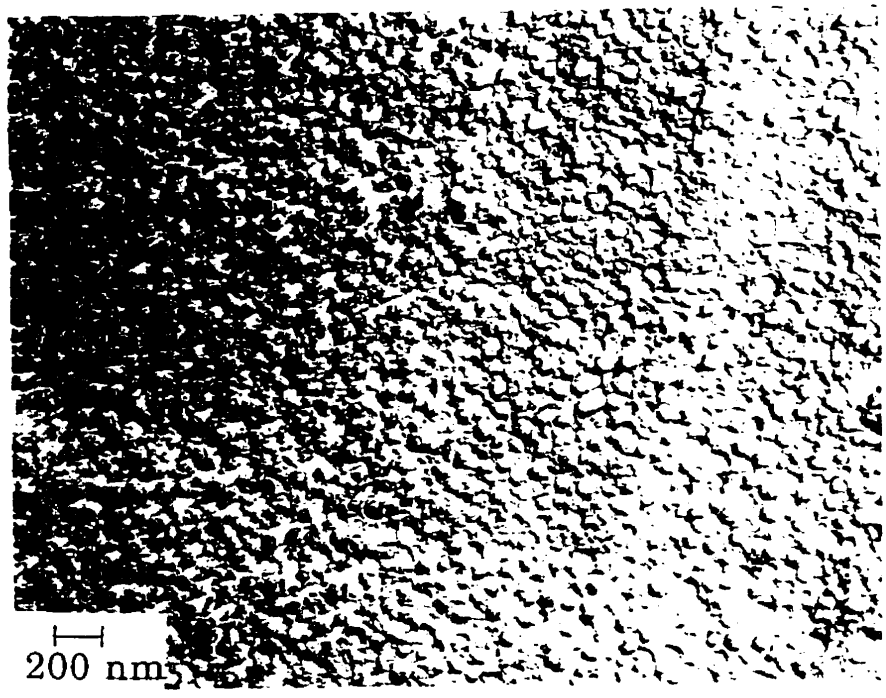

Figure IV-5. FFTEM image of a latex blend film containing a 1 : 1 mixture of 110 nm PMMA particles and P(BMA-co-BA) particles of d = 32 nm and Tg of -6.9°C. The film was fractured at -170°C, and shadowed with platinum-carbon.

IV-3-2-2 Clustering of hard particles in turbid films

When turbid films are obtained from latex blends, we always observe aggregation of the hard particles. This is particularly true for films consisting of hard particles with sizes larger than ~250 nm and small soft particles (50 nm or smaller).[7] We also have some evidence that when the surfactant is removed from the blend dispersion, the tendency to aggregation is enhanced.[7] The most interesting result observed in these experiments is that when the size ratio between the hard and soft particles is far from unity (e.g. 10), macroscopic phase separation occurs. In films comprised of 400 nm diameter PMMA latex and 50 nm P(BMA-co-BA) latex, clear regions and turbid domains are apparent to the eye. In the SEM, no PMMA spheres are seen in certain regions of the film surface (Figure IV-6A), which we associate with the transparent domains, whereas aggregates are clearly apparent in other domains (Figure IV-6B) which likely are turbid. This type of phase separation with a large size ratio of the particles is seen reproducibly in other

films, for example, in films prepared from a dispersion of 1000 nm PMMA plus 100 nm P(MMA-co-BA) particles.

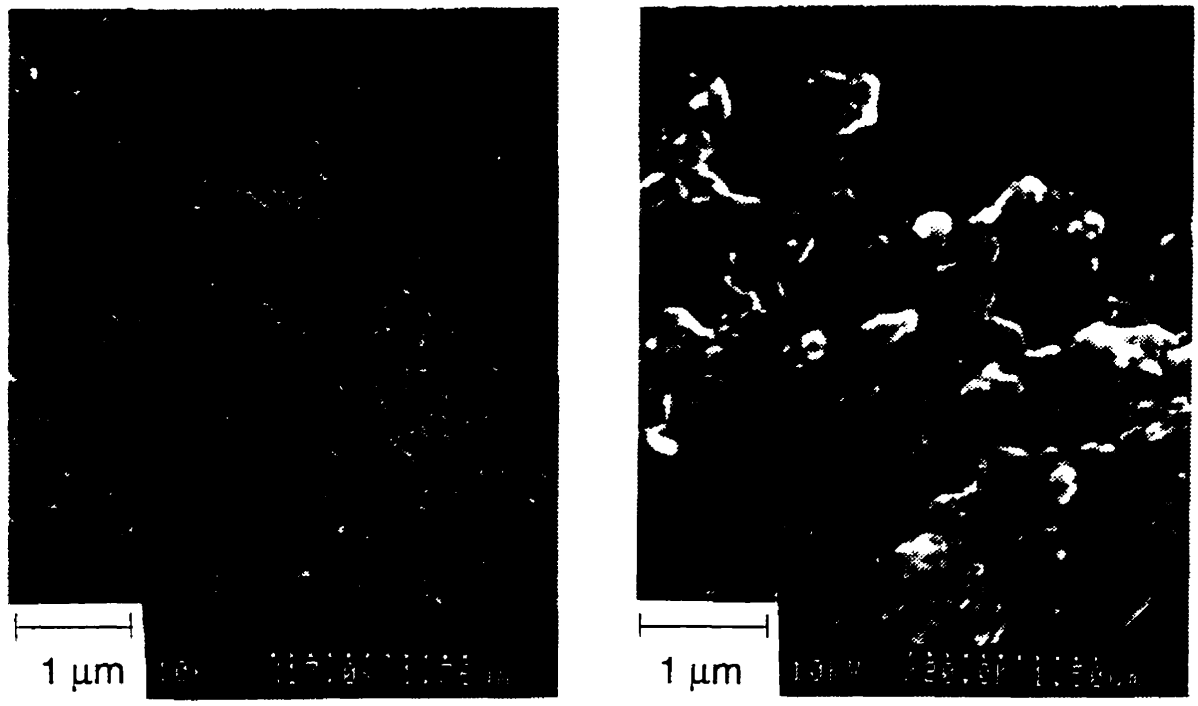

(a) (b)

Figure IV-6. SEM images of a film exhibiting a clear region and a turbid region, prepared from a hard latex of 400 nm and a soft latex of 50 nm: (a) an image with no hard particles observable, and (b) an image showing clustering of hard particles.

It would be useful in understanding the generation of film morphology to have information about the distribution of particles in binary colloidal mixtures. We believe that the film morphology is derived from the particle packing structure in the concentrated dispersion before the particles come into close contact. Once close-packing occurs, morphology change can not be reversed. This nature of this state in the concentrated dispersion should relate primarily to the colloidal properties of the particles (i.e. particle sizes), and only indirectly to the polymer composition within the particle. Some information on particle distribution in binary colloidal mixtures has recently become available.

Isrealachivili[15] has commented that there is always an effective attraction between particles of the same species in a binary mixture in dispersion. Bartlett and Ottewill[16] used small angle neutron scattering (SANS) to examine colloidal dispersions composed of mixtures of particles of

different sizes. We note that their colloidal systems are different from our latex dispersions, both in the choice of particles and the type of medium. For their system they pointed out that in a binary mixture of particles, A and B, the average microstructure might have either a tendency toward "dispersion," in which an A species will have on average both A and B particles as neighbors, or a tendency toward "association", in which separate clusters of A and B will form. They presented evidence for the clustering of small spheres in the presence of large spheres in some samples, but no sign of macroscopic fluid phase separation when the particle size ratio was not too far from unity. From their experiments, together with the work of Biben and Hansen,[17] they suggested that when the diameter ratio of binary particles in a mixture is less then 0.2, the colloidal mixture may phase separate. This is consistent with our observations. Our results lend support to the idea that the particle packing state in a dried latex film is largely determined by fluid phase structures in the concentrated binary dispersion during the drying process.

IV-3-2-3 Surface morphology in relation to transparency phase diagram

The surface morphologies were also examined by AFM. By comparison, we noticed that using a small brush to coat a thin film gave flatter surface than simply casting a film from dispersion on mica for AFM measurements. The AFM images mentioned here were taken by Mr. Abhi Patel during his summer visit in this lab. Figure IV-7 shows AFM images of P(MMA-co-BA) latex blend films of different compositions. In these blends, the hard particles (Tg = 48 °C) and soft particles (Tg = 17 °C) are of similar size (d = 110 nm). In pure hard latex, no films can be formed at room temperature and the particles retain spherical shape, as seen in Fig IV-7A. The size of these spheres is close to that evaluated by DLS. At a soft particle volume fraction of 0.2, the hard particles are still apparent as undeformed spheres, held together by a "glue" of deformed soft particles, as seen in Figure IV-7B. At Φ_{soft} = 0.4 (Fig. IV-7C) and 0.6 (Fig.IV-7D), further soft particle coalescence can be seen. The most striking feature of these images in blends is the presence of bumps which appear larger than the size of either of the individual hard or soft particles. This may be formed by clustering of certain number of soft and hard particles. Because the bumps are quite smooth and resemble boulders more than spheres, it is reasonable to suppose that they are formed by coalescence of soft particles over the underlying hard particles. This idea is supported by the observation that as the hard particle volume fraction is decreased, the number of bumps also decreases, as seen in the image for a Φ_{soft} = 0.8 film (Fig. IV-7E). With pure soft latex, we observe that the particles have deformed into polyhedral structure with high degree of ordering, as shown in Fig IV-7F.

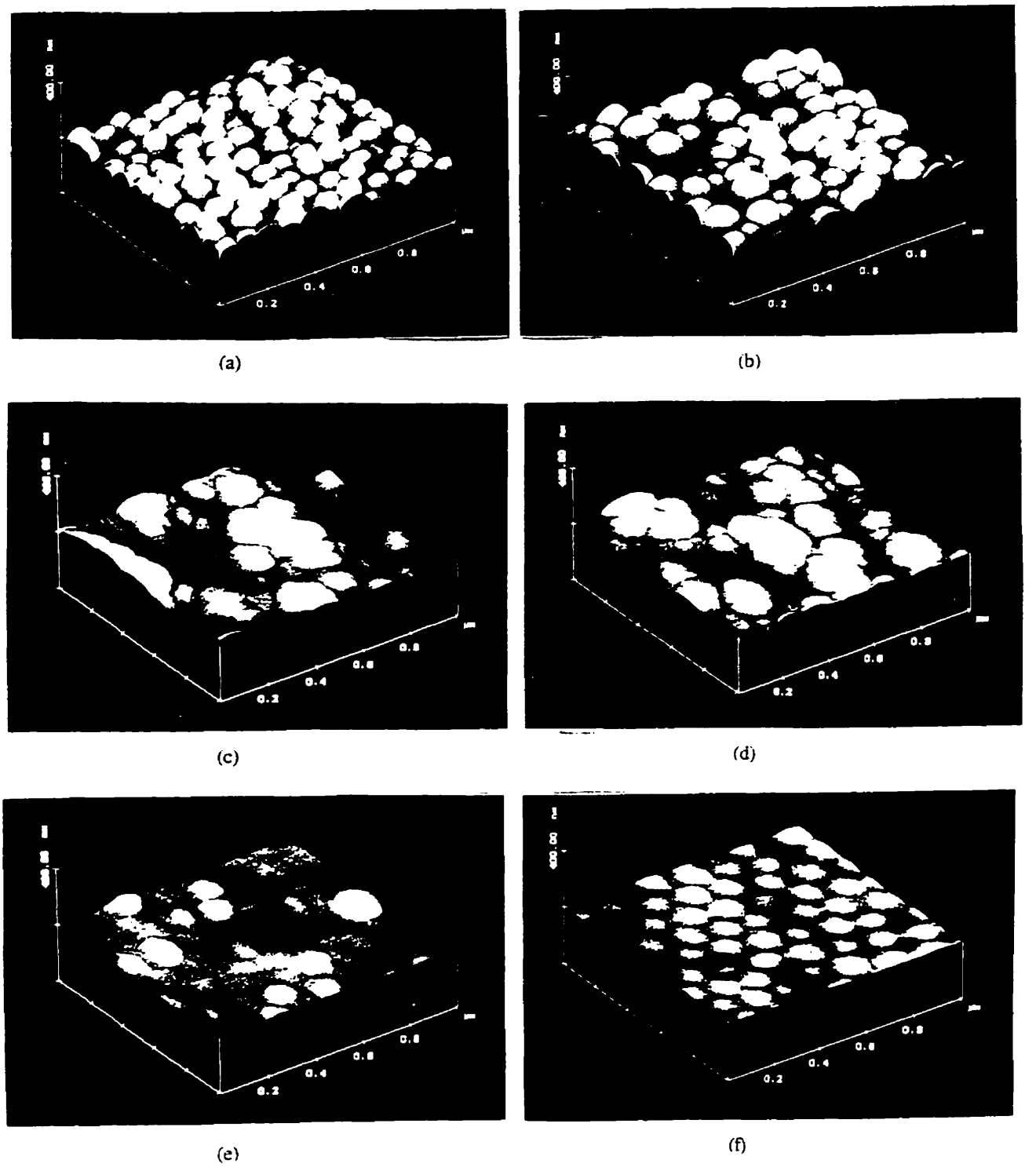

Figure IV-7. AFM images (3-dimensional, 1 μm x 1 μm x 400 nm) of the surface of blends of high Tg and low Tg P(MMA-co-BA) samples (both d ≈ 110 nm) with compositions of Φ_{soft} = (A) 0, (B) 0.2, (C) 0.4, (D) 0.6, (E) 0.8, and (F) 1.0, respectively.

The AFM surface images correlate with the phase diagram shown in Fig. IV-3B. In the sample of Φ_{soft} = 0.2 film, void spaces between hard particles are apparent, suggesting the presence of extensive voids within. The phase diagram indicates a transition to void-free films at Φ_{soft} = ca. 0.5. In the AFM images of the Φ_{soft} = 0.4 and Φ_{soft} = 0.6 films, possible voids between particles are much harder to discern. The film surfaces are not very smooth, although the roughness is on the order of a particle diameter. If there is clustering of the higher Tg latex in the sample of Φ_{soft} = 0.5, this would be unlikely to lead to turbidity because of the very small difference of refractive indices between the two polymers. In the sample with Φ_{soft} = 0.8, the soft polymer forms the matrix. There are no voids, and the hard particles are well dispersed.

IV-3-2-4 Morphology Evolution upon Annealing

The preceding discussion treats the latex film morphology as though it is fixed at close contact, and that no subsequent rearrangement can occur. One reason we chose the Tg of the soft component as a variable was to look for morphology evolution in the film. Another way to accelerate changes within the film is through annealing. We have carried out a limited number of experiments involving sample annealing at 100 °C, just below the Tg of the PMMA microspheres, and at 140 °C, above its Tg.

Upon annealing at 100 ^{o}C for 2 hours, we see that for the film of 1 : 1 blend of d_{hard} = 110 nm and d_{soft} = 55nm (very similar to the sample in Figure IV-4) the population of hard particles on the film surface become much smaller, probably due to the preference of the soft polymer to move to the surface. Interestingly, the hard particles remaining on the surface tend to form small clusters but do not undergo fusion (Fig. IV-8A). Here the annealing temperature was not high enough to allow the PMMA particles (Tg=105 ^{o}C) to deform or to fuse with each other. When a similar film was annealed at 140 ^{o}C for 16 hours, we observe that the hard particles have coalesced, forming clusters up to several micrometers in size (Fig. IV-8B). These films exhibit varying degrees of turbidity.

From these experiments we learn that while initial film morphology is dominated by processes that occur in the dispersion, the film that is produced can rearrange, and phase separation of the components can occur. From a practical point of view, one ought to be able to suppress this rearrangement by cross-linking the continuous low Tg phase subsequent to film formation. Some current coatings technologies make use of this concept. We will present our strategies for latex film crosslinking in Chapter VII.

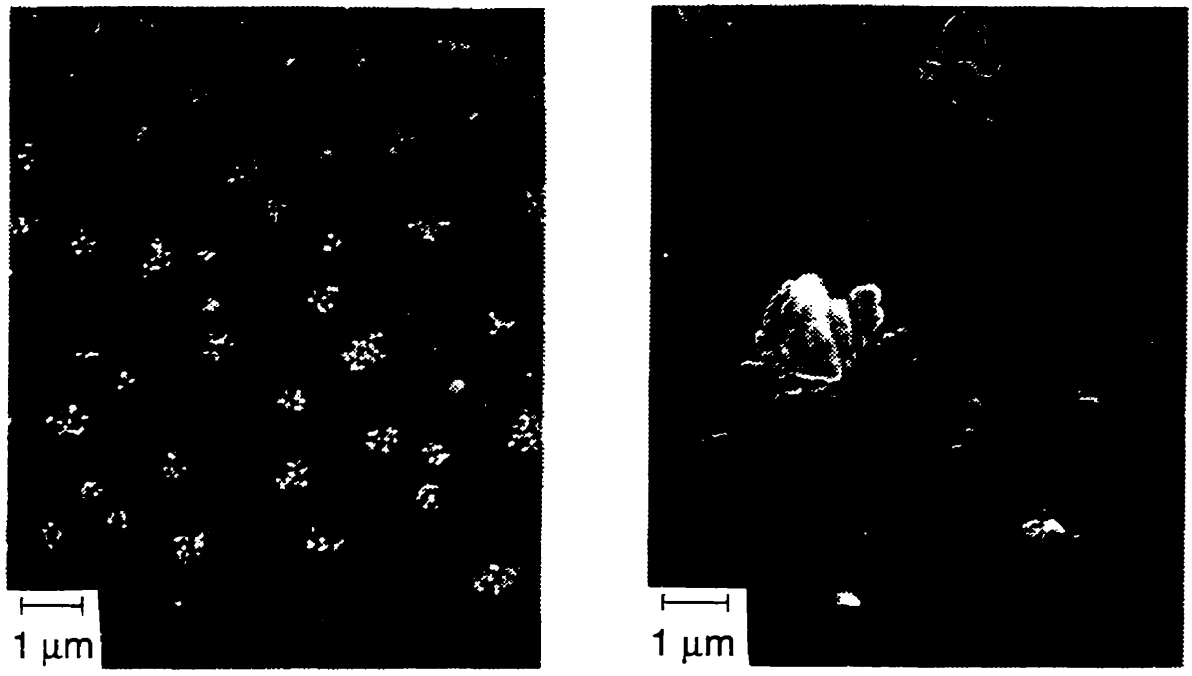

Figure IV-8. Redistribution of particles for 1 : 1 blend films after annealing under different conditions: (A) 100°C, 2 h and (B) 140°C, 16 h. The films were prepared with d_{hard} = 110 nm, d_{soft} = 55 nm, and Tg_{soft} ≈ 5.1°C.

IV-3-3 Mechanical Properties

One of the reasons that latex blend films represent a useful strategy for zero VOC coatings is that the films have enhanced mechanical properties. There appears to be a strong interaction between the hard latex and the soft matrix, which gives useful mechanical coupling between them. In this section, we examine briefly the nature of this interaction.

Blend films of PMMA and P(BMA-co-BA) were investigated by dynamic mechanical analysis (DMA). Figure IV-9A shows a typical result for a blend film sample with Φ_{hard} = 0.5. We show changes in the storage modulus E', the loss modulus E", and loss tangent (tanδ) vs. T (°C). The first transition, characterized by the sharp decrease of E', and peaks for E" and tanδ at about -10 °C, reflects the glass transition of the soft component. The second transition occurs at T > 110 °C, where the PMMA hard particles begin to soften, and the composite starts to flow. The most interesting information comes from comparing samples with different blend

compositions. For this purpose, in Figure IV-9B we plot the storage modulus vs. temperature for film samples with Φ_{hard} = 0, 0.25, and 0.50, respectively.

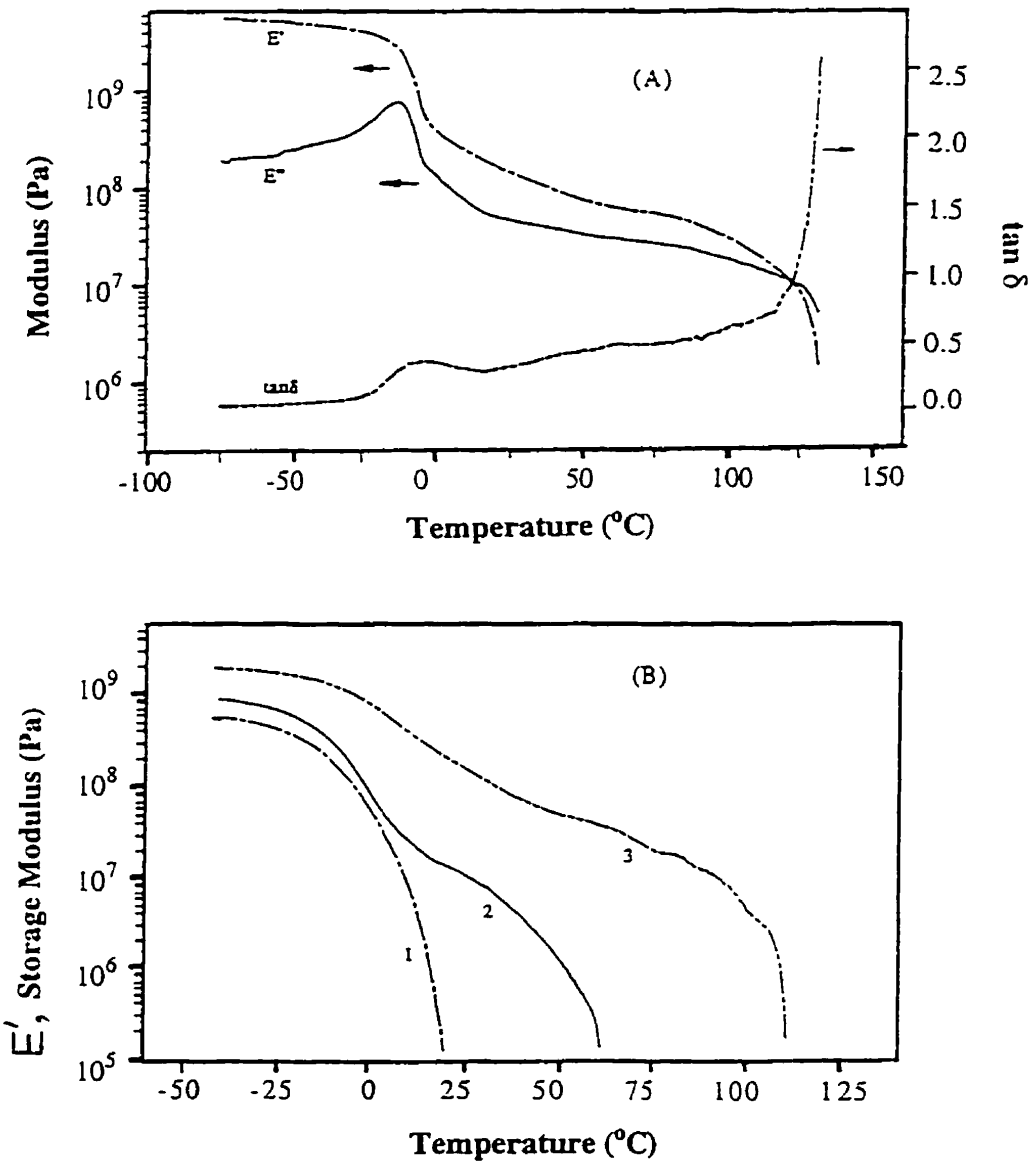

Figure IV-9. Dynamic mechanical analysis of latex films composed of 110 nm PMMA particles and P(BMA-co-BA) soft polymer: (A) Log plots of E', E" and tanδ versus T under controlled-strain conditions (strain 0.04%, frequency 1 Hz) for a blend film of Φ_{hard} = 0.5; (B) Log plots of the dynamic storage modulus (E') versus temperature (strain 0.025%; frequency 1 Hz) for blend films of Φ_{hard} = 0 (curve 1), 0.25 (curve 2), and 0.50 (curve 3), respectively.

There are several noteworthy features in Figure IV-9. First, we see that the overall film modulus is significantly increased when the soft polymer is blended with the hard latex. Second, the high modulus region of the DMA spectrum extends to a much higher temperature when the hard component is present. In addition, the glass transition of the soft component becomes broader and shifts to higher temperature when the amount of hard particles increases, indicating that the physical properties of the soft polymer itself have been modified due to the interaction with the hard particles. These results are of particular importance for the use of latex blends in coatings. These dispersions form films at room temperature without the need for any coalescing aid, yet the films that form have a much higher modulus at room 22°C (E' on the order of 10^8 Pa) than the low Tg latex polymer.

The dynamic mechanical properties of these latex blend films resemble those of polymers compounded with inorganic filler.[18,19] Physical models[20,21] of polymer/filler systems invoke the idea that a layer of soft polymer adjacent to a hard surface becomes stiffer. NMR studies [22,23] reveal that there is a reduction of molecular mobility of the soft polymer adjacent to the filler particles that causes the shift of glass transition position and the increase of the modulus of the matrix. When the volume fraction of hard particles increases, the fraction of soft component that is influenced by the hard particles increases, and the effect of reinforcement becomes more pronounced.

Table IV-3 shows the results of block resistance tests for blend films of different compositions. We see that the pure soft latex films have very poor block resistance, while blending 25% or higher amount of PMMA particles increases the block resistance to a high degree. The degree of block resistance 10 indicates that the blend films are not sticky. The pencil hardness tests give the same trends: blending the soft latex with a hard latex increases the film hardness significantly.

Table IV-3. Block resistance Vs. blending composition in PMMA and P(BMA-co-BA) blend films

PMMA (110 nm) + P(BMA-co-BA) (38 nm, Tg = 4.1 °C)			
Φ_{hard}	0	0.25	0.50
Block resistance	0-2	~8	10
PMMA (110 nm) + P(BMA-co-BA) (43 nm, Tg = -33 °C)			
Φ_{hard}	0	0.25	0.50
Block resistance	0	6-8	10

The PMMA particles in the soft polymer matrix act as reinforcing filler in our blend films. They increase the modulus, the hardness and the block resistance of these films. This effect is rather remarkable, considering that there is no obvious source of chemical interaction between the components, as one would have between an acrylate polymer and a silica or TiO_2 surface. There seems to be strong interactions at the interfaces between these dissimilar polymers which provide a significant adhesion.

IV-4 SUMMARY

Polymer blend films were prepared by air drying of dispersions containing mixtures of hard and soft latex particles. At least one soft latex is required so that coherent films can be formed at room temperature. The soft latex particles undergo complete coalescence and serve as a binder for the high Tg latex. Images by FFTEM and SEM show that in these films the hard particles retain their spherical shape and original size and are surrounded by the deformed soft particles after film drying. When the hard particles are very uniformly distributed in the soft polymer matrix, the films are transparent; when they aggregate, turbid films are obtained. The factors that affect film clarity appear to operate in the concentrated dispersion before the particles are forced into close contact by evaporation of water.

The formation of transparent films is ultimately governed by a phase diagram. Dispersions which contain an excess of hard particles do not form transparent films. There is a critical volume fraction of soft polymer Φ_c above which clear films will be obtained. Φ_c is an important parameter for characterizing film formation from binary or multicomponent latex systems.

In these blend films, the hard particles in the soft polymer matrix act as a reinforcement filler and provide a remarkable improvement in the mechanical properties of the films formed. They significantly increase the modulus, the hardness and the block resistance for the coated films.

CHAPTER V INTERFACE CHARACTERIZATION IN BLEND LATEX FILMS BY DIRECT NON-RADIATIVE ENERGY TRANSFER

V-1 INTRODUCTION

V-1-1 Direct Non-radiative Energy Transfer

Direct non-radiative energy transfer (DET) involves the transfer of the excited state energy from a donor (D) molecule to an acceptor (A) molecule through resonant coupling of the transition dipoles.[1] Because of this energy transfer the decay rate of the excited donors is increased. Figure V-1 shows the decay paths of an excited donor. When there is no acceptor, the donor will decay to ground state through fluorescence emission with a rate constant k_f and by other non-radiative paths with a rate constant k_{nr}. In this case the time-resolved decay of donor fluorescence $I_D(t)$ will follow a single exponential decay law as shown by Eq.(V-1).

$$I_D(t) = A \exp(-t/\tau_D^{\circ}) \qquad (V\text{-}1)$$

where $\tau_D^{\circ} = 1/(k_f+k_{nr})$ is the fluorescence lifetime of the donor in the absence of acceptor. When acceptor molecules are present, the excited donor molecules can transfer their energy to acceptors with a rate $\omega(r)$.

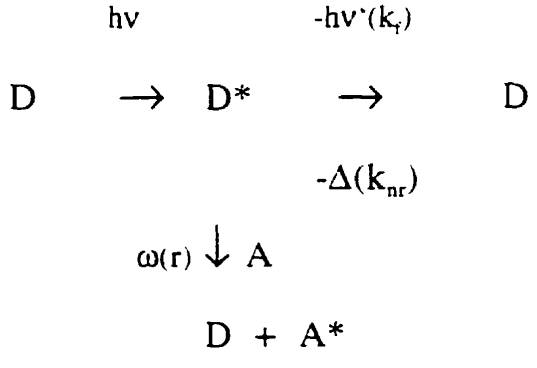

Figure V-1 The deexcitation pathways of an excited donor (D) in the presence of an acceptor (A) chromophore.

The rate of energy transfer $\omega(r)$ depends on the extent of overlap of the emission spectrum of the donor with the absorption spectrum of the acceptor, the relative orientation of the D and A transition dipoles, and the distance r between these molecules.[2] For the simple case of donor-acceptor pairs being separated by a fixed distance r, the rate constant of energy transfer $\omega(r)$ from a specific donor to an acceptor is given by[2,3]

$$\omega(r) = 1/\tau_D^{\circ} (R_o/r)^6 \qquad \text{(V-2)}$$

where τ_D° is the lifetime of the donor in the absence of acceptor, and R_o is a characteristic distance, the Förster distance, at which the efficiency of energy transfer is 50%,[2] i.e. the transfer rate $\omega(r)$ is equal to $1/\tau_D^{\circ} = (k_f + k_{nr})$. R_o is defined by

$$R_o^6 = [9000 (\ln 10) \kappa^2 \phi^{\circ}_D / (128\pi^5 N_A n^4)] \int_0^{\infty} F_D(\nu) \varepsilon_A(\nu) d\nu / \nu^4 \qquad \text{(V-3)}$$

where ϕ°_D is the quantum yield of donor fluorescence in the absence of acceptor, n is the refractive index of the medium, N_A is Avogadro's number, $F_D(\nu)$ is the corrected fluorescence intensity in the wave number range ν to $d\nu$, with the total intensity normalized to unity. $\varepsilon_A(\nu)$ is the extinction coefficient of the acceptor at ν, and κ^2 is a factor describing the relative orientation of the transition dipoles of the donor and the acceptor. The integral here expresses the degree of spectral overlap between the donor emission and the acceptor absorption.

The quantum efficiency of energy transfer Φ_{ET} is defined by[1]

$$\Phi_{ET} = \omega(r) / [k_f + k_{nr} + \omega(r)] \qquad \text{(V-4)}$$

In the above expressions, we consider D-A pairs separated by a fixed distance. In this case, a single transfer rate $\omega(r)$ is found and, as a consequence, the decay of fluorescence intensity will be exponential, but with a lifetime $\tau_D = 1/[k_f + k_{nr} + \omega(r)]$ shorter than the unquenched lifetime $\tau_D^{\circ} = 1/[k_f + k_{nr}]$. In cases where D and A molecules are separated by a distribution of distances, the donor fluorescence decay is no longer exponential, and more complex expressions are required. Such expressions are generally derived by integrating the transfer rate over the assumed D-A distribution.

The quantum efficiency of energy transfer (Φ_{ET}) is frequently calculated, in the case of steady-state measurements, from the relative fluorescence yield as [1]

$$\Phi_{ET} = 1 - I_D / I_D^{\circ} \qquad \text{(V-5)}$$

where I_D, I_D° are the intensities of donor fluorescence in the presence and absence of acceptors, respectively. For the time resolved donor decay through δ-pulse excitation, the Φ_{ET} is expressed by the integrals of the decay function $I_D(t)$ as [1]

$$\Phi_{ET} = 1 - [\int_0^\infty I_D(t)\,dt] / [\int_0^\infty I_D^\circ(t)\,dt] \qquad \text{(V-6)}$$

where $\int_0^\infty I_D^\circ(t)dt = \tau_D^\circ$. The integral of the donor emission, $\int_0^\infty I_D(t)dt$, can be evaluated from the areas obtained experimentally under the donor decay curves (normalizing the decay curves at decay time zero), giving

$$\Phi_{ET} = 1 - Area_D / Area_D^\circ \qquad \text{(V-7)}$$

where $Area_D$, $Area_D^\circ$ are the areas under the normalized decay curves of donor fluorescence in the presence and absence of acceptor, respectively.

An important factor which affects the rate and hence the efficiency of energy transfer is the orientation factor κ^2. κ^2 is generally assumed to be 2/3 for mobile, randomly distributed D and A molecules, and 0.475 for immobile, randomly distributed dyes.[1,4]

The distance dependence of DET also leads to its dependence on the concentration and concentration distribution of dye molecules in the system. A reference concentration C_{A_0} is often used signifying the concentration of acceptor molecules at which an acceptor molecule is expected to be found inside a sphere of radius R_0 and is given by [2-4]

$$C_{A_0} = 3000 / (2\pi^{3/2} N_A R_0^3) \qquad \text{(V-8)}$$

V-1-2 Interface Characterization by DET

DET is a powerful technique for studying morphology and dynamics in solid materials, particularly for looking at events occurring at interfaces in these systems. It involves energy transfer from excited donors to acceptors when they are sufficiently close, usually in the interfacial region between the donor- and acceptor-containing phases. When all the donors in a system can be considered equivalent, the kinetics of excited donor decay can be described by the Klafter-Blumen expression.[3] This equation applies to infinite media, where the donors are related by translational equivalence, and to restricted geometries such as the surface of a small sphere, where donor positions are related by symmetry. The term restricted geometry refers to a confining space with at least one dimension on the order of R_0, the characteristic distance for energy transfer to take place. This model has been used to fit experimental fluorescence decay curves obtained from systems in which the donor and acceptor dyes are adsorbed to silica[3b] or polymer latex[5] microspheres. Such types of analyses provide information about the surface

structure (dimensionality or roughness) of the inorganic or polymeric particles in their colloidal dispersions. It has also been applied to the study of interfaces in block copolymer melts.[6]

In many applications, the dyes have a rather complicated distribution and the requirement for donor equivalence is not met. An example is the study of molecular mixing in polymers to learn about compatibility in blends[7] and polymer diffusion in homopolymer films,[8] where the donors and acceptors are distributed with a concentration gradient near the interfacial region.

One can use two types of strategies to study interfaces by DET in a system with a complex spatial distribution of dyes. One can derive a new model of the fluorescence decay function which reflects the details of the distance distribution between all the D-A pairs in the system. Alternatively, one can choose simple parameters which characterize the extent of energy transfer to analyze aspects of the structure of the system. For example, the quantum efficiency of energy transfer (Φ_{ET}) can be used to characterize the amount of DET, and this amount should be related to the interface thickness between phases labeled with D and A, respectively, when appropriate sample structure is designed.

V-1-3 Latex Films

We are concerned with DET measurements to obtain information about the interface structure and its evolution in latex films. The films consist of mixtures of latex particles labeled covalently with a small amount of donor and acceptor, respectively. In newly formed films, the donors and acceptors are isolated in separate domains (particles), presumably without any significant interpenetration. Even under this condition, each donor near the interface is affected by acceptors in the neighboring domain to a degree that depends on the distance of their separation. As we will show in this chapter, a certain amount of energy transfer can be observed across a sharp interface separating two polymer phases labeled with donors and acceptors, respectively. Upon annealing, polymer interpenetration occurs, accompanied by the increase in intimacy between the donors and acceptors and hence the growth in efficiency of energy transfer.

An important quantity to determine in the above-mentioned systems is the extent of energy transfer occurring across a sharp interface, where donors and acceptors are intimate enough to undergo DET but are located in separated phases. For polymer diffusion, this is the starting condition of the process, and proper determination of DET is important for characterizing the subsequent processes of diffusion. We choose a model system in which the donors and acceptors labeling the polymer chains are separated into two phases by a sharp interface. This was achieved by preparing polymer films from aqueous dispersions of donor-labeled hard particles and acceptor labeled soft particles. The soft latex particles (e.g. acceptor-labeled), having a polymer Tg below room temperature, deform during drying to form a continuous phase.

The hard particles (e.g. donor-labeled) are dispersed in the soft polymer matrix. The hard polymer has a Tg well above room temperature and, hence, no large-scale chain motion is possible in the formed films. For this reason, we anticipate very limited interpenetration between the two polymer components. Thus this system represents a good model for us to measure the amount of energy transfer across a sharp interface.

V-2 EXPERIMENTAL

We choose poly(methyl methacrylate) [PMMA] as the high Tg latex sample, and poly(butyl methacrylate-co-butyl acrylate) [P(BMA-co-BA)], as the low Tg sample. The PMMA particles were labeled with a fluorescent donor, phenanthrene (Phe), and P(BMA-co-BA) with an acceptor, anthracene (An), or *vice versa*. These labeled samples were all synthesized by two-stage semi-continuous polymerization, as has been described in Chap. II and previously.[9] Both labels have a concentration of 1 mol% (with respect to the base monomer units) in the polymers. By gel permeation chromatography (GPC) analysis, we find that the dyes (e.g. Phe and An) can be randomly distributed in the polymer chains.[10] Due to the uniformity and the low content of dye labeling, we believe that within each particle the dyes are randomly distributed in space. The GPC measurements also give the molecular weight and molecular weight distribution of the polymers, relative to PMMA standards. The particle diameters of various labeled PMMA samples prepared range from 45 to 165 nm with narrow size distributions, as evaluated by dynamic light scattering (DLS). The sizes of some of the hard latex samples were also confirmed by scanning electron microscopy (SEM). The labeled soft latexes have sizes of 50-55 nm and Tg values in the dry state of 5-10 °C. The Tg values were evaluated with a differential scanning calorimeter (DSC). The characteristics of latex particles used are listed in Table V-1. In many cases, the latex dispersions were treated with an ion exchange resin to remove the surfactant, sodium dodecyl sulfate, and other ionic substances before use in film formation.

Table V-1. List of Latex Characteristics

Sample	PhePMMA				AnPMMA	Phe-Soft	An-Soft
Diameter (nm)	160	110	65	45	110	55	50
Polydispersity	0.01	0.01	0.01	0.01	0.01	0.08	0.08
Tg (°C)	-	105	-	-	-	5.1	9.9
Mw ($\times 10^{-5}$)	-	2.1	5.6	4.6	2.1	5.1	1.1
Mw/Mn	-	2.3	2.0	3.7	3.1	5.5	6.9

The polymer films were formed by spreading mixed dispersions of the labeled hard and soft latex particles onto quartz plates, followed by air drying at room temperature. We have found that transparent, coherent films can be formed at room temperature from the mixtures of these two types of latex particles.[9,11] Some films were annealed for a certain time at 70, 100 and 140 °C, respectively.

Fluorescence decay profiles were measured at room temperature by using the time-correlated single-photon-counting technique. Samples were excited at 298 nm, and the emission was detected at 366 nm. A bandpass filter (320-390 nm) was mounted between the sample and the phototube detector to minimize the scattered light and the interference due to possible fluorescence from directly excited acceptors. The donor decay data were collected over four decades of decay. These measurement conditions were similar to those in the previous work on poly(butyl methacrylate) films.[8]

The energy transfer efficiencies, Φ_{ET}, were calculated from the areas under the normalized decay profiles. To obtain accurate areas, we fit each experimental decay profile to a mathematical function, and then integrated the function. In most cases, a function in the form of $I_D(t) = A_1 \exp(-t/\tau_D^\circ) + A_2 \exp[-t/\tau_D^\circ - p(-t/\tau_D^\circ)^{1/2}]$ gives satisfactory fits. Data were fitted by nonlinear least squares using the mimic lamp method. A small correction due to scattered light was introduced in the fitting. The goodness of the data fitting to a selected decay function was determined by chi-square (< 1.2 for most of fits and not >1.4 for other fits).

Data were also analyzed in terms of donor lifetime distributions using the Maximum Entropy Method (MEM) using software supplied by PTI Co., Canada. The method uses a series of exponentials (up to 100 terms) as a probe function with fixed, logarithmically-spaced lifetimes and variable pre-exponential amplitudes. By fitting to a decay profile, the lifetime distributions of the system are recovered.

V-3 RESULTS AND DISCUSSIONS

V-3-1 Energy Transfer Across An Interface

We begin by considering the structure as shown in Figure V-2. The system brings into contact two polymer phases: one labeled with a fluorescent donor (D) in a spherical particle, and another labeled with an acceptor (A) as the imbedding medium. Following excitation of the donors (at 298 nm for Phe), energy transfer from donors to acceptors will take place across the interface between the phases. The efficiency of DET is related to the interfacial area relative to the volume of the labeled phases, and also to the extent of phase penetration, if any.

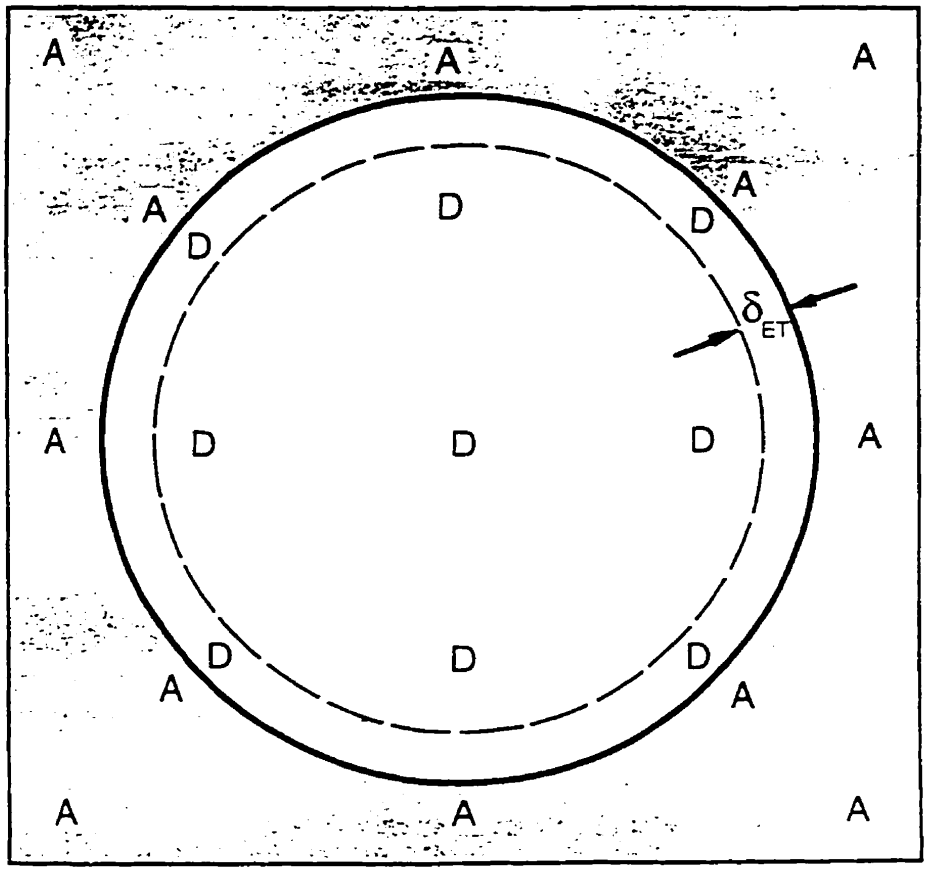

Figure V-2. A cartoon showing the interfacial contact between a donor-labeled sphere and an acceptor-labeled matrix phase. Energy transfer will take place between the D and A located near the interfacial region. The effective distance (δ_{ET}) within which DET takes place is also shown.

In our latex blend systems, we either labeled PMMA particles with an energy donor (Phe), and P(BMA-co-BA) particles with an energy acceptor (An), or *vice versa*. Blend films were formed from these two types of particles with various compositions. Energy transfer between Phe donors and An acceptors can occur when they are sufficiently close (ca. 2 nm).[4,8] We use the quantum efficiency of energy transfer (Φ_{ET}), measured from the fluorescent decay profiles, to quantify the amount of DET and to characterize the interface.

V-3-1-1 Varying blend composition and hard particle size

To form a coherent blend film, it is essential that soft particles deform to form a continuous phase, and that the hard spheres be well dispersed in the soft matrix. Clusters of hard spheres can generate microscopic voids, and if these voids are significantly large they can scatter visible light to give turbidity or create large cracks due to weak adhesion. The probability that hard particles encounter each other in the system is strongly dependent on the number fraction of hard particles, and hence the blend composition and hard particle size. The existence of local clustering of hard spheres will reduce the interfacial area between the hard sphere and the soft matrix, and this should be in principle reflected in the energy transfer signal. On the other hand, when the hard particles are well dispersed in and fully surrounded by the soft polymer matrix, we anticipate a finite amount of observable ET. To test this idea, we prepared blend films consisting of An-labeled soft particles (50 nm before film formation) and Phe-labeled hard spheres of various diameters ranging from 45 to 160 nm, with various blending compositions. Fluorescence energy transfer analysis was carried out for these films.

Figure V-3 shows donor fluorescence decay profiles for blend films with different volume ratios of acceptor-labeled soft polymer to donor-labeled hard particles (V_A/V_D or V_{soft}/V_{hard}) and with various diameters of donor-labeled hard particles (d_D). In Figure V-3(a) we show the profiles for films with d_D = 160 nm. The uppermost line (line 1) corresponds to a film formed with donor-labeled hard particles and non-labeled soft particles. A straight line is obtained for this film with donor labels only. This is also found in films with other sizes of donor-labeled hard spheres in the absence of acceptors. The donor lifetimes, obtained from exponential fits from various samples, varied in a narrow range of 43.0 to 43.5 ns. These values are also close to those previously found in our lab or reported in literature. Curve 2 and 3 are for films with V_A/V_D = 1 and 3, respectively. One sees that there is a small amount of ET occurring in these two films, indicated by their slightly steeper decay curves. The decay profiles of these two films essentially overlap, with very similar Φ_{ET} values (Table V-2). A similar phenomenon is seen in films with d_D = 110 nm [Figure V-3(b)] when varying V_A/V_D from 1 to 4. This indicates that when the hard particles have a size of 110 - 160 nm, at V_A/V_D = 1, the interfacial contact area between the two polymer phases has already reached a finite value, so that the amount of ET is close to that for the film with a much greater V_A/V_D Another finding here is that the ET efficiency is independent of the volume of acceptor-labeled soft polymer phase when V_A/V_D exceeds certain value.[12]

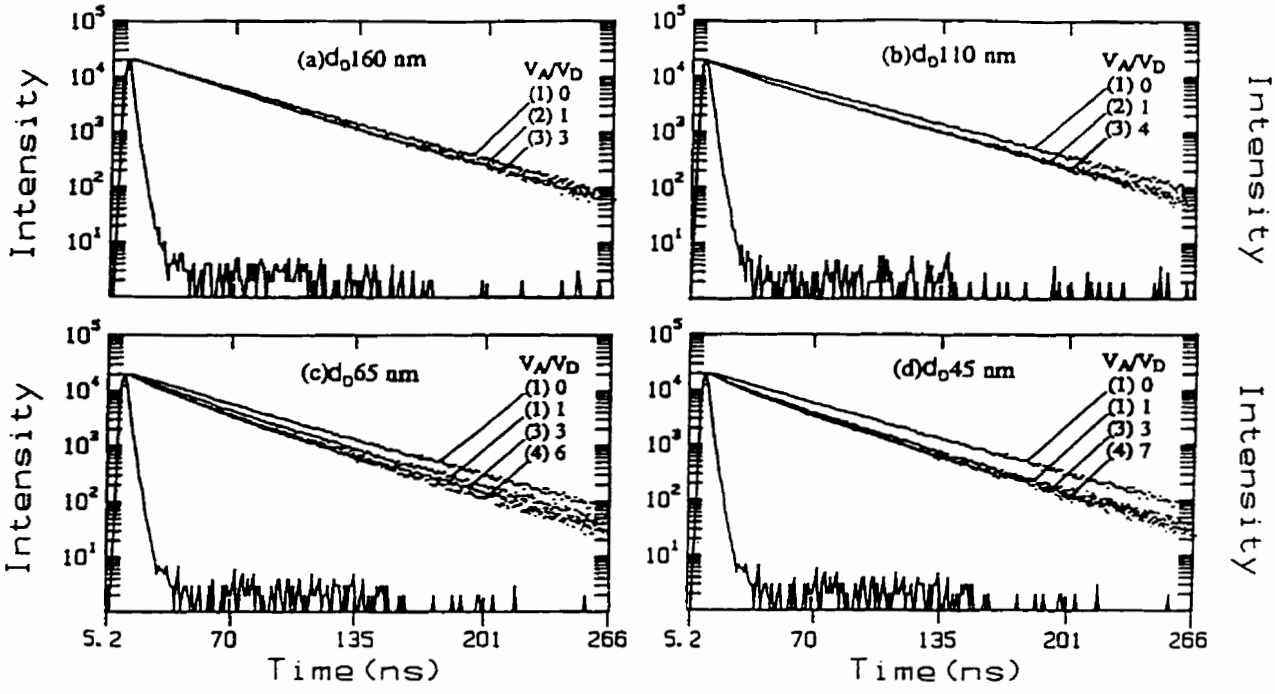

Figure V-3. Donor fluorescence decay profiles for latex blend films with various volume ratios of acceptor-labeled soft polymer to donor-labeled PMMA (V_A / V_D). The diameters of the D-labeled hard particles (d_D) are (a) 160, (b) 110, (c) 65, and (d) 45 nm, respectively.

Table V-2. Areas under donor decay curves ($Area_D$) and Φ_{ET} values for blend films consisting of An-labeled soft particles and Phe-labeled hard particles of various diameters (d_D) with various blending compositions (V_A/V_D)

d_D (nm) / V_A/V_D	160		110		65		45	
	$Area_D$	Φ_{ET}	$Area_D$	Φ_{ET}	$Area_D$	Φ_{ET}	$Area_D$	Φ_{ET}
0	43.5	0	43.5	0	43.1	0	43.1	0
1	38.4	0.12	37.1	0.15	31.4	0.27	28.1	0.35
3	37.7	0.13			27.3	0.37	25.3	0.41
4			36.0	0.17				
6					26.4	0.39		
7							24.4	0.43

When the hard spheres have smaller sizes (e.g. 65 and 45 nm), the differences in the amount of energy transfer between films of $V_A/V_D = 1$ and films of $V_A/V_D \approx 3$ are much more pronounced, as seen in the curvature in early times of the decay profiles in Figure V-3(c) and (d) and in the Φ_{ET} values in Table V-2. This indicates that as the size of hard spheres decreases, more soft particles are needed to fully surround the hard ones. With further increasing V_A/V_D from 3 to 6 or 7, the increase in energy transfer signal is not significant (Table V-2), indicating that nearly a saturated contact between the phases has been reached when V_A/V_D is close to 3.

The above results must be related to how the hard spheres are distributed in the film and how the soft polymer flows to bind the hard spheres. We need to point out that in the above film samples the surfactant originally present in the dispersions is removed. We have reported previously that in films formed from surfactant-containing dispersions the hard spheres of similar size (45 - 110 nm) are quite uniformly distributed in the soft polymer phase, while in the absence of surfactant the tendency for them to aggregate is relatively more pronounced.[9] When the hard spheres have a high concentration (e.g. $V_A/V_D = V_{soft}/V_{hard} \approx 1$) and have a similar size to the soft ones, there may be local clusters of hard spheres in which the soft polymer is not able to fill all the interstitial space, leading to less coverage of soft polymer on the hard particle surface, as depicted in the triangle in Figure V-4a. Although the soft polymer has an ability to flow, the flow can be retarded in the channels between close-packed hard particles since a soft polymer layer on a hard surface is stiffer than in bulk.[13,14] Also, when the distances between a pair of hard spheres are less than the order of energy transfer distance, i.e. 2 nm, there will be a reduced amount of ET even when the interstitial space is filled with soft polymer.

When the soft polymer fraction is increased (e.g. $V_{soft}/V_{hard} \approx 3$), the probability of hard sphere aggregation is smaller and the soft polymer should be able to fully cover the hard surface (Figure V-4b). When the hard spheres are larger than the soft ones (e.g. 2 times), for the same volume of hard and soft particles ($V_{soft}/V_{hard} \approx 1$), one hard sphere corresponds to about ten soft particles, which should be sufficient to isolate the hard one, as depicted in Figure V-4c.

We should point out that for a transparent and mechanically coherent film, the overall extent of clustering should be low and the size of interstitial voids, if any (as shown in Figure V-4a), should be very small (e.g. less than a few nanometers). In fact, when the hard spheres are very small ($d_{hard} < 60$ nm), films with composition of $V_{soft}/V_{hard} \approx 1$ often exhibit high transparency, although from energy transfer measurements we learn that the two polymers do not achieve maximum contact. This is an indication that the energy transfer technique is very sensitive to distances of fine scale, with much higher resolution than the optical density

measurement. For many samples with d_{hard} = 110 nm, d_{soft} = 50 nm and V_{soft}/V_{hard} = 1, we find that the films show high transparency. Here the energy transfer analysis shows that the two polymer phases reach a maximum contact, indicating the formation of dense films with a good dispersion of hard spheres in the soft polymer matrix.

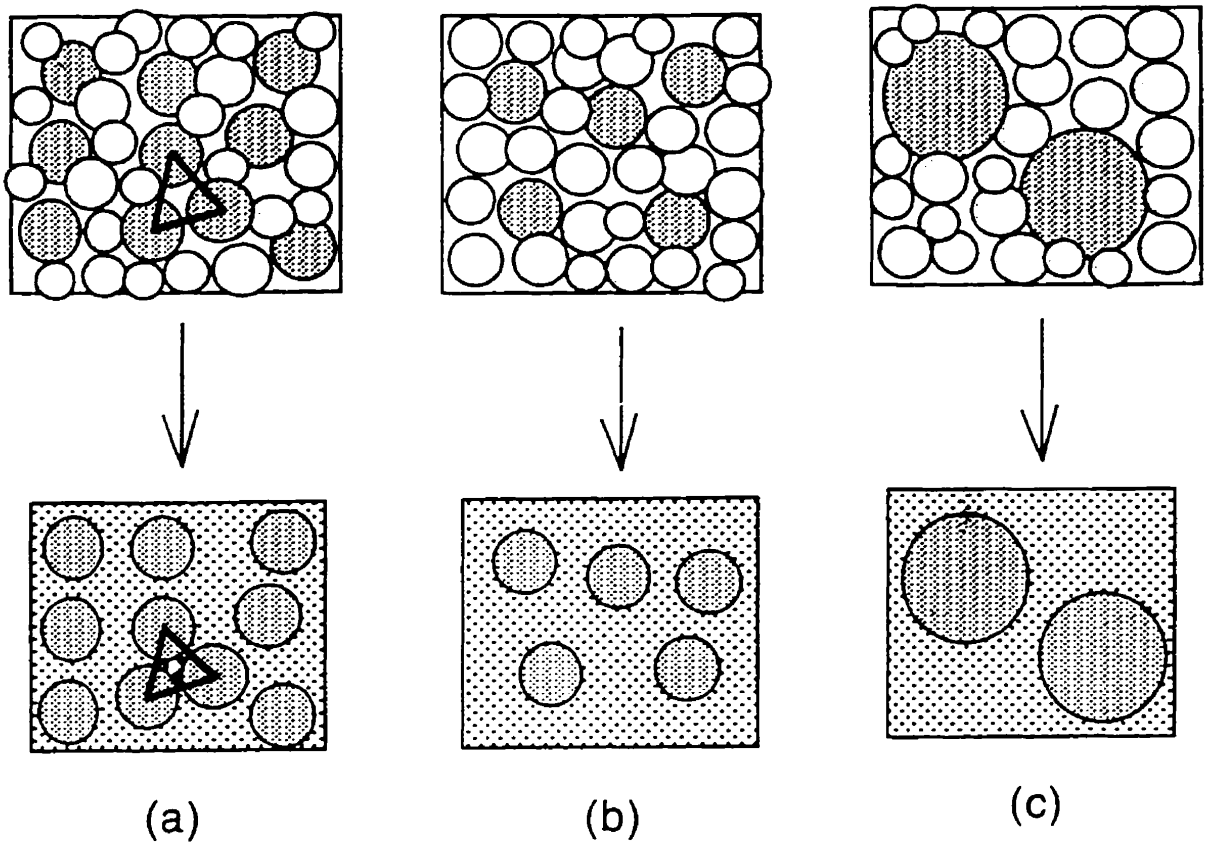

Figure V-4. A cartoon showing the extent of contact between the hard particles and the continuous soft phase. In (a) we show that when there are local clusters of hard particles and when the amount of soft polymer is not sufficient to fill all the interstitial spaces, small voids may exist in the film which lead to a reduced contact area between the two phases. In (b) we show that when the fraction of soft polymer is large, the hard spheres are isolated and fully covered by the soft polymer. When the hard particles are larger (c), for the same composition as in (a) the relative number of soft particles become much larger and are more easily able to flow to surround the hard particles.

To show the above results more clearly, in Figure V-5 we plot Φ_{ET} Vs V_A/V_D for various hard particle sizes. We did not investigate films with $V_A/V_D < 1$, since we found that as V_A/V_D (V_{soft}/V_{hard}) becomes smaller than 1, most of the films change, with a sharp transition, from clear to turbid or even powdery. Turbidity indicates the presence of large voids in the film.

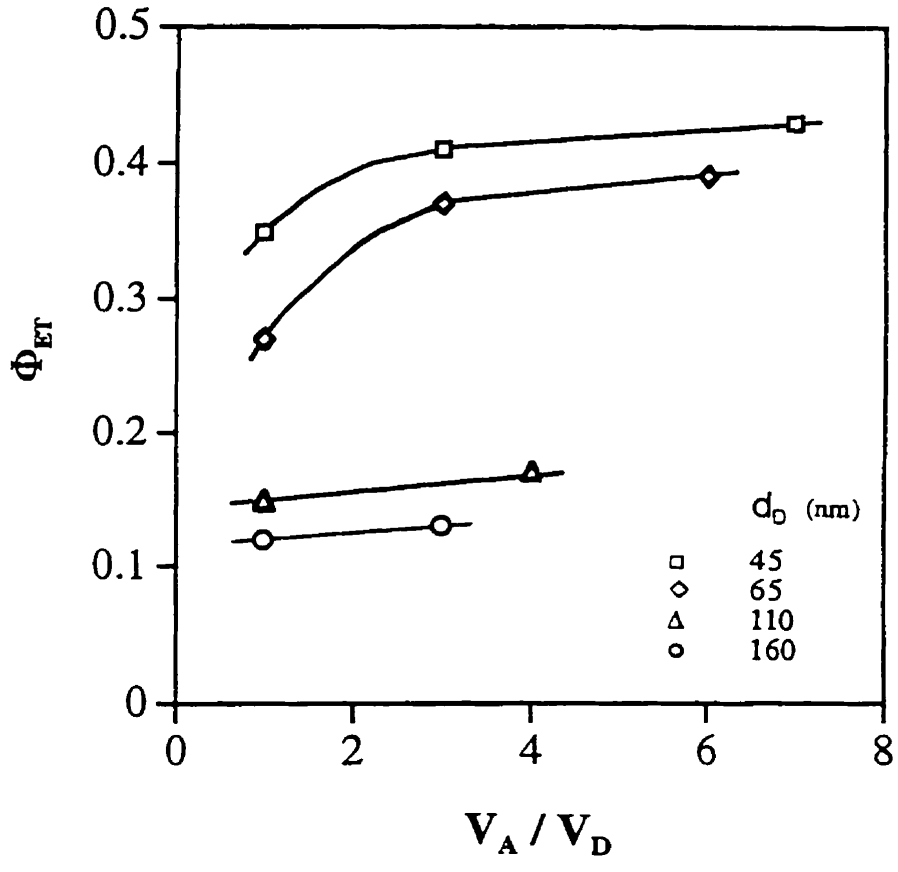

Figure V-5. Variation of extent of energy transfer (Φ_{ET}) vs composition (V_A / V_D) for blend films prepared with 50 nm An-labeled soft particles and donor-labeled hard particles having diameters of 160, 110, 65, and 45 nm, respectively.

V-3-1-2 The dependence of energy transfer on interfacial area

An interesting result here is that the amount of energy transfer clearly increases as the donor-labeled hard spheres decrease in size. The amount of DET should be related to the interfacial area between hard and soft polymer phases. We have previously established, by electron microscopy and by dynamic mechanical measurements,[9-11] that in latex blend films of the sort studied here one obtains a good distribution of hard particles in the soft polymer matrix, with intimate contact (good wetting) at the polymer-polymer surface. For a given volume of donor-labeled hard spheres, the surface area of the donor-labeled particles is proportional to $1/d_D$. In Figure V-6 we plot the values of Φ_{ET} vs. $1/d_D$, obtained from film samples prepared with different sizes of donor-labeled PMMA particles. Four samples of donor-labeled particles with

mean diameters of 160, 110, 65, and 45 nm, respectively, were used to prepare these films. Φ_{ET} values are evaluated using films with a large fraction of acceptor-labeled polymer (ϕ_{soft}). The plot of Φ_{ET} vs. $1/d_D$ is linear. We infer from this that the amount of DET is proportional to the interfacial area. This is useful because one can estimate the interfacial area of contact between the two phases of a given system by a simple measurement of Φ_{ET}

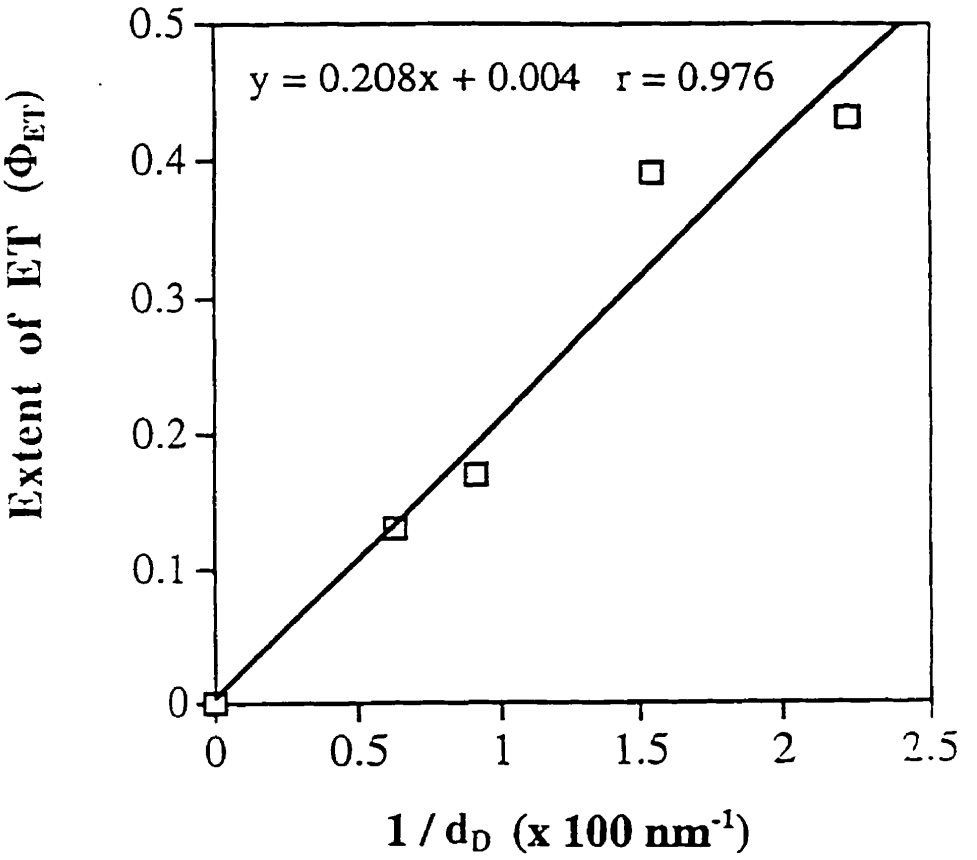

Figure V-6. A plot of Φ_{ET} for films with $\phi_{soft} \geq 0.75$ Vs. inverse of diameter of donor-labeled hard particles ($1/d_D$). The blend films were prepared with 50 nm An-labeled soft particles and donor-labeled hard particles having diameters of 160, 110, 65, and 45 nm, respectively.

An alternative way to look at the dependence of ET on hard particle size is to show the lifetime distributions of the samples studied. In Figure V-7 the lifetime distribution profiles are presented. We see in Fig. V-7a that for d_D = 160 nm, a large fraction of donors has lifetimes distributed along 40-45 ns with a small fraction having shorter lifetimes at about 20-25 ns. The small peak characterizing shorter donor lifetimes must arise from energy transfer and is not

observable for films with donors only. For d_D = 110 nm (Fig. V-7b), similar distribution behavior to Fig. V-7(a) is seen except that the second small peak seems to be shifted further to shorter lifetime (ca. 17-20 ns). When d_D decreases further to 65 and 45 nm (Fig. V-7c and 7d), the fraction of donors with short lifetimes (at 8-20 ns) increases and the lifetime distribution is also broadened, indicating that a larger number of donors are influenced by acceptors due to energy transfer.

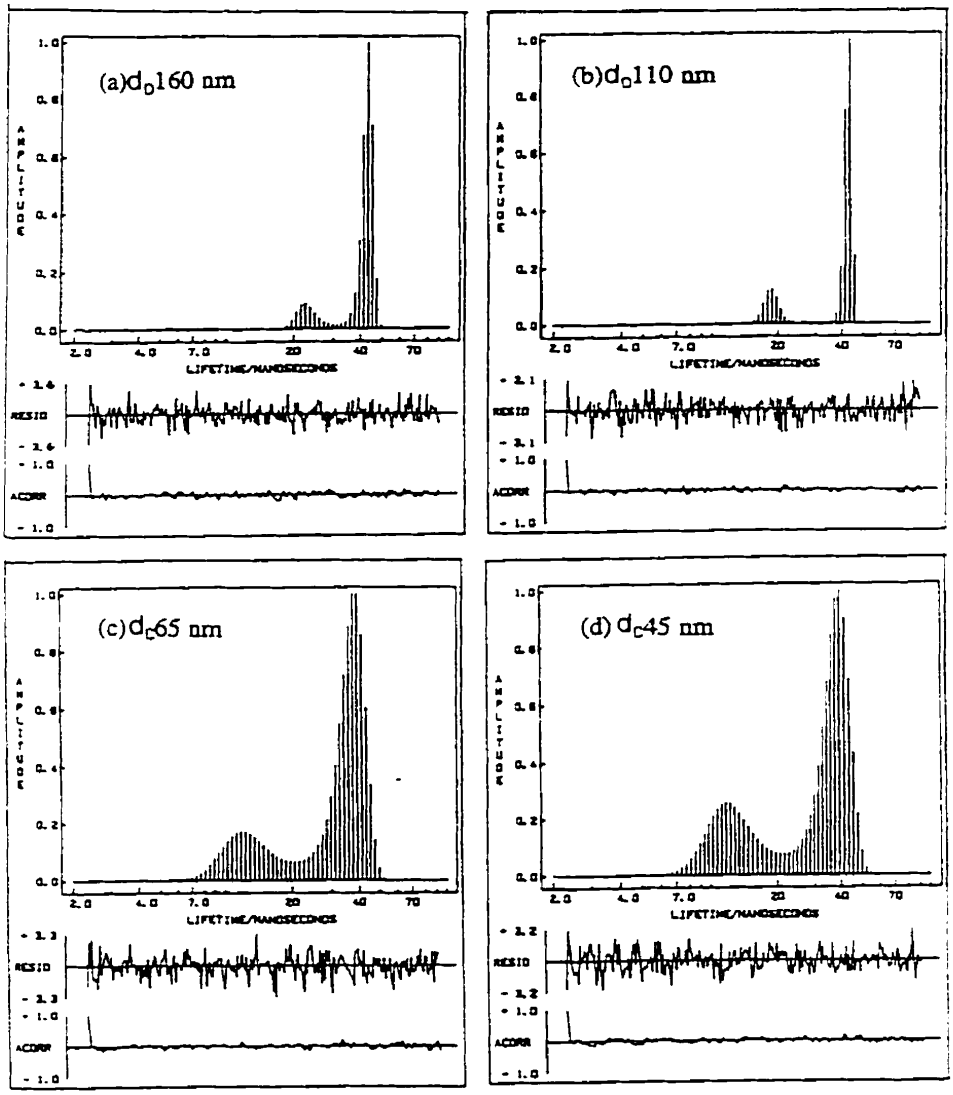

Figure V-7. Donor lifetime distribution profiles for blend films prepared with An-labeled soft polymer and donor-labeled hard particles having diameters of (a) 160, (b) 110, (c) 65, and (d) 45 nm, respectively. The blend compositions, V_A / V_D, in the samples are (a) 3, (b) 4, (c) 6, and (d) 7, respectively.

V-3-1-3 Variation of the means of labeling

To further examine the condition of contact between the hard and soft polymer phases, we chose an alternative means of labeling in the blend films. Here we labeled PMMA spheres with An acceptor, and soft particles with Phe donor. We chose PMMA spheres having size of 110 nm, since this is a size conventionally used both in scientific research and in practical applications. Films with blending composition of $V_A/V_D = V_{hard}/V_{soft} = 1$ were prepared. Four repeated fluorescence decay measurements for the films of the same composition were carried out. The areas under normalized decay curves as well as the energy transfer efficiencies calculated are present in Table V-3. We see that the Φ_{ET} values lie in a narrow range with an average of 0.14. This value is very close to that for films in which the polymer phases are reversibly labeled but are prepared with the same blending composition and hard particle size.

Table V-3. Areas under decay curves and Φ_{ET} values for 1 : 1 blend films consisting of Phe labeled soft particles and An labeled 110 nm hard particles

Sample	Phe-Soft	Phe-Soft + An-Hard (1:1)				
$Area_D$	45.0	39.2	38.8	38.4	39.3	38.9 (average)
Φ_{ET}	0	0.13	0.14	0.15	0.13	0.14 (average)

V-3-1-4 Influence of the presence of surfactant

In the above mentioned film samples, the ionic surfactant originally present in the dispersions was removed. In some other samples, the surfactant, 4-6 wt% based upon latex solids, was carried forward into the films, allowing us to examine the influence of surfactant on the extent of energy transfer in the films.

It has been pointed out that there are several possible locations in latex films in which the surfactant may be present.[15-17] Depending on the compatibility between the surfactant and the latex polymer, the surfactant may penetrate into the particles, form separated domains, be exuded onto film surface, or be trapped in the contact region between particles. We have found that part

of the SDS was exuded onto the film surface in these samples.[9] It is often reasonable to presume that part of the surfactant remain in the interparticle boundary. Fluorescence decay profiles for films with and without surfactant, respectively, were measured. The Φ_{ET} value calculated for the surfactant-containing film is indeed 30–40% smaller than that for the surfactant-free film. This difference is significant. We repeated these experiments with similar films and the same trend was found in all pairs of samples. The results are summarized in Table V-4. These results indicate that surfactant in the film decreases the contact between adjacent particles.

Table V-4. Areas and Φ_{ET} values for 1 : 1 blend films of An-labeled soft particles and Phe labeled hard particles in the presence and absence of surfactant

Sample	With surfactant			Without surfactant		
$Area_D$	39.0 [a]	39.6 [b]	39.6 [b]	37.6 [a]	38.3 [b]	38.2[b]
Φ_{ET}	0.10	0.09	0.09	0.14	0.12	0.12

a. The hard spheres have a diameter of 110 nm in these samples. b. The hard spheres have a bimodel size distribution at 100 nm and with a small fraction at 200 nm.

V-3-2 Interface Structure in Nascent Blend Films

In the nascent blend films consisting of 1 : 1 Phe-labeled soft polymer plus An-labeled 110 nm hard particles, the observed DET efficiency, Φ_{ET}, was always ca. 0.14, as shown in Table V-3. A very similar Φ_{ET} value (0.15) was found when the films were prepared with 1 : 1 An-labeled soft particles and Phe-labeled 110 nm hard particles. Moreover, the Φ_{ET} value did not change significantly when we varied the volume ratio of acceptor-labeled soft matrix to donor-labeled hard spheres (V_{soft}/V_{hard}) from 1 up to 4 (Table V-2). We also found a similar Φ_{ET} value when films were carefully prepared to avoid penetration from 1 : 12 Phe- and An- labeled poly(butyl methacrylate) latex particles of the same size (110 nm). These results indicate that in our blend films, a complete, intimate contact between the two components is achieved so that the amount of ET is not dependent on the means of labeling and the fraction of the hard spheres up to ca. 0.5. Note that Φ_{ET} will vary if we change the concentration of A in the A-labeled phase.

Φ_{ET} reflects the population fraction of dyes located in a thin layer of small volume near the interface within which ET can take place. For simplification, we define the thickness of this layer as an effective distance of energy transfer, δ_{ET} , and assume that outside of this layer the donors are not influenced by acceptors in the adjacent phase. This simple concept has been used previously,[8] and is further suggested by Dr. Ahmad Yekta. Note that this assumption ignores the dependence of energy transfer on the distribution of distances between the donors and acceptors. From a simple spherical geometric consideration (c.f. Figure V-2), the volume of this layer (V_{ET}) relative to the total volume of donor-labeled sphere (V_{total}) of diameter d_D is given by

$$V_{ET}/V_{total} = \Phi_{ET} = 6\,\delta_{ET} / d_D \qquad \text{(V-9)}$$

We have shown in Figure V-6 a plot of Φ_{ET} vs. $1/d_D$ obtained from our experiments. The slope of this linear plot, corresponding to $6\delta_{ET}$ in Eq.(V-9), gives a value of δ_{ET} = 3.5 nm.

This analysis provides a possibility for estimating the interface thickness between the two polymers of the nascent films. It has been pointed out [3] that for a given pair of dyes energy transfer can occur over a maximum separation distance, R_{max},

$$R_{max} = [3/2 \langle\kappa^2\rangle\ t_{max}/\tau_D^{\circ}]^{1/6}\ R_o \qquad \text{(V-10)}$$

where t_{max} is the maximum time to detect the donor fluorescence signal during decay, and $\langle\kappa^2\rangle$ is the orientation factor. A reasonable numerical value for (t_{max}/τ_D°), suggested by Klafter et al.[3] is 4ln10, equivalent to measuring four decades of the fluorescence decay. Considering that $\langle\kappa^2\rangle$ is 2/3 for randomly oriented, mobile dyes, and 0.475 for randomly oriented, immobile dyes in solid films, R_{max} for DET estimated from Eq.(V-10) is on the order of 1.37 R_o - 1.45 R_o. For the Phe/An pair, R_o is 2.3 nm.[4,8] Therefore in our experiments the probe distance is 3.1 - 3.3 nm.

The effective distance of energy transfer (δ_{ET}) we find in our experiments is almost equal to or only slightly larger than the maximum probe distance (R_{max}) of the dye pair used. This indicates that the energy transfer we observed can be attributed to the dyes located on the two sides of a boundary which is sharp (little molecular penetration). If there were any significant penetration (e.g. > 2 nm) between the phases, one would expect that the effective layer thickness of DET would be significantly larger than the probe distance of the dye pair.

V-3-3 Interface Evolution in Annealed Films

In these blend films containing PMMA and soft polymer (Tg < 10 °C) particles, aging at room temperature does not change the interface structure. We observe no changes of Φ_{ET}, the extent of energy transfer, over a period of months after sample preparation. To facilitate

interpolymer mixing, films were annealed at higher temperatures and their energy transfer was analyzed after cooling the films to room temperature.

Polymer diffusion only occurs at temperatures that allow the polymer chains to undergo microbrownian motion, i.e. above Tg. Here the PMMA particles have Tg = 105 °C and the soft particles have Tg < 10 °C.

In the nascent films, the value of Φ_{ET} corresponds to the ET at the boundary separating the two polymer phases. When the films are aged or annealed, the measured Φ_{ET} should reflect both the initial ET and the increase in ET due to molecular mixing upon aging or annealing. To relate the extent of molecular mixing to the ET signal, we define a parameter, f_m , the extent of mixing, or the net increase of extent of ET due to annealing (or aging) from time zero to time t_a normalized by the maximum detectable signal at full mixing,[8]

$$f_m = \frac{\Phi_{ET}(t_a) - \Phi_{ET}(0)}{\Phi_{ET}(\infty) - \Phi_{ET}(0)} \qquad \text{(V-11)}$$

f_m can be rewritten in the form of Eq.(V-12) with the areas under the donor decay curves according to Eqs. (V-7) and (V-11):

$$f_m = \frac{Area(0) - Area(t_a)}{Area(0) - Area(\infty)} \qquad \text{(V-12)}$$

We are particularly interested in the growth of interface thickness, which should be reflected by the increase in the extent of energy transfer. By approximation, we have previously regarded[8a,b] the term f_m as the apparent volume fraction of mixing. We then estimated the increase in apparent interface thickness ($\Delta\delta_{INT}$) from the f_m values, as the interfacial area between the hard spheres and the soft matrix can be obtained from the hard sphere size.

The energy transfer efficiencies for blend films before and after annealing were determined by single photon counting. Examples of the decay profiles obtained for our films are shown in Figure V-8. The uppermost line corresponds to a film consisting of donor labeled P(BMA-co-BA) and non-labeled PMMA particles, which gives a single exponential decay with a decay time of 45 ns. Curve 2 is for a nascent film prepared with 1 : 1 volume ratio of Phe-labeled soft particles and An- labeled hard spheres. A slightly increased curvature seen in curve 3, which indicates an increase in the rate of donor decay, is due to the annealing at 100 °C for 21 h for a film having the same composition as that in curve 2. The lowermost curve is for a model system corresponding to the state in which all dye molecules have been fully mixed. This film is prepared by solvent-casting 1 : 1 volume ratio of dry PMMA particles labeled with donors and acceptors, respectively, with the same chromophore concentrations as those polymers used for preparing the blend films.

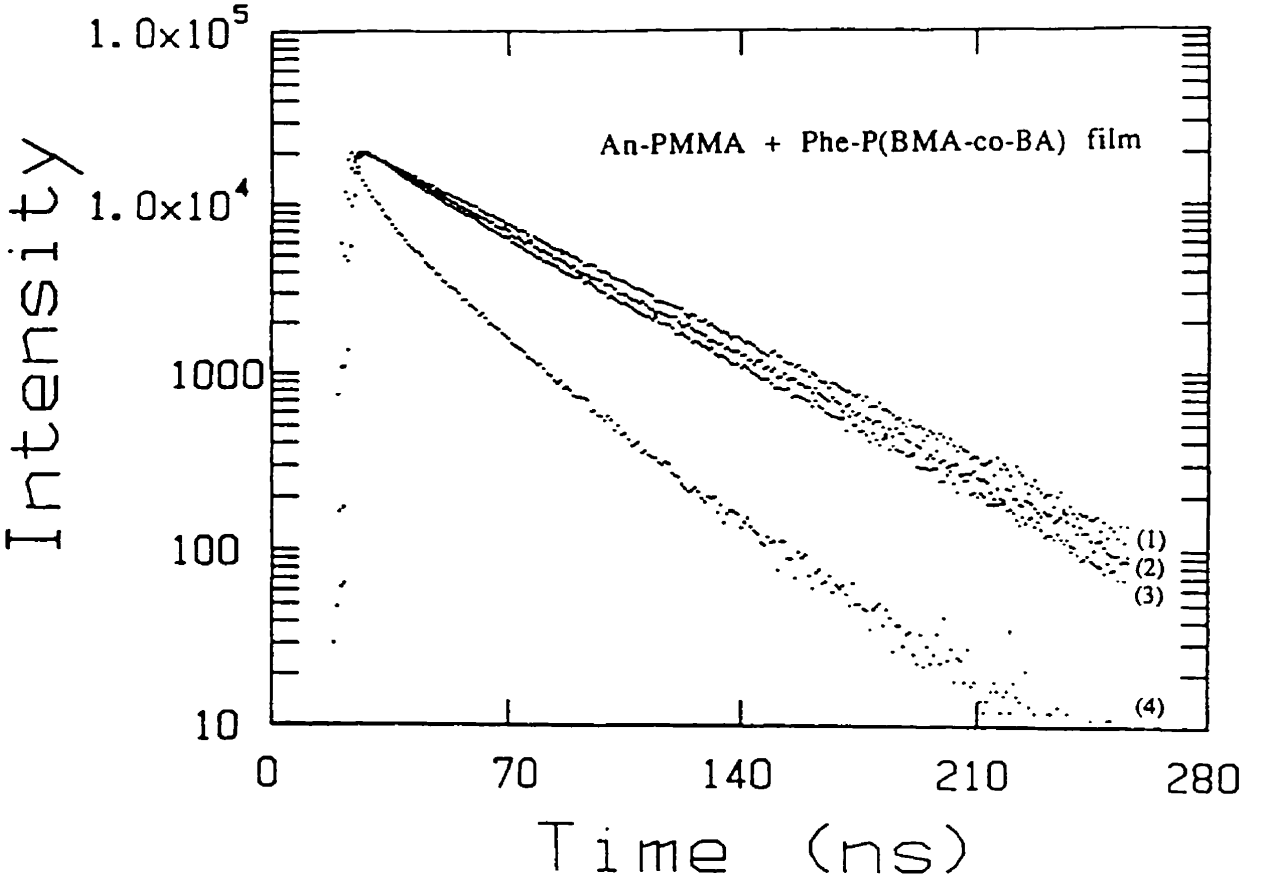

Figure V-8. Donor fluorescence decay profiles for films consisting of (1) Phe-labeled soft particles and non-labeled hard particles; (2) 1 : 1 Phe-labeled soft polymer and An-labeled 110 nm hard particles without annealing; (3) 1 : 1 Phe-labeled soft polymer and An-labeled 110 nm hard particles after annealing at 100 °C for 21 h; and (4) 1 :1 Phe- and An-labeled PMMA particles formed by solvent-casting.

Table V-5 presents the results of extent of mixing (f_m) calculated from energy transfer data for films annealed at 70, 100, and 140 °C, respectively. The evolution of interface thickness, $\Delta\delta_{INT}$, is also shown.

At an annealing temperature of 70 °C, one would expect that P(BMA-co-BA) chains in soft particles might be so flexible that they might diffuse into the hard particles across the boundary in a way similar to swelling of polymer particles by fluid organic solvents. However, the results from fluorescence measurements indicate that the material mixing between two types of particles upon annealing at 70 °C only occurs to a small extent, as shown in Table V-5. At an annealing temperature of 100 °C, which is close to the Tg of PMMA (105 °C), an increased extent of molecular mixing is seen, indicated by an increase of 3 to 5 nm in interface thickness. For an annealing temperature of 140 °C, where we know that PMMA chains have become effectively mobile,[18] we obtain a larger extent of penetration. The interface thickness increases from about 4 nm up to nearly 7 nm during the annealing process.

Table V-5. The apparent volume fraction of mixing (f_m) and increase of interface thickness ($\Delta\delta_{Int}$) in blend films annealed at 70, 100 and 140 °C

Time(h) / Temp(°C)		1	2	4	7	16	21
70	f_m	0.004	0.07	0.07	-	0.04	-
	$\Delta\delta_{Int}$ (nm)	0.1	2.5	2.5		1.5	
100	f_m	0.10	0.08	0.12	0.13	-	0.12
	$\Delta\delta_{Int}$ (nm)	3.7	2.9	4.4	4.8		4.4
140	f_m	0.10	0.10	-	-	0.20	-
	$\Delta\delta_{Int}$ (nm)	3.7	3.7			7.3	

Note that the f_m and $\Delta\delta_{INT}$ values at high temperature (e.g. 140 °C) for long annealing time may only reflect the amount of DET in relation to phase penetration but are not a direct measure of interface thickness, since some of the PMMA spheres have undergone coalescence under these conditions (see Chap. IV and ref. 9) and the interfacial area is reduced. Also, the miscibility in polymer blends may depend on the molecular weight and molecular weight distribution of the

polymers. Nevertheless, the overall extent of mixing between the two blend polymers here is small. The f_m also does not increase significantly when a film with the same composition was dissolved in a solvent, re-cast from the solution and analyzed in the same way. This indicates that there is only limited miscibility between the blended polymer components. This is common in polymer systems even when the polymers have very similar chemical structures.

V-4 SUMMARY

We chose a model system in which fluorescent donors and acceptors attached to their own polymer chains were randomly distributed in their respective phases separated by a sharp interface. A certain amount of direct non-radiative energy transfer (DET) across the interfaces between the labeled polymer phases was observed by fluorescence decay measurements. The quantum efficiency of energy transfer (Φ_{ET}) was used to quantify the amount of DET. The Φ_{ET} value increases as the interfacial contact area between the phases increases and is inversely proportional to the diameter of the donor-labeled dispersed particles when they are prepared in the form of hard spheres. The presence of ionic surfactant reduces the interfacial energy transfer to an extent of 30-40%. Upon annealing the films, the energy transfer efficiency increases to a small extent, indicating that there is a small increase in the interface thickness between the polymer pairs used in our blend films.

CHAPTER VI POLYMER DIFFUSION ANALYSIS BY FLUORESCENCE ENERGY TRANSFER IN LATEX FILMS AND FACTORS AFFECTING THE DIFFUSION RATE

VI-1 INTRODUCTION

VI-1-1 Polymer Diffusion

Polymer diffusion across interfaces has been a subject of intense interest for over a decade. Technologically, interest has arisen from issues related to welding of polymer slabs,[1] crack healing,[2] sintering of polymer powders by compression molding,[3,4] and the formation and aging of latex films.[5,6] Scientifically, it is desired to obtain information about the diffusion rate of the polymer and its relation to the evolution of mechanical properties,[3,4] as well as to test those theories related to polymer dynamics and interfacial phenomena.[7-10]

In many cases, polymer self-diffusion is a result of the Brownian motion of the molecules and therefore the motion is assumed to be random-walk. The diffusion thus follows the Fickian model and, as a consequence, the mean square of displacement $\langle r^2 \rangle$ of the substance is 6Dt. The so-called diffusion coefficient D (in units of cm^2/s), which is an important parameter characterizing the diffusion rate, is defined by equation (VI-1) referred to as Fick's First Law[11]

$$F = -D\,\partial C/\partial x \qquad \text{(VI-1)}$$

where F is the flux or the rate of transfer of diffusion molecules through unit cross-sectional area (in $mole/cm^2s$) and $\partial C/\partial x$ is the concentration gradient (in $mole/cm^3/cm$).

The Fickian second law allows one to find expressions of the concentration of the diffusing substance at certain position in the diffusion system in terms of the time t and diffusion coefficient D. For example, for diffusion in spherical geometry, if the diffusing substance is initially distributed uniformly through a sphere of radius R with a concentration C_o, the concentration C(r,t) at radius r and time t is given by[5,11]

$$C(r,t) = \frac{C_0}{2}\left[\mathrm{erf}\left(\frac{R+r}{2\sqrt{Dt}}\right) + \mathrm{erf}\left(\frac{R-r}{2\sqrt{Dt}}\right)\right] - \frac{C_0}{r}\sqrt{\frac{Dt}{\pi}}\left\{\exp\left[-\frac{(R-r)^2}{4Dt}\right] - \exp\left[-\frac{(R+r)^2}{4Dt}\right]\right\} \qquad \text{(VI-2)}$$

The fraction of the diffusing substance f_D that has diffused across the original boundary at time t is:

$$f_D = 1 - \frac{3}{4\pi R^3 C_0}\int_0^R C(r,t)\, 4\pi r^2\, dr \qquad \text{(VI-3)}$$

The diffusion process can be characterized in many ways. The most profound description of the process is to show the concentration profile of the diffusing substance expressed by C(r,t) and its evolution with time.

In many cases, the concentration profile is not convenient to quote, and simple parameters are preferred. The diffusion coefficient, D, is one of the most important ones characterizing the rate of molecular diffusion in the system. The mass fraction of diffusion, f_D, is also a useful parameter characterizing the diffusion in a 3-dimensional manner.

Another parameter often used for characterizing the diffusion process is the interpenetration depth d_i, which for spherical system is defined in terms of the change in radius of gyration of the labeled particles.

$$d_i = [R_g^2(t) - R_g^2(0)]^{1/2} = [\int c(r,t)\, r^2\, dr / \int c(r,t)\, dr - \int c(r,0)\, r^2\, dr / \int c(r,0)\, dr\,]^{1/2} \qquad \text{(VI-4)}$$

which simplifies to [12]

$$d_i = [R_g^2(t) - R_g^2(0)]^{1/2} = (6Dt)^{1/2} \qquad \text{(VI-5)}$$

Note that $(6Dt)^{1/2}$ is also commonly referred to as the diffusing distance.

VI-1-2 Analysis of Polymer Diffusion by DET

We are concerned with DET measurements to monitor the polymer diffusion process in latex films. One type of particles is composed of a polymer randomly labeled with donor, and the other type is composed of an identical polymer but labeled with acceptors. The particles can deform into void-free polyhedra structure but with little molecular diffusion at a temperature just above the Tg of the polymer, and upon annealing the labeled polymer molecules diffuse to mix, which can be monitored by the increase in energy transfer efficiency.

In earlier analyses of polymer diffusion carried out in our laboratory, we assumed that there were three domains in the system during the diffusion process: a donor-labeled domain, an acceptor-labeled domain, and a mixed domain in which donors and acceptors are uniformly distributed.[5] By this simplification, a decay expression analogous to that of the Klafter-Blumen model was used to analyze for the diffusion process in terms of the observable change in the extent of DET. The decay expression used is also called a Förster mixing equation as

$$I_D(t) = A_1 \exp[-t_d/\tau_D^{\circ} - p(t_d/\tau_D^{\circ})^{1/2}] + A_2 \exp(-t_d/\tau_D^{\circ}) \qquad \text{(VI-6)}$$

where the first term with a prefactor A_1 reflects the donors that undergo energy transfer (ET) in the mixed domain, and the second term with a prefactor A_2 reflects the donors that are not influenced by acceptors in the unmixed domain. τ_D° is the unquenched donor lifetime, and t_d is the decay time.

Dhinojwala et al[13] and Liu et al[14] proposed an alternative data analysis technique, taking the concentration gradient of the dye-labeled polymers into account. These models allow one to describe the diffusion process in terms of the evolution of concentration profile C(r,t) and the change in the density distribution of acceptors surrounding the donors. In this approach, the concentration profile is subdivided into thin slices with locally uniform donor and acceptor concentrations. Mathematical expressions were derived describing the DET between donor and acceptors attached to polymer chains diffusing across the interface. Recently, Yekta et al[15] derived a general expression in systems of planar symmetry for the fluorescence decay of excited donors in the presence of acceptors under conditions where the donor/acceptor concentrations are nonuniformly distributed. Based on this work, a more comprehensive model[16] was developed which allows one to analyze systems with sharp concentration profiles.

The data from DET studies of polymer diffusion can be analyzed at various levels of sophistication. Although comprehensive models of DET and polymer diffusion provide more accurate absolute values of the diffusion coefficients in the system,[14-16] a simpler approach to data analysis is preferable for most of latex films. One approach which we have employed in the past is to try to estimate the extent of mixing due to diffusion from comparison of the fluorescence decay curves. A simple measure of the extent of mixing, $f_m(t)$, is expressed in terms of the fractional growth in energy transfer efficiency[5] as

$$f_m(t) = \frac{\Phi_{ET}(t) - \Phi_{ET}(0)}{\Phi_{ET}(\infty) - \Phi_{ET}(0)} = \frac{\text{area}\,(0) - \text{area}\,(t)}{\text{area}\,(0) - \text{area}\,(\infty)} \qquad \text{(VI-7)}$$

where $[\Phi_{ET(t)} - \Phi_{ET(0)}]$ represents the change in DET efficiency between the initially prepared film and that annealed for time t. In our experience, the most reliable way to obtain Φ_{ET} is from the area under the normalized fluorescence decay curve. $f_m(t)$ itself is an important parameter for characterizing the extent of mixing or polymer diffusion by DET technique.

To proceed more deeply into the analysis of the diffusion process, we calculate apparent mean diffusion coefficients D_{app} characterizing the rate of movement of the polymers across the interparticle interface in the samples. The diffusion coefficients were calculated by fitting the data obtained from energy transfer to a spherical diffusion model which satisfies Fick's laws of diffusion.[11] The details of the analysis and discussion have been presented previously.[5] In the

analysis, a parameter, f_D, namely the fraction of substance (donor-labeled polymer under consideration here) which has diffused across the initial boundaries after a certain time, is needed. The key step for us is thus to find a relation between f_D and the extent of mixing f_m.

The terms f_m and f_D both reflect the fraction of diffusion, and both are proportional to $t^{1/2}$ at early times of the diffusion process. The proportionality constant between f_m and f_D over this initial range depends on the extent of acceptor-labeling in the system. In most of the latex samples examined previously in our laboratory, we used an equal number of An- and Phe- labeled particles ($N_{An} : N_{Phe} = 1$).[5] Our approach has been to assume a proportionality of unity and calculate apparent mean diffusion coefficients (D_{app}). Under our conditions we estimate that D_{app} may differ from the true D by a factor of 2 to 5. We are normally interested in changes in D caused by changes in some external variable. In this case, the absolute D values become less important.

In other cases in which we intend to analyze the diffusion by more sophisticated models, a $N_{An} : N_{Phe}$ ratio of 12 is required.[14] In most of the films described in this study, we chose a $N_{An} : N_{Phe}$ ratio of 12 to match the conditions for spherical diffusion model, as described in ref. 14. The f_D value we use for diffusion coefficient calculations is $1/2f_m$. One notices that the relationship between f_D and f_m for 12:1 An/Phe mixture differs by a factor of 2 from that for 1:1 mixture. From a geometric consideration, this is not difficult to understand. In the case of $N_{An} : N_{Phe} = 12$, each donor particle is primarily surrounded by an acceptor medium, whereas in 1:1 mixtures, each Phe-labeled particle has only half the number of An-labeled neighboring particles. Thus for the same mass fraction of diffusion (f_D), the energy transfer signal one would observe in $N_{An}/N_{Phe} = 1$ film is half of that for $N_{An}/N_{Phe} = 12$ film.

We have found experimentally that the diffusion coefficients obtained from films of $N_{An}/N_{Phe} = 12$ by assuming $f_D = 1/2f_m$ are very close to those obtained from films of $N_{An}/N_{Phe} = 1$ by setting $f_D = f_m$, especially at early times of diffusion. We also found that the diffusion rate analyzed by using $f_D = 1/2f_m$ for $N_{An}/N_{Phe} = 12$ are very similar to those analyzed by a model considering the concentration profile developed by Liu et al for the same samples.[14] We thus obtain f_D values, from energy transfer data by setting $f_D = 1/2\ f_m$, for each sample ($N_{An}/N_{Phe} = 12$) at each diffusion time and are able to calculate the diffusion coefficients of the polymers.

VI-1-3 Examining Factors Affecting Polymer Diffusion Rate

One of the most important issues is how the presence of various substances affects the rate of polymer diffusion and the development of film properties. Major substances present in latex systems include water, polymers in microspheres, surfactant, coalescing aid, and other additives. Wang et al[5c,17] found that normal coalescing aids added to coatings formulations could greatly increase the diffusion coefficient of the polymers. Kim et al[18] found that carboxylated poly(butyl methacrylate) (PBMA) diffuses much slower than the pure PBMA, and that, upon

neutralization of the carboxylated sample by inorganic bases, the retardation of diffusion is even more pronounced. It is also found that poly(ethylene oxide)-based nonionic surfactants can enhance the diffusion of PBMA while ionic surfactant has little effect.[19]

Water is one of the most important ingredients in latex systems. It plays an important role in latex film formation process in providing a stabilizing and suspending medium for the particles that allows for thermal motion of the system to permit approach to close packing of the particles. Brown[20] proposed that the presence of water in the drying film is also essential to the deformation of particles associated with the capillary compression. An important issue is how the presence of water affects the polymer diffusion rate in latex films. Since there can be always a certain amount of water in the films either from the original dispersion or from air, it is of extreme importance to examine the role of water in polymer diffusion process in latex films.

Other components present in latex system include a small amount of oligomers, which are produced mainly by polymerization of a small fraction of monomer in the aqueous phase, or in some cases are due to one's design of synthesis. These species have nearly the same molecular structure as the major high polymer, but have much higher free-volume and mobility. It is interesting to examine whether or not there is a plasticizing effect of these species on the latex polymer.

Our experiments consist mainly of monitoring the polymer diffusion process by fluorescence energy transfer technique. We compare the diffusion rates between latex films aged or annealed in dry environment and those treated under wet conditions, and the behavior of water effect on diffusion between hydrophobic and hydrophilic latex polymers. We examine the polymer diffusion rates for films prepared with different amounts of oligomers. Our experiments are the first scientific study on the influence of water and oligomeric species on high polymer diffusion. We show that those simplest substances such as water can alter greatly the dynamics and thus property development for certain polymers.

VI-2 EXPERIMENTAL

VI-2-1 Latex Sample

The latex polymers used in this study include poly(butyl methacrylate) [PBMA], regarded as the hydrophobic polymer, and a copolymer of butyl methacrylate and 5 wt% methacrylic acid [P(MAA-co-BMA)], as the more hydrophilic polymer. The polymers were either labeled with a fluorescence donor, phenanthrene (Phe), or an acceptor, anthracene (An). The synthesis of labeled latexes has been described in Chapter II. The characteristics for the samples used are listed in Table VI-1. Since each pair of Phe- and An- labeled latex samples was prepared using almost the same recipe and under strictly identical conditions, we obtained

similar particle size and size distribution, and, more importantly, the molecular weight and molecular weight distribution of them essentially fall in the same range.

Table VI-1. Latex characteristics

Polymer	PBMA-VI-1		PBMA-VI-2		P(MAA-co-BMA)	
Label	Phe	An	Phe-	An-	Phe-	An-
Diameter [a] (nm)	128	128	125	125	132	132
Size polydispersity [a]	0.02	0.02	0.02	0.02	0.03	0.03
Mw ($x10^3$ or K)	370	400	35	34	39	37
Mn ($x10^3$ or K)	130	130	17	18	16	16
Mw / Mn	2.8	3.0	2.1	1.9	2.4	2.3

a. The particle sizes are nearly identical with both a narrow size distribution for each pair of Phe- and An- labeled latex samples, and the results shown here were measured for 12 : 1 An/Phe mixtures of the pairs of ion-exchanged samples, which are thus directly used in our diffusion analysis.

VI-2-2 Film Formation and Characterization

Before film formation, all latex dispersions were cleaned by ion-exchange to remove the surfactant and other ionic substances.

Films were formed by spreading mixed dispersions of An- and Phe- labeled particles onto thin quartz plates and dried in a temperature-control oven. The drying temperature for PBMA-VI-2 latex samples was 25 °C, close to room temperature, and that for PBMA-VI-1 and P(MAA-co-BMA)-based samples was 32 °C. The drying time for each dispersion was ca. 3 h. A typical thickness of our films prepared here is ca. 150 μm. For each set of samples for comparison, the films were dried under identical conditions.

In most of our films, the number ratio of An- to Phe- labeled particles is 12 : 1. For P(MAA-co-BMA) samples, some films were formed when the -COOH groups were in the protonated form, and others were prepared from dispersions of the latex mixed with NH_3 or NaOH (molar ratios $[NH_3]/[\text{-COOH}]$ or $[NaOH]/[\text{-COOH}] \approx 2.5$) to neutralize the -COOHs.

To examine the oligomer effect on polymer diffusion, some PBMA dispersions were mixed with different amounts of BMA oligomers. The oligomers were obtained as follows: a surfactant-free emulsion polymerization of BMA was carried out, and the oligomer species were separated from particles by centrifuging the latex dispersion. The clear aqueous solution in

which oligomers were dissolved was collected. BMA segments are hydrophobic and we expect that the oligomers soluble in water have short chain lengths with the number of monomer units per molecule on the order of 10 or less. Some ionic initiator used for polymerization remained in the clear liquid, and the amount of oligomers was determined by ^{1}H-NMR based on the acrylic ester content in dried sample dissolved in $CDCl_3$. The oligomer solution was then post-added to dispersion mixtures of Phe- and An-labeled particles to prepare oligomer-containing films.

To examine water effect on films, the dried films were treated under different humidity conditions. Some were further dried under vacuum for 2-3 days to remove possible residual water and then kept in a dry environment in a sealed test tube. Others were either placed, with glass beads as a support, on the top of a water layer in a test tube covered with a rubber septum, with an internal humidity of ca. 100% RH, or directly immersed in liquid water, for 2 days to obtain an equilibrium water content. The dry and wet films were then annealed at 60 °C in an oven. To minimize the water loss from the wet films upon heating, the wet films were either placed on the top of a water layer in a sealed test tube and heated in high humidity (100% RH) or heated directly in liquid water. To prevent the increase in water vapor pressure during heating, the internal vapor was connected to the open air with a small needle inserted through the rubber septum. After carrying out a fluorescence decay measurement on an annealed wet film, it was placed back in its wet environment at room temperature to reach saturated water content, and then reheated for an additional amount of time. For each set of samples to be compared, the films were heated simultaneously.

The water contents of the films were measured gravimetrically. Film transparency was determined with a UV-vis spectrometer (Hewlett-Packard 8452A Diode Array) as its percent transmittance (%T) in the visible range (400-700 nm). Fluorescence decay measurements were carried out by using the time-correlated single-photon-counting technique. The measurement conditions were similar to those mentioned in Chapter V and previously.[5]

VI-3 RESULTS AND DISCUSSIONS

VI-3-1 Energy Transfer and Diffusion Analysis

We consider the Phe-labeled molecules as the diffusing substance in our films. Since the number ratio of donor- (D) to acceptor- (A) labeled particles is 1/12, it is reasonable to assume that each donor particle is encircled by an acceptor medium, as depicted in Fig. VI-1. Upon annealing, polymer diffusion occurs and a certain amount of donor molecules will diffuse out of its original sphere and enter into the surrounding particles, with a fraction of $f_D(t)$. The size of cluster bearing donor molecules will gradually increase, as shown in Fig. VI-1.

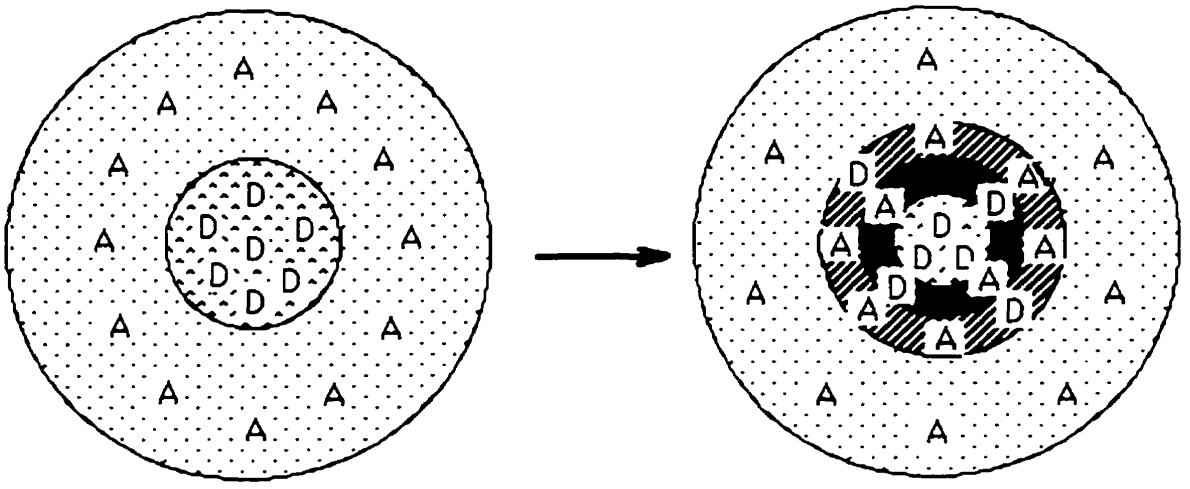

Figure VI-1. Illustration of diffusion upon annealing at (a) t = 0, and (b) t > 0.

Fluorescence decay measurements were carried out on our film samples as a means of assessing the extent of energy transfer as a function of annealing history or of film composition. Figure VI-2 shows examples of fluorescence decay profiles obtained for a set of our P(MAA-co-BMA) films in the dry state before and after annealing. Films prepared from a dispersion of Phe-labeled particles only exhibit an exponential decay profile (top straight line) with a lifetime of 45 when excited at 298 nm. Films prepared from a mixture of Phe- and An- labeled particles show a slightly increased curvature at early times in the decay profiles followed by a long exponential tail (curve 2). This corresponds to a small amount of energy transfer between donors and acceptors located in the initial interparticle boundary region in the nascent films. When the films are annealed at elevated temperatures, this increased curvature becomes more pronounced, as seen in curve 3 and 4 for films heated at 60 °C for 40 and 190 min., respectively. This indicates that molecular mixing has occurred between donor- and acceptor-labeled polymers and the extent of energy transfer is increased, leading to a fast decay of donor fluorescence.

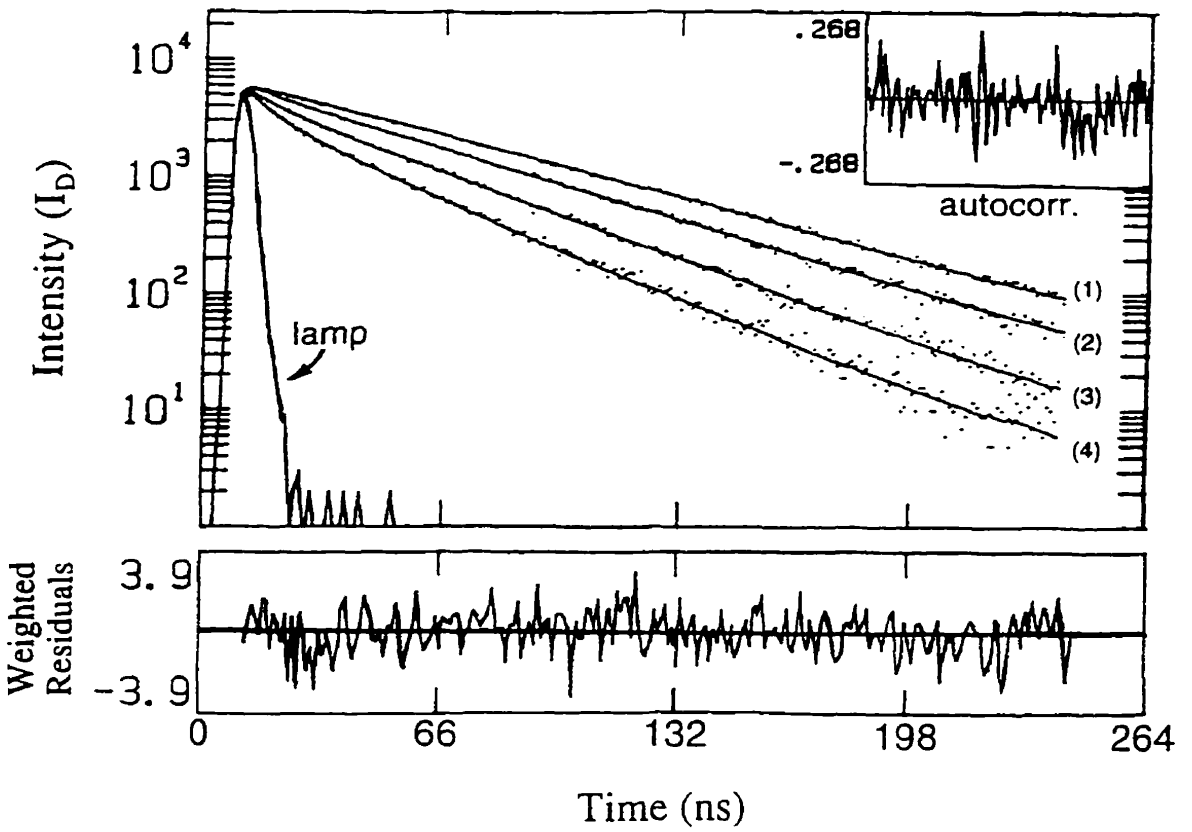

Figure VI-2. Representative donor fluorescence decay profiles for dry P(MAA-co-BMA) films. Curve 1 corresponds to a film with donor particles only and curve 2 is for a film freshly prepared with 1 : 12 mixture of Phe- and An- labeled particles. Curve 3 and 4 are for the acceptor-containing films annealed in dry environment at 60 °C for 40, and 190 min., respectively. These curves are integrated to obtain the areas under them in our data analysis, as described in the text. The decay function used for integration is: $I_D(t) = A_1 \exp[-t_d/\tau_D' - p(t_d/\tau_D')^{1/2}] + A_2 \exp(-t_d/\tau_D')$. In the Figure we also display the weighted residuals and their autocorrelation for curve 4 when fitted to the above expression.

The extent of mixing expressed in terms of the fractional growth of ET efficiency, $f_m(t)$, can be obtained via Eq. (VI-7). This is done by measuring the decay profiles and comparing the areas under the profiles for films without annealing [*area(0)*], annealed for certain times [*area(t)*], and annealed for sufficiently long time to approach a minimum value of area [*area(∞)*]. *area(∞)* can also be obtained from films prepared by solvent-casting. Representative data of f_m values for our films as a function of annealing time will be presented in the following sections. We will also show the polymer diffusion coefficients for our samples calculated based on the f_m values.

VI-3-2 Role of Water in Polymer Diffusion

VI-3-2-1 Film Transparency and Water Content

(a) Water content in latex films. In the fresh films of PBMA (Sample ID PBMA-VI-2) prepared under our conditions, the films had an initial water content of 1.4 wt%. A similar value was found for newly formed P(MAA-co-BMA) films in the protonated form in our case, while the values were much larger (up to 8.9 wt%) when the carboxylic acid groups were neutralized by NH_3 or NaOH. The water contents increased significantly when all these films were exposed to a vapor of high water content (100% RH). When immersed directly in liquid water, ca. 15 wt% water could be detected. This level of water content can include water uptake into cracks in the film. Table VI-2 shows the water contents measured for our latex films when exposed to water at room temperature and when heated at 60 °C at high humidity.

Table VI-2. Water contents (wt%) in latex films treated in water vapor (100% RH) or in water liquid

Latex	PBMA	P(MAA-co-BMA)		
		-COOH	$+NH_3$	+NaOH
Newly dried film	1.4	1.4	5.3	8.9
Immersed in liquid water (3 days)	15.0	16.2	swollen	swollen
Exposed to wet vapor (~100% RH, 3days)	3.4	5.7	5.9	13.8
Heated at 60 °C in water vapor [a]				
40 min	2.3	5.4	5.0	13.7
90 min	2.2	4.6	3.3	10.5
Heated for 2h at 60 °C and exposed to wet vapor again [b]	3.5	5.5	5.8	14.0

a: The water contents after heating were immediately measured before more water entered into the film upon cooling; b: The well-heated films were placed in water vapor again to reach an equilibrium water content.

When the wet films are heated, water is evaporated out the film. When the heating was carried out in a wet environment (e.g. air vapor of 100% RH), a significant amount of water remained in the film (Table VI-2), which allowed us to observe its effect on polymer diffusion.

We do not intend to consider the above results as the standard quantities of water absorbed or solublized in the polymers. Rather, these are the data obtained in conjunction with our energy transfer measurements for the same samples and are useful for us to compare and to interpret our results, as we will show in the following.

(b) Film transparency. When dense, crack-free films are formed from latex dispersions, they are often transparent or sometimes semi-transparent depending on the film microhomogeneity, film thickness, and water content. Due to the microheterogeneous nature of newly formed latex films, the transparency of latex films is often to some extent lower than that of films cast from a homogeneous solution of the same polymer in an organic solvent. In other cases highly transparent films are obtained, especially when the temperature of film formation is well above the MFT. In films formed at high temperatures, some interparticle polymer diffusion may have occurred during the film formation process.

Films dried under our conditions were fairly transparent with a percent transmittance (%T) of 70% over the visible wavelength range. This value would be higher if thinner films were prepared. For both PBMA- and P(MAA-co-BMA)- based samples, annealing at elevated temperatures (e.g. 60 °C) in dry environment leads to an increase in %T to over 80%.

When PBMA films are exposed to a water vapor or immersed in water liquid for a sufficient time (e.g. 2 days), they turned highly turbid, with %T < 20%. The water content for a PBMA film placed in water vapor was 3.5 wt%, and that for a film immersed in liquid water could be as high as 15 wt%. The film immersed in liquid water also showed large cracks and became too brittle to resist mechanical forces. This result is similar to that seen by Joanicot et al.[21] We infer from this result that water would be more concentrated in the interparticle boundary region richer in polar groups (e.g. $-SO_3H$) than the core region. This inhomogeneity of water distribution in the films would be the reason causing turbidity for films exposed either to water vapor or to liquid water.

When the water-containing turbid PBMA films are heated in a low humidity environment and water is evaporated, the film transmittance increases and the films soon become clear. When these heated clear films are placed back into water vapor or liquid water, they become highly turbid again. Figure VI-3 shows the visible transmittance spectra for a PBMA film newly formed, a film exposed to water vapor, that well-heated in low humidity, and that placed into wet atmosphere again after heating.

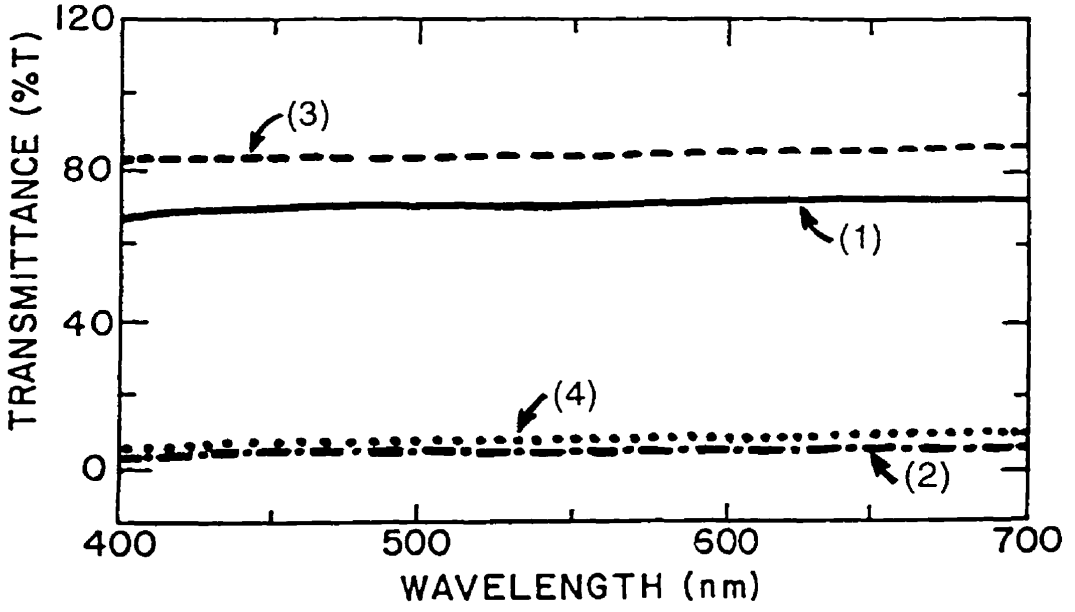

Figure VI-3. Visible transmittance spectra for PBMA films: (1) a nascent film, (2) a film exposed to wet vapor for 2 days, (3) a film heated in low humidity at 60 °C for 2 h, and (4) the well-heated film placed into wet vapor for 2 days.

What is surprising here is that turbidity under wet conditions is found for films that have been well-heated and the polymer molecules have reached a high extent of mixing. We also observed a high turbidity for wet films prepared initially by solvent-casting. What one would expect is that as polymer molecules are well mixed, the heterogeneity in the initial latex films gradually disappears, and the hydrophobic polymer matrix would be more resistant to water. From our results, we infer that while the molecular mixing increases overall the homogeneity of the system, some degree of non-uniformity of distribution of polar groups would exist throughout the mixing process. When the films are open to water, domains rich in polar substituents would take up more water and these regions might be sufficient to scatter light. As a consequence, the water-containing films remain turbid in any state of the polymer interdiffusion process.

The above results also lead us to consider a possible phenomenon occurring in a similar way to the case of surfactant assembly. When surfactant molecules are placed in a hydrophobic medium, the hydrophilic ends may aggregate into certain domains and the hydrophobes may penetrate into the medium. Our PBMA latex polymers are made of hydrophobic chains with polar groups at the ends (e.g. -OSO_3H groups from the initiator). When the polymer molecular weights are much higher than common surfactant, the tendency for the hydrophilic ends to assemble should be overcome by the tendency towards random distribution of the chain ends

driven by the polymer conformational preference. In the case here, however, the polymer molecular weights (Mw = 35K, Mn = 17K) are smaller than normal latex polymers, with some portions of the molecules distributed along molecular weight of only ca. 1000 to several thousand. In these molecules, each chain contains only ten or a few tens of monomer units and two polar end groups, which may be able to aggregate into hydrophilic domains distributed in hydrophobic environments. This process can be possible when the films are heated so that the molecules are mobile enough to rearrange their distribution in space. We should point out that even with much high molecular weights, there is always some amount of oligomers possibly present in latex systems.[22] Oligomer species are believed to be hydrophilic.

P(MAA-co-BMA) films behave differently. When clear P(MAA-co-BMA) films are exposed to water, the saturated amount of water was ca. 5.7% in 100 %RH vapor and >15% in liquid water. However, these water-containing films remain transparent, with almost identical transmittance to those films in dry state. This implies that there is a relatively uniform distribution of water in the film. This may be related to the distribution of polar groups in the latex. In this type of samples, along each polymer chain the polar groups (mainly carboxyls) are likely statistically distributed, although detailed information about chemical composition distribution is unknown. In each particle, the density of polar groups ($-SO_3H$ and -COOH) at the surface may be comparable to that within the particle, since 5 wt% MAA were incorporated into the polymer throughout the second stage of polymerization. There is a seed core made of PBMA, corresponding to ca. 10 wt% of the entire particle, but it ought to be well mixed with the second-stage polymer during polymerization (at 80 °C). Thus, on a microscopic level, there maybe no preferred domains in which the polar materials are highly concentrated in these films.

VI-3-2-2 Effect of Water on Polymer Diffusion Rate

Figure VI-4 shows the diffusion data at 60 °C for PBMA (M_w=35K, M_n=17K) films treated in dry environment and in a vapor of high humidity, respectively. In Fig. VI-4a we plot the fraction of mixing f_m vs. annealing time, and in Fig. VI-4b the plots of apparent diffusion coefficient D_{app} vs. time are shown. We see that the extent of mixing in the films increases with time and approaches unity on a time scale of 2 to 3 hours in both sets of samples. The diffusion coefficients obtained are on the order of 0.1 nm^2/s at early times and are slightly lower at later times. This can be explained by the fact that our samples have a range of chain lengths, and those shorter chains should have higher diffusivity and dominant the measurement at early times. The larger polymer molecules having smaller diffusion coefficients, make their contribution to the DET measurement at later times. Comparing the data between dry and wet PBMA films, we see that the diffusion rate for the wet film appears to be slightly higher than that for the dry film, but the difference is not significant. For both experiments the diffusion coefficients fall in the same range. This indicates that water has little effect on the diffusion rate of PBMA samples.

The only exception observed repeatedly in our experiments is that in the very beginning of annealing (e.g. the first 10 min), the f_m for the wet film is significantly larger than that for the dry film, and the calculated diffusion coefficient for the wet film is also noticeably larger (e.g. 2 times, see Figure VI-4). We think that this is related to the presence of a small portion of molecules having shorter chain lengths than the average, including those oligomer-like species. This portion of molecules can have not only high diffusivity but also high hydrophilicity. These combined factors lead to a faster mixing in the early times in the wet films than in the dry films. Over most of the times of annealing, however, the influence of water on diffusion of PBMA is quite small, indicating that PBMA is hydrophobic with little plasticization from water.

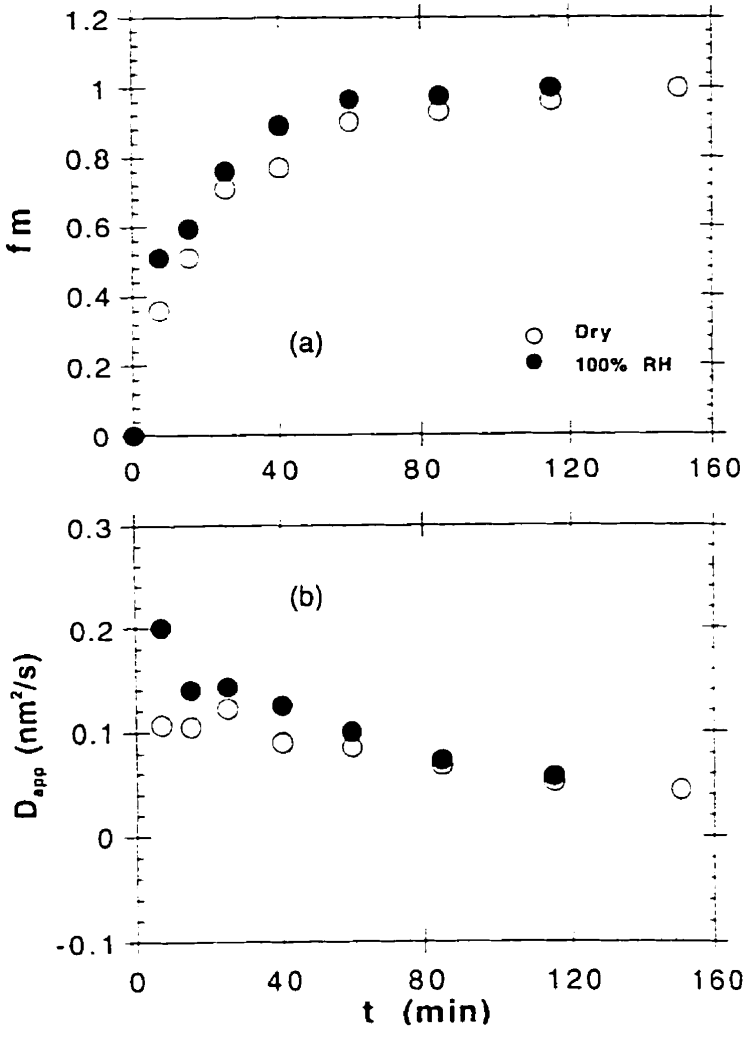

Figure VI-4. Comparison of diffusion rate of PBMA (M_w=35K) at 60°C between dry samples (O) and wet films (●) treated in high humidity. In (a) and (b) the plots of extent of mixing (f_m) and the apparent diffusion coefficient (D_{app}, in nm^2/s), respectively, Vs. time (in min) are shown. Similar types of plots are involved in the following Figures.

For P(MAA-co-BMA) samples (M_w=38K, M_n=16K), the diffusion data for films under dry and wet conditions are presented in Figure VI-5. Three sets of films are under consideration here: one is in its dry state, one is exposed to water vapor, and the other is immersed in liquid water. The wet films, either treated in a wet vapor or immersed in water, show similar diffusion rates upon heating at the same temperature. Note that the amount of water in the film was 5 wt% during heating in wet vapor and larger when the film was immersed in liquid water (see Table VI-2). Although there is an excess of water present in the film immersed in water compared to that in the wet vapor, this does not impose further hydroplastic effect on the polymer. We also notice here that the diffusion coefficient for the wet films at the very beginning of annealing (e.g. 10 min) is distinguishably larger than that at later times. This effect is similar to that found for PBMA samples, and points to a contribution from the highly diffusive, hydrophilic short-chain molecules. The most important results here is that the diffusion occurs much faster for films under wet conditions than those in dry state. As seen in Fig. VI-5a, the f_m values for the wet films are much larger (2 times up to 2h) and approach unity sooner than the dry films. The D_{app} values found for the dry P(MAA-co-BMA) film are ca. 0.01 nm^2/s, whereas those for the wet films are about 5 times larger, for annealing times up to 2 h (Fig. VI-5b). This difference is significant. It clearly indicates that the presence of water in P(MAA-co-BMA) films increases the diffusion rates of the polymers by about half an order of magnitude.

Comparing the data for PBMA samples (Fig. VI-4) with those for P(MAA-co-BMA) (Fig. VI-5) of similar molecular weights examined under the same conditions, we see that overall the PBMA diffuses faster than P(MAA-co-BMA). This difference can be attributed to the increase in Tg, and corresponding decrease in mobility, when the MAA component is incorporated into the PBMA, as discussed previously.[18] In the dry state, the D_{app} values found for PBMA are about 10 times larger than those for P(MAA-co-BMA), whereas in the wet state, the ratio of diffusion coefficients becomes only a factor of 2. This comparison further demonstrates that water has much larger effect on the diffusion of the hydrophilic P(MAA-co-BMA) than the hydrophobic PBMA.

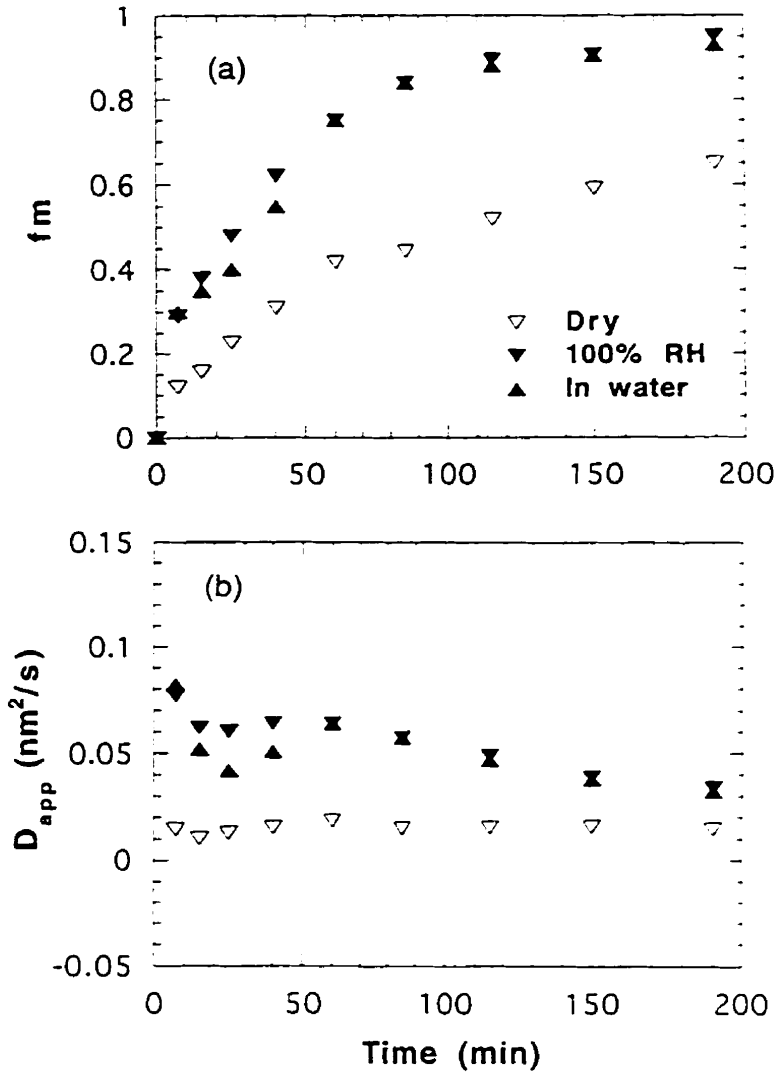

Figure VI-5. Comparison of diffusion rates at 60 °C between dry and wet films for P(MAA-co-BMA) (M_w=38K). The symbols ∇, ▼, and ▲ represent films treated in dry environment, in wet vapor, and in liquid water, respectively.

VI-3-2-3 Water Effect on Neutralized P(MAA-co-BMA)

Some of our P(MAA-co-BMA) films were prepared from ion-exchanged dispersions in which the carboxylic acid groups were in the protonated form. Others were prepared when the -COOH groups were subsequently neutralized with NH_3 or NaOH. We wish to compare diffusion between unneutralized and neutralized films, under dry and wet conditions.

Figure VI-6 shows diffusion data for dry P(MAA-co-BMA) films without addition of base, and those neutralized by NH_3 and NaOH, respectively. We see that the diffusion rate for

NaOH-neutralized sample is much smaller than that for the unneutralized (-COOH) film, with the diffusion coefficient ratio of almost an order of magnitude (0.001 vs 0.01 nm^2/s). NH_3-neutralization causes some retardation of the diffusion, but the difference is not as large for the NaOH-neutralized film. We attribute the decrease in diffusion rate upon neutralization of the -COOH groups to the increase in Tg when the polymer changes from its uncharged state to an ionomer.[18,23] The difference between NH_3- and NaOH- treated films maybe due to the evaporation of NH_3 upon heating, leading to its smaller effect on polymer diffusion.

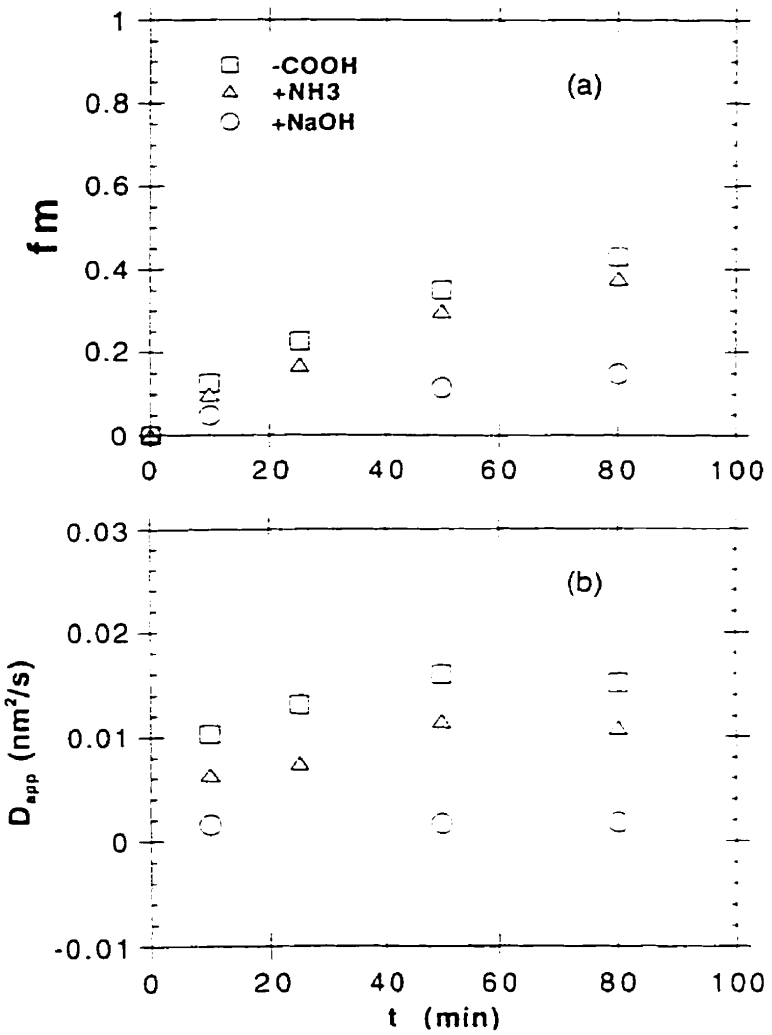

Figure VI-6. Comparison of diffusion rate at 60 °C for dry films of P(MAA-co-BMA) in which the carboxyl groups were unneutralized (□), neutralized with NH_3 (△) and with NaOH (○), respectively.

In Figure VI-7 the diffusion data for films similar to those in Figure VI-6 but treated under wet conditions (in wet vapor) are shown. Comparing Fig. VI-7 and VI-6 for the respective wet and dry films examined simultaneously, one sees that the diffusion rates in wet films for all sets of samples are larger than those in dry films. This indicates that water plasticizes all these samples. What is interesting here is that in the dry state the diffusion in NaOH-film occurs slowest, and that in -COOH-film occurs fastest, while under wet conditions this trend has been reversed. The NaOH-film sample diffuses faster than the -COOH-film sample in the presence of water. What is impressive is that the ratio of the apparent diffusion coefficients between the wet and dry NaOH-treated samples is about 80 to 100 (D_{app} 0.1 vs 0.001 nm^2/s). A large difference is also observed between the wet and dry NH_3-neutralized films. For the -COOH-films, the ratio of D_{app} values between wet and dry samples is still significant (5 to 8) but much smaller than that for neutralized films. These results indicate that water has much larger enhancement effect on the P(MAA-co-BMA) diffusion in neutralized samples than those in protonated from.

Some other observations may be also instructive to the understanding of the above results. For example, we found that the unneutralized P(MAA-co-BMA) sample could preserve its film integrity when both exposed to water vapor and liquid water. The NaOH-neutralized film was physically stable in the presence of water vapor but fell apart when immersed in liquid water. When a NaOH-neutralized P(MAA-co-BMA) film is immersed in water, it gradually loses its film features and becomes a white suspension of small polymer pieces in water, indicating that a large amount of water swells the film and the material is no longer able to retain its properties as a coherent film. In energy transfer measurements for newly-formed P(MAA-co-BMA)-based films, the quantum efficiency of energy transfer for a NaOH-film is already noticeably (20%) lower than a -COOH film, indicating that water plasticizes the NaOH-neutralized polymer even during film formation.

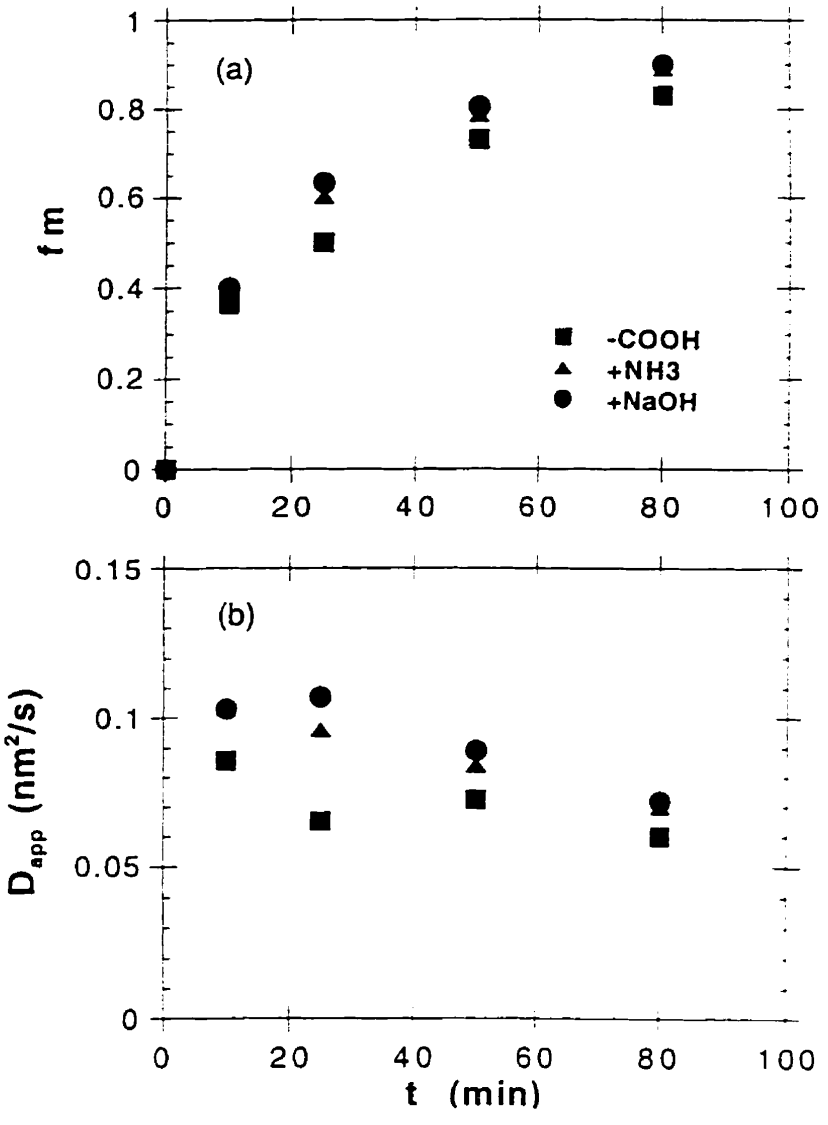

Figure VI-7. Comparison of diffusion rate of P(MAA-co-BMA) at 60°C in water vapor for samples unneutralized (■), neutralized with NH_3 (▲) and with NaOH (●), respectively.

VI-3-3 Effect of Oligomers on Polymer Diffusion

This work was carried out in collaboration with Ms. Ewa Odrobina in the Winnik lab. Most of the experiments were performed by Ewa, and the details of the results will be described in her Ph.D. thesis. I present here an example of the data we obtained.

The BMA oligomers in an aqueous solution were added into dispersions of ion-exchanged PBMA latex (M_w = 370K, M_n = 130K) containing Phe- and An-labeled particles to

form films. Films were annealed at 70 °C and their fluorescence decay profiles were measured, allowing us to measure the diffusion rates.

Figure VI-8 shows comparison for diffusion rates measured for PBMA without and with post-addition of different amounts of BMA oligomers to the system. One observes a clear trend that with increasing amount of oligomer, the diffusion rate of the polymer increases. The D_{app} values are increased by about 6 times upon addition of only 3 wt% oligomers, and are much higher for films with 6 or 9 wt% oligomers. This indicates that oligomers can plasticize and enhance greatly the diffusivity of the high polymer.

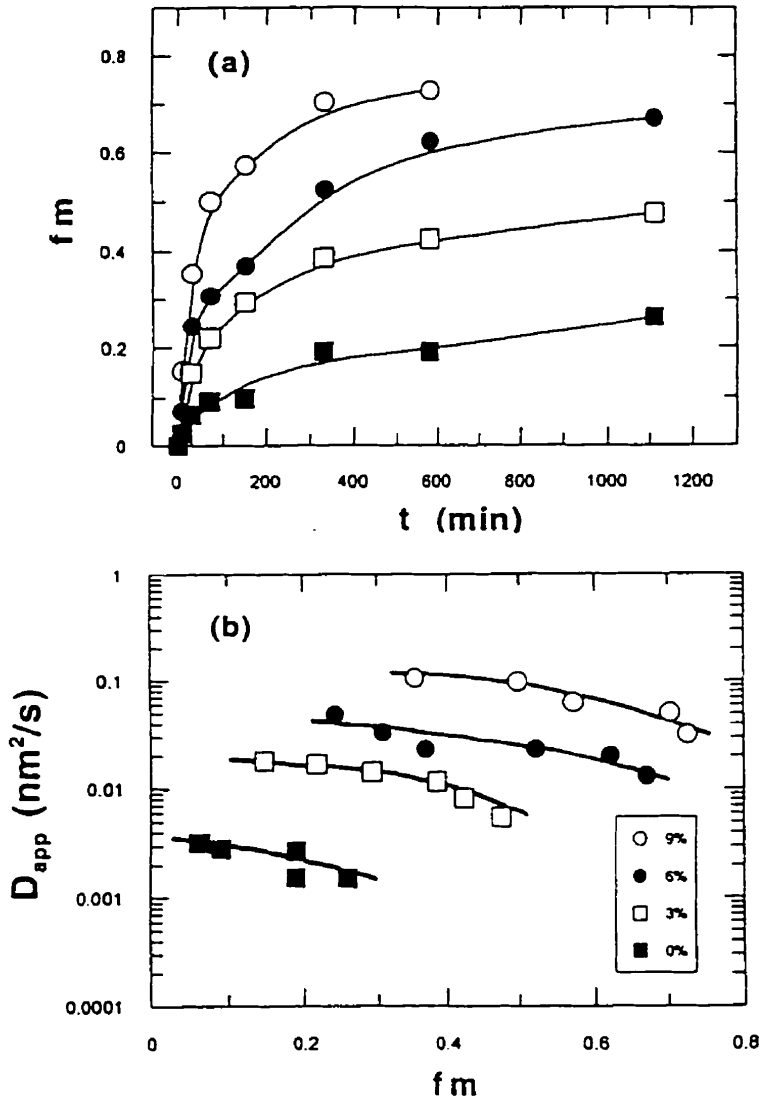

Figure VI-8. Comparison of diffusion rates for PBMA (M_w=370K) at 70°C without post-addition (■) and with addition of 3 (□), 6 (●), and 9 wt% (○) of BMA oligomers.

While both water and oligomers might contribute in many ways to enhancement of polymer diffusion, the most likely mechanism is that they dissolve into the polymer and act to increase the free volume in the sample. Comparing oligomers, which can be regarded as *in situ* surfactant, to an ionic surfactant (SDS), we find that SDS can reduce the interparticle contact in the nascent films (c.f. Chap. V) but has negligible effect on diffusion rate of PBMA in annealed films.[19a] It is likely that SDS surfactant has much less miscibility with PBMA than the BMA oligomer. Upon annealing the films, the SDS can either be exuded to the surface[24a] or form separate phases in the films.[24b] The oligomers, however, may become distributed into the polymer matrix and can plasticize the polymer.

In practical latex films, there may be always some amount of water, oligomer, and lower-molar-mass polymer present. Also, latex polymers often consist of not only hydrophobic components but also significant amounts of hydrophilic components (e.g. polymers containing carboxyl groups) either initially present in the shell or distributed within the particles. Thus the above results have appealing importance for latex coatings.

VI-4 SUMMARY

The diffusion process of latex polymers was monitored by fluorescence energy transfer for films annealed at 60 or 70 °C. The effects of various components on the polymer diffusion rate were examined.

The role of water in polymer diffusion was investigated by comparing films kept in dry state with those wetted by either exposing to water vapor or immersing in liquid water both before and during heating. For a hydrophobic polymer [PBMA], water has little influence on the polymer diffusion rate. Water absorbed into the films increases film turbidity both for nascent films and for well-annealed films in which polymer molecules have approached an equilibrium mixing state. For a more hydrophilic polymer [P(MAA-co-BMA) with 5wt% MAA component, the presence of water (e.g. 5wt%) increases the diffusion coefficient by more than a factor of 5 at 60 °C. Upon neutralization the carboxylic acid groups of P(MAA-co-BMA) with NaOH, the polymer diffusion is much retarded in dry films, but enhanced in wet films. Water shows tremendous effect on the diffusion rate of NaOH-neutralized P(MAA-co-BMA) sample: the polymer diffusion coefficient measured for wet films is about two orders of magnitude larger than that for the corresponding dry films examined under the same conditions. Neutralization with NH_3 results in intermediate diffusion rates between unneutralized and NaOH-neutralized films under both dry and wet conditions.

The addition of BMA oligomers to PBMA latex enhances the polymer diffusion rate. We find that the presence of 3 wt% oligomers increases the diffusion coefficient of the polymer by almost an order of magnitude.

CHAPTER VII FORMATION AND CHARACTERIZATION OF LATEX FILMS CROSSLINKABLE UNDER AMBIENT CONDITIONS

VII-1 INTRODUCTION

Polymer latex particles bearing functional groups at the particle surfaces or within the particles have many practical applications. The functional groups can provide a latex with specific properties such as improved colloidal stability, modified rheological behavior, enhanced binding capacity for biomolecules or surface active substances, better adhesion to a given substrate, as well as increased mechanical performances of the films obtained from these latex samples.[1] When the functional groups are chemically reactive, they are capable of participating in various post-polymerization reactions.[2] Increasing interest has been paid to utilizing these reactive latex polymers to form crosslinkable films when they are applied as water-borne paints, coatings or adhesives.

Although latex coatings reduce the amount of volatile organic emissions and display excellent performance in the areas of applications, thermoplastic latex films lack the tensile strength, abrasion resistance, chemical resistance and general durability. These properties can be greatly improved by introducing crosslinks in the systems.[3] The properties displayed by crosslinking will depend upon the nature and amount of the curing agent, the crosslink density, and the location of the crosslink sites.

Film curing can be conventionally achieved by thermal treatment or sometimes by high energy (e.g. UV) radiation. In many applications of coatings systems, these conditions are not easily applicable and crosslinking under ambient conditions is desired.

VII-1-1 Brief Review of Thermal-cure Systems

Reactive latex particles which can form crosslinkable films are conventionally prepared by copolymerizing the base monomers with a functional monomer during the emulsion polymerization process. Carboxyl, hydroxyl and amide functionalities are frequently introduced into latex systems, particularly at the particle surface, with the use of monomers such as methacrylic acid, 2-hydroxyethyl methacrylate or N-methyloacrylamide.[1] An example of the applications of these latex samples is the use of multi-stage acrylic latex, with surface carboxyl and hydroxyl functional groups, in automotive basecoat.[4] Crosslinking can be achieved by reacting the hydroxyl groups with an added melamine crosslinker at a high baking temperature

(normally 140-160 °C). Of the various reactive monomers, N-methylol(meth)acrylamides (N-MAA or N-MMAA) are commonly used to develop crosslinking emulsions.[3,5] The methylol groups of N-MAA or N-MMAA can self-condense upon conventional thermal curing (e.g. at 200 °C). Ethers of N-methylol acrylamide (e.g. N-(iso-butoxymethyl) acrylamide)) have also been used as functional monomers to prepare crosslinkable latexes, by self-condensation or reacting with amines, hydroxyls, and carboxyls, under the conditions of heat.[2,6,7] Glycidyl (meth)acrylates (GA or GMA) are very useful reactive monomers. They contain both an epoxy group and a double bond and can be used in either nucleophilic substitution or radical reactions.[8] These monomers can copolymerize with unsaturated base monomers to produce latex particles bearing epoxy groups, preferably at low polymerization temperature to preserve the epoxy content.[9,10] Films formed from these particles can be cured with reactive substances such as carboxylic acids at elevated temperature.[8,11] Thiirane-functional monomers, e.g. 2,3-epithio-propyl methacrylate, have also been used to produce crosslinkable emulsions and the reactivity of the thiirane group has some differences compared to oxiranes introduced via GMA.[12]

VII-1-2 Brief Review of Ambient-cure Systems

An important goal for novel latex-based coatings is to cure the films at ambient temperature. This requires that the reactive substances have high reactivity. An interesting type of reactive monomer is acetoacetoxyethyl methacrylate.[13,14] The functional (acetoacetoxy) groups can be easily incorporated into acrylic latex, and crosslinking can be achieved at ambient temperature by reacting with difunctional amines, aldehydes, and electron-deficient olefins through the Michael reaction. The acetoacetoxy functionality offers unique versatility to the coatings formulators. Other reactive systems include maleimide-containing emulsions prepared with 6-(3-chloromaleimido)hexyl acrylate.[15] The maleimide unsaturation may be able to react with nucleophiles such as amines by addition reactions at ambient temperature. Epoxy-containing latexes prepared with GMA may also crosslink with diamines at temperatures close to room temperature.[11,16] Another type of application of GMA is to use the C=C double bond as the reactive functionality.[8,17] Latex particles bearing carboxylic acid groups at the surface may be prepared first. After post-reaction of the carboxyl groups with GMA, an unsaturated latex is obtained, and its films can be crosslinked under ambient conditions,[17] using a curing procedure similar to that employed for unsaturated oils or alkyd resins. Film curing based on hydrazone formation between a carbonyl and a hydrazine residue has also been widely investigated.[18] Other mechanisms involve esterfication between oxazoline and -COOH,[19,20] Schiff base formation between primary amine and C=O groups.[21]

VII-1-3 Our Approaches to Ambient-cure

While the heat curable latex systems have been described in both the patent literature and in scientific journals, there have been very few reports systematically examining films prepared from reactive latex particles that are curable at room temperature.

As a start in this direction, we have prepared latex samples containing the acetoacetoxy functionality and examined its reaction with diamines. Another approach involves preparing films with unsaturated functionality and air cure the films by reactions among the double bonds in a manner resembling polymerization reactions. This project has been in collaboration with the German Group in the Netherlands and was initialized during my visit in their group. We do not intend to invent new curing chemistry here. Rather, we think that these are attractive strategies for ambient cure of latex films.

For latex films the crosslinks need to be formed in a special way: one needs entanglements between polymer molecules from adjacent latex particles to generate strength in the system. Crosslinks between polymers originating in the same latex particles will only make the film weaker. The technology depends upon a proper balance between the rate of polymer interdiffusion to generate entanglements, and the rate of crosslinking to lock the entanglements in place. There is very little known about the rates of interdiffusion and crosslinking in these systems. This issue of the rates of polymer diffusion across interfaces in competition with crosslinking reactions which retard diffusion is a topic of intense interest, both to the academic and industrial communities. In this chapter, I describe systems in which we measure both rates, which are important for the development of mechanical properties of the films. In this way we hope to provide some useful knowledge for the curing technology of latex films.

VII-2 EXPERIMENTAL

VII-2-1 Latex Samples

One type of latexes contains acetoacetoxy (AA) groups as the reactive functionality. These are copolymers of either butyl methacrylate (BMA), or 2-ethylhexyl methacrylate (EHMA), with 10 wt% acetoacetoxyethyl methacrylate (AAEMA), referred to as AA-PBMA or AA-PEHMA. Most of these copolymerization reactions were carried out at 20 °C using a redox initiation system by a batch process, as described in Chap. II. Some AA-PEHMA samples were labeled with phenanthrene (Phe), and some with anthracene (An), referred to as Phe-AA-PEHMA and An-AA-PEHMA. These labeled samples were prepared at 80 °C, with the help of Mr. Hung Pham, using potassium persulfate as the initiator and dodecyl mercaptan (DM) as the chain transfer agent, via a semi-continuous process. The preparation conditions for these labeled

latexes are similar to those for the labeled PBMA as described in Chap. II, with nearly 100% of dye fraction reacted and randomly incorporated into polymer chains. We found that it was difficult to obtain an efficient and uniform dye labeling when polymerizations were carried out at 20 °C using the redox initiators, either via a batch or via a semi-continuous process.

The other type of latex has unsaturated (U) bonds as functionality. They were prepared by reacting glycidyl methacrylate (GMA) with the carboxyl groups covalently attached to latex polymers, as described in Chap. II. The latex samples before introducing unsaturation were terpolymers of BMA (70.5 wt%), BA (23.5 wt%) and methacrylic acid (MAA, 6.0 wt%). This composition was chosen based on the consideration that the resulting Tg of the polymer should be below 22 °C and the amount of BA should be small enough to avoid premature branching or crosslinking. One such a carboxylated latex was prepared at 20 °C (latex C-1), while the other was prepared at 60 °C and with the addition of a chain transfer agent (DM) (latex C-2) for lowering the molecular weight of the polymer and hence for the ease of characterization in solution. After introducing unsaturation, the respective latexes are referred to as U-1 and U-2. We estimated that about 80% of -COOH groups had been reacted to form unsaturated bonds. The details of latex preparation and characterization have been described in Chap. II.

Some important characteristics for these reactive latexes are presented in Table VII-1.

Table VII-1 Characteristics of latexes containing acetoacetoxy and unsaturated-bond functionalities

Latex	AA-PBMA	AA-PEHMA			U-1	U-2
Label	Non-	Non-	Phe-	An-	Non-	Non-
Diameter (nm)	54.2	50.8	85	85	58.1	39.7
Polydispersity	0.082	0.078	0.02	0.02	0.044	0.090
Tg (°C)	18	-9	-9	-9	2	2
Solids (wt%)	10.6	10.5	26.0	25.4	11.4	11.6
Mw ($x10^4$)	78	-	4.7	4.8	70	11
Mn ($x10^4$)	28	-	1.7	1.5	22	2.7

a. The Tg values here are estimated by the Fox equation using the Tg values of 20, -10, 5, -55, and 130 °C (see Table II-1) for PBMA, PEHMA, PAAEMA, PBA, and PMAA, respectively.

VII-2-2 Film Formation, Crosslinking, and Measurements

Our latex dispersion samples had a solid content of ca. 10 wt%, and it took 3-5 hours for them to dry in the open air (50-65 %RH) to form films (ca. 50 μm thick). The drying rates of dispersions were analyzed by gravimetric water loss measurements.

For crosslinking the acetoacetoxy-functionalized films, a certain amount of 5% aqueous solution of 1,6-hexane diamine (Aldrich, 98%), with a molar ratio $NH_2(CH_2)_6NH_2$: AA = 1 : 2, was added into the dispersions and the mixtures were dried, giving solid films. Some films were further aged in air for 3 days or a week.

For crosslinking the films with unsaturated bonds, the latex dispersions (e.g. latex U-1) were mixed with 0.1-0.5 wt% (based upon polymer) of a "drier", cobalt octoate in its xylene emulsion or cobalt naphthenate (Fluka). A few drops of the mixed dispersion was placed on a glass substrate, dried, and further aged in air.

The extent of crosslinking was characterized by solvent extraction and swelling measurements. Film specimens (weight: W_0, dimensions: ~15 x 15 x 0.1 mm^3) were immersed in 1,4-dioxane for 72 h to attain swelling and dissolution equilibrium. The remaining film specimens were then carefully removed from dioxane, and the solvent attached to the surface was wiped off with filter papers. The weight of the film (W_1) was measured. This procedure was completed as immediately as possible (in 5 seconds) to assure accurate and consistent measurements. The film was then dried again to a constant weight (W_2) in a vacuum oven. The gel content (%) and swelling ratio are calculated from the following expressions:

$$\text{Gel content (\%)} = (W_2 / W_0) \times 100\% \qquad \text{(VII-1)}$$

$$\text{Swelling ratio} = (W_1 / W_2) \qquad \text{(VII-2)}$$

Films were also characterized by spectroscopic measurements, for example, by NMR and FTIR techniques. In the FTIR measurements, films were prepared by casting very dilute latex dispersions onto water-resistant IR plates and then placed in the sample chamber equipped with N_2 flow. ^{1}H-NMR measurements were performed for non-crosslinked polymers in solution or for lightly-crosslinked polymers in the swollen state in organic solvents, on a Varian 200-MHz NMR spectrometer. Sometimes the use of mixture of solvents (e.g. d-chloroform and d-toluene) was necessary to allow the polymer to be well suspended in the tube. For highly crosslinked films, ^{13}C solid-state high-resolution NMR spectra were measured in the laboratory of Prof. Peter M. Macdonald, employing various techniques including magic-angle spinning, cross-polarization, and decoupling to minimize the line broadening.

For polymer diffusion analysis by direct non-radiative energy transfer, fluorescence decay measurements were carried out for labeled films. The measurement conditions and data analysis technique were similar to those described in Chap. V and VI.

VII-3 RESULTS AND DISCUSSIONS

VII-3-1 Acetoacetoxy (AA) System

The AA-PBMA latex forms turbid films with large cracks at room temperature (22 °C), whereas the AA-PEHMA latex forms soft, clear films under the same conditions. This is consistent with the difference in Tg (and MFT) values between these two latex polymers.

Both pure AA-PBMA and pure AA-PEHMA latex samples give films soluble in organic solvents such as dioxane (Only after long storage do the films form gels in a good solvent due to light crosslinking). This indicates that negligible crosslinking occurred during the preparation of the above two kinds of copolymer latex particles. The low temperature polymerization by the use of a redox initiator system favors the production of linear polymers (avoiding crosslinking reactions between functional groups). Also, the AA content in the copolymers is sufficiently low to avoid gel formation (Note that a latex homopolymer of acetoacetoxyethyl methacrylate, PAAEMA, prepared under similar low-temperature conditions, is partially gelled).

Crosslinking of the AA-containing copolymer latex systems was achieved by adding hexane diamine into the dispersions and air drying the dispersions to form films.

VII-3-1-1 The drying behavior and pseudoplastic rheological effect

When the above AA-containing latex samples are mixed with diamine in the dispersion and air dried, the drying behavior and appearance of the dispersions show many differences. First, these dispersions increase their viscosity and turn into nearly an immobile state when the drying reaches only about 15 wt% solids (in about 40 min). In contrast, the wet dispersions in the absence of diamine remain liquid-like until the drying is much closer to the end. Second, from the very beginning of the drying process, dispersions with diamine exhibit much higher turbidity than those of the pure latex, implying the occurrence of association of individual particles into larger-sized groups. We infer from the above results that there may be interactions between the diamine molecules and particles, which cause association of the particles and the increase in turbidity and viscosity. This high viscosity can exist easily under conditions of little mechanical disturbance or low shear rate. At high shear rate, the physical association between the latex particles and the diamino molecules must be destroyed, and the viscosity becomes low. This rheological effect is known as pseudoplastic characteristics,[22] which is useful for many coatings applications. The pseudoplastic properties can arise from many different types of interactions, e.g. the hydrogen bonding and the association between polar or hydrophobic

groups.[4] An example of such a kind of systems is a latex dispersion containing carboxylic acid and hydroxyl groups at the particle shell, which exhibits pseudoplastic behavior upon addition of melamine to the system.[4] In the present system, the interaction is likely the hydrogen bonding between the amino groups and the acrylic ester groups or the polar groups at the particle surface. This is confirmed by a similar rheological effect observed for dispersions of PBMA latex without the AA-functional groups but in the presence of diamine.

In addition to the possible physical association between the amino groups and the particle surfaces, the crosslinking reactions between the diamine molecules and the acetoacetoxy groups at the particle surface can give rise to an additional effect on the viscosity increase. We found that the AA-containing PBMA dispersions became highly viscous during drying much earlier (e.g. 40 vs. 90 min) than the AA-free PBMA samples, both in the presence of diamine and with the same initial solid content (10 %). Also, as will be pointed out below, the crosslinking reactions in the AA-containing system occur well before the dispersions are dried. This type of chemical bridging of particles leads to the formation of microgel, and unlike physical association, it is in fact an irreversible process.

Another important phenomenon is that dispersions with diamine dry uniformly across the surface, while those without diamine dry with a drying front, showing a dry film at the edge which grows towards the center. The drying front is always seen in a normal latex system, related to the flux of liquid water and particles in the substrate plane.[23] This indicates that no macroscopic particle motion across the film plane is possible due to the presence of diamine in the drying dispersions. This drying behavior is consistent with the high viscosity observed for dispersions with diamine present.

Comparison of drying rate: Due to the large difference in drying behavior between dispersions with and without diamine, we carried out experiments in which we monitored the drying rates of these samples. Figure VII-1 shows drying curves for a AA-PBMA latex dispersion with and without diamine. One sees that the addition of diamine to the dispersion increases significantly the drying rate. It takes less time (ca. 4.3 h Vs. 5 h) for the amino-containing dispersion to reach 97% solids than for the dispersion without amine. Comparing the drying behavior between pure PBMA latex (no AA) with and without diamine, we observe a very similar behavior: the amino-containing dispersion dries faster than the amino-free dispersion. In our experiments, some samples were ion-exchanged to remove ionic substances (e.g. surfactant) before addition of diamine, some were used without cleaning. The presence of surfactant and other ionic species changes slightly the rate difference between the amino-containing and amino-free dispersions. This, however, does not alter the trend of drying rates: the presence of diamine always facilitates drying. We attribute the fast drying rate because of the presence of diamine to its creation of hydrophilic channels between particles which allows for water transport. This concept has been illustrated previously for the enhancement effect of ionic surfactant on drying rate.[23] Another

reason for the fast evaporation in the sample with diamine would be that such a latex dispersion dries uniformly across the surface, while in the sample without diamine the wet dispersion decreases in surface area during drying.

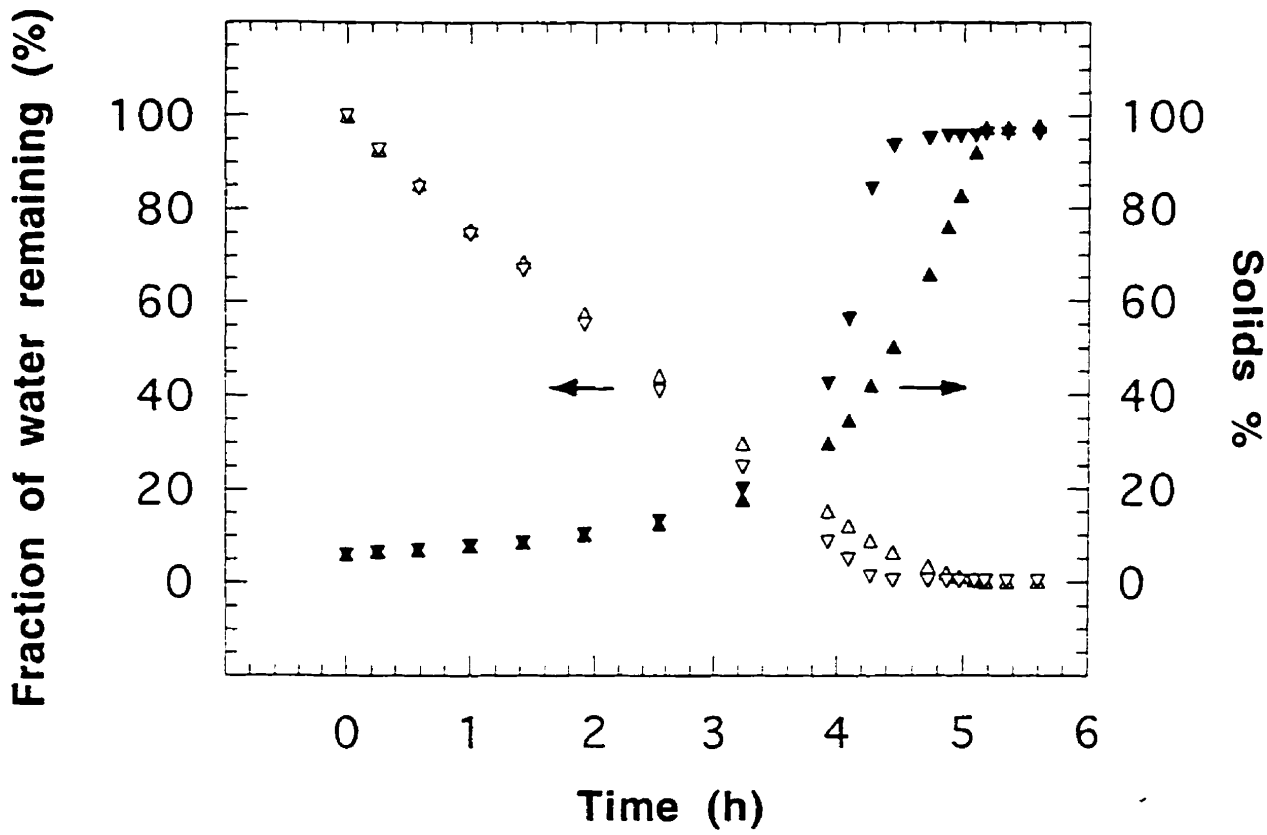

Figure VII-1. Plots of percent solids (%, filled symbols) and the fraction of water remaining (%, open symbols) as a function of drying time (in h) for an AA-PBMA latex dispersion in the presence (∇▼) and absence (Δ▲) of hexane diamine.

VII-3-1-2 Characterization of the crosslinking reactions

Films formed from dispersions containing the diamino compound were not soluble in dioxane or other organic solvents, neither the AA-PBMA nor the AA-PEHMA latex samples. This indicates that reaction between amino and acetoacetoxy groups occurs during air drying and

aging, resulting in sufficient crosslink density in the latex films to resist organic solvents. Note that after drying, the AA-PBMA latex, which only formed powdery films upon drying at room temperature, produced continuous, highly transparent films when mixed with diamine.

The gel content and swelling ratio in dioxane were measured for films either newly formed or aged, allowing us to look at the crosslinking capacity of the reactive species in the films. Table VII-2 summarizes the results for these samples and also for those samples in the absence of diamino crosslinker.

Table VII-2. Gel content and swelling ratio in dioxane for films formed from AA-PBMA and AA-PEHMA latex samples with or without diamines

Latex	AA-PBMA			AA-PEHMA			
	No amine	with amine		No amine	with amine		
		fresh	3 days		fresh	3 days	7 days
Gel content (%)	0	98	97	0	90	92	92
Swelling ratio	∞	3.1	3.0	∞	1.8	1.9	1.9

The addition of diamine to both AA-PBMA and AA-PEHMA latex dispersions led to crosslinked films with only a small weight fraction extractable in a good solvent. The extractable part might include trace amounts of water, monomer, unreacted diamine and a small amount of polymer. The major part of the film formed a stable network, only swellable but not soluble in solvent. When comparing the AA-PBMA latex films with the AA-PEHMA films, the latter had a relatively lower degree of swelling. One would expect that the lower Tg AA-PEHMA copolymer would provide higher mobility for achieving higher density of crosslinking than the relatively higher Tg AA-PBMA copolymer. A lower gel content observed for AA-PEHMA films compared to the AA-PBMA films would be due to either composition heterogeneity or lower miscibility of amine in the AA-PEHMA sample.

The results also show that there is virtually no significant difference between the newly formed films and those aged for 3 days or a week, for both AA-PBMA and AA-PEHMA latex samples in the presence of diamine. A possible explanation is that the crosslinking reaction takes place at a rapid rate. Thus after our films were dried (e.g. 3h), the crosslinking reactions had occurred to a large extent, and further aging would not increase significantly the crosslinking

density. We will confirm this point below.

The mechanism of reaction between acetoacetoxy and amino groups is believed to be the formation of enamino ester,[13,14] as shown in Eq. (VII-3):

$$-OCO-CH_2-COCH_3 + H_2N-R \rightarrow -OCO-CH=C(CH_3)NH-R + H_2O \qquad (VII-3)$$

We attempted to employ spectroscopic techniques to further characterize the crosslinking reactions or, if possible, to quantify the extent of these reactions occurred in the films. The first technique we employed was FTIR. Based on the above reaction mechanism, the crosslinking reaction between an acetoacetoxy and an amino group should be characterized by the formation of a C-N bond and the cleavage of a C-O and a N-H bond. Unfortunately, in the IR spectra we obtained (not shown), the absorbance peaks for the C-N bonds or C-O bonds largely overlap with those peaks from the base polymer and those from the added diamino compound. Yet, the characteristic peak at 3300 cm^{-1} for N-H bonds is always masked by the presence of trace amounts of water in the film or in the sample chamber. This problem is unavoidable, even when the films are stored under vacuum and examined in a nitrogen environment. We are thus unable to observe the changes associated with crosslinking from IR measurements.

We used NMR technique to characterize these films. High-resolution solid-state ^{13}C NMR spectroscopy was investigated as a means of determining the extent of crosslinking with hexanediamine. Figure VII-2 shows spectra for a homopolymer of acetoacetoxyethyl methacrylate (PAAEMA) before and after mixing with diamine in THF for 24 hr, followed by drying. The PAAEMA sample was prepared under conditions similar to the AA-PBMA and AA-PEHMA copolymers. The addition of hexanediamine to PAAEMA in this case should produce a model sample with a high extent of crosslinking, allowing us to observe clearly the changes associated with the reactions. In our assignment for each individual resonance shown below, standard spectra of relevant compounds in refs. 24 and 25 were used for comparison.

In the spectrum of pure PAAEMA (Fig. VII-2a), one can readily identify resonances associated with the methacrylate backbone methyl (16 ppm), ternary carbon (45 ppm), and carbonyl (178 ppm), although the backbone methylene (55 ppm) is obscured by other resonances. In particular, the ethoxy methylenes are expected to occur in the region of 63 ppm where there is a broad ill-resolved group of resonances. Likewise, the methylene of the acetoacetoxy, flanked by carbonyls, occurs in this region of the spectrum (50 ppm). The terminal methyl of the acetoacetoxy group is clearly resolved (30.3 ppm), as are the carboxyl carbonyl (168.2 ppm) and the aldehyde carbonyl (202.2 ppm). Because these ^{13}C NMR spectra were acquired using cross-polarization the resonance intensities cannot be used quantitatively.

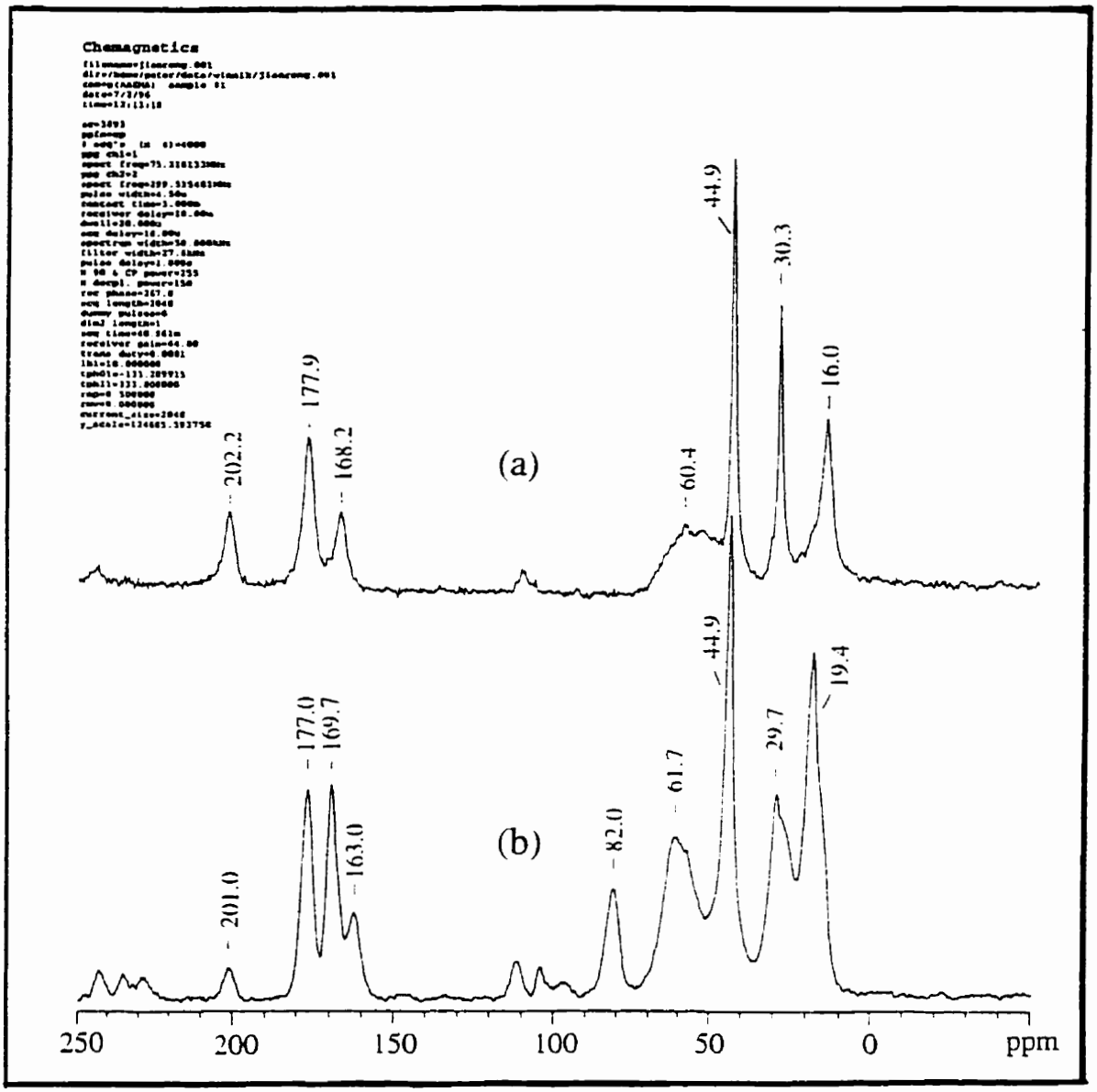

Figure VII-2. ^{13}C high-resolution solid-state NMR spectra for samples of: (a) PAAEMA, and (b) PAAEMA crosslinked with diamine for 24 h in THF followed by drying.

When the PAAEMA polymer is mixed with diamine to undergo crosslinking reactions, we observed some important changes in ^{13}C-NMR spectrum (Fig. VII-2b). The resonances from the crosslinker hexanediamine itself occur in the region of 29 ppm for the methylenes beta and gamma to the secondary amine, and at about 50 ppm for the alpha methylene, although the latter resonance cannot be resolved from the ethylmethacrylate resonance occurring in the same region of the spectrum. Major changes in this spectrum include the loss of the terminal methyl resonance at 30.3 ppm and the acetoacetoxy aldehyde carbonyl resonance at 202 ppm. The latter is not completely absent, indicating that 100% crosslinking was not achieved. New resonances appear at 169.7 ppm corresponding to the ester carbonyl in its new environment next to a site of unsaturation, at 163.0 ppm corresponding to the methyne unit of the enamine, and at 82.0 ppm corresponding to the ternary carbon of the enamine. These results clearly indicate that the ^{13}C-NMR is capable of both detecting crosslinking with hexanediamine and identifying the resulting product. In particular, the carbonyl region of the spectrum yields the most clear-cut information. Our results lend supports to the reaction mechanism between acetoacetoxy and amine groups proposed previously.[13,14]

When copolymers of BMA or EHMA with 10% AAEMA, after crosslinking with hexanediamine, were investigated via ^{13}C-NMR under the same conditions, it was observed that the particular resonances corresponding to the AAEMA units were too low in intensity to be useful as a means of quantifying crosslinking.

VII-3-1-3 Film formation rate vs. crosslinking rate

a. Crosslinking rate. To have information about the crosslinking rate, we monitored the change of gel content of the polymer with reaction time. Since it is observed that a high extent of crosslinking has occurred in the newly dried films, we start this measurement for samples in the dispersion state well before complete drying. Each dispersion was quickly freeze-dried after a certain time of reaction, and the dried powder was placed into dioxane and stirred, and then the insoluble part (gel) formed due to crosslinking was obtained by centrifugation. Figure VII-3 shows the plot of gel content (%) as a function of time for an AA-PBMA latex mixed with diamine. Here the starting reaction time was the time when the dispersion (latex + diamine) was placed onto a glass substrate, after the two reactive components had been mixed and stirred for 5 min. We see that a fast crosslinking occurs between the reactive moieties: the gel content reaches above 80% after drying for 5 min. At reaction time 60 min., the gel content reaches 95%, quite close to that (ca. 97%) for the film completely dried (after 210 min). Similarly, a fast crosslinking rate is observed for the AA-PEHMA sample.

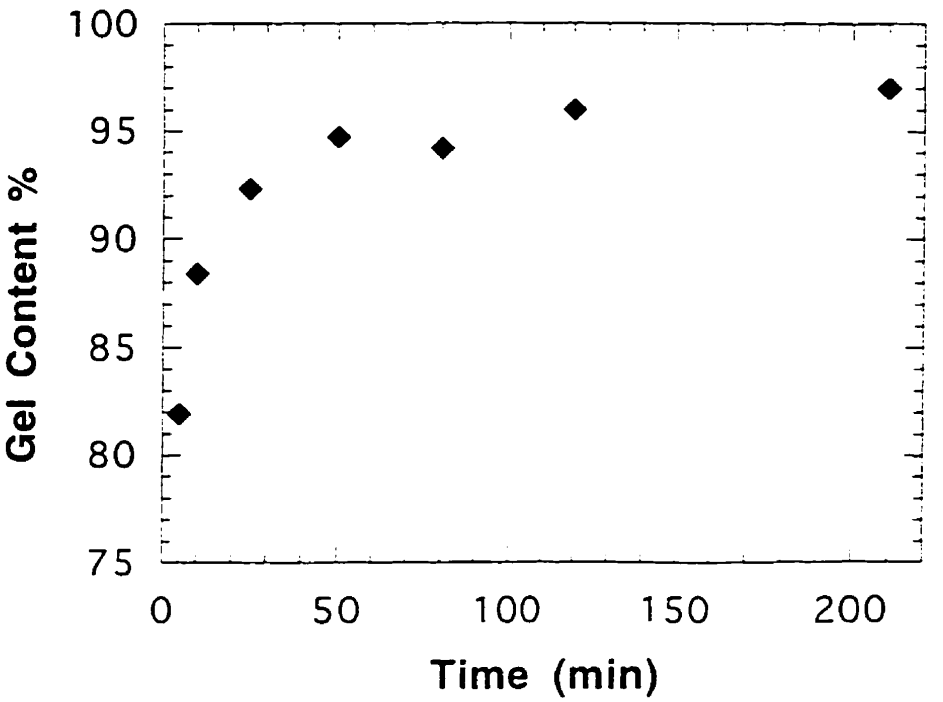

Figure VII-3. A plot of gel content (%) Vs. time for an AA-PBMA film crosslinked with diamine.

b. Ambient diffusion rate of polymers. In case of PBMA samples, we have found that polymer diffusion is negligible at room temperature when the polymer molecular weight is high (e.g. Mw > 10^5). Such a high molecular weight is characteristic of many emulsion polymers. We have a pair of labeled PBMA samples with lower molecular weight (Mw = 3.5 x 10^4, Mn = 1.7 x 10^4, Tg ≈ 20 °C). By fluorescence energy transfer analysis, we monitored the growth of the extent of mixing (f_m) with diffusion time and evaluated the polymer diffusion coefficient D_{app} (in nm^2/s) for this polymer at 22 °C. Table VII-3 shows these results. We also show the increase in interpenetration depth d_i (in nm), defined as $(6Dt)^{1/2}$ in Chap. VI, with time.

Table VII-3. The extent of mixing (f_m), diffusion coefficient (D_{app}), and interpenetration depth (d_i) at 22 °C for PBMA (Mw = 3.5 x 10^4, d = 125 nm)

t (h)	f_m	D_{app} (nm^2/s)	d_i (nm)
0	0	-	0
12	0.14	6.4 x 10^{-4}	13
72	0.28	4.3 x 10^{-4}	25
264	0.58	5.9 x 10^{-4}	58

One notices that for the given molecular weight, the PBMA can effectively diffuse at room temperature on a time scale of days. If we estimate the average penetration depth per minute (d_i/dt), we find values of 0.02 nm/min or less. As mentioned above, the crosslinking reaction for the AA-containing PBMA with diamine occurs on a time scale of minutes. From these results it is clear that the PBMA diffusion rate is too slow to allow for sufficient penetration and entangling before crosslinking, even for a quite low molecular weight.

We also carried out diffusion experiments for the lower Tg (-7 °C, as measured by DSC) PEHMA samples. The Phe- and An- labeled PEHMA samples (d = 85 nm, Mw = 4.7 x 10^4, Mn = 1.6 x 10^4, see Table VII-1) are AA-containing terpolymers made of 89 wt% EHMA, 10 wt% AAEMA, and 1 wt% fluorescent monomer. We intended to examine both the interdiffusion and crosslinking processes on the same samples. Figure VII-4 shows donor decay profiles for AA-PEHMA samples (no diamine) aged for different times. Since the diffusion time for this polymer is shorter, we prepared thick films (ca. 300 μm) to minimize the measurement time (< 8 min) for each decay profile.

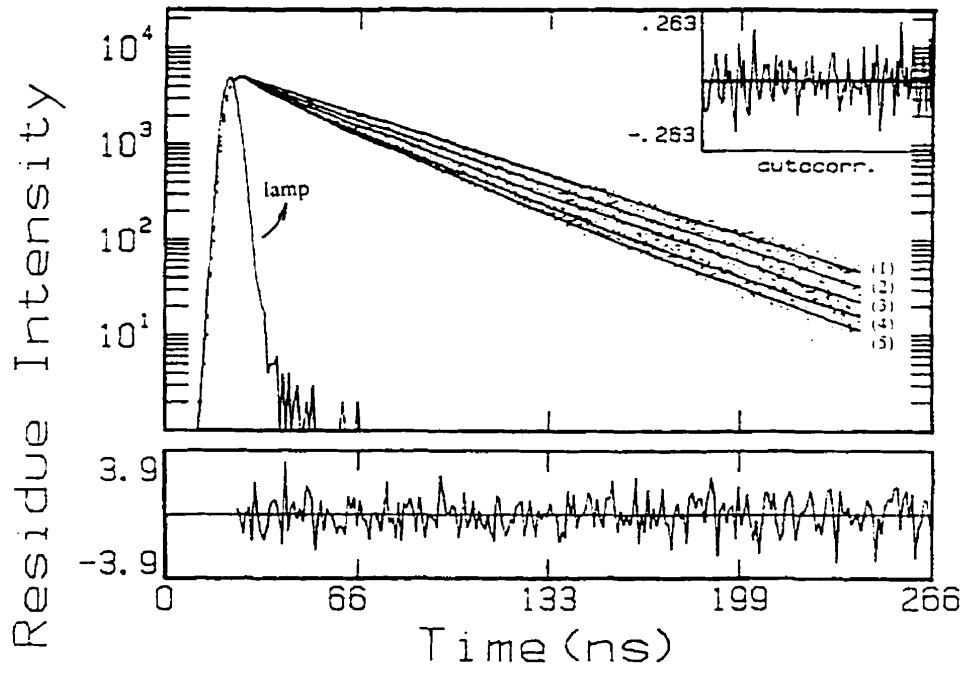

Figure VII-4. Donor fluorescence decay profiles for AA-PEHMA latex films (Mw = 4.7 x 10^4, d = 85 nm, Phe : An = 1 : 1) with diffusion time of: (1) 0, (2) 30, (3) 60, (4) 120, (5) 180 min, respectively. These curves are integrated to obtain the areas under them in our data analysis, as described in Chap. VI. A decay function expressed as: $I_D(t) = A_1 \exp[-t_d/\tau_D^\circ - p(t_d/\tau_D^\circ)^{1/2}] + A_2 \exp(-t_d/\tau_D^\circ)$, is used to fit the curves for area integration. In the Figure we also display the weighted residuals and their autocorrelation for curve 2 when fitted to the above expression.

From the decay profiles we analyze the diffusion rate for the polymer. The results are shown in Table VII-4.

Table VII-4. The extent of mixing (f_m), diffusion coefficient (D_{app}), and interpenetration depth (d_i) at 22 °C for AA-PEHMA (Mw = $4.7x10^4$, d = 125 nm)

t (min)	f_m	D_{app} (nm^2/s)	d_i (nm)
0	0	-	0
30	0.41	6.5×10^{-2}	26
60	0.61	8.3×10^{-2}	42
120	0.84	1.2×10^{-1}	72
180	0.90	1.2×10^{-1}	90

We notice that this polymer diffuses to a significant extent within 30 min. The diffusion distance per minute (d_i/dt) estimated for this sample is ca. 1 nm/min at early times and 0.5 nm/min at later times. For an aging time as short as 10 min, a significant amount of penetration (e.g. 5-10 nm) can be observed. Thus the interdiffusion rate for this polymer is much more comparable to the crosslinking rate in the given system.

We carried out similar experiments in which the Phe- and An- labeled AA-PEHMA particles were mixed in the presence of diamine to produce films, in which both the growth of energy transfer efficiency and the crosslinking reactions occurred. An unexpected result of donor fluorescence decay is observed for such a system. An example of a donor decay profile for such a film (aged for 10 h after drying) is shown in Figure VII-5 (curve 1). One sees that in addition to the energy transfer from donors to acceptors causing the deviation of the decay from exponential, a very fast decay component is seen at early times of the decay. The decay behavior of this component is much different from that due to energy transfer to anthracene, as seen in the profiles in Fig. VII-4. This fast component is more pronounced for films aged for longer time and less pronounced for freshly-formed films. Since this decay behavior is not seen when we examine films prepared from latex without AA-functional groups but with the addition of diamine (curve 2), it is clear that it is related to the crosslinking reactions. Species produced from the reactions might act as a quencher for the donor fluorescence. What is surprising is that when we measure a film prepared from Phe-AA-PEHMA particles (no An-labeled particles) mixed with

diamine, the donor decay rate is not influenced by the crosslinking reactions (curve 3). We then suspect that the fast decay component would arise from cooperative action from both the An molecules and the crosslinking reaction products. This interaction may produce either a new short-lifetime fluorescent species or an efficient quencher to Phe- emission. The presence of this decay component complicates our data analysis for interdiffusion in competition with crosslinking. It, however, serves as an indicator for the crosslinking reactions.

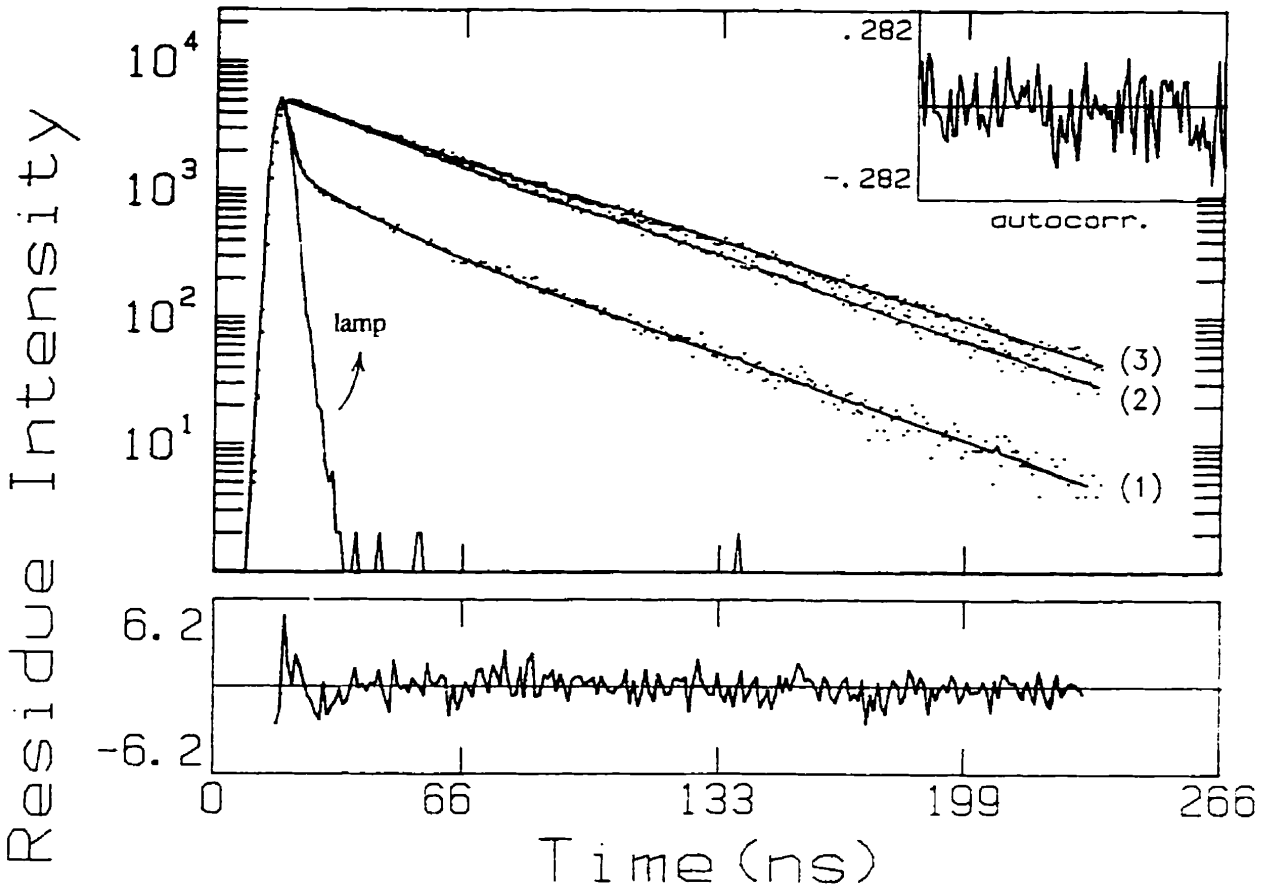

Figure VII-5. Donor decay profiles for films: (1) prepared from 1 : 1 Phe- and An- labeled AA-PEHMA particles in the presence of diamine and aged for 10 h after drying; (2) prepared from 1 : 1 Phe- and An- labeled particles without AA-functional groups but with the addition of diamine; (3) prepared from Phe-AA-PEHMA particles (no An-labeled particles) mixed with diamine.

While the crosslinking strategy presented here based on acetoacetoxy/amino functionalities provides an efficient way for film crosslinking, one can expect that the crosslinking rate is too fast to form well-mixed, coherent latex films. The fact that a significant extent of crosslinking occurs before the dispersion is dried is particularly undesired. Even for the

above-mentioned AA-PEHMA sample which can diffuse a few nanometers in several minutes, negligible interdiffusion can be detected for such a film sample before dried (e.g. at 92% solid content, 30 min before completely dried). The decay profile for this sample (not shown) overlaps with curve 3 in Fig. VII-5. Thus the crosslinking reaction here always precedes the polymer interdiffusion rate.

To decrease the crosslinking rate, one can either reduce the amount of AA content in the latex or change the type of amino compounds.

VII-3-1-4 Loss of functionality during storage and upon heating

We noticed in our experiments that the AA-functionalized samples gradually decreased their efficiency for crosslinking with diamine. Table VII-5 shows our comparison of crosslinking capacity between newly prepared AA-PEHMA latex and the same latex stored for 6 months. One sees that after storage the gel content is decreased, and the swelling ratio is considerably increased. We also observed that the AA-PEHMA films in the absence of diamine became lightly crosslinked (gel content ca. 50 % in dioxane) after storage for 6 months, while those fresh films were completely soluble. This gel formation is another indication that the functional groups have undergone chemical reactions, in relation to the loss of AA content, during the aging period.

Table VII-5. Gel content and swelling ratio in dioxane for AA-PEHMA/ diamine films using the latex freshly prepared and stored for 6 months

Film	AA-PEHMA latex + Diamine	
	Fresh	**Stored for 6 months**
Gel content (%)	90-92	83-87
Swelling ratio	1.8-1.9	2.5-3.5

To monitor the changes in polymers, ^{1}H-NMR spectra were measured. Comparing the spectra for a fresh and an aged latex polymer, we observed that the intensity of the peaks for the AA groups has significantly decreased (e.g. by 35% for PBMA and more for PEHMA after storage for 6 months).

When the latexes are heated or prepared at high temperatures, a noticeable amount of AA functionality is lost. Figure VII-6 shows ^{1}H-NMR spectra for a fresh AA-PBMA latex (prepared at 22 °C) and for the same sample after heating at 70 °C for 5 h and 20 h. One sees that after heating for 5 h, the intensity of the peak at 3.6 ppm for the methylene group and that at 2.3 ppm

for the methyl group in AA unit have both decreased by ca. 25%. A factor of 40% of decrease is observed for the sample heated for 20 h. We also found that the labeled AA-PEHMA samples prepared at 80 °C with a total polymerization time of 8 h had an AA content to some extent (ca. 30%) lower than that of the theoretical value, although a significant level of AA was still preserved, and the polymer was completely organic soluble.

It has been proposed that the loss of functionality in such a system is mainly due to the hydrolysis of the acetoacetoxy group, giving decomposition products such as acetone and carbon dioxide.[26] Some coatings formulators have tried to add stabilizers such as ammonia, employing the enamine formation mechanism, to prevent this hydrolysis. [26]

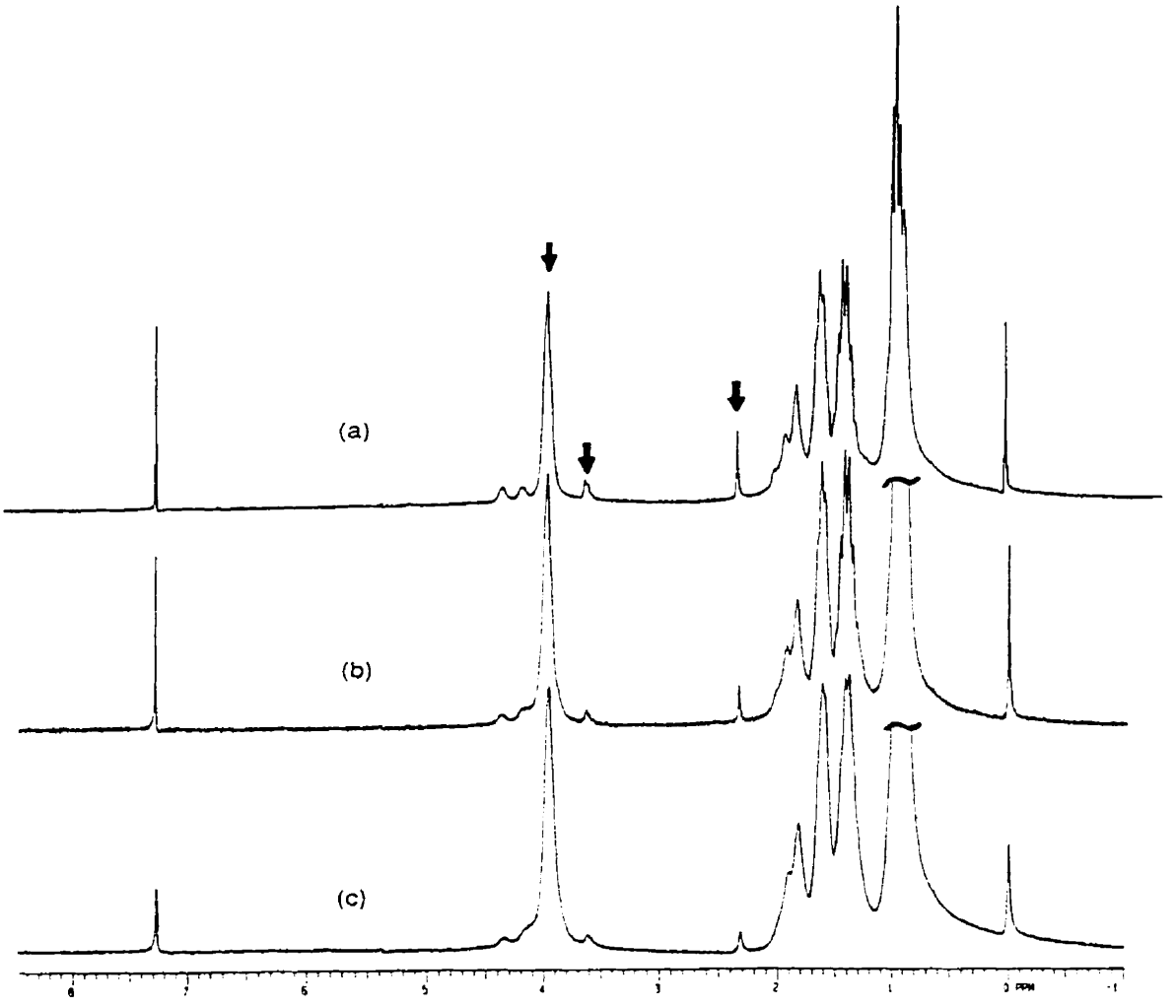

Figure VII-6. ^{1}H-NMR spectra for a fresh AA-PBMA latex polymer (prepared at 22°C) (curve a) and the sample in (a) after heating at 70 °C for 5 h (curve b) and 20 h (curve c). The arrows indicate the peak at 3.6 ppm for the active methylene group, that at 2.3 ppm for the methyl group in AA unit, and that at 3.9 ppm for the -C$\underline{H}_2$-OCO protons in PBMA. The relative intensities of these peaks are used to monitor the change of AA content.

VII-3-2 Unsaturated (U) SYSTEM

Perhaps the most interesting approach to ambient cure of latex films involves a system with air-curable functionality. The patent by Mylonakis describes reacting surface acid groups on a latex in water with glycidyl methacrylate to introduce surface unsaturated groups.[17] Perhaps because of the low solubility of O_2 in water, the unsaturated bonds remain unreactive in the dispersion, but polymerize in the dry film exposed to air. Union Carbide reported alternative post-functionalization chemistry based upon carbodiimide methacrylates.[27] Here we examine the strategy based on the Mylonakis approach.

We first prepared carboxylated P(BMA-co-BA) latex samples. We then carried out a reaction of the -COOH groups with glycidyl methacrylate (GMA), which contains both a double bond and an epoxy group that could react with -COOH. In this way unsaturated (reactive) latex samples were prepared.

Films were formed on glass substrate from dispersions of the unsaturated latex (U-1), mixed with a small amount of "drier" (e.g. cobalt octoate). The dry films were then cured in air for 7 days or longer. The procedure was similar to that used in the Mylonakis patent.[17] The crosslinking of these films was evaluated by solvent extraction and swelling. Films formed from saturated latex samples (before post-reaction) were also compared. Table VII-6 summarizes the results.

Table VII-6. Gel content and swelling ratio for films formed from unsaturated and saturated latexes and cured in air with or without a drier agent

Latex	Saturated latex		Unsaturated latex		
	No drier	with octoate	No drier	with octoate	
				7 days	12 days
Gel content (%)	0	0	0	87	87
Swelling ratio	∞	∞	∞	13	12

Films formed from saturated latex were completely soluble in solvent (i.e. 0% gel in dioxane) either in the absence or presence of a curing agent. For the unsaturated latex films, crosslinking also did not occur after 7 or 12 days when no curing agent was present. In contrast, films formed from unsaturated latex in the presence of cobalt octoate were crosslinked after aging for ca. 7 days.

A normal cure time for such a system is 30 days.[17] We have shown above that for this crosslinking rate, a low Tg latex (e.g. PEHMA) can diffuse to well mix. Even for a latex polymer having a Tg close to room temperature (e.g. PBMA), the polymer can effectively diffuse when the molecular weight is not high (e.g. Mw = 3.5×10^4). Thus the approach here based on air-cure of unsaturated latex represents a slow cure approach, which can allow for sufficient interdiffusion.

VII-4 SUMMARY

Reactive latex particles were prepared and characterized. These latex particles were of two types: one bearing acetoacetoxy groups and the other with post-incorporated unsaturated groups as the reactive functionalities. Film formation was carried out and film air-curing was performed for both types of reactive latex samples. Significant crosslinking was achieved for both types of latex films, as indicated by their solvent resistance. The approach based on unsaturated functionality represents a slow-air-curing strategy, while that based on reaction between acetoacetoxy and diamine provides a rapid crosslinking process. Both reaction routes tested for low temperature latex film crosslinking were deemed to be successful.

APPENDICES

Appendix II-1 Recipes for Preparation and Characteristics of P(BMA-co-BA) Latexes

Table AII-1-1. Recipes for Preparation of P(BMA-co-BA) Latexes

Sample	III-1-1	III-1-4	III-1-5	III-1-6	III-1-7	III-1-8	III-1-9	III-1-10[a]	III-1-11[b]
Batch Stage									
BMA[c] (ml)	3.5	2	0	1	2	0	5	2	2
BA[d] (ml)	3.5	0	2	1	0.5	0	1.2	0.5	0.5
Water (ml)	100	100	100	100	100	500	500	485	485
KPS[e] (g)	0.085	0.085	0.085	0.085	0.085	0.425	0.425	0.30	0.30
SDS[f] (g)	0.44	0.44	0.44	0.33	0.33	1.65	1.65	0.66	0.66
$NaHCO_3$ (g)	0.09	0.09	0.09	0.09	0.09	0.45	0.45	0.45	0.45
Temp. (°C)	70	70	70	70	70	70	70	70	70
Time (h)	1	2	2	2	2	0	1	1	1
Semi-batch	**Stage**								
BMA (ml)	-	-	-	-	-	2.0	10	13	13
BA (ml)	-	-	-	-	-	0.5	2.55	3.25	3.25
AnMA[g] (g)	-	-	-	-	-	-	-	0.32	-
PheMMA[h] (g)								-	0.32
Water (ml)	-	-	-	-	-	-	-	15	15
KPS (ml)	-	-	-	-	-	-	-	0.15	0.15
SDS (g)	-	-	-	-	-	-	-	1.0	1.0
Temp. (°C)	-	-	-	-	-	70	70	70	70
Time (h)	-	-	-	-	-	4	4	4	4

a. Anthracene-labeled latex; b. Phenanthrene-labeled latex; c. Butyl methacrylate; d. Butyl acrylate; e. Potassium persulfate; f. Sodium dodecyl sulfate; g. (9-Anthryl) methacrylate; h. (9-Phenanthryl) methyl methacrylate.

Table AII-1-2 Properties of P(BMA-co-BA) Latexes

Sample	III-1-1	III-1-4	III-1-5	III-1-6	III-1-7	III-1-8	III-1-9	III-1-10 [a]	III-1-11 [b]
Diameter (nm)	43	25	28	28	32	21	38	49	55
Polydispersity	0.008	0.042	0.088	0.018	0.026	0.13	0.017	0.077	0.082
Solid content (wt%)	6.16	2.27	2.37	1.82	2.57	2.58	2.78	3.62	3.78
Tg [c] (°C)	-33.0	22.9	-55	-33.8	-6.9	-1.9	4.1	9.9	5.1
Mw ($x10^{-5}$)	8.4	2.8	-	-	6.7	1.3	3.5	1.1	5.1
Mw/Mn	1.7	2.1	-	-	1.9	3.0	24	6.9	5.5
Labeling (mol%)	-	-	-	-	-	-	-	1.0	1.0

a. An-labeled; b. Phe-labeled; c. Only one Tg was observed by DSC for each copolymer.

Appendix II-2 Recipes for the Preparation and Characteristics of P(BMA-co-BA-co-MAA) Latexes

One such a latex was prepared by a batch method at 20 °C (C-1), while the other was prepared at 60 °C and with the addition of a chain transfer agent (C-2) for lowering the molecular weight of the polymer and hence for the ease of characterization of the resultant polymer in solution. No buffer (e.g. $NaHCO_3$) was used during the polymerization process to avoid possible enhancement of homopolymerization of MAA in aqueous phase upon neutralization. The recipes for preparing the latex particles and some of their characteristics are given in Table AII-2-1. The solids content and monomer conversion were measured gravimetrically. Particle sizes and polydispersities were determined by dynamic light scattering.

Table AII-2-1 Recipes for preparation and characteristics of P(BMA-co-BA-co-MAA) latex samples

Latex code	C-1	C-2
Recipe		
BMA [a] (g)	70.52	70.55
BA [b] (g)	23.54	23.26
MAA [c] (g)	6.01	6.04
Water (g)	820	825
NaPS [d] (g)	2.377	2.373
$NaHSO_3$ (g)	1.038	1.034
$CuSO_4$·EDTA [e] (μ mol)	1.50	1.50
SDS [f] (g)	2.888	2.881
DM [g] (g)	0	3.068
Temp (^oC)	20-22	60
Time (h)	20	20
Characteristics		
Solids content (wt%)	11.43	11.60
Monomer conversion (%)	99.7	100
Mean diameter (nm)	58.1	39.7
Size polydispersity	0.044	0.090

a. BMA: Butyl methacrylate; b. BA: Butyl acrylate; c. MAA: Methacrylic acid; d. NaPS: Sodium persulfate; e. EDTA: Ethylene diamine tetraacetic acid, sodium salt; f. SDS: Sodium dodecyl sulfate; g. DM: Dodecyl mercaptan.

Appendix III-1. Calculation of the percent solids (S_{wet}%) and thickness (δ_{wet}) of the wet dispersion domain during drying of latex dispersions

The calculation is based on the total solids content (S_{total} %) of the film and the fractional area of the wet dispersion ($A_{wet}/A°_{wet}$, or F_{wet}), at each time of the drying process, measured in our drying experiments.

The total weight of the polymer film after complete drying is known. We simply use the value of 0.015 g here, for 0.300 g dispersion of initial solids content 5.0 wt%. We assume that the film after drying has a uniform thickness over the surface. This is reasonable to our observations: we find that surfactant-free dispersions often give quite uniform films after drying, and that the rim formed at the edge for surfactant-containing dispersions is small with respect to the total weight (or volume) of the entire film. We also find that the dry film, once formed, has high solids content (e.g. 97%) with negligible amount of water. Thus the solid weight of this dry film part is $0.015\ (1- F_{wet})$. If the percent solids of the wet dispersion is S_{wet} (in %), and the weight of the wet dispersion (solids + water) is W_{wet} (in g), we have a relation

$$W_{wet}\ S_{wet} + 0.015\ (1- F_{wet}) = 0.015 \qquad \text{(AIII-1)}$$

where we have ignored the drying boundary between the dry film and the wet domain, since it is rather sharp and has little contribution to the total polymer solids.

The above parameters must also relate to the total percent solids of the drying film (S_{total}, in %) as

$$0.015 / [W_{wet} + 0.015\ (1- F_{wet})] = S_{total}\,\% \qquad \text{(AIII-2)}$$

In Eq. (AIII-1) and (AIII-2) there are only two unknown parameters, S_{wet} and W_{wet}, which can thus be easily calculated.

Once the F_{wet} is measured, and the W_{wet} (in g) is calculated, the thickness of the wet domain (δ_{wet}) can be estimated. The density of our dilute dispersions is close to 1 (in g/cm^3), and thus the volume of the wet dispersion is numerically identical to W_{wet}. The surface area of the initial dispersion is known, to be 5 cm^2. Assuming a flat surface of the wet domain (reasonable at early or intermediate drying times), the thickness of the wet dispersion (δ_{wet}, in μm) is thus obtained via Eq. AIII-3.

$$\delta_{wet} = 10^4\ W_{wet} / (5\ F_{wet}) \qquad \text{(AIII-3)}$$

Appendix VI-1 Comparison of polymer diffusion analysis by DET for film samples of different number ratio of donor to acceptor-labeled particles or with different sample geometries and by using different analytical techniques

AVI-1-1 Objectives

In the polymer diffusion analysis by direct non-radiative energy transfer (DET or ET) measurements carried out in our laboratory, two types of sample geometries have been used. One involves an equal number of donor-labeled (D) and acceptor-labeled (A) particles, prepared from a 1 : 1 mixture of D and A particles. The other type of sample is characterized by a structure in which each D particle is almost completely surrounded by A particles, and is prepared from a 1 : 12 mixture of D and A particles.

In this section, I compare the results of these two types of experiments by using the same analytical technique but from these two different sample geometries. In addition, I describe a preliminary experiment for a sample with a lamellar geometry which can be analyzed in a manner proposed by Torkelson et al.[1]

AVI-1-2 Experimental

The two latex samples are PBMA labeled with 1 mol% phenanthrene (Phe, D) and anthracene (An, A), respectively, synthesized with the help of Ms. Ewa Odrobina, using a recipe similar to that shown in Table II-5 (Chap. II). The pair of samples have nearly the same particle size, average molecular weight, and molecular weight distribution. We also confirmed this by measuring these properties with 1 : 1 mixture of the two samples. The mean values are: d = 128 nm, Mw = 380 K, Mn = 130 k, and Mw/Mn = 2.9.

Latex films were prepared by air drying the dispersions on quartz substrate at an intermediate drying rate (total time ca. 5 h) at 32 °C in an oven. Films with either 1 : 1 or 1 : 12 mixture of D and A labeled particles were obtained. It is well-known that the latex particles deform into space-filling polyhedra after the films are formed at a temperature just above the softening point of the polymer.

One film sample used here is a lamellar-type prepared in two steps. First, a D-labeled polymer layer was prepared by solvent-casting a sample of the dry D-labeled latex particles after dissolving it in toluene. In this way a film of thickness 8 μm was obtained after drying. The thickness is quite homogeneous over the substrate surface and is close to that (i.e. 10 μm) calculated from the amount of polymer used and the area of the substrate surface occupied by the film. The second A-labeled layer was prepared by directly casting the An-labeled latex in water on the top of the first layer at 32°C. The thickness of this layer was 16 μm. The uniformity of thickness of this layer is not very important in the model of diffusion analysis.

These films, placed in sealed test tubes filled with N_2, were annealed at elevated temperatures (i.e. 70 and 110 °C). Fluorescence decay measurements were carried out for the polymer films with D and A labels.

AVI-1-3 Comparison between 1 : 1 and 1 : 12 D/A mixture

AVI-1-3-1 Geometric consideration

We illustrate the expected structures for films with 1 : 1 and 1 : 12 D/A mixtures, respectively, in Figure AVI-1. In the nascent films, the particles have deformed into polyhedra with sharp interfaces, and there is no significant penetration between the D and A phases. On the top of the Figure we show 2-dimensionally that in case 1:1 D/A mixture, each D particle has half of its neighbors as D-labeled particles and half as A labeled particles. In 1:12 D/A mixture each D particle is surrounded by A particles. With time during annealing the molecules in the two phases interdiffuse, and therefore more and more D and A groups diffuse into proximity. The diffusion is a 3-dimensional process and the particles and phases have a spherical relationship, as depicted in the bottom of the Figure. Since energy transfer (DET) reflects the fraction of donors that are quenched by acceptors, it will provide a measure for the extent of mixing during the diffusion process.

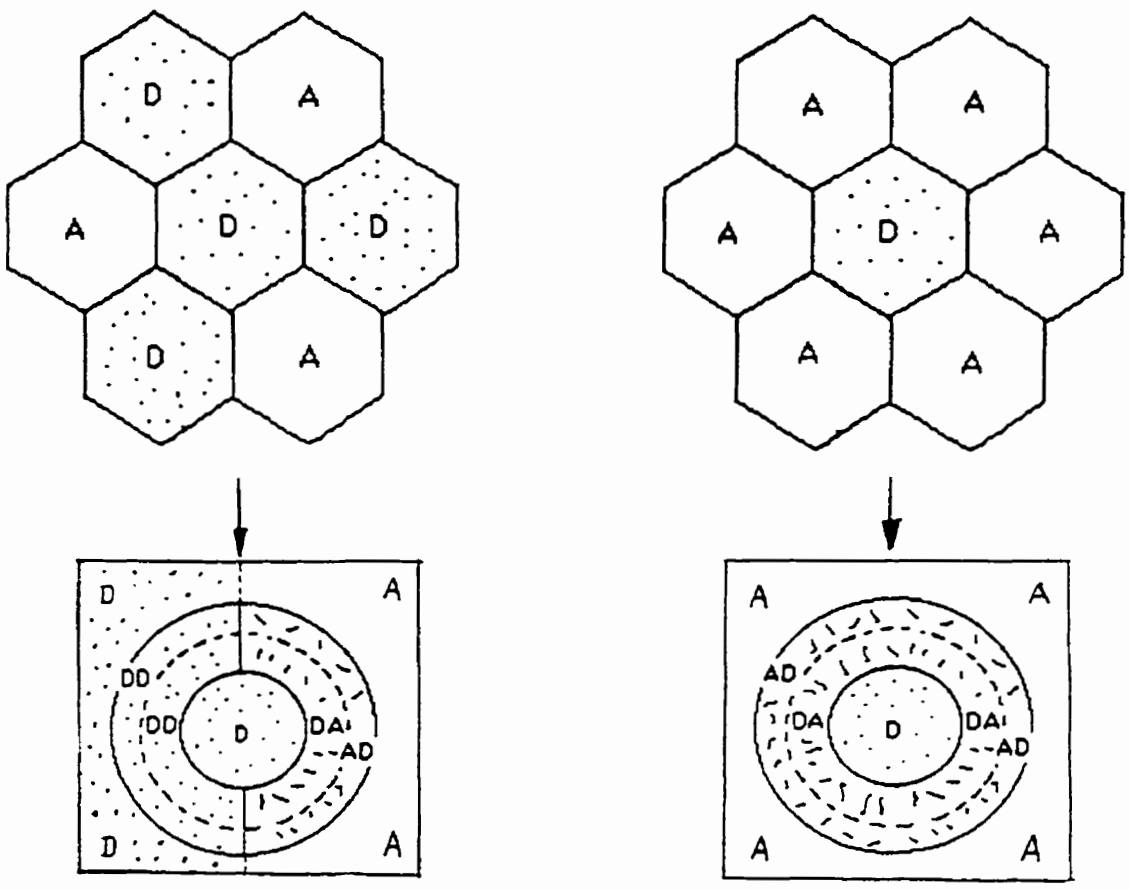

Figure AVI-1. Illustration of the structures of various phases in films prepared with D and A labeled particles with the number ratio of D to A of 1/1 and 1/12, respectively. In the 1:1 D/A mixture, each D particle has half number of both D and A neighboring particles, and in the 1:12 D/A mixture, most D particles are surrounded by A particles. Before annealing, the D and A phases are present as polyhedra, as shown on the top, with sharp interfaces separating them. After annealing, D and A phases will mix 3-dimensionally. Each D particle under consideration here is drawn as sphere together with its related surrounding phases. Part of the D molecules enter into the A phases, forming a mixed phase referred to as AD, and the same amount of A molecules enter into the D phase, forming a mixed phase referred to as DA. In the 1:1 D/A mixture, half of the D molecules which diffuse out of their original particle mix with D molecules in the neighboring D phases, forming an identical phase referred to as DD.

From simple geometric considerations, one would expect that for the same extent of molecular mixing, the observable ET signal in the 1 : 1 D/A mixture would be half of that in the 1 : 12 mixture, since only half the number of neighboring particles in 1 : 1 mixture would be acceptor-labeled. Our intent here is to examine whether or not this factor of 2 with respect to DET holds for these two geometries.

To examine this point more carefully, we need to establish some relationships between the parameters characterizing energy transfer and those for the extent of mixing. We analyze this process with a simple approach. We assume that there are three regions in the films during diffusion: an unmixed D-labeled region, an unmixed A-labeled region, and a region in which D and A have been mixed (e.g. DA, AD phases) with a concentration of half of their initial values and where DET takes place. In many cases, the donors and acceptors have almost the same initial concentration C_o, and thus the concentration of D and A in the mixed region is assumed to be $0.5C_o$. These are rough approximations, since the labeled polymers should be distributed with a concentration gradient rather than as a three-region step-function. However, analysis in a simple fashion is desired and helpful to understand a system in which reality is more complex than the current models or theories available, in the areas of both energy transfer and polymer diffusion.

In case of 1 : 1 D/A mixture, the extent of ET can be characterized by the number fraction of donors undergoing DET (f'_{ET}) by

$$f'_{ET} = 0.5C_o(V_{DA}+V_{AD})/[C_o(V_D+V_{DD}) + 0.5C_o(V_{DA}+V_{AD})] = V_{DA}/(2V_{DA}+V_D) \qquad \text{(AVI-1)}$$

The apparent fractional volume of mixing, f'_m, can be easily obtained by

$$f'_m = (V_{DA}+V_{DD})/[V_{DA}+V_{DD}+V_D] = 2V_{DA}/(2V_{DA}+V_D) \qquad \text{(AVI-2)}$$

The mass fraction of diffusion is calculated here by the apparent mass (or volume) fraction of diffuse substance (considering donor molecules here) that has diffused out of the original boundary, f'_D, by

$$f'_D = 0.5C_o(V_{DD}+V_{AD})/[C_oV_D + 0.5C_o(2V_{DD}+V_{DA}+V_{AD})] = V_{DA}/(2V_{DA}+V_D) \qquad \text{(AVI-3)}$$

From these relationships, one sees that $f'_{ET} = f'_D$, but $f'_m = 2\,f'_{ET} = 2\,f'_D$. In the previous publications from this laboratory,[2] the parameter f'_{ET} was in fact ignored, and f'_m was used instead. Here we find that for the simple step-function model these two parameters (the extent of ET vs. the extent of mixing) are not equivalent but differ by a factor of 2. This confusion in the previous descriptions arises from the derivation of the relationship between the extent of energy transfer and fractional volume of mixing only for 1-dimensional planar diffusion,[2a,b] and in such a case the above two parameters are equivalent. In fact, Wang et al[2b] pointed out that in the 1 : 1 D/A latex films, their term f_m, which is the f_{ET} here, reflects only part of the extent of mixing by considering only the contribution of donors entering into acceptor-environment to the volume mixing and ignoring the same amount (volume) of acceptor-labeled molecules diffusing into the donor phases. Nevertheless, in the diffusion coefficient analysis carried out previously they assumed that the extent of energy transfer is equivalent to the mass fraction of diffusion, i.e. f_{ET} =

f_D. This is reasonable for the simple picture presented here for the 1 : 1 mixture. Thus for the evaluation of diffusion coefficients there does not appear to be any conflict.

In case of D/A 1 : 12 mixtures, the above three parameters become:

$$f'_{ET} = 0.5C_o(V_{DA}+V_{AD})/[C_oV_D + 0.5C_o(V_{DA}+V_{AD})] = V_{DA}/(V_{DA}+V_D) \quad \text{(AVI-4)}$$

$$f'_m = V_{DA}/[V_{DA}+V_D] \quad \text{(AVI-5)}$$

$$f'_D = 0.5C_oV_{AD}/[C_oV_D + 0.5C_o(V_{DA}+V_{AD})] = 0.5\ V_{DA}/(V_{DA}+V_D) \quad \text{(AVI-6)}$$

Here, $f'_{ET} = f'_m$, but $f'_D = 0.5\ f'_{ET} = 0.5\ f'_m$

Thus, one would expect that for the same level of mixing (f_m), the ET signal (f_{ET}) in D/A=1/1 would be half of that in D/A=1/12. For diffusion analysis using the mass fraction of diffusion (f_D), one may simply set $f_D = f_{ET}$ for 1 : 1, but one should use $f_D = 0.5f_{ET} = 0.5f_m$ for 1 : 12 mixtures. These relationships are close to those predicted by Wang et al[2b] with a formula of f_D/f_m as a function of the number fraction of acceptor-labeled particles.

AVI-1-3-2 Analysis of energy transfer efficiency

We first analyze the diffusion process in terms of the change in quantum efficiency of energy transfer (Φ_{ET}). Φ_{ET} is obtained simply by measuring the integrated area under the decay profile for a sample containing D and A particles annealed at time t and that for a sample without A labels, after normalizing the decays at $t_d = 0$.

$$\Phi_{ET} = 1 - \text{Area}(t) / \text{Area}(\text{no ET}) = 1 - \text{Area}(t)/45 \quad \text{(AVI-7)}$$

where 45 ns is the lifetime of Phe (D) attached to PBMA in films.

Figure AVI-2 shows the growth in Φ_{ET} as a function of annealing time for samples annealed at 70°C. In (a) we show plots of Φ_{ET} vs. time for D/A=1 and D/A=1/12, respectively, and in (b) we show the ratio of Φ_{ET} between these two cases [i.e. $\Phi_{ET}(D/A=1/12)/\ \Phi_{ET}(D/A=1)$] vs. time. One sees that before annealing (t=0), the Φ_{ET} value found for D/A=1/12 is almost exactly 2 times of that found for D/A=1. During early times of diffusion, this factor 2 is preserved. These results indicate that the ratio of energy transfer signals for the two cases follows the prediction by simple geometric consideration. With further increasing diffusion time or Φ_{ET}, the ratio slightly decreases to about 1.75. It is very likely that with increasing diffusion, the assumption for case D/A=1 that each donor particle is surrounded by a half-number of both acceptor- and donor-labeled neighboring particles no longer holds, since these donor neighboring particles ought to be partially mixed with acceptors. Thus the ET efficiency for such a system may be higher than that expected, and hence the ratio of Φ_{ET} between D/A=1/12 and D/A=1 is lower than 2. Nevertheless, at early times of diffusion, this deviation is rather small. Note that the maximum Φ_{ET} value here is ca. 0.5 for case D/A = 1/12 and ca. 0.3 for D/A = 1. We have other sets of data

in which Φ_{ET} changes over a larger range. One set is shown in Figure AVI-3 with plots similar to those shown in Figure AVI-2, using similar films but annealed at 110°C. One sees again that before annealing, or at early times of annealing, a factor of 2 is obtained, but this ratio decreases gradually to about 1.5 as diffusion proceeds to larger Φ_{ET} values.

The above results confirm the idea that the amount of substance diffused, reflected by energy transfer efficiency, is proportional to the cross-sectional area for mass transfer.

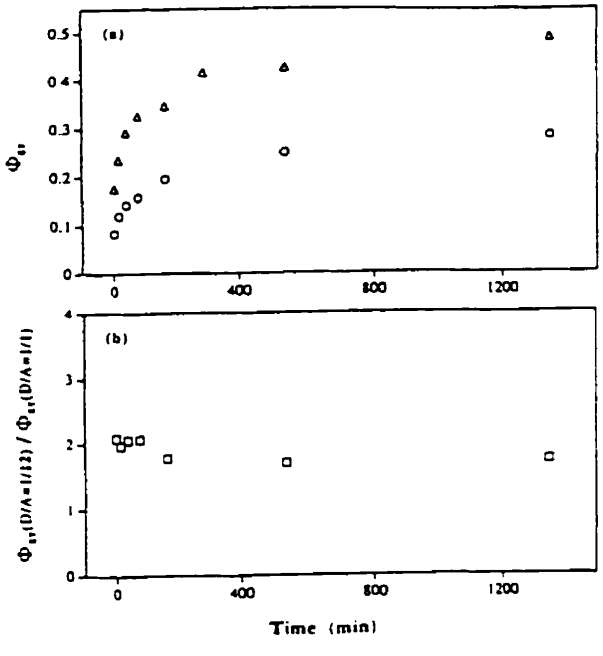

Figure AVI-2. Variation of Φ_{ET} vs. diffusion time for samples annealed at 70°C: (a) plots of Φ_{ET} vs time, and (b) plots of the Φ_{ET} ratio between case D/A=1/12 and case D/A=1/1 vs. time.

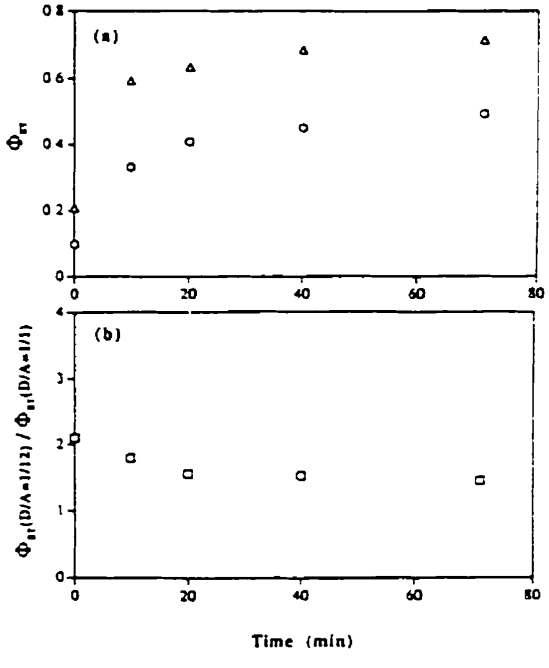

Figure AVI-3. Variation of Φ_{ET} vs. diffusion time for samples annealed at 110°C: (a) plots of Φ_{ET} vs. time, and (b) plots of the Φ_{ET} ratio between case D/A=1/12 and case D/A=1/1 vs. time.

AVI-1-3-3 The net increase of energy transfer efficiency

In studying a diffusion process by DET, one has to take into account the energy transfer across the initial sharp interface. If this is significant, it is the increase in energy transfer efficiency ($\Delta\Phi_{ET}$) due to diffusion that provides meaningful data for evaluating the extent of diffusion. $\Delta\Phi_{ET}$ is obtained by subtracting the initial Φ_{ET} before diffusion [Φ_{ET} (t=0)] from the signal at certain diffusion time t [Φ_{ET}(t)]. Figure AVI-4(a) shows plots of $\Delta\Phi_{ET}$ vs. time, derived from Figure AVI-2(a), and in Figure AVI-4(b) we show the ratio of $\Delta\Phi_{ET}$ between the two cases of different dye concentrations vs. time, for samples annealed at 70 °C. One sees that at early times the increase in ET efficiency for D/A=1/12 is about 2 times of that for D/A=1, pointing to the validity of the simple geometric relationship, and with time this ratio decreases to ≈ 1.5, implying the deviation from simple geometric relationship as diffusion proceeds. The data obtained at the annealing temperature 110 °C show similar behavior.

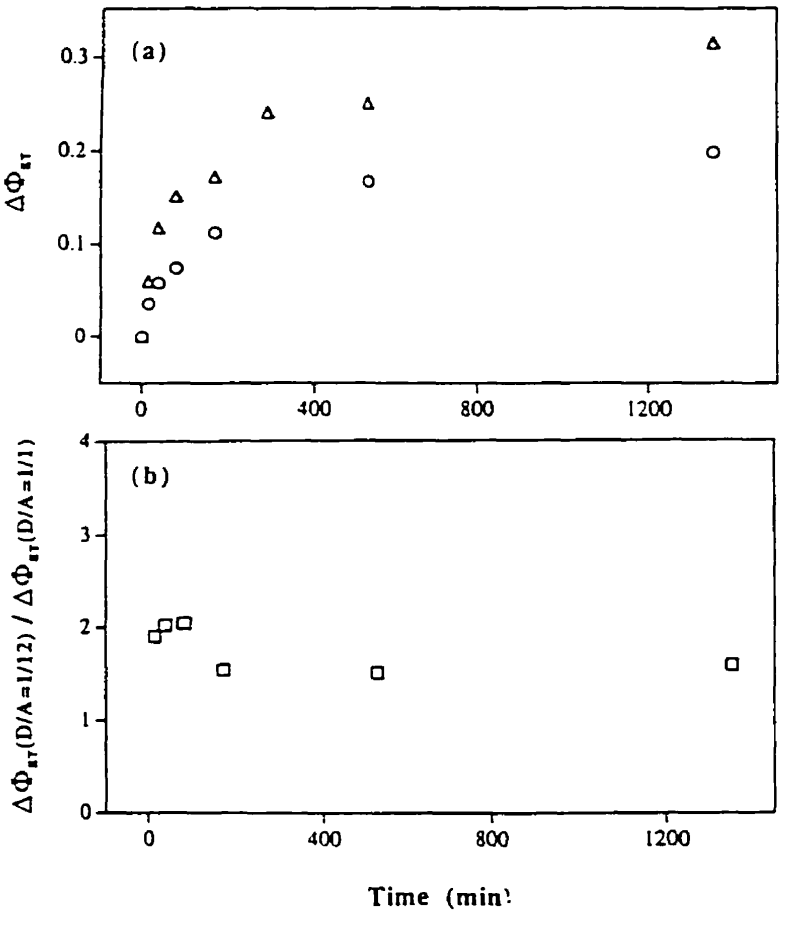

Figure AVI-4. The increase in energy transfer efficiency $\Delta\Phi_{ET}$ vs. diffusion time for samples annealed at 70°C: (a) plots of $\Delta\Phi_{ET}$ vs time, and (b) plots of the $\Delta\Phi_{ET}$ ratio between case D/A=1/12 and case D/A=1/1 vs. time.

The increase in energy transfer efficiency characterizes the mixing of the polymer. In the past, we have used a modified parameter, the fractional growth of ET efficiency, as a measure for the extent of mixing (f_m). f_m is obtained from the net increase in ET efficiency ($\Delta\Phi_{ET}$) normalized by its maximum detectable quantity [$\Phi_{ET}(\infty)$-$\Phi_{ET}(t=0)$], as

$$f_m = [\Phi_{ET}(t)-\Phi_{ET}(t=0)] / [\Phi_{ET}(\infty)-\Phi_{ET}(t=0)] \qquad \text{(AVI-8)}$$

Here the $\Phi_{ET}(\infty)$ value was obtained from solvent-cast film of a mixture of D and A labeled latex polymers, as a model for the state in which the molecules have reached maximum mixing.

Figure AVI-5(a) shows f_m values vs time at an annealing temperature of 70 °C for films with D/A=1 and 1/12, respectively. In Figure AVI-5(b) we show the f_m ratio between the two cases vs. time. One observes that at early times, the f_m ratio is about 1.7, showing some deviation but not too far from 2. With time, this ratio decreases and becomes closer to 1. Note that $\Phi_{ET}(\infty)$ has lost most of the information about the initial conditions, and f_m is not exactly proportional to the initial contact area.

Although the relationship between f_m values for D/A=1 and those for D/A=1/12 shows increased complexity as compared to the Φ_{ET} and $\Delta\Phi_{ET}$ values, some simple features can be discerned. The difference between $\Delta\Phi_{ET}$ and f_m is only a factor of $1/[\Phi_{ET}(\infty)-\Phi_{ET}(t=0)]$. This factor is in fact a constant, irrespective of the diffusion time and only dependent on the number ratio of D to A particles. We found $\Phi_{ET}(\infty)=0.60$, $\Phi_{ET}(0)=0.08$, and $[\Phi_{ET}(\infty)-\Phi_{ET}(0)] = 0.52$ for D/A=1, and $\Phi_{ET}(\infty)=0.80$, $\Phi_{ET}(0)=0.17$, and $[\Phi_{ET}(\infty)-\Phi_{ET}(0)] = 0.63$ for D/A=1/12. These values were found repeatedly, in various experiments, from the areas under the decay curves: Area(∞)=17.5 and Area(0)=41.5 for D/A=1, and Area(∞)=8.5, Area(0)=37.5 for D/A=1/12. The $[\Phi_{ET}(\infty)-\Phi_{ET}(0)]$ values found for the two cases are not exactly equal but differ by 15%, and this is the reason that the f_m ratios are = 1.7 rather than 2, which is the factor for $\Delta\Phi_{ET}$ values for short diffusion times. This systematic difference at early times is rather small. At intermediate times of diffusion, the f_m ratios will decrease to lower values, since the simple geometric relationship no longer exists as many D particles become acceptor-containing phases in 1:1 D/A mixture. One can imagine the importance of this effect when the film is near the end of mixing process, and when no single pure D phase is present. The trend that f_m eventually reaches unity for both cases is expected, since it is obtained by normalization.

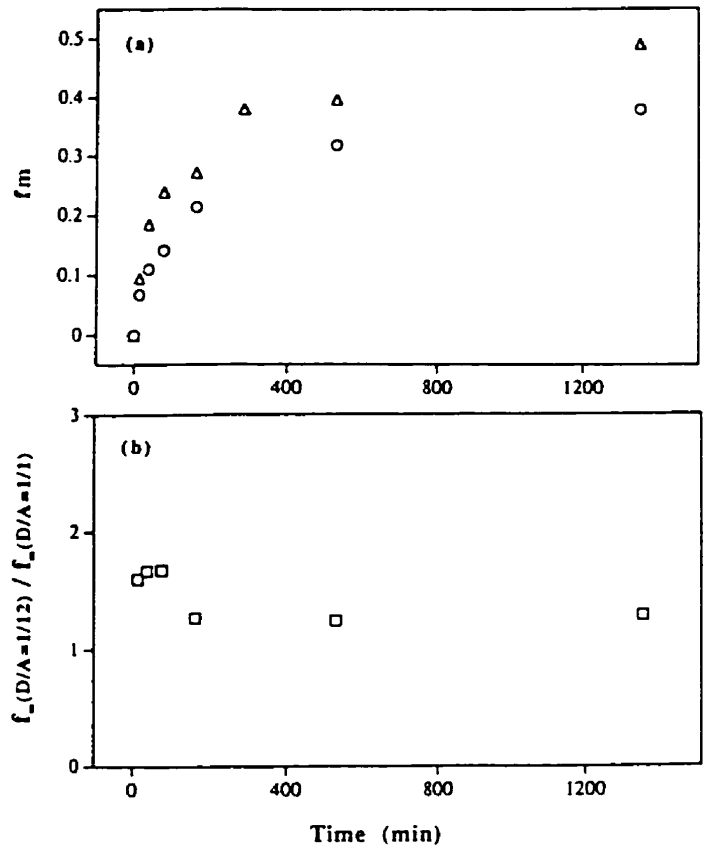

Figure AVI-5. The fractional growth in ET efficiency (fm) vs. diffusion time for samples annealed at 70°C: (a) plots of fm vs time, and (b) plots of the fm ratio between case D/A=1/12 and case D/A=1/1 vs. time.

AVI-1-3-4 Calculation of diffusion coefficient

To calculate the diffusion coefficient for the polymers, we need the mass fraction of diffusion (f_D), and then have to relate this f_D value to a concentration function of the diffuse substance, from which the diffusion coefficient can be obtained. As shown previously, a concentration function can be found by assuming a diffusion model (e.g. Fickian diffusion in a spherical geometry).[2,3] The key parameters for us to access are the f_D values.

We have in the past simply set the mass fraction of donor molecules diffused out of the original particles (f_D) to be equal to the fractional growth of energy transfer efficiency (f_m) in our previous analysis for 1:1 D/A mixtures. This relationship will be used here for the 1: 1 case. As mentioned above, from a geometric consideration it is more reasonable to set $f_D = 0.5\ f_m$ for the case of D/A 1:12 mixture. The f_D values used below for diffusion coefficient calculations are obtained in this way.

Figure AVI-6 shows the apparent diffusion coefficients (D_{app}) calculated for the same polymers at 70 °C at different diffusion times for two films of different D/A particle number ratios. The diffusion coefficients are all of the same order of magnitude, within 0.005 - 0.007 nm^2/s at early times, and decrease to 0.001 - 0.0025 at later times. The difference in diffusion

coefficient values obtained for the two sample geometries (D/A 1/1 vs. 1/12) is very small at early times, but becomes larger (e.g. by a factor of 2-3) as the diffusion proceeds. Considering that in latex samples the mean diffusion coefficients can decrease by as much as a factor of 5 from the beginning to the later stages of the diffusion process, due to the broad polymer molar mass distribution, the above difference between the two sample cases is not very large. For films annealed at 110 °C with larger extents of mixing, a similar behavior is observed: the D_{app} (nm^2/s) values obtained from D/A=1/12 by setting $f_D=0.5f_m$ is only slightly (i.e. less than a factor of 2) lower than those obtained from D/A=1 by setting $f_D=f_m$ in the beginning. With time the difference in D_{app} values between the two sets of data increases to a factor of ca. 3.

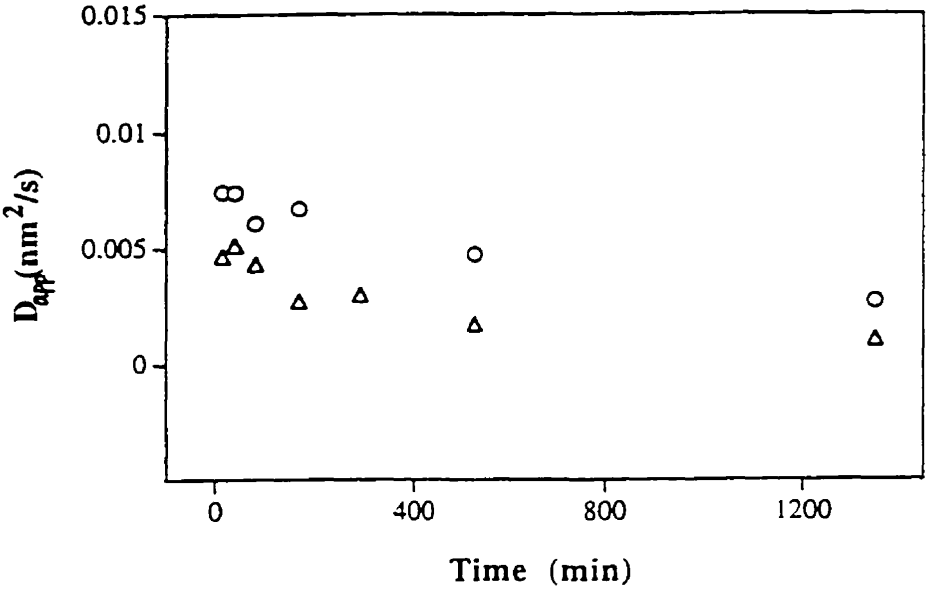

Figure AVI-6 Diffusion coefficients for PBMA films annealed at 70°C obtained from 1:1 D/A mixture (circles) by setting $f_D=f_m$ and from 1:12 D/A mixture (triangles) by setting $f_D=0.5f_m$.

It is difficult to conclude which sample geometry is better for these experiments. For the 1:1 case, one obtains a higher signal of donor emission. Thus a relatively short time is required for individual fluorescence decay measurements. As shown above, there is a problem with lateral mixing in the later stages of diffusion, but this is not very serious with respect to experimental errors, sample limitations, as well as theoretical complexities. For the 1:12 case, one obtains a simpler phase structure with respect to either spherical or planar diffusion, and with less serious lateral diffusion problem. The donor emission signal is weaker, and hence a longer measurement time or thicker film is required.

There is a dependence of energy transfer on the concentration of acceptors and donors, and this may cause the difference of ET measurements between the two sample cases. However,

we have shown that in the way we analyze the process by ET efficiency (Φ_{ET}) or the increase in Φ_{ET}, a simple geometric relationship follows at the beginning, and it only deviates from this simple behavior at later times when the structures of the system become more complex. Even for the f_m parameter, the growth in ET efficiency normalized by $[\Phi_{ET}(\infty)-\Phi_{ET}(0)]$, its dependence on the sample geometry under the two cases considered here is quite simple and predictable at early stages of interdiffusion. Moreover, the $[\Phi_{ET}(\infty)-\Phi_{ET}(0)]$ values found for the two sample cases are not very different (e.g. 0.52 vs. 0.63), indicating that the two samples of different D/A particle number ratios give similar detection sensitivity (signal gap).

AVI-1-3-5 The $t^{1/2}$ dependence of energy transfer at short times

Figure AVI-7a shows plots of Φ_{ET} vs. $t^{1/2}$, and in Figure AV-7b we show plots of f_m vs. $t^{1/2}$. The data are derived from Figure AV-2 and AV-5 and are for films annealed at 70°C. One observes in Figure AVI-7a that at short diffusion times the plots of ET efficiency vs. $t^{1/2}$ are essentially linear lines for both samples with D/A = 1/1 and 1/12. With diffusion, the plots become curved, and the increase in Φ_{ET} levels off. The plots of f_m vs. $t^{1/2}$ show a similar behavior, as seen in Figure AVI-7b. The $t^{1/2}$ dependence of Φ_{ET} and f_m at short diffusion times is observed repeatedly in our experiments in latex films with both D/A=1 and D/A=1/12 cases.

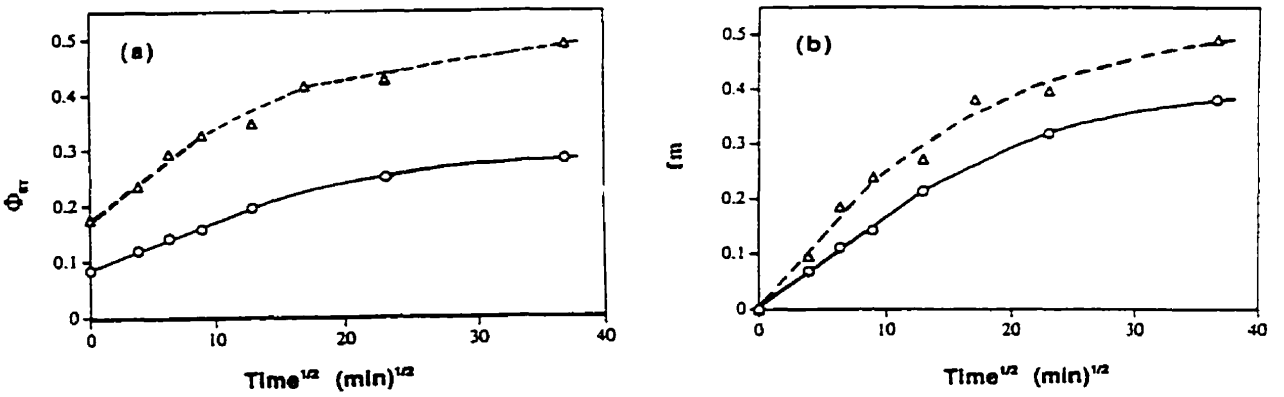

AVI-7. Plots of (a) Φ_{ET} vs. $t^{1/2}$ and (b) f_m vs. $t^{1/2}$ for film samples with D/A = 1/1 (circles) and 1/12 (triangles). The data are derived from Figure AVI-2 and AVI-5.

AVI-1-3-6 Evidences of non-uniform chromophore concentration distribution (the correlation holes)

de Gennes [4] pointed out that in a polymer system, each monomer unit is surrounded by a "correlation hole," inside which the concentration of monomer units from other chains is reduced. This correlation hole effect is dependent on the polymer chain dimensions, and the correlation hole size is comparable with the overall size of one chain. Fredrickson[5] proposed an approach based on DET technique for verifying intramolecular and intermolecular correlations. By using de Gennes's correlation function for a melt of end-labeled chains and examining a system of end-labeled polymers where one polymer chain is labeled with a donor chromophore and n ($n >> 1$) chains are labeled with acceptors, Fredrickson related the donor fluorescence intensity decay to intermolecular correlations. This procedure involves modifying Förster's original expression for energy transfer in a purely random system of chromophores to take into account the correlations in a labeled polymer system. Torkelson and coworkers [6] extended this idea to include the chain statistics and intermolecular interactions in the donor fluorescence decay function on a more quantitative basis, for both melt of end-labeled monodisperse polymer and semidilute solutions. Due to mathematical complications, this theoretical work has not so far been extended to polymer systems with randomly labeled chromophores.

For polymers randomly labeled with fluorescent chromophores, the existence of correlation holes implies that at short distances, the density allowed for other chains near a monomer site of a selected chain is reduced, and hence the concentration of other chromophores (e.g. acceptors) surrounding a given chromophore (e.g. a donor) also drops. Since energy transfer experiments measure short distances (e.g. on the order of 2 nm), one would expect that the correlation hole effect would alter the efficiency of energy transfer.

We attempt to examine the above point using films in which the polymer molecules, labeled with D and A respectively, have reached a state close to maximum mixing, either by diffusion for a sufficiently long time or by solvent-casting. In this case, the dyes are assumed to be uniformly distributed in a 3-dimensional system and the donor decay obeys the Förster mixing expression (Eq. AVI-9) as [2]

$$I_D(t') = A_1 \exp[(-t'/\tau_D^\circ) - P(-t'/\tau_D^\circ)^{1/2}] + A_2 \exp(-t'/\tau_D^\circ) \qquad \text{(AVI-9)}$$

where t' is the decay time and τ_D° is the donor lifetime (45 for Phe in PBMA). A_1, A_2, and P are fitting parameters which can be obtained by fitting an experimental decay profile to Eq. (AVI-9). P is related to the effective acceptor concentration C_A (in mol/l) by

$$P = 2\, C_A/C_{Ao} = (4\pi^{3/2} N_A R_o^3 / 3000)\, C_A \qquad \text{(AVI-10)}$$

where C_{Ao} is the reference acceptor concentration in energy transfer system defined as

$$C_{A0} = [3000/(2\pi^{1.5} N_A R_0^3)] \quad \text{(AVI-11)}$$

Here R_0 is the characteristic distance for energy transfer, whose value has been determined to be 2.3×10^{-7} cm, [2] and N_A is Avagadro's number.

For a PBMA film sample with Mw = 380 K, a D/A particle number ratio of 1:12, and an initial acceptor content of 1.0 mol% in A particles, the calculated average acceptor concentration $[A]_{cal}$ in a fully mixed film is 0.0689 mol/l. From fluorescence decay measurements and data fitting of the decay to Eq. (AVI-9), we obtained a P value of 2.462 for this film. The effective acceptor concentration $(C_A)_{exp}$ obtained from such an experiment and calculated via Eq. (AVI-10) is 0.0453 mol/l. We noticed that the acceptor concentration probed by energy transfer experiment is significantly smaller than the calculated bulk average value. The quantum efficiency of energy transfer determined by decay measurement, $(\Phi_{ET})_{exp}$, is also noticeably lower than that calculated by integrating Eq. (AVI-9) based on $C_A = [A]_{cal} = 0.0689$ mol/l, $(\Phi_{ET})_{cal}$. These data are shown in Table AVI-1. For comparison, I also show similar results obtained for films consisting of the same labeled polymers but prepared with a 1:1 D/A ratio.

Table AVI-1. Comparison of calculated and probed acceptor concentrations and energy transfer efficiencies (PBMA, Mw = 380K)

	$[A]_{cal}$ mol/l	$(C_A)_{exp}$ mol/l	$(\Phi_{ET})_{cal}$	$(\Phi_{ET})_{exp}$
D/A = 1/12	0.0689	0.0453	0.89	0.81
D/A = 1/1	0.0373	0.0229	0.76	0.60

When films were prepared using lower molecular weight (M) PBMA (Mw = 35 K) but with the same D/A particle number ratio (i.e. 1/12) and a nearly identical initial acceptor labeling content (0.99 mol%) in A-labeled particles, the results are shown in Table AVI-2. In Table AVI-2 we also show results for films with the same D/A ratio and acceptor concentration but prepared using a carboxylated PBMA, a copolymer of BMA and 5 wt% methacrylic acid [P(MAA-co-BMA)] (Mw = 38 K).

Table AVI-2. Comparison of calculated and probed acceptor concentrations and energy transfer efficiencies for lower M PBMA (Mw = 35 K, D/A = 1/12) and P(MAA-co-BMA) (Mw = 38 K, D/A = 1/12)

	$[A]_{cal}$ mol/l	$(C_A)_{exp}$ mol/l	$(\Phi_{ET})_{cal}$	$(\Phi_{ET})_{exp}$
PBMA	0.0682	0.0515	0.89	0.84
P(MAA-co-BMA)	0.0682	0.0571	0.89	0.86

One notices first that the probed acceptor concentration becomes closer to the calculated bulk concentration when the lower M PBMA is used, as compared to the higher M PBMA. The observed energy transfer efficiency for lower M film is also increased to 0.84. These show that the chromophore concentration reduction arising from the correlation hole effect is less pronounced when the polymer molecular weight is low. This is consistent with the description by de Gennes.

It is also interesting to note that for a P(MAA-co-BMA) copolymer sample of quite low M (Mw = 38 K), a high level of ET efficiency (0.86), close to the calculated value (0.89), is obtained, and that the probed acceptor concentration is closer to the bulk value (0.57 Vs. 0.68).

AVI-1-3-7 Calculation of the characteristics distance for energy transfer (R_o)

In the above analysis, we have assumed a R_o value of 2.3 nm. We now assume that the dye concentration distribution in a solvent-cast film is reasonably uniform and that the local acceptor concentration equals to the bulk concentration, i.e. $C_A = [A]_{cal}$. We then calculate the R_o values using Eq. (AVI-10) based on the P values measured from decay experiments.

For this purpose, we choose the sample data from films that give very high extent of energy transfer when fully mixed (e.g. from solvent-casting). These samples are PBMA (Mw = 35 K, D/A = 1/12) and P(MAA-co-BMA) (Mw = 38K, D/A = 1/12), both having an acceptor concentration of 0.0682 mol/l. The ET efficiencies found for these samples are as high as 0.84-0.86 (with the areas under decay curves of 7.2 and 6.2 ns), the highest among all our samples examined so far. From the decay profiles measured and data fitting, the P parameters are obtained, from which we obtain the $(R_o)_{cal}$ values. Table AVI-3 shows the results.

Table AVI-3. P parameters and R_o values determined by fluorescence decay measurements on fully mixed films

	Area	$(\Phi_{ET})_{exp}$	P	$(R_o)_{cal\ nm}$
PBMA (Mw=35 K, D/A=1/12)	7.2	0.84	2.80	2.1
P(MAA-co-BMA) (Mw=38 K, D/A=1/12)	6.2	0.86	3.10	2.2

The R_o values determined in this way are 2.1-2.2 nm. These values are close to that obtained previously[2] and that we have often used (i.e. 2.3 nm).

AVI-1-4 Strategies for Comparison Between Latex-Structured and Lamellar-layered Films

A lamellar-layered (sandwiched) film was prepared by solvent-casting first a thin film layer of donor-labeled polymer, and then coating it with an acceptor-labeled polymer layer from a latex dispersion of acceptor-labeled particles. Here the thickness of the D-labeled layer is 8 μm.

The film exhibits single exponential decay in fluorescence decay measurements before annealing, and thus $\Phi_{ET}(t=0) = 0$. It is then annealed at 110 °C (at the same time as the latex films described above with D/A=1 and 1/12, respectively).

The energy transfer efficiency (Φ_{ET}) for the lamellar film is obtained in the same way as for the latex-structured film. The diffusion coefficients are calculated from a simple relationship between Φ_{ET} and diffusion coefficient proposed by Torkelson[1] as follows:

$$\Phi_{ET} = k\,(D_p t)^{1/2} / x \qquad \text{(AVI-12)}$$

where D_p is the polymer self-diffusion coefficient, x is the thickness of the donor-labeled layer, and k is a constant which is dependent on $C_A(0)/C_{Ao}$. Here $C_A(0)$ is the initial acceptor concentration before diffusion, calculated here to be 0.0747 mol/l for 1 mol% labeling content in PBMA. C_{Ao} is the reference concentration of acceptors defined as Eq. (AVI-11), and is equal to of 0.0368 mol/l for Phe-An pair. Thus the $C_A(0)/C_{Ao}$ value in our case is 2.03. From the plot of k vs. $C_A(0)/C_{Ao}$ shown in Figure 2 in ref. 1, we obtain for k a value of 1.35. Since in our case x

= 8000 nm, we have a simple equation from which the D_p values can be calculated based on Φ_{ET} measurements.

The condition for the above simple relation between Φ_{ET} and D_p to be valid is $t < x^2/(16D_p)$. This is always a case when the x is not very small. According to Torkelson et al. one could also use a simple relation between the normalized energy transfer efficiency (f_m in our case) and D_p. However, in this situation, the constant k is not only a function of the initial acceptor concentration, but also the thickness ratio of the A- and D- labeled layers. For Φ_{ET}, its magnitude is only dependent on the diffusion distance with respect to the D-labeled layer thickness, but not dependent on the thickness of A-labeled layer over much of the diffusion process.

For films annealed at 110 °C, the diffusion coefficients found for latex-structured films analyzed in the above-mentioned ways are on the order of 0.3-0.5 nm^2/s at early times and 2-3 times lower at later times. For the lamellar-layered films, we obtain D_p values nearly 10 times larger (between 2-5 nm^2/s). It is important to point out that the data quality for the lamellar-layered films is rather poor. A major reason is that the change in ET signal is too small, even at such a high temperature. This can be seen in Table AVI-4 which lists the areas, Φ_{ET} and D_p values for several data points obtained. This is the disadvantage of employing the lamellar-layered films for diffusion analysis, since very long times or very high temperatures are required for obtaining a significant signal. In the lamellar case, one follows diffusion over a distance of micrometers, whereas for the latex films, diffusion is monitored over a distance of 50-100 nm.

Table AVI-4. Variation of Areas and Φ_{ET} values and the calculated D_p values for lamellar films at 110°C

t (min)	Area (ns)	Φ_{ET}	D_p (nm^2/s)
0	45	0	
20	44.43	0.0127	4.7
40	44.5	0.0111	1.8
120	44.06	0.0209	2.1
190	43.25	0.0389	4.66

The reason that the D values obtained from lamellas are much larger than those from latex films may be that my experiments with the sandwiched film detect only diffusion at very early stages. At these times, only a portion of lower molar mass polymer is able to diffuse in the

lamellar films. In the latex films, our measurements are carried out to a very high extent of mixing over the same time scale. Another reason for the large difference may arise from different analytical techniques and different diffusion geometries (spherical vs. lamellar). Torkelson et al[1] claimed that the analysis by the simple step-function approach which ignores the concentration profile may significantly underestimate the diffusion coefficient. This point may be valid under certain circumstances but is not a serious concern to our experiments. As we show below, the results from the simple "step-function" approach are very consistent with those obtained by using a model developed for the same latex-structured case with the same spherical diffusion equation but considering the concentration profile.

Further experiments are required if one would like to clarify the above point. One way to improve data quality would be to prepare films with a much thinner D-labeled layer. In such a case, the extent of ET would be increased, but at the same time the donor fluorescence signal would be very much reduced. It may even be difficult to measure. In contrast, with latex-structured films one is able to obtain both high ET signal due to high surface area for diffusion and significant donor fluorescence sensitivity by preparing films of enough thick (e.g. 100 μm).

AVI-1-5 Comparison of analysis between the "step-function" approach and the "concentration-gradient" approach

AVI-1-5-1 Simulated data

Liu and Winnik developed a model which considers the concentration gradient in the decay functions and fits the decay functions to the Fickian spherical diffusion model. The details of the model have been described in refs. 3a and 3b.

Liu assumed a diffusion coefficient of 0.1 nm^2/s for a polymer system of initial particle d = 120 nm with 1 : 12 D/A particle number ratio. By using this model, he obtained a series of decay functions at different diffusion time by simulation. He then recovered a diffusion coefficient value of 0.1 nm^2/s by reanalyzing these decay functions using the model.

The decay functions Liu simulated allowed me to calculate the integrals of these decay functions (corresponding to the areas under the decay profiles), the fractional growth of ET (f_m), and the diffusion coefficients (D_{app}). The D_{app} values were obtained by setting $f_D = 0.5\ f_m$, using the simple "step-function" approach as described above and in Chap. VI. The results of analysis I obtained are shown in Table AVI-5.

Table AVI-5. The results of diffusion analyzed by the "step-function" approach for decay functions generated by simulation from the "concentration-gradient" approach by assuming a diffusion coefficient value of 0.1 nm^2/s

Time (s)	0	120	600	1200	2400	3800	6000	∞
Area	45	37	28	23	17	13	10	6.7
f_m	0	0.21	0.44	0.57	0.73	0.84	0.91	1.0
f_D	0	0.10	0.22	0.29	0.37	0.42	0.45	-
D_{app} (nm^2/s)	-	0.11	0.10	0.090	0.080	0.064	0.048	-

From Table AVI-5 one sees that the D_{app} values obtained by the "step-function" approach are very close to that recovered from the "concentration-gradient" approach using the same set of decay functions. Only at the very late stages of diffusion in which the D and A phases have been largely mixed do the D_{app} values decrease and deviate much from the assumed diffusion coefficient. This indicates that the "step-function" approach does not appear to lead to very large errors, at least numerically, in the diffusion coefficient analysis, and that in the "step-function" method the assumption of 2-factor between f_D and f_m in 1:12 D/A mixture for diffusion analysis is reasonable.

AVI-1-5-2 Experimental data

The film samples were prepared with 1:12 D/A mixture and annealed at 90 °C. The latex characteristics here were d = 116 nm, Mw = 2.6×10^5, Mn = 7.5×10^4 and with a labeling content of 0.8 mol%. Fluorescence decay profiles were measured after each diffusion time interval and the diffusion coefficients were obtained from these decay profiles by using the two analytical methods. Table AVI-6 presents the results.

Table AVI-6. Diffusion coefficients for PBMA films with 1:12 D/A mixture at annealing temperature 90 °C analyzed by the "step-function" and the "concentration-gradient" approach

Time (s)	0	6	20	55	125	∞
f_D (f_D=0.5f_m)	0	0.20	0.32	0.42	0.43	-
D [a] (nm^2/s)	-	0.20	0.12	0.072	0.032	-
D_{app} [b] (nm^2/s)	-	0.14	0.11	0.071	0.032	

a. by the "concentration-gradient" approach; b. by the "step-function" approach.

From Table AVI-6, one sees that the diffusion coefficient values found independently from the two analytical techniques essentially fall into the same range. This further indicates that using a simple approach with the growth in ET efficiency can give reasonable numerical values of diffusion coefficients, although the concentration gradient is ignored in the analysis.

AVI-1-6 Concluding Remarks

By comparing the energy transfer efficiency (Φ_{ET}) in the diffusion process in latex films with different number ratios of donor- to acceptor- labeled particles, it is established that the amount of diffusion is proportional to the initial contact area of the polymer phases. To analyze the diffusion for different sample geometry, it is reasonable to consider the factor of contact area between the initial phases arising from the different geometric configuration. By considering this factor, the apparent diffusion coefficients (D_{app}) analyzed for films with D/A=1 are close to those analyzed for D/A=1/12 at early times of the diffusion process. The D_{app} values obtained by a simple approach ignoring the concentration gradient are consistent with those obtained through a model which considers the concentration profile.

REFERENCES

Chapter I

1. G. Odian, "Emulsion Polymerization", in "Principles of Polymerization", 2nd Ed., John Wiley & Sons: New York, p319, 1981.
2. I. Piirma, "Emulsion Polymerization", Academic Press: New York, 1982.
3. H. F. Mark, N. Bikales, C. Overberger, and G. Menges, "Encyclopedia of Polym. Sci. Eng.", Vol. 6, 2nd Ed., John Wiley & Sons: New York, 1986.
4. R. M. Fitch, M. B. Prenosil, and K. J. Sprick, J. Polym. Sci., C27, 95 (1969).
5. F. K. Hansen, and J. Ugelstad, J. Polym. Sci.: Polym. Che. Ed., 16, 1953 (1978).
6. C. P. Roe, Ind. Eng. Chem., 60, 20 (1968).
7. R. L. Zollars, J. Appl. Polym. Sci., 24, 1353 (1979).
8. F. K. Hansen, and J. Ugelstad, J. Polym. Sci.: Polym Chem. Ed., 17, 3033 (1979).
9. W. D. Harkins, (a) J. Chem. Phys., 13, 381 (1945); (b) J. Chem. Phys., 14, 47 (1946); (c) J. Am. Chem. Soc., 69, 1428 (1947).
10. J. L. Gardon, "Emulsion Polymerization", in "Polymerization Process", C. E. Schildknecht, Ed., Chap.6, Wiley-Interscience: New York, 1977.
11. W. V. Smith, R. H. Ewart, (a) J. Chem. Phys., 16, 592 (1948); (b) J. Am. Chem. Soc., 70, 3695 (1948).
12. (a) R. G. Gilbert, "Emulsion Polymerization - A Mechanistic Approach", Academic Press: San Diego, 1995; (b) B. Hawkett, D. H. Napper, and R. Gilbert, J. Chem. Soc., Faraday Trans. I, 76, 1323 (1980).
13. H. Gerrens, Adv. Polym. Sci., 1, 234 (1959).
14. S. Chatterjee, M. Banerjee, and R. Konar, J. Polym. Sci.: Polym. Chem. Ed., 17, 2193 (1979).
15. M. S. El-Aasser, in "An introduction to Polymer Colloids", F. Candau and R. H. Ottewill Eds., Kluwer: Dordrecht, p1 1990.
16. R. A. Wessling, and D. S. Gibbs, J. Macromol. Sci. Chem., A7 (3), 647 (1973).
17. F. Wall, C. Delbecq, and R. E. Florin, J. Polym. Sci., 9, 177 (1952).
18. G. van Doremaele, "Model Prediction, Experimental Determination and Control of Emulsion Copolymer Microstructure", Ph.D thesis, The Anton German Group, Eindhoven University of Technology, The Netherlands, 1990.
19. T. C. Paton, "Paint Flow and Pigment Technology", Wiley: New York, 1979.

20. G. Turner, "Introduction to Paint Chemistry and Principles of Paint Technology", 3rd ed., Chapman and Hall: London, 1985.
21. (a) S. Voyutski, J. Polym. Sci., part A, 32, 528 (1958); (b) S. Voyutski, "Autohesion and Adhesion of High Polymers", Wiley-Interscience: New York, 1963.
22. J. W. Vanderhoff, E. B. Bradford, W. K. Carrington, J. Polym. Sci.: Symp. No. 41, 155 (1973).
23. M. A. Winnik, "The Formation and Properties of Latex Films", in "Emulsion Polymerization and Emulsion Polymers", M. El-Aasser and P. Lovel (ed.), to be published.
24. D. P. Sheetz, J. Appl. Polym. Sci., 9, 3759 (1965).
25. S. G. Croll, (a) J. Coat. Tech. 58 (734), 411 (1986); (b) J. Coat. Tech., 59 (571), 81 (1987).
26. (a) M. Joanicot, K. Wong, J. Maquet, Y. Chevalier, C. Pichot, C. graillat, P. Lindner, L. Rios, and B. Cabane, Prog. Colloid Polym. Sci., 81, 175 (1990); (b) Y. Chevalier, C. Pichot, C. graillat, M. Joanicot, K. Wong, P. Lindner, and B. Cabane, Colloid Polym. Sci., 270, 806 (1992).
27. N. D. Denkov, O. D. Velev, P. A. Kralczevsky, I. B. Ivanov, H. Yoshimura, K. Nagayama, Langmuir, 8, 3183 (1992).
28. (a) A. van Tent, K. te Nijenhuis, J. Colloid Interfac. Sci., 150, 97 (1992); (b) A. van Tent, K. te Nijenhuis, Prog. Org. Coatings, 20, 459 (1992).
29. (a) J. Feng, M. A. Winnik, R. Shivers, and B. Clubb, Macromol., 28, 7671 (1995); (b) M. A. Winnik, J. Feng, J. Coat. Tech., 68 (852), 39 (1996).
30. R. E. Dillon, L. A. Matheson, E. B. Bradford, J. Colloid. Sci., 6, 108 (1951).
31. G. L. Brown, J. Polym. Sci., 22, 423 (1956).
32. J. W. Vanderhoff, H. L. Tarkowski, M. C. Jenkins, and E. B. Bradford, J. Macromol. Chem., 1, 361 (1966).
33. S. T. Eckersley, and A. Rudin, J. Coat. Tech., 62 (780), 89 (1990).
34. G. Mason, Br. Polym. J., 5, 101 (1973).
35. K. Kendall, J. Padget, Int. J. Adhes. Adhes., 2, 149 (1982).
36. (a) F. Dobler, T. Pith, M. Lambla, Y. Holl, J. Colloid Interface Sci., 152, 1 & 12 (1992); (b) F. Dobler, Y. Holl, Trends in Polymer Science, 4 (5), 145 (1996).
37. P. R. Sperry, B. Snyder, M. O'Dowd, and P. Lesko, Langmuir, 10, 2619 (1994).
38. T. F. Protzman, G. L. Brown, J. Appl. Polym. Sci., 4, 81 (1960), and ASTM D-2354.
39. W. A. Henson, D. A. Taber, and E. B. Bradford, Ind. Eng. Chem., 45, 735 (1953).
40. D. Distler, G. Kanig, Colloid Polym. Sci., 256, 1052 (1978).
41. (a) B. J. Roulstone, M. Wilkinson, J. Hearn, A. Wilson, J. Polym. Int., 24, 87 (1991); (b) B. J. Roulstone, M. Wilkinson, J. Hearn, J. Polym. Int. 27, 43 (1992).

42. Y. Wang, A. Kats, D. Juhue, M. A. Winnik, R. Shivers, C. Dinsdale, Langmuir, 8, 1435 (1992).
43. (a) Y. Wang, D. Juhue, M. A. Winnik, O. Leung, and M. C. Goh, Langmuir, 8, 760 (1992); (b) M. C. Goh, D. Juhue, O. Leung, Y. Wang, and M. A. Winnik, Langmuir, 9, 1319 (1993).
44. R. Zallen, "The Physics of Amorphous Solids", Wiley-Interscience: New York, 1983.
45. A. Patel, J. Feng, M. A. Winnik, J. Vancso, and C. McBain, Polymer, 1996, in press.
46. E. B. Bradford, and J. W. Vanderhoff, J. Macromol. Chem., 1, 335 (1966).
47. M. El-Aasser, and A. Robertson, J. Paint Tech., 47 (611), 50 (1975).
48. M. Chainey, and M. Wilkinson, J. Polym. Sci.: Polym. Chem. Ed., 23, 2947 (1985).
49. (a) K. Hahn, G. Ley, H. Schuller, R. Oberthur, Colloid Polymer Sci., 264, 1092 (1986); (b) K. Hahn, G. Ley, H. Schuller, R. Oberthur, Colloid Polymer Sci., 266, 631 (1988).
50. (a) M. Linné, A. Klein, G. Miller, L. H. Sperling, G. Wignal, J. Macromol. Sci., Phys., B27 (2 & 3), 217 (1988); (b) J. Yoo, L. H. Sperling, C. Glinka, A. Klein, Macromolecules, 23, 3962 (1990); (c)) J. Yoo, L. H. Sperling, C. Glinka, A. Klein, Macromolecules, 24, 2868 (1991).
51. (a) N. Mohammadi, J. N.Yoo, A. Klein, and L. H. Sperling, J. Polym.Sci. Part B: Polym. Phys., 30, 1311 (1992); (b) N. Mohammadi, K. D. Kim, A. Klein, L. H. Sperling, J. Coll. Interfac. Sci., 157, 124 (1993); (c) N. Mohammadi, A. Klein, L. H. Sperling, Macromolecules, 26, 1019 (1993).
52. K. D. Kim, L. H. Sperling, A. Klein, G. D. Wignall, Macromolecules, 26, 4624 (1993).
53. (a) C-L Zhao, Y. Wang, Z. Hruska, M. A. Winnik, Macromolecules, 23, 4082 (1990); (b) Y. Wang, M. A. Winnik, J. Chem. Phys., 95, 2143 (1991); (c) Y. Wang, M. A. Winnik, J. Phys. Chem., 97, 2507 (1993); (d) Y. Wang, M. A. Winnik, Macromolecules, 26, 3147 (1993).
54. (a) Y. Wang, M. A. Winnik, F. Haley, J. Coatings Technol., 64(811), 51 (1992) ; (b) D. Juhué, Y. Wang, M. A. Winnik, Makromol. Chem. Rapid Comm., 14, 345 (1993).
55. (a) Y. S. Liu, E. Odrobina, J. Feng, and M. A. Winnik, to be published; (b) S. Kawagouchi, E. Odrobina, and M. A. Winnik, to be published.
56. (a) H. Strametz, Prog. Org. Coatings, 20, 447 (1992); (b) A. Broek, Prog. Org. Coatings, 22, 55 (1993).
57. B. G. Bufkin, and J. R. Grawe, J. Coatings Tech., 50 (641), 41 (1978).
58. M. Ooka, and H. Ozawa, Prog. Org. Coatings, 23, 325 (1994).
59. G. Vandezande, and A. Rudin, J. Coatings Tech., 66 (828), 99 (1994).
60. (a) P. Jansse, J. Oil & Color Chemists' Assoc., 12, 478 (1989); (b) J. C. Padget, J. Coatings Tech., 66 (839), 89 (1994).

Chapter II

1. (a) H. F. Mark, N. M. Bikales, C. G. Overberger, and G. Menges (Ed.), Encyclopedia of Polym. Sci. and Eng., Vol. 1, p234, John Wiley and Sons: New York, 1985; (b) R. G. Gilbert, "Emulsion Polymerization - A Mechanistic Approach", Academic Press: San Diego, 1995; (c) J. Feng, unpublished results. Data were estimated by measuring weight gain after immersion in water vapor (100 %RH) for 2 days of polymer films initially prepared by solvent-casting from latex samples cleaned by ion-exchange.
2. C. Zhao, Y. Wang, Z. Hruska, and M. A. Winnik, Macromol., 23, 4082 (1990).
3. H. Kim, Y. Wang, and M. A. Winnik, Polymer, 35, 1779 (1994).
4. J. Brandrup, and E. H. Immergut, Polymer Handbook, 2nd Ed., Interscience: New York, 1966.
5. G. Markl, and A. Merz, Synthesis, 1973, 295.
6. W. Tagaki, I. Inoue, Y. Yano, and T. Okonogi, Tetrahedron Lett., 1974, 2587.
7. (a) L. Egan, Ph.D. Thesis, University of Toronto, Canada, 1985; (b) J. Feng, unpublished reports, 1992.
8. S. Sosnowski, J. Feng, M. A. Winnik, J. Polym. Sci.: Polym. Chem., 32, 1497 (1994).
9. (a) S. Mori, J. Chromatogr., 411, 355 (1987); (b) Z. Grubisic-Gallot, J. P. Lingelser, and Y. Gallot, Polym. Bull., 23, 389 (1990).
10. G. H. J. Van Doremaele, "Model Prediction, Experimental Determination and Control of Emulsion Copolymer Microstructure", Ph.D thesis, Eindhoven University of Technology, The Netherlands, Berlicum, 1990.
11. M. S. El-Aasser, in "An Introduction to Polymer Colloids", F. Candau and R. H. Ottewill (Eds.), P. 1, Kluwer Academic Publishers: Dordrecht, 1990.
12. T. G. Fox, Bull. Amer. Phys. Soc., 1, 123 (1956).
13. J. Snuparek, Makromol. Chem. Suppl., 10/11, 129 (1985).
14. F. Candau, "Polymerization in Microemulsions", in "Polymerization in Organized Media", C.M. Paleos (Ed.), Gordon and Breach Science Publ.: Philadelphia, 1992.
15. (a) M. Antonietti, W. Bremser, D. Muschenborn, C. Rosenauer, B. Schupp, M. Schmidt, Macromolecules, 24, 6636 (1991); (b) M. Antonietti, S. Lohmann, C. Niel, Macromolecules, 25, 1139 (1992).
16. I. Capek, P. Potisk, J. Polym. Sci.: Polym. Chem. Ed., 33, 1675 (1995).
17 H. Shirahama, and T. Suzawa, Polym. J., 16, 795 (1984).

18. B. Emelie, C. Pichot, and J. Guittot, (a) J. Disp. Sci. Tech., 5, 393 (1984); (b) Makromol. Chem., 189, 1879 (1988).
19. A. Zosel, W. Heckmann, G. Ley, and W. Maechtle, Colloid Polym. Sci., 265, 113 (1987).
20. L. B. Bangs, "Uniform Latex Particles", Seradyn, Indianapolis, 1984.
21. M. S. El-Aasser, F. Loncar, J. W. Vanderhoff, Makromol. Chem. Suppl. 10/11, 335 (1985).
22. J. W. Taylor, M. J. Collins, and D. R. Bassett, "Proceedings of the ACS: Division of Polym. Mater. Sci. Eng.", 73, 102 (1995).

Chapter III

1. G. L. Brown, J. Polym. Sci., 22, 423 (1956).
2. D. P. Sheetz, J. Appl. Polym. Sci., 9, 3759 (1965).
3. J. W. Vanderhoff, E. B. Bradford, W. K. Carrington, J. Polym. Sci.: Symp. No. 41, 155 (1973).
4. F. Dobler, Y. Holl, Trends in Polymer Science, 4 (5), 145 (1996).
5. N. Pramojaney, G. W. Poehlein, and J. W. Vanderhoff, Drying'80, vol. 2, p93-100 (1980).
6. S. G. Croll, J. Coat. Tech. 58 (734), 41 (1986).
7. S. G. Croll, J. Coat. Tech., 59 (571), 81 (1987).
8. M. Joanicot, K. Wong, J. Maquet, Y. Chevalier, C. Pichot, C. Graillat, P. Lindner, L. Rios, and B. Cabane, Prog. Colloid Polym. Sci., 81, 175 (1990).
9. Y. Chevalier, C. Pichot, C. Graillat, M. Joanicot, K. Wong, P. Lindner, B. Cabane, Colloid Polymer Science, 270, 806 (1992).
10. P. K. Isaacs, J. Macromol. Chem., 1, 163 (1966).
11. B. R. Vijayendran, J. Appl. Polym. Sci., 23, 733 (1979).
12. S. T. Eckersley, A. Rudin, Progress in Organic Coatings, 23, 387 (1994).
13. T. Crowley, A. Sanderson, J. Morrison, M. Barry, A. J. Morton-Jones, and A. R. Rennie, Langmuir, 8, 2110 (1992).
14. N. D. Denkov, O. D. Velev, P. A. Kralchevsky, I. B. Ivanov, H. Yoshimura, K. Nagayama, Langmuir, 8, 3183 (1992).
15. J. S. Mackie, P. Meares, Proc. R. Soc. London, A 1955, 232, 498.
16. D. A. Sullivan, J. Paint Techn., 47 (610), 60 (1975).

17. (a) F. B. Stieg, J. Paint Techn., 39 (515), 701 (1967); (b) F. B. Stieg, Prog. Org. Coatings, 1, 351 (1973).
18. E. Schaller, J. Paint Techn., 40 (525), 433 (1968).
19. J. Feng, M. A. Winnik, R. Shivers, B. Clubb, Macromolecules, 28, 7671 (1995).
20. M. A. Winnik, J. Feng, J. Coat. Tech., 68 (852), 39 (1996).

Chapter IV

1. T. L. Patton, Paint Flow and Pigment Dispersion, Wiley-Interscience: New York, 1979.
2. D. R. Karsa, Additives for Water-based Coatings, Royal Society of Chemistry: London, 1990.
3. A. D. Broek, Prog. Org. Coatings, 22, 55 (1993).
4. M. A. Winnik, Y. Wang, and F. Haley, J. Coatings Tech. 64 (811), 51 (1992).
5. J. Friel, European Patent Application, 0466 409 A1 (1992).
6. B. S. Snyder, United States Patent, 5308890 (1994).
7. J. Feng, M. A. Winnik, R. Shivers, B. Clubb, Macromolecules, 28, 7671 (1995).
8. M. A. Winnik, J. Feng, J. Coatings Tech., 68 (852), 39 (1996).
9. A. Patel, J. Feng, M. A. Winnik, J. Vancso, C. McBain, Polymer, 1996, in press.
10. Y. Wang, A. Kats, D. Juhué, M. A. Winnik, R. Shivers, C. Dinsdale, Langmuir, 8, 1435 (1992).
11. ASTM D 3363-92a, "Standard Test Method for Film Hardness by Pencil Test", ASTM, Philadelphia, PA 19103.
12. ASTM D4946-89, "Standard Test Method for Blocking Resistance of Architectural Paints", ASTM, Philadelphia, PA 19103.
13. L. Bohn, in "Polymer Handbook," Brandrup, J. and Immergut, E. H. (Ed), 2nd Ed. Wiley-Interscience, N.Y., 1975, p. IV-211.
14. S. L. Rosen, Polymer Eng. Sci., 7 (2), 115 (1967).
15. J. N. Israelachvili, Intermolecular and Surface Forces, Academic Press: London, 1985.
16. P. Bartlett, R. H. Ottewill, Langmuir, 1992, 8, 1919.
17. T. Biben, J. P. Hansen, Phys. Rev. Lett. 1991, 66, 2215.
18. D. R. Paul, S. Newman, Polymer Blends; Vol. 1-2, Academic Press: New York, 1978.
19. I. S. Miles, Multicomponent Polymer Systems, Burnt Mill: Harlow, 1992.
20. V. A. Mations, Polym. Eng. and Sci., 9, 90 (1969).
21. P. H. T. Vollenberg, and D. Heikens, Polymer, 30 (9), 1656 (1989).
22. D. C. Douglass, and V. J. Mcbrierty, Polym. Eng. and Sci., 19 , 1054 (1979).

23. D. Mahoney, and E. V. Meerwall, J. Polym. Sci Polym. Phys., 31, 1029 (1993).

Chapter V

1. J. R. Lakowicz, "Energy Transfer", in "Principles of Fluorescence Spectroscopy". Plenum Press: New York, 1983.
2. (a) T. Forster, Ann. Phys., 2, 55 (1948); (b) T. Forster, Discuss. Faraday Soc., 27, 7 (1959).
3. (a) J. Klafter, and A. Blumen, J. Phys. Chem. 80, 875, 1984; (b) P. LeVtz, J. Drake, and J. Klafter, "Energy Transfer at Interfaces: Silica Gels as Model Systems", in: Molecular Dynamics in Restricted Geometries . John Wiley & Sons: New York, 1989.
4. I. B. Berlman, "Energy Transfer Parameters of Aromatic Compounds". Academic Press, New York, 1973.
5. K. Nakashima, Y. Liu, P. Zhang, J. Duhamel, J. Feng, and M. A. Winnik, Langmuir 9, 2825 (1993).
6. S. Ni, P. Zhang, Y. Wang, and M. A. Winnik, Macromolecules 27, 5742 (1994).
7. H. Morawetz, Science , 240, 172 (1981).
8. (a) Y. Wang, C. Zhao, and M. A. Winnik, J. Chem. Phys., 95, 2143 (1991); (b) M. A. Winnik, Y. Wang, and F. Haley, Journal of Coatings Technology, 64 (811),51-61 (1992); (c) Y. Liu, J. Feng, and M. A. Winnik, J. Chem. Phys., 101, 9096 (1994).
9. J. Feng, M. A. Winnik, B. Clubb, and R. Shivers, Macromolecules, 28, 7671 (1995).
10. S. Sosnowski, J. Feng, M. A. Winnik, J. Polym. Sci.: Polym. Chem., 32, 1497 (1994).
11. M. A. Winnik, and J. Feng, J. Coatings Tech., 68 (852), 39 (1996).
12. Increasing the total number of acceptors will increase significantly the reabsorption of donor fluorescence (trivial energy transfer). This doesnot affect the donor decay profile. But one needs a longer detection time for the experiments.
13. V. A. Mations, Polym. Eng. Sci., 9, 90 (1969).
14. P. Vollenberg, and D. Heikens, Polymer, 30, 1656 (1989).
15. C. Bindschaedler, R. Gurny, and E. Doelker, J. Appl. Polym. Sci., 34, 2631 (1987).
16. (a) C. Zhao, Y. Holl, T. Pith, and M. Lambla, Colloid Polym. Sci., 265, 823 (1987); (b) C. Zhao, Y. Holl, T. Pith, and M. Lambla, British Polym. J., 21, 155 (1989).
17. (a) M. Urban, Evanson, Polym. Commun., 31, 279 (1990); (b) T. Thorstenson, M. Urban, J. Appl. Polym. Sci., 47, 1387 (1993).
18. L Li, Y. Wang, J. Feng, M. A. Winnik, H. Yan, T. North, to be submitted for publication.

Chapter VI

1. J. Whitlow, R. P. Wool, Macromolecules, 24, 5926 (1991).
2. (a) R. P. Wool, K. M. O'Conner, J. Appl. Phys., 52, 5194, 5993 (1981); (b) Y. H. Kim, R. P. Wool, Macromolecules, 16, 1115 (1983).
3. J. N. Yoo, L. H. Sperling, C. Glinka, A. Klein, Macromolecules, 23, 3962 (1990); (b) J. N. Yoo, L. H. Sperling, C. Glinka, A. Klein, Macromolecules, 24, 2868 (1991).
4. (a) Y. Wang, M. A. Winnik, Macromolecules, 26, 3147 (1993); (b) L. Li, Y. Wang, J. Feng, M. A. Winnik, H. Yan, T. H. North, to be submitted for publication.
5. (a) C. Zhao, Y. Wang, Z. Hruska, M. A. Winnik, Macromolecules, 23, 4082 (1990); . (b) Y. Wang, C. Zhao, M. A. Winnik, J. Chem. Phys., 95, 2143 (1991); (c) Y. Wang, M. A. Winnik, F. Haley, J. Coat. Technol., 64 (811), 51 (1992); (d) Y. Wang, M. A. Winnik, J. Phys. Chem., 97, 2507 (1993).
6. (a) K. Hahn, G. Ley, H. Schuller, R. Oberthur, Colloid Polym. Sci., 264, 1092 (1986); (b) K. Hahn, G. Ley, R. Oberthur, Colloid Polym. Sci., 266, 631 (1988); (c) A. Zosel, G. Ley, Macromolecules, 26, 2222 (1993).
7. (a) P.-G. de Gennes, J. Phys., 9, 457 (1971); (b) P.-G. de Gennes, Scaling Concepts in Polymer Physics, Cornell University Press: Ithaca, 1979.
8. (a) E. Kramer, P. Green, C. Palmstrom, Polymer, 25, 473 (1984); (b) P. Green, E. Kramer, Macromolecules, 19, 1108 (1986).
9. T. P. Russell, V. Delvie, W. Dozier, G. Felcher, G. Agrawal, R. P. Wool, J. Mays, Nature, 365, 235 (1993).
10. (a) H. Sillescu, Makromol. Chem. Rapid Commun., 5, 519 (1984); (b) H. Sillescu, Makromol. Chem. Rapid Commun., 8, 393 (1987).
11. J. Crank, The Mathematics of Diffusion, Clarendon: Oxford, 1974.
12. M. Eu, R. Ullman, Proceedings of the American Chemical Society: Division of Polymeric Materials: Science and Engineering, vol 73, p10, Fall 1995, Chicago, U.S.A.
13. A. Dhinojwala, J. Torkelson, Macromolecules, 27, 4817 (1994).
14. (a) Y. Liu, J. Feng, M. A. Winnik, J. Chem. Phys., 101, 9096 (1994); (b) Y. Liu, M. A. Winnik, Makromol. Chem. Symp., 92, 321 (1995).
15. A. Yekta, J. Duhamel, M. A. Winnik, Chem. Phys. Lett., 235, 119 (1995).
16. J. Farinha, J. M. G. Martinho, A. Yekta, M. A. Winnik, Macromol., 27, 4817 (1994).
17. D. Juhué, Y. Wang, M. A. Winnik, Makromol. Chem. Rapid Comm., 14, 345 (1993).

18. (a) H. Kim, Y. Wang, M. A. Winnik, Polymer, 35, 1779 (1994); (b) H. Kim, M. A. Winnik, Macromolecules, 27, 1007 (1994); (c) H. Kim, M. A. Winnik, Macromolecules, 28, 2033 (1995).
19. (a) Y. S. Liu, E. Odrobina, J. Feng, and M. A. Winnik, to be published; (b) S. Kawagouchi, E. Odrobina, and M. A. Winnik, to be published.
20. G. L. Brown, J. Polym. Sci., 22, 423 (1956).
21. (a) Y. Chevalier, C. Pichot, C. Graillat, M. Joanicot, K. Wong, J. Maquet, P. Lindner, B. Cabane, Colloid Polym. Sci., 270, 806 (1992); (b) M. Joanicot, K. Wong, B. Cabane, submitted for publication.
22. Z. Wang, A. Paine, A. Rudin, J. Polym. Sci.: Polym. Chem., 33, 1597 (1995).
23. (a) A. Eisenberg, Macromolecules, 4, 125 (1971); (b) H. Matsuura, A. Eisenberg, J. Polym. Sci. Polym. Phys. Ed., 14, 1201 (1976).
24. (a) D. Juhué, Y. Wang, J. Lang, O. M. Leung, M. C. Goh, M. A. Winnik, J. Polym. Sci.: Polym. Phys., 33, 1123 (1995); (b) Y. Wang, A. Kats, D. Juhué, M. A. Winnik, R. Shivers, C. Dinsdale, Langmuir, 8, 1435 (1992).

Chapter VII

1. C. Pichot, Makromol. Chem.: Macromol. Symp., 35/36, 327 (1990).
2. D. A. Upson, J. Polym. Sci.: Polym. Symp., 72, 45 (1985).
3. B. G. Bufkin and J. R. Grawe, J. Coatings Techn., 50 (641), 41 (1978).
4. A. J. Backhouse, U.S. Patent, 1983, 4,403,003.
5. V. I. Yeliseeva, Br. Polym. J., 7, 33 (1975).
6. D. R. Basset, M. A. Sherwin, and Hager, S. L., J. Coatings Techn., 51 (657), 65 (1979).
7. K. Makuuchi, A. Katakai, and H. Nakayama, J. Coatings Techn., 55(698), 29 (1983).
8. M. Yoshino, M. Shibata, M. Tanaka, and M. Sakai, J. Paint Techn., 44 (564), 116 (1972).
9. B. Schlund, T. Pith, and M. Lambla, Makromol. Chem. Suppl., 10/11, 419 (1985).
10. M. Okubo, Y. Nakamura, and T. Matsumoto, J. Polym. Sci.: Polym. Chem. Ed., 18, 2451 (1980).
11. J. A. Simms, J. Appl. Polym. Sci., 5 (13), 58 (1961).
12. R. M. O'Brien, S. A. Brown, B. G. Bufkin, and J. R. Grawe, J. Coatings. Techn., 53 (673), 49 (1981).
13. (a) R. J. Clemens, and F. D. Rector, J. Coatings Techn., 61 (770), 83 (1989); (b) F. D. Rector, W. W. Blount, and D. R. Leonard, J. Coatings Techn., 61 (771), 31 (1989).

14. L. van der Ven, R. Lamping, P. Geurink, Proceedings of the XXII Fatipec Congress, Budapest, May 1994.
15. J. R. Grawe and B. G. Bufkin, J. Coatings Techn., 53(676), 45 (1981).
16. S. Magnet, J. Guillot, A. Guyot, and C. Pichot, Prog. Org. Coatings, 20, 73 (1992).
17. S. G. Mylonakis, U.S. Patent, 1981, 4,244,850.
18. M. Ooka, and H. Ozawa, Prog. Org. Coatings, 23, 325 (1994).
19. Y. Kawamura, Proc. Toryokoza, Tokyo, Japan, Oct. 13, 27 (1992).
20. Polymeric crosslinkers, K-1000 series, Tech. Bull. Nippon Shokubai.
21. ICI Resins, Jpn. Patent, 1990, No. 2 024 370.
22. J. C. Padget, J. Coatings. Tech., 66 (839), 89 (1994).
23. M. A. Winnik, J. Feng, J. Coat. Tech., 68 (852), 39 (1996).
24. L. F. Johnson, W. C. Jankowski, Carbon-13 NMR Spectra, John Wiley & Sons: New York, 1972.
25. H. Kalinowski, S. Berger, S. Braun, ^{13}C-NMR Spectroscopy, Wiley: New York, 1988.
26. D. A. Bors, European Patent Application, 1992, 0 492 847 A2.
27. J. W. Taylor, J. Collins, D. Bassett, U.S. Patent, 1994, 5,371,148.

Appendix VI-1

1. A. Dhinojwala, J. Torkelson, Macromolecules, 27, 4817 (1994).
2. (a) C. Zhao, Y. Wang, Z. Hruska, M. A. Winnik, Macromolecules, 23, 4082 (1990); (b) Y. Wang, C. Zhao, M. A. Winnik, J. Chem. Phys., 95, 2143 (1991); (c) Y. Wang, M. A. Winnik, J. Phys. Chem., 97, 2507 (1993).
3. (a) Y. Liu, J. Feng, M. A. Winnik, J. Chem. Phys., 101, 9096 (1994); (b) M. A. Winnik, Y. Liu, Makromol. Symp., 92, 321 (1995).
4. (a) P.-G. de Gennes, J. Phys. (Paris), 31, 235 (1970); (b) P.-G. de Gennes, "Scaling Concepts in Polymer Physics", Cornell University Press: London, p62, 1979.
5. G. H. Fredrickson, Macromolecules, 19, 441 (1986).
6. A. Mendelsohn, M. Cruz, J. Torkelson, Macromolecules, 26, 6789 (1993).

LIST OF PUBLICATIONS

(I) Published

(1) J. Feng, A. Yekta, M. A. Winnik, **Chemical Physical Letters**, 260, 296 (1996).
"Direct Non-radiative Energy Transfer Across A Sharp Polymer Interface"

(2) J. Feng, M. A. Winnik, **Journal of Coatings Technology**, 68 (852), 39 (1996).
"Latex Blends: An Approach to Zero Volatile-Organic-Compound Coatings"

(3) X. Jin, L. Chen, J. Feng, M. A. Winnik, **Journal of Polymer Science: Polymer Chemistry**, 34, 2045 (1996).
"Thermal Decomposition Behavior of Naphthalene-labeled Polyethylene"

(4) J. Feng, M. A. Winnik, R. Shivers, B. Clubb, **Macromolecules**, 28, 7673 (1995).
"Polymer Blend Latex Films: Morphology and Transparency"

(5) S. Sosnowski, J. Feng, M. A. Winnik, **Journal of Polymer Science: Polymer Chemistry**, 32, 1497 (1994).
"Dye Distribution in Fluorescent-labeled Latex Prepared by Emulsion Polymerization"

(6) Y. Liu, J. Feng, M. A. Winnik, **Journal of Chemical Physics**, 101, 9096 (1994).
"Study of Polymer Diffusion Across Interfaces through Direct Energy Transfer Experiments"

(7) K. Nakashima, Y. Liu, P. Zhang, J. Duhamel, J. Feng, M. A. Winnik, **Langmuir**, 9, 2825 (1993).
"Surface Characterization of Colloidal Particles by Direct Energy Transfer"

(II) In press, submitted or in prepararion

(8) A. Patel, J. Feng, M. A. Winnik, J. Vancso, **Polymer**, 1996, in press.
"Characterization of Latex Blend Films by Atomic Force Microscopy"

(9) J. Feng, M. A. Winnik, **Journal of Coatings Technology**, submitted, 1996.
"Role of Water in Polymer Diffusion in Latex Films"

(10) J. Feng, M. A. Winnik, **Macromolecules**, to be submitted, 1996.
"Polymer Diffusion in Latex Films at Ambient Temperature"

(11) J. Feng, H. Pham, P. M. Macdonald, M. A. Winnik, J. M. Geurts, H. Zirkzee, S. van ES, A. L. German, **Progress in Organic Coatings**, to be submitted, 1996.
"Preparation of Reactive Latex and Formation of Latex Films Crosslinkable under Ambient Conditions: using acetoacetoxy groups as the reactive functionality"

(12) Y. Liu, E. Odrobina, J. Feng, M. A. Winnik, in preparation.
"Effect of Ionic and Nonionic Surfactant on Polymer Diffusion in Latex Films"

(13) E. Odrobina, J. Feng, M. A. Winnik, in preparation.
"Oligomer Effect on Diffusion Rate of High Polymers"

(14) J. Feng, M. A. Winnik, in preparation.
"Interface Characterization of Latex Blend Films by Energy Transfer"

(15) L. Li, Y. Wang, J. Feng, M.A. Winnik, H. Yan, T. North, to be submitted.
"Polymer Diffusion and Mechanical Property Development in Poly(methyl methacrylate) Films Prepared by Melt-compressing Latex Particles"

(October 25, 1996)

IMAGE EVALUATION
TEST TARGET (QA-3)

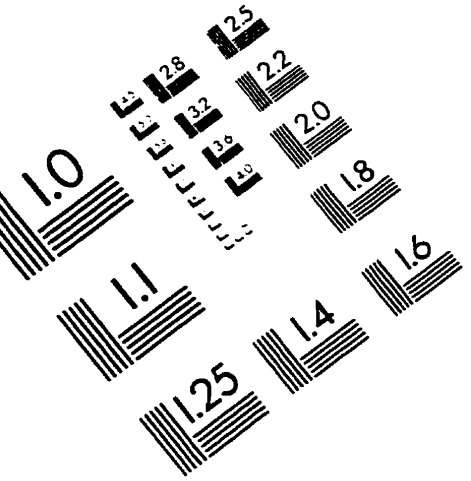

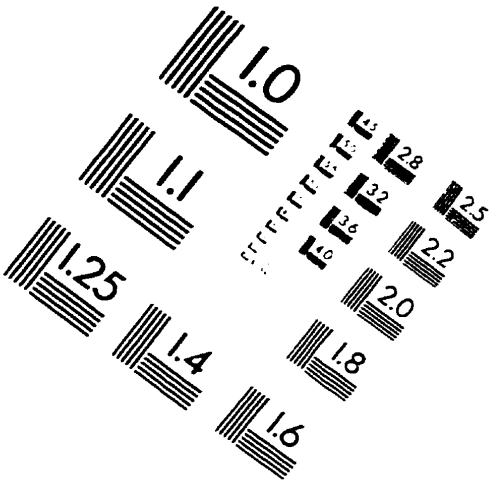

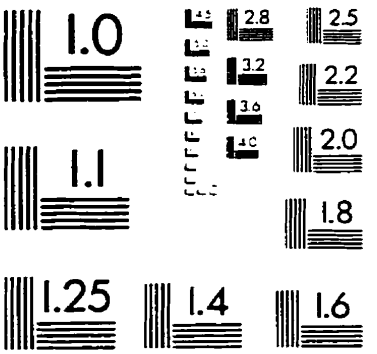

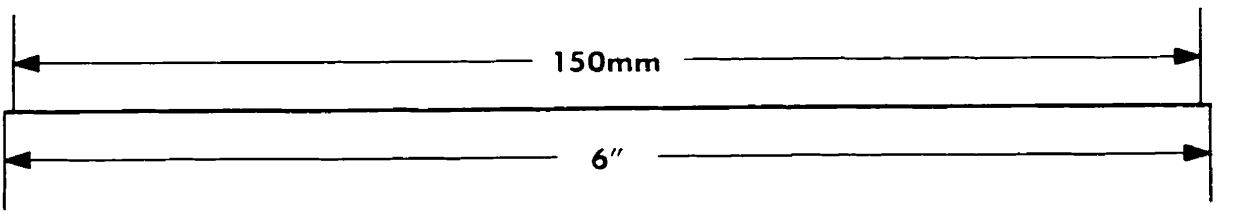

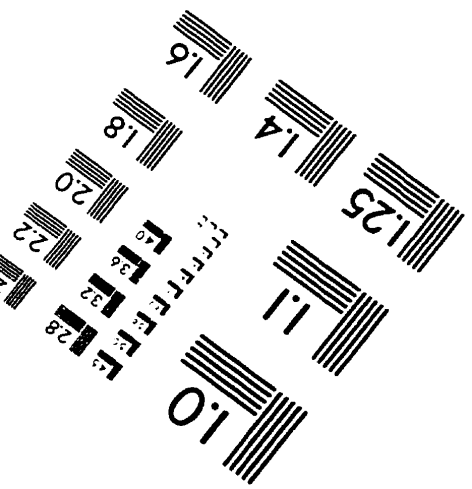

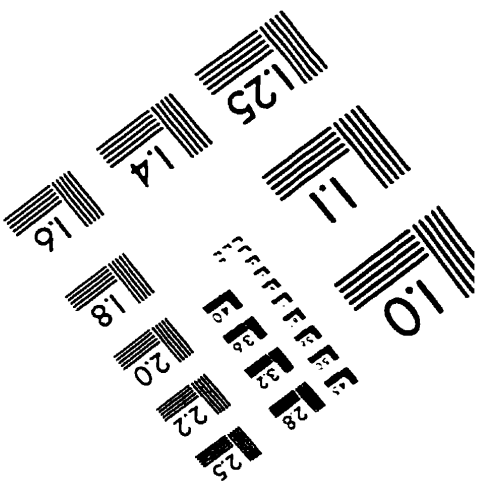

APPLIED IMAGE, Inc
1653 East Main Street
Rochester, NY 14609 USA
Phone: 716/482-0300
Fax: 716/288-5989